Preclinical investigations of genetic and pharmacological therapeutic strategies for *MECP2*-related neurodevelopmental disorders

By

Sheryl Anne Daguimol Vermudez

Dissertation

Submitted to the Faculty of the

Graduate School of Vanderbilt University

in partial fulfillment of the requirements

for the degree of

DOCTOR OF PHILOSOPHY

in

Pharmacology

January 31, 2022

Nashville, Tennessee

Approved:

Lisa Monteggia, Ph.D.

Colleen M. Niswender, Ph.D.

P. Jeffrey Conn, Ph.D.

Jeffrey Neul, M.D., Ph.D.

Eric Delpire, Ph.D.

For my grandparents and parents –

Your sacrifices have set me up for success,

And I will always be grateful.

ACKNOWLEDGEMENTS

I have been very fortunate that my path to and time in graduate school have been filled with tremendous support from numerous people. I would first like to thank my mentor Colleen Niswender for allowing me to rotate in her lab and taking a chance on me. Colleen resembles everything that I wanted in a mentor, supportive, communicative, exuding confidence that was contagious and a big proponent of independent research. Her motto of “try it once” and value of letting people drive their careers have both been a huge component of my dissertation project and my development as a scientist and a person, especially in instilling confidence in myself. Her initial message prior to officially joining the lab was “Bring it!”, and it has served as a constant motivation. Colleen, I hope that I have brought it and contributed to the lab; a big Mahalo for your support throughout these years. Thank you to my committee members Lisa Monteggia, Jeff Conn, Jeff Neul and Eric Delpire. You all have been supportive and encouraging throughout these years. Aside from the occasional nervousness, I have always felt positive during and after my committee meetings. Your commitment and investment to my success during graduate school and my future plans have been remarkable.

I would also like to thank Rocco Gogliotti for serving as a second mentor to me. Rocco showed me the ropes from when I first rotated in the lab and he has been integral in the progression of my projects even after he transitioned to a faculty position (woohoo!) in another university. His meticulousness and detailed eye have been valuable for presentations, and I have always been very grateful for that. A big thank you to my undergraduate mentors, Claire Wright and Bulent Terem, for believing in me and giving me the opportunity to grow as a scientist. Bulent, you have always showed unwavering support, and Claire, you inspired me to pursue translational research, especially in the context of the neuroscience. At difficult times, I questioned why I listened to your speeches about the value of graduate education, but I am forever grateful to you both.

Thank you to everyone, past and present, in the Niswender and Conn labs. A special thank you to current and former members in “Team Rett/MeCP2/mGlu$_7$” – Rocco, Nicole Fisher, Chris Hofmann, Bright Arthur, Kelly Weiss, Aditi Buch, Yuta Moxley, Clarissa Morales, James Melchior, and Geanne Freitas; members of the electrophysiology group for your patience and time in teaching me – Sean Moran, James Maksymetz, Branden Stansley, Dan Foster, Zixiu Xiang and Shalini Dogra; members of the Molecular Pharmacology group for showing me your sophisticated screening machines and big data – Vince Luscombe, Marc Quitilag, Matt Loch, Alice Rodriguez and Aidong Qi; and the undergraduate students for shaping me as a mentor – Chiaki Santiago, Susmi Chennareddy and Hershey Rajpal. The camaraderie within the lab, especially a big one, is hard to come by, and I have been lucky to work in an environment that has been supportive, inclusive and always felt like family.

I also would like to thank John Allison for his training at the Mouse Neurobehavioral Core, as well as his patience for seeing me there constantly. Thank you to the Pharmacology and IMSD community and leadership – Joey Barnett, Ege Kavalali, Christine Konradi, Karen Gieg, Roger Chalkley, Linda Sealy and Christina Keeton – for fostering a sense of community with rigorous training. At the graduate school, thank you to Don Brunson and Beth Bowman for helping me during my decision to attend Vanderbilt and transition to Nashville. Lastly, I would like to thank the VPMM program, especially Sarika Peters for giving me the opportunity to meet patients with Rett syndrome and cultivate my passion for translational research.

To my friends from Hawaii and in Nashville, thank you for being my 'Ohana and for your constant support, belief and countless memories. My Hawaii friends, Kahealani Uehara, Lauren Uson, Keri Fujiwara, Alexis Peterson, Maria Sciulli and Kiana Annunziata, a big Mahalo; we always pick up where we left off and I look forward to celebrating all your successes in life. To Mark Crowder and Jamal Bryant, I cannot thank you enough; you both have been my family in Nashville and I am

excited to see your careers take off. I know that the despite where we all are, I can always count on all of you and I will be there for you all too. A special thank you to Jamie Hatfield – you have been there with me through the beginning of graduate school and thank you for always believing in me and reminding me of life outside of lab. I look forward to finally not having hours and thousands of miles between us, *Je vous aime.*

Finally, to my family, you have been my rock – Salamat po. Thank you to my parents for leading by example on what hard work entails and the value of humility in every achievement. You have always encouraged me to follow my aspirations, supported my decisions even the ones that led me to the mainland (many times in the South), and instilling core values of perseverance, dedication and humility. Thank you to my brother, Mark Wayne for pretending to listen while I talk science, just like when I pretend to listen when you talk cars. I can always count on you to not only drive me around but to enjoy the smallest things that life offers. Thank you to my grandparents for your sacrifices in order for all your children and grandchildren to live a better life. To the rest of my immediate and extended family, thank you for always welcoming me back home and for your endless support. I love you all.

TABLE OF CONTENTS

LIST OF TABLES

LIST OF FIGURES

LIST OF SUPPLEMENTARY DATA

Supplementary data are provided in additional external files.

LIST OF ABBREVIATIONS

Abbreviation	Definition
aa	Amino acids
AAV	Adeno-associated virus
AC	Adenylyl cyclase
AD1 / AD2	Activation domain 1 / 2
(A)ERP	(Auditory) event-related potential
AGAT	Glycine amidinotransferase
AS	Angelman syndrome
ASD	Autism spectrum disorder
ASO	Anti-sense oligonucleotides
ASR	Acoustic startle response
BA	Brodmann area
BBB	Blood brain barrier
BCA	Bicinchoninic acid
bHLH	Basic helix-loop-helix
BNDF	Brain-derived neurotrophic factor
bp	Base pair
BP	Biological process
C-term / CTD	C-terminus
CA1 / CA3	Hippocampal cornu ammonis 1/3
cAMP	cyclic-AMP
CBP	CREB binding protein
CC	Cellular component
CDD	Cerebral creatine deficiency

cDNA	Complementary DNA
CER	Cerebellum
CF	Conditioned fear / Fear conditioning (contextual)
CK / *CK*	Creatine kinase
CNP	2',3'-Cyclic nucleotide 3'-phosphodiesterase
CNS	Central nervous system
CRD	Cysteine-rich domain
CREB1	Cyclic AMP-responsive element-binding protein 1
CRH	Corticotropin-releasing hormone
Ct	Cycle threshold
CTGF	Connective tissue growth factor
CTX	Cortex
dB	Decibel
DEG	Differentially expressed gene
DGCR8	DiGeorge syndrome critical region 8
E-box	Ephrussi box
ECD	Extracellular domain
EDTA	Ethylenediaminetetraacetic acid
EEG	Electroencephalogram
EGFP / GFP	(Enhanced) green fluorescent protein
ELISA	Enzyme-linked immunosorbent assay
ERK1/2	Extracellular signal-regulated kinase 1/2 (
Ex/Em	Excitation / emission
EZM	Elevated zero maze
FC	Fold change
FDR	False discovery rate

FST	Forced-swim test
FXS	Fragile X syndrome
GABA	γ-Aminobutyric acid
Gamt / GAMT	Guanidinoacetate methyltransferase
GIRK	G-protein-gated inwardly rectifying potassium channels
GO	Gene ontology
GPCR	G-protein couple receptor(s)
GRIP	Glutamate receptor-interacting protein
GRK	GPCR kinase
GTP	Guanosine-5'-triphosphate
HDAC	Histone deacetylase
hmC	Hydroxymethylcytosine
HPC	Hippocampus
hr / hrs	Hour(s)
i.p.	Intraperitoneal
ICV	Intracerebroventricular
ID	Interdomain
Id	Inhibitors of DNA binding
IGF-1	Insulin-like growth factor 1
iGlu	Ionotropic glutamate receptor
Indel	Insertion or deletion
iTF2	Immunoglobulin transcription factor 2
ITI	Inter-trial interval
kDa	Kilodaltons
kg	Kilogram
LOF	Loss-of-function

LTD	Long-term depression
LTP	Long-term potentiation
mA	Milliamp
MAPK	Mitogen-activated protein kinase
MBD	Methyl-binding domain
MCBR	Molecular cell biology resource core
MDS	MECP2 Duplication syndrome
MECP2 / *Mecp2* / MeCP2	Methyl-CpG-binding protein 2
MF	Molecular function
mg	Milligram
mGlu	Metabotropic glutamate receptor
min	Minutes
miRNA	microRNA
mM	Millimolar
MNL	Mouse neurobehavioral lab
MOG	Myelin oligodendrocyte glycoprotein
MOR	μ-opioid receptor
mPFC / PFC	(Medial) prefrontal cortex
mRNA	Messenger RNA
msec	Milliseconds
mTOR	Mechanistic target of rapamycin
N-term	N-terminus
NAM	Negative allosteric modulator
NCOR	Nuclear receptor co-repressor
ng	Nanogram
NG2	NG2 chondroitin sulphate proteoglycan

NHERF	Na^+/H^+ exchanger regulatory factors 1 and 2
NID	NCOR/SMRT interaction domain
NLS	Nuclear localization signal
nm	Nanometer
NMDA	N-methyl-D-aspartate
ns	Not significant
OF	Open field
OL	Oligodendrocyte
PAM	Positive allosteric modulator
PCP	Phencyclidine
PCR	Polymerase chain reaction
PDZ	PSD-95/Discs-large/ZO1
PICK	Protein interacting with protein kinase C
PKA	Protein kinase A
PLC	Phospholipase C
PP2Cα	Protein phosphatase 2Cα
PPF	Paired-pulse facilitation
PPI	Pre-pulse inhibition
PPR	Paired-pulse ratio
PSD	Post-synaptic density
PTEN	Phosphatase and tensin homolog deleted on chromosome 10
PTHS	Pitt-Hopkins syndrome
PTX	Picrotoxin
qRT-PCR	Quantitative real-time polymerase chain reaction
rhIGF-1	Recombinant human IGF-1
RIPA	Radioimmunoprecipitation assay

RNA-seq	RNA-sequencing
rpm	Revolutions per minute
RT	Room temperature
RTT	Rett syndrome
SAGA	Spt-Ada-Gcn5 acetyltransferase
SAHA	Suberoylanilide hydroxamic acid
SC	Schaffer collateral
scAAV	Self-complementary adeno-associated virus
SDS	Sodium dodecyl sulfate
sec	Second
SEF2	SL3-3 enhancer factor 2
SEM	Standard error of the mean
SLC6A8	Creatine transporter
SMRT	Silencing mediator of retinoic acid and thyroid hormone receptor
SNP	Single nucleotide polymorphism
STR	Striatum
TBS	Tris-buffered saline
TCF4 / Tcf4	Transcription factor 4
TG / Tg	Transgene
TMD	Transmembrane domain
Trb	Tropomyosin receptor kinase B
TRD	Transcriptional repression domain
TS	Tone-shock
TSC	Tuberous sclerosis
TST	Tail suspension test
VFD	Venus flytrap domain

vGlut2	Vesicular glutamate transporter 2
WBP	Whole-body plethysmography
WT	Wild-type
XCI	X-chromosome inactivation
YB-1	Y box-binding protein 1
µg	Microgram
µL	Microliter

CHAPTER 1

INTRODUCTION

1.1 *MECP2*-Related Neurodevelopmental Disorders

A group of rare, pediatric diseases that are linked to the gene *Methyl-CpG-binding Protein 2* (*MECP2*) are classified as *MECP2*-related neurodevelopmental disorders. These disorders have similar clinical presentations including intellectual disability, motor and speech abnormalities, breathing disturbances, and seizures (*1*). These common features resemble those of autism spectrum disorder (ASD), and thus have also been referred to as syndromic ASDs. Two disorders, Rett syndrome (RTT) and *MECP2* Duplication syndrome (MDS) are directly associated with abnormal MeCP2 protein expression and function. Several others, including *FOXG1* syndrome, *CDKL5* deficiency disorder and Pitt-Hopkins syndrome (PTHS), are broadly classified as atypical RTT or RTT-like disorders due to their history of a RTT clinical diagnosis despite the lack of *MECP2* mutation. This dissertation will focus on RTT, MDS and PTHS, all which currently lack effective treatments.

1.1.1 Methyl-CpG-binding Protein 2 (MeCP2)

The *MECP2* gene is located on the X-chromosome (Xq28) and encodes for the transcription factor, MeCP2 (*2*, *3*). There are two isoforms of MeCP2, e1 and e2, which differ at the N-terminus due to the inclusion of exon 2 (*4*–*6*). Translation from exon 1 and bypassing exon 2 leads to the major and slightly longer isoform MeCP2-e1, which consists of 498 amino acids (aa) (*5*, *6*). The shorter protein, MeCP2-e2 (486 aa), was actually identified first and only includes exons 2-4 (*2*, *4*). Although the e1 isoform is more abundantly expressed (*6*), the structure of MeCP2, and thus subsequent identification of mutations in MeCP2, are referred by their location in the MeCP2-e2 protein.

The structure of MeCP2 includes four core domains, the methyl-binding (MBD), transcriptional repression (TRD), nuclear localization signal (NLS) and NCOR/SMRT (Nuclear receptor co-repressor / Silencing mediator of retinoic acid and thyroid hormone receptor) interaction (NID) regions (Figure 1). These functional domains are responsible for MeCP2's role in binding to DNA and regulating gene transcription; thus, MeCP2 is predominantly known as a transcriptional modulator. DNA binding is facilitated through the MBD, and at regions of methylated DNA, specifically methylated di- and tri-nucleotides including mCpG, mCpA, mCAC and hydroxymethylcytosine (hmC) (*7*–*14*). Additional findings of MeCP2 interacting with non-methylated DNA (*9*) support MeCP2's function in chromatin regulation. To exert its impact on transcription, MeCP2 utilizes its TRD and/or NID regions to recruit other co-factors to either activate or repress gene transcription (*15*). In particular, protein complexes involving histone deacetylases (HDACs), such as the Sin3a and NCOR/SMRT complexes, are recruited via the TRD or NID, respectively, to inhibit transcription (*16*, *17*). The role of MeCP2 in promoting transcription was observed in transcriptomic studies, in which *Mecp2* deficiency resulted in downregulated genes; recruitment of co-activators such as cyclic AMP-responsive element-binding protein 1 (CREB1) are thought to mediate this function of MeCP2 (*15*).

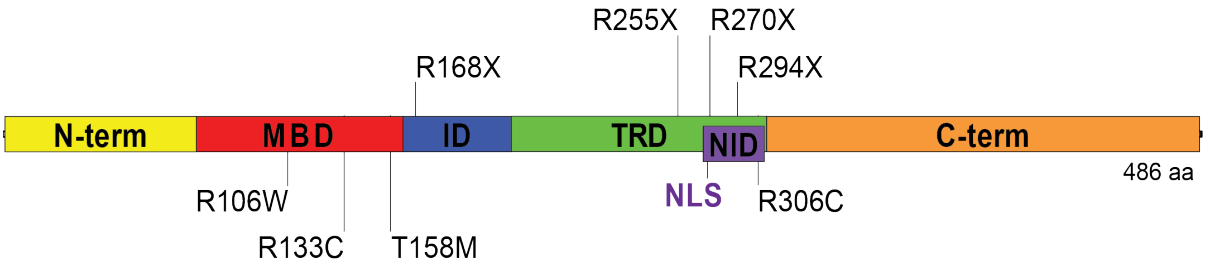

Figure 1: MeCP2 protein and common mutations leading to RTT. Illustration of key domains in the MeCP2 protein, isoform e2 (486 aa), and common pathological mutations leading to Rett syndrome (RTT). N-terminus (N-term), methyl-CpG-binding domain (MBD), interdomain (ID), transcriptional repressor domain (TRD), nuclear localization signal (NLS), NCOR/SMRT interaction domain (NID), C-terminus (C-term).

In addition to chromatin and transcriptional regulation, MeCP2 has been proposed to have other roles including alternative splicing and microRNA (miRNA) regulation (*18*–*21*). Young *et. al.* demonstrated that MeCP2 binds to the RNA-binding protein and splicing factor Y box-binding protein 1 (YB-1) to regulate alternative splicing (*22*). Since then, other splicing factors have been linked to MeCP2, with most interacting with the C-terminus regions of the protein (*23*–*25*). A recent study showed that MeCP2 modulates splicing events initiated by spatial learning, implicating the protein in cognitive function (*26*). Despite this, our understanding of the significance of MeCP2's relationship with the spliceosome and role in alternative splicing is still limited.

miRNAs are short non-coding RNAs that bind to 3' or 5' untranslated regions (UTRs) of target genes to, respectively, promote degradation and repress translation or regulate transcription through the Drosha/DiGeorge syndrome critical region 8 (DGCR8) machinery (*27*). Studies have shown contrasting roles of MeCP2 in miRNA regulation; Cheng *et. al.* demonstrated that MeCP2's interaction with DGCR8 inhibits miRNA function, which is consistent with downregulation of miRNAs in *in vitro* and *in vivo Mecp2* deficient models (*28*–*30*). miRNA upregulation was also observed with *Mecp2* deficiency (*29*), and congruently, reports have presented that MeCP2 promotes miRNA processing (*31*, *32*). For example, miR-199 activity is enhanced by MeCP2 and promoted mechanistic target of rapamycin (mTOR) signaling, which is dysregulated in *Mecp2* deficient models (*32*–*34*). However, a conflicting report recently showed that increased miR-199 activity led to aberrant neuronal development similar to *Mecp2 deficient* model (*35*). Therefore, the relationship between MeCP2 and miRNA regulation is still unclear. However, the roles of MeCP2 beyond transcriptional regulation has potential implications in studying *MECP2*-related disorders, especially with the expression profile of MeCP2.

MeCP2 is ubiquitously expressed with high levels in the central nervous system (CNS) (*36*). Within the CNS, MeCP2 is found mostly in neurons and with reduced but significant expression

in glial cells (*10*, *36*). Predominant expression in post-mitotic neurons suggest that MeCP2 is critical for neuronal maturation and maintenance of neuronal function (*10*, *37*). These roles are also influenced by MeCP2 in glia through non-cell-autonomous mechanisms (*38–41*). In particular, MeCP2 deficiency in either neurons or glial cells resulted in abnormal neuronal dendritic morphology. Thus, the function and expression of MeCP2 in different cell types could explain the delayed manifestation of disease phenotypes in and/or the developmental regression characteristic of *MECP2*-related disorders.

1.1.2 Rett syndrome (RTT)

RTT was initially observed in female patients by Andreas Rett in the 1960s and then later reported in the 1980s by Bengt Hagberg (*42*, *43*). Rett and Hagberg initially described that after normal development during the first 6-18 months of life, RTT patients undergo rapid regression, suffering from motor, cognitive and social symptoms as well as breathing abnormalities and stereotypic behaviors such as repetitive hand wringing (*42*, *44–46*). Almost 20 years later, the etiology was discovered to be loss-of-function (LOF) mutations in *MECP2* (*47*). The location of *MECP2* on the X-chromosome results in females being primarily affected with an occurrence of 1 in 10,000 (*46*). The mosaicism observed in RTT is due to X-chromosome inactivation (XCI), wherein one X-chromosome, thus one copy of the *MECP2* gene is inactivated (*48–50*). Favorable XCI skewing, or substantially higher expression of the X chromosome with the wild-type (WT) *MECP2* allele compared to the mutant allele, leads to milder disease presentation (*49*, *51*). This lack of mosaic expression of normal and mutant MeCP2 in males causes lethality in the majority of cases. However, studies have described cases of male patients with mutations in MeCP2 and/or present with symptoms that fulfill the clinical diagnosis of RTT (*52–55*).

1.1.2.1 MeCP2 mutations and clinical severity

Pathological mutations in MeCP2 decrease protein expression and render the protein completely or partially non-functional. Currently, there are almost 200 known pathological mutations in MeCP2, which are documented in accessible online databases such as RettBASE and InterRett (*56*, *57*). The most prevalent mutations are those in core regions of MeCP2, including the MBD and TRD, and are associated with symptom severity (*21*, *46*, *58–60*) (Figure 2). For example, patients with early truncating mutations in MeCP2 that disrupt DNA binding or transcriptional regulation, including R168X and R255X have more severe phenotypes than mutations in the C-terminus (e.g. R306C), which disrupt protein stability (*46*, *58–60*). Additionally, patients that have partial LOF or hypomorphic mutations, such as R133C and R294X, exhibit less severe phenotypes.

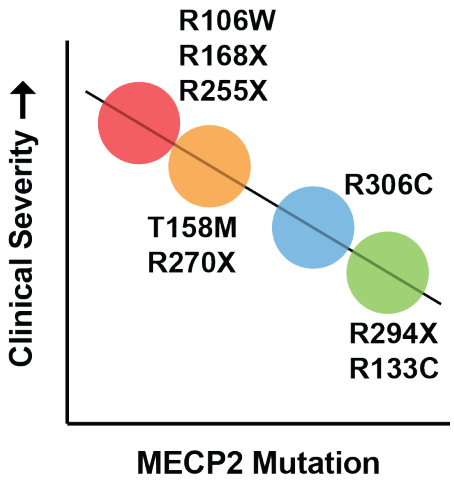

Figure 2: Genotype-phenotype correlation in RTT. Clinical severity of common pathological *MECP2* mutations based on (*60*). Modified from (*61*).

1.1.2.2 Mouse models of Rett syndrome

Seminal studies have demonstrated that clinical symptoms are recapitulated in rodent models lacking MeCP2, which have been comprehensively reviewed (*59*, *62–64*). These mouse models

exhibit anatomical abnormalities and neuronal dysfunction such as aberrant dendritic complexity, as well as deficits in synaptic neurotransmission and synaptic plasticity. In addition, behavioral deficits are also observed including motor (e.g. abnormal gait and hypolocomotor activity), cognitive (e.g. contextual and cued associative learning and memory), and social (e.g. decreased social recognition) defects. The hand-wringing stereotypy seen in patients is also mirrored as a hindlimb clasping phenotype in animal models. Lastly, these mouse models also display neurophysiological features such as irregularities in respiratory function, as well as abnormalities in electroencephalogram (EEG) recordings and auditory event-related potentials (AERPs), which possess stronger translatable value (*41*, *65*–*84*).

The most abundantly used mouse models are *Mecp2*^{Birdtm1} and *Mecp2*^{Jae}, which lack MeCP2 and were independently developed by the laboratories of Adrian Bird and Rudolph Jaenisch, respectively (*85*, *86*). In both mouse models, the Cre-lox recombination system was utilized, in which a conditional *Mecp2* allele was created with the insertion of loxP sites flanking exon 3 only (*Mecp2*^{Jae}) or exons 3 and 4 (*Mecp2*^{Birdtm1}). In *Mecp2*^{Birdtm1}, *Mecp2* is ubiquitously deleted; in contrast, *Mecp2*^{Jae} mice have *Mecp2* specifically deleted in the CNS with a nestin-Cre transgene, and in post-mitotic neurons using CamK-Cre93. Guy *et. al.* also developed mice lacking *Mecp2* only in the brain (*85*); both studies showed that the phenotypes observed in *Mecp2 null* mice are of neurological origin. These mouse models have been commonly used in understanding RTT and the role of MeCP2, as well as in discovering treatment strategies that either modulate MeCP2 directly, or associated proteins or pathways that are downstream of MeCP2.

Despite the abundant progress these mouse models have allowed, they only model 30% of the clinical cases, which are reflective of the most common mutations that have higher clinical severity score (T158M, R168X, R255X, R270X, R106W) (*56*, *57*, *60*). Many *in vitro* studies have explored the implications of these human MeCP2 mutations, in particular the impact on MeCP2 expression

and function in binding to its targets and regulating processes such as chromatin dynamics, and transcriptional repression and activation (*87*–*92*). On the other hand, *in vivo* studies of these human MeCP2 mutations have been sparse. These recent rodent studies of human MeCP2 mutations have shown that there are key functional domains in MeCP2 that contribute to the pathophysiology of RTT (*93*–*95*). The genotype-phenotype correlation observed clinically has also been recapitulated in mouse models bearing human MeCP2 mutations especially the most common pathological mutations (*17*, *65*, *74*, *78*, *82*–*84*, *94*–*100*).

1.1.2.3 MeCP2-targeted genetic therapy

Using these animal models, research has focused on uncovering treatment strategies that specifically target MeCP2. A breakthrough in the field came from early studies showing that genetically replacing MeCP2 could ameliorate phenotypes in mouse models (*71*, *101*). Since then, numerous rodent studies of genetic manipulation of MeCP2, either through reactivation or replacement methods have been conducted. Post-natal reactivation of the silenced *Mecp2* allele in the *Mecp2*^{tm2Bird} or *Mecp2*$^{tm1.1Jae}$ mouse has been conducted multiple times using the Cre-lox system (*41*, *71*, *102*–*104*). Ubiquitous reactivation of *Mecp2* at ~70-80% efficiency in male and female *Mecp2*^{tm2Bird} animals corrected several RTT-like characteristics including decreased dendritic complexity, long-term potentiation (LTP) deficits, decreased survival, and breathing and motor abnormalities (*71*, *102*). Cell-type specific reactivation of *Mecp2*, particularly in astrocytes and microglia, also reversed phenotypes in male *Mecp2*^{tm2Bird} or *Mecp2*^{Jae} mice (*41*, *103*). However, these studies are conflicted by a report showing that *Mecp2* reactivation in microglia of several RTT mouse models using bone marrow transplantation does not exert efficacy (*104*).

Contrary to the reactivation of an endogenous *Mecp2* allele, MeCP2 replacement methods involve the germline introduction of human *MECP2* or mouse *Mecp2* transgenes in RTT mice. An early study showed that *Mecp2*$^{tm1.1Jae}$ mice also expressing *Tau-Mecp2* or MeCP2 specifically in post-

mitotic neurons extended survival as well as reversed the attenuated body and brain weight and locomotor activity observed in *Mecp2*$^{tm1.1Jae}$ animals (*101*). Subsequent studies have since replicated the efficacy of germline MeCP2 replacement strategy using *MECP2* or *Mecp2* alleles that are expressed either throughout the body, in the CNS or specifically in neurons or glial cells of *Mecp2 mutant* mice (*105*–*108*). Interestingly, two reports of post-natal activation of the *MECP2* or *Mecp2* transgenes in neurons conflict, with one study demonstrating partial rescue of RTT-like phenotypes while the other describe no beneficial effects (*106*, *109*). Differences in the use of the human or mouse alleles and the activation techniques of the Cre-lox system versus the tetracycline (Tet)-regulated system could explain the opposing results from these studies. Recent studies have capitalized on these early findings by introducing *MECP2* or *Mecp2* in RTT mouse models with human MeCP2 mutations such as T158M, R255X, and R306C, and illustrating recapitulation of phenotypes observed in humans (*74*, *82*, *94*, *95*).

The beneficial effects of rescuing RTT-like phenotypes using MeCP2-reactivation or -replacement strategies further support the idea that RTT is amenable to MeCP2-targeted therapy. Moreover, these studies have led to the current state in the field in which gene therapy using adeno-associated viral vectors (AAVs) is the front-runner for a treatment. A multitude of preclinical reports demonstrate the optimization and feasibility of viral-mediated MeCP2-replacement gene therapy for RTT (*93*, *110*–*118*). It is important to note that these studies have been conducted in male *Mecp2 knockout or null* animals, with the exception of three contradictory studies that utilized female *Mecp2 null* animals (*113*, *117*, *118*). These latter reports show conflicting results of toxicity at high doses of AAV-expressing MeCP2. In particular, Luoni *et. al.* did not observe adverse effects, which contrast with the two studies describing Parkinsonian-like phenotypes or liver toxicity in female *Mecp2 null* animal administered with high doses of AAV-MeCP2 (*113*, *117*, *118*). These adverse effects could be further confounded by different MeCP2 mutations. Nonetheless, AAV-MeCP2 has progressed in the drug discovery pipeline. Novartis initially reported the safety

of gene therapy in non-human primates; however, this has unfortunately been recently terminated (*119*). Although it has not been disclosed, lack of efficacy or toxicity could underly the termination. To combat toxicity issues caused by MeCP2 overexpression, the gene therapy program led by Taysha Gene Therapies is using an AAV-expressing MeCP2 (TSHA-102) with a built-in inhibitory regulatory element known as miRARE, a synthetic miRNA (*120*). TSHA-102 has recently been demonstrated to be safe and efficacious in preclinical models, and is on track for clinical trials.

1.1.2.4 Pharmacological modulation of MeCP2 targets

The role of MeCP2 in regulating gene transcription presents potential targets that could be amenable to pharmacological modulation. Additionally, results from transcriptomic studies from RTT human and mouse samples have yielded a number of proteins that are dysregulated in RTT and could be involved in the pathophysiology of the disease (*15*, *121–125*). To date, the most studied protein linked to MeCP2 is the brain-derived neurotrophic factor (BDNF) due to early reports illustrating that MeCP2 directly binds to the *Bdnf* gene to regulate its transcription and that *Mecp2 null* mice exhibit decreased levels of Bdnf (*8*, *126–128*). These molecular findings have led to *in vivo* preclinical studies showing the beneficial effects of modulating BDNF levels and activity in *Mecp2 mutant* mice, including genetic BDNF overexpression, pharmacological stimulation of neuronal activity to indirectly increase BDNF levels, and activation of the BDNF receptor tropomyosin receptor kinase B (Trkb) (*127–130*).

With the poor ability of BNDF in crossing the blood brain barrier (BBB), another growth factor of interest is insulin-like growth factor 1 (IGF-1). IGF-1 has the capacity to cross the BBB and plays a role in enhancing synaptic neurotransmission (*131*, *132*). Thus, several forms of IGF-1 peptides have been investigated in *Mecp2 mutant* mice and shown efficacy in correcting abnormal neuronal and synaptic architecture and plasticity as well as behavioral phenotypes such as in extending survival and reversing deficits in locomotor activity and respiratory function (*133*, *134*).

One report, however, raised caution in IGF-1 treatments with the findings that high doses of full-length IGF-1 worsened neurological and metabolic phenotypes in *Mecp2 null* mice, suggesting that a narrow therapeutic exists with this strategy (*135*). Nonetheless, these studies demonstrate that BDNF and IGF are attractive therapeutic targets as well as implicate normalization of reduced or altered neuronal activity as a treatment option.

Several studies have already explored this treatment option in regards to synaptic neurotransmission and plasticity with focus on neurotransmitter systems. Concerning the maintenance of the excitatory and inhibitory balance by the glutamatergic and γ-Aminobutyric acid (GABA)-ergic systems, reports have demonstrated the efficacy of targeting the glutamate receptors, ionotropic glutamate receptor N-methyl-D-aspartate (NMDA) and metabotropic glutamate receptor (mGlu, discussed in detail below), which are both reduced in RTT human and/or mouse samples (*67*, *68*, *124*, *136*, *137*). NMDA receptor inhibition with memantine or ketamine restored synaptic function and plasticity in *Mecp2 null* mice, specifically forebrain hypofunction and LTP at the Schaffer collateral (SC)-CA1 synapse in the hippocampus (*138*–*140*). Moreover, acute or chronic treatment of low-dose ketamine reversed or delayed behavioral deficits, in particular stereotypic behavior and abnormal sensorimotor gating and breathing in *Mecp2 null* animals (*139*, *140*). Parallel investigations that increase the activity of several subtypes of the mGlu receptors also reversed impaired SC-CA1 LTP and long-term depression (LTD) and various phenotypic domains encompassing motor, social, cognitive and respiratory function of *Mecp2 null* mice (*124*, *136*, *137*). Another neurotransmitter system of interest involve the monoamine neurotransmitters given evidence of monoamine reduction in RTT human and mice (*77*, *141*, *142*). Studies that pharmacologically manipulate monoamine transporters, including inhibition of norepinephrine reuptake by desipramine, noradrenergic and serotonergic receptors by mirtazapine, and serotonergic and dopaminergic receptors by sarizotan restored normal respiratory function in *Mecp2 mutant* animals (*143*–*146*).

These preclinical evaluations of possible therapeutic targets for RTT have translated to clinical investigations. Some studies demonstrated safety and efficacy in RTT patients, while others reported the development of adverse side effects and/or showed no improvements in symptoms (*46*, *147*, *148*). In a Phase I clinical trial, glatiramer acetate, which enhances BDNF levels, unfortunately caused severe adverse events with RTT patients developing apneas and seizures, leading to early termination of the trial (*149*). A similar compound, Fingolimod that has shown efficacy in multiple sclerosis patients was used in RTT patients, where it was deemed safe yet lacking efficacy (*150*). Two promising candidates in the area of growth factors with safe profiles are the recombinant human IGF-1 (rhIGF-1) mecasermin and IGF-1 tripeptide analog trofinetide (*151–153*). Phase II trials indicated that rhIGF-1 treatment did not improve RTT symptoms, whereas trofinetide significantly did at the highest dose, which has prompted a Phase 3 clinical trial by Acadia Pharmaceuticals (ClinicalTrials.gov, number NCT04181723) (*152–155*).

Targeting the monoaminergic neurotransmitter systems, two drugs, sarizotan and desipramine, have been evaluated in RTT patients for correction of breathing abnormalities. Unfortunately, the clinical trial using sarizotan was terminated early due to lack of efficacy (ClinicalTrials.gov, number NCT02790034). Desipramine treatment also did not significantly improve breathing function, although it was noted that a positive correlation existed between desipramine levels and improvement of apneas and hypopneas (e.g. shallow breathing), warranting further studies targeting the noradrenergic pathway (*156*). Drugs that target the glutamate neurotransmitter system, including dextromethorphan and ketamine, which are both NMDA receptor antagonists appear to be more favorable. The initial trial with dextromethorphan lacked a placebo control and did not affect the primary endpoint of EEG spike activity, but showed efficacy in reducing seizure frequency and hyperactivity and improving cognitive behavior (*157*). This study is promising given that ketamine is currently being investigated in RTT patients (ClinicalTrials.gov, number

NCT03633058). Overall, several candidates show potential in alleviating clinical phenotypes in RTT, and these studies have enhanced our understanding of the disease.

1.1.3 *MECP2* Duplication syndrome (MDS)

MDS is a much rarer neurodevelopmental disorder than RTT accounting for approximately 1 in 100,000 live births of males and 1-2% of intellectual disability in males (*158*, *159*). Contrary to RTT, MDS is associated with increased expression of MeCP2 due to either duplication or triplication of the *MECP2* gene (*160*). Moreover, MDS is of maternal origin and the majority of the cases are inherited; due to its X chromosome location, more than 90% of symptomatic MDS patients are males (*160*). Females are also affected, presenting with neuropsychiatric symptoms such as anxiety and depression (*161*). However, due to favorable XCI skewing (near 100%), severity especially relating to intellectual disability is comparably reduced in female patients (*161*–*163*). Male MDS patients exhibit infantile hypotonia, developmental delay that spans motor, cognitive and social abilities, and seizures, which are analogous to RTT and other ASDs (*21*, *160*). Interestingly, MDS patients also undergo developmental regression similar to RTT, with the average age of onset between 3-5 years old (*164*). Recent studies have demonstrated that this regression mostly encompasses loss of functional skills, such as motor and communication skills, and is also associated with the likelihood and onset of epilepsy (*164*–*166*). Furthermore, clinical severity is positively correlated with age and size of the Xq28 duplication (*166*, *167*).

1.1.3.1 Mouse models of MDS

The clinical phenotypes of MDS are recapitulated in mouse models that overexpress MeCP2 (*101*, *105*, *108*, *168*). Luikenhuis *et. al.* described that a *Tau-Mecp2* transgene expression in wild-type mice caused a 4-6 fold increase in MeCP2 expression and led to abnormal phenotypes that were restricted to animals with homozygous expression of the transgene (*101*). In particular, these mice overexpress MeCP2 only in neurons and displayed reduced body weight and motor

abnormalities such as ataxic gait, which was also later observed in mice overexpressing MeCP2 in forebrain neurons (*107*). These detrimental effects, including decreased survival, were also reported in a more recent study (*94*). A subsequent paper characterized the behavior of the *Tau-Mecp2* animals, which presented with impaired motor coordination, enhanced cued and contextual fear conditioning, impaired fear extinction learning and a recognition memory deficit (*168*). In association with the learning phenotypes, hippocampal synaptic plasticity was also altered, with heightened short-term plasticity in the form of paired-pulse facilitation (PPF) and attenuated LTP. These studies demonstrate that, similar to RTT, neuronal alteration of MeCP2 is sufficient to cause abnormal phenotypes.

To mimic the widespread overexpression of MeCP2 in humans, a human *MECP2* transgene was ubiquitously expressed in WT mice (*105*). In agreement with the *Tau-Mecp2* mice, animals with MeCP2 overexpression exhibited progressive neurological abnormalities such as forepaw clasping, kyphosis and hypoactivity, and the onset of phenotypes was correlated to MeCP2 levels, with mice expressing a 3-fold increase presenting increase severity earlier until mortality at 3 weeks of age. In addition, mice with a 1-fold increase in MeCP2 ($MECP2^{Tg1}$) survived at least to 20 weeks, at which phenotypes began to manifest, including reduced anxiety, aggressiveness and increased frequency of seizures and EEG spikes. These phenotypes were also observed in related mouse models of two different genetic strains that overexpressed mouse *Mecp2* fused to the enhanced green fluorescent protein (EGFP) (*108*, *169*). Interestingly, the delayed onset of phenotypes appeared to be correlated to alterations in dendritic complexity, which was increased in young mice, and spine density, which decreased in adult mice (*169*, *170*).

$MECP2^{Tg1}$ animals also displayed abnormal enhancement in motor learning and contextual and cued fear conditioning, as well as increased PPF and LTP. These latter phenotypes mostly conflict with the behavior observed in *Tau-Mecp2* mice, which could be explained by differences in animal

genetic strain and age, in the use of mouse versus human MeCP2, and in the ubiquitous versus cell-type specific overexpression of MeCP2. The effects of strain difference are somewhat reconciled, as *MECP2*^{Tg1} animals of mixed F1 hybrid genetic strain also exhibit enhanced motor learning and LTP, although again these mice overexpress human MeCP2 (*171*). Moreover, F1 hybrid MeCP2-overexpressing mice display heightened anxiety, deficiencies in sociability and social recognition, and hypoactivity, the latter of which is conserved in all MDS mice regardless of genetic background, species-origin of MeCP2 and localization of MeCP2 overexpression (*171*, *172*). Despite the discrepancies, these studies demonstrate the detrimental morphological, synaptic physiological and behavioral effects of MeCP2 overexpression in preclinical models, providing evidence that MeCP2 dosage is critical.

1.1.3.2 Therapeutic discovery and development for MDS

The availability and validity of MDS mouse models provide opportunities to evaluate treatment strategies similar to those conducted with RTT animals. Although the studies are sparse, emerging reports excitingly show that MDS phenotypes are reversible in mice with genetic manipulation of MeCP2 expression (*82*, *94*, *171*) or modulation of MeCP2- and/or MDS-associated targets (*172*, *173*). The efficacy of increasing MeCP2 levels in RTT mice postulates the feasibility of the converse scenario of normalizing MeCP2 to WT levels in MDS mice. Such an approach was first genetically conducted in conditional MDS mice that expressed a human *MECP2* allele in addition to the endogenous conditional mouse *Mecp2* allele (*171*). Removal of the endogenous *Mecp2* allele using an inducible Cre-lox system reduced total MeCP2 levels in MDS mice and reversed an array of abnormal phenotypes, including deficits in locomotor activity and social behavior, and heightened anxiety, motor learning and LTP. A similar, more translatable strategy employed antisense oligonucleotides (ASOs), which bind the precursor mRNA of human *MECP2* and reduce MeCP2 expression (*171*). Again, behavioral efficacy, including reduction of EEG spikes and seizures, was observed with ASO treatment, which is posited to be correlated to

the reversal of pathogenic molecular changes as interrogated with hippocampal-specific transcriptomic studies.

A related approach to mitigate MeCP2 expression is to introduce mutant MeCP2 in MDS mice. One study, reported in the context of treating RTT, genetically supplemented WT mice with a mouse *Mecp2* transgene bearing the MBD-mutation T158M (*82*). Despite a 1-fold increase in total MeCP2, mice with the *Mecp2*^{T158M} transgene displayed normal behavior compared to WT animals, regardless of sex. A similar study was recently conducted wherein overexpression of the mutant MeCP2 was restricted to neuronal cells using the Tau promoter (*94*). In agreement with the latter study, male WT mice overexpressing *Tau-Mecp2*^{T158M} did not exhibit overt phenotypes apart from a progressively worsening hindlimb clasping phenotype that manifested at 10 weeks of age. Interestingly, overexpression of another MBD mutation, R133C, in WT animals decreased body weight and exacerbated hindlimb clasping starting at 6 weeks old. These effects of *Tau-Mecp2*^{R133C} overexpression are thought to be due to the retention of DNA binding ability with the MeCP2 R133C mutant protein; this is supported by the similar increase in total MeCP2 levels between *Tau-Mecp2*^{R133C} and heterozygous *Tau-Mecp2* animals, which did not exhibit any abnormal phenotypes. Moreover, the increase in stereotypic behavior appeared to be restricted to overexpression of MBD mutants, as a *Tau* transgene expressing the NID-mutation R306C resulted in similar phenotypes to WT littermates despite a 4-fold increase in total MeCP2, a level that caused early mortality in homozygous *Tau-Mecp2* mice. These studies suggest that disrupting MeCP2 function, but not necessarily expression, is sufficient to alleviate MDS-related phenotypes. Moreover, NID dysfunction in MeCP2 is preferred over diminished DNA binding capability in achieving these beneficial effects for MDS.

The previous report presented an intriguing possibility that MDS phenotypes could be reversed by inhibiting the interaction of MeCP2 with NCOR complexes using small molecules. Although

this has not yet been investigated, it parallels other perspectives in using small molecules to modulate MeCP2- or MDS-related proteins. In particular, one study demonstrated that chronic treatment with the $GABA_A$ receptor antagonist picrotoxin (PTX) in *Tau-Mecp2* animals improved recognition memory, motor learning and synaptic plasticity features of PPF and LTP (*173*). These results, along with studies implicating GABAergic pathways in MDS and other ASDs (*72*, *174*), suggest that inhibition of $GABA_A$ receptors is a promising therapeutic strategy. It is important to note that PTX treatment did not amend all phenotypes in MDS mice, including associative learning in either cued or contextual fear conditioning and increased anxiety. Interestingly, a potential therapeutic strategy to modulate anxiety could be to target the corticotropin-releasing hormone (CRH) signaling pathway. A recent paper from Huda Zoghbi's lab showed that *Crh* is upregulated in MDS mice and genetic knockdown of *Crh* ameliorated the heightened anxiety phenotype of MDS mice (*172*). This group also reported that genetic attenuation of another upregulated gene in MDS, *Oprm1*, which encodes for the G protein–coupled μ-opioid receptor MOR, reversed sociability and social recognition memory in MDS mice. Overall, these studies provide potential therapeutic targets to alleviate MDS phenotypes.

1.1.4 Pitt-Hopkins syndrome (PTHS)

The prevalence of PTHS is estimated to be even lower than MDS, with a diagnosis rate of 1 in 225,000 to 300,000 individuals, despite similarly affecting males and females (*175*). This could be confounded by the challenge of differential diagnosing PTHS from RTT and Angelman syndrome (AS) given the overwhelmingly similar clinical presentation between these neurodevelopmental disorders. Indeed, these overlapping clinical features, including motor and cognitive dysfunction, breathing abnormalities and seizures (*175*–*182*), have historically led clinicians to diagnose PTHS patients with RTT, thereby characterizing PTHS as atypical RTT. However, PTHS lacks some core symptoms of RTT, especially developmental regression (*45*) and patients exhibit distinct physical characteristics such as a wide mouth, which was first

observed by Australian physicians David Pitt and Ian Hopkins in two unrelated patients (*183*). In an effort to assist accurate identification of PTHS patients, an international consensus of clinical diagnostic criteria was recently developed (*175*). This score-based system relies heavily on distinctive facial features and, if needed, it can be followed with molecular/genetic diagnosis to screen for mutations in the *Transcription Factor 4* (*TCF4*) gene. Therefore, although so far *TCF4* is the only identified causative gene for PTHS, PTHS patients may be clinically diagnosed with the disorder but may not have pathological mutations in *TCF4*.

4.2.1.1 Transcription Factor 4 (TCF4): Isoforms and molecular functions

The human *TCF4* gene is expressed from chromosome 18 and encodes for the class I basic helix-loop-helix (bHLH) transcription factor TCF4, which has also been known as E2-2, immunoglobulin transcription factor 2 (ITF2), or SL3-3 enhancer factor 2 (SEF2) (*184*). These different names were derived from the ability of TCF4 to bind the promoters and enhancers of different genes, e.g. immunoglobins and the SL3-3 gene of murine leukemia virus through Ephrussi boxes (E-box), which express the consensus sequence CACCTG. The C-terminal bHLH domain (exon 18) (Figure 3) also facilitates TCF4's capacity to form homodimers or heterodimers with other HLH proteins (*185*). In particular, heterodimerization with inhibitors of DNA binding (Id) proteins, specifically ID2, prevent the ability of TCF4 to bind DNA (*186*–*188*). A similar DNA binding inhibition mechanism involves binding of the Ca^{2+} sensor calmodulin to TCF4's bHLH domain (*189*). Additionally, TCF4 can heterodimerize with class II bHLH proteins, which are tissue-specific and require heterodimerization with other HLH proteins (*190*). These include the proneural proteins ATOH and ASCL1/MASH1 and the oligodendrocyte (OL) protein OLIG2, which are all important in neuronal and OL differentiation and specification (*191*–*195*). TCF4's ability to dimerize and regulate transcription is impacted by the N-terminal domains, NLS and activation domains AD1 and AD2 (Figure 3) (*196*). Without the NLS domain, TCF4 must rely on heterodimerizing with other HLH proteins to translocate to the nucleus. Additionally, the AD1 and

AD2 domains modulate the transcriptional activity of TCF4 through recruitment of co-activators and co-repressors. For example, TCF4 can promote transcription through AD1's activity in recruiting the Spt–Ada–Gcn5 acetyltransferase (SAGA) histone complex or CREB binding protein (CBP) (*197*, *198*). In the same manner, AD2 binds to the histone deacetylase (HDAC) complexes to inhibit transcription (*199*).

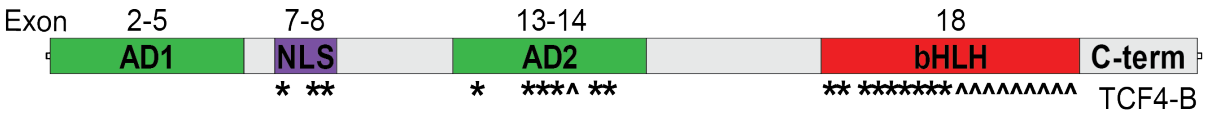

Figure 3: TCF4 protein and PTHS-associated mutations. Illustration of key domains in TCF4 protein, isoform B, and variants leading to PTHS are noted (excluding intragenic deletions and frameshift variants) based on (*175*). Activation domain (AD1, AD2), nuclear localization signal (NLS), basic helix-loop-helix domain (bHLH), C-terminus (C-term), *truncation mutations, ^missense mutations.

The functions of TCF4 also depend on the expression of various protein isoforms. Sepp *et. al.* identified that the gene, consisting of 21 exons, leads to 18 N-terminally distinct proteins and additional isoforms due to alternative splicing (*196*). Interestingly, all isoforms include the AD2 and bHLH domains; thus, function of the majority of the N-terminal variants is dependent on the presence and activity of the AD1 domain. Despite the characterization of these isoforms, only two TCF4 proteins have been extensively studied, correspondingly named TCF4-A and TCF4-B. TCF4-A lacks a large portion of the N-terminus and is missing domains AD1 and NLS, which reduces the ability of this isoform to activate transcription and localize to the nucleus (*196*, *200*). On the other hand, TCF4-B is a longer protein, containing all major functional domains. Interestingly, TCF4-B with both activation domains exhibits increased *in vitro* transcriptional activity compared to a construct lacking one activation domain as well as to TCF4-A, suggesting a synergistic effect of these two regulatory domains (*196*).

TCF4 is a ubiquitously expressed gene and protein with high expression in the CNS (*196*, *201–204*). However, several studies have shown that mRNA and protein expression is dependent on transcript variants or protein isoforms, age and tissue (*196*, *201*). Interestingly, although longer transcripts and higher molecular weight isoforms are detected, shorter variants and smaller isoforms are more prominent in peripheral and CNS tissues (*196*). In the CNS, TCF4 is expressed embryonically and in the fetal brain, consistent with the role of TCF4 in brain development (*196*, *201*, *204*). Moreover, TCF4 is highly expressed in the cerebellum, cortex and subcortical regions such as the hippocampus, and is conserved in tissues of adult human, non-human primates and mice (*196*, *202–204*). It is important to note that TCF4 levels in CNS tissues likely reduce with age, although this is confounded by the lack of sensitivity of antibodies and the numerous isoforms. A recent study utilized a GFP reporter to track TCF4, and indeed demonstrated that TCF4 maintains high expression only in the cerebellum throughout age (*204*). The authors also characterized TCF4 distribution in specific cell types within brain regions and discovered that, consistent with the proneural and OL-specific heterodimerization partners of TCF4, inhibitory and excitatory neurons as well as glial cells express TCF4.

4.2.1.2 TCF4 mutations: Impact on function and severity

The link between *TCF4* haploinsufficiency and PTHS was not discovered until 2007 when independent studies associated *de novo* LOF or dominant-negative mutations in TCF4 and translocations or deletions in chromosome 18 with symptoms of facial dysmorphism, intellectual disability, breathing abnormalities and seizures (*205–207*). Functional studies have shown that pathological mutations impair protein stability, DNA binding ability and/or dimerization capability, thus altering transcriptional activity (*201*, *206*, *208*). However, as Sepp *et. al.* comprehensively described, the degree of functional loss varies and is dependent on the domain site of the mutation or encoded transcripts (*208*).

Intragenic deletions or translocations that lead to the abolishment of exons 10-21, which include the AD2 and bHLH domains, do not produce any functional transcripts, thereby causing severe phenotypes. This severity is also the case with indel or nonsense mutations that cause premature stop codons and result in loss of the bHLH region. The importance of the bHLH domain is further exemplified with missense mutations, which encompass the majority of the pathological TCF4 mutations (~20%) and are clustered in the bHLH domain (*178*, *209*). These missense mutations mostly affect arginine residues and impair DNA binding or destabilize TCF4, but interestingly, do not impact heterodimerization. The intact heterodimerization capacity can reverse the DNA-binding and transactivation deficits of mutant TCF4. Conversely, mutant TCF4 can be dominant-negative and inhibit the DNA-binding ability and transcription activity of its dimer pair, whether that is the WT TCF4 or another HLH protein (*208*).

These functional effects of pathological TCF4 variants translate to the disease presentation and severity of symptoms. One study confirmed the latter observation that core features of PTHS manifested with bHLH disruption (*209*). Another report described that missense mutations, likely within the bHLH, were correlated with increased seizure frequency as well as breathing abnormalities, which have been observed to be more prevalent with and preceding epilepsy (*201*, *210*). On the other hand, the preservation of the C-terminal domains, such as AD2 and bHLH, led to only mild intellectual disability or PTHS-like phenotypes (*209*, *211*).

4.2.1.3 Tcf4 mutant mouse models

The most frequent mouse model to study PTHS and the functions of TCF4 is the *Tcf4* haploinsufficient mouse, $Tcf4^{+/-}$, which was first developed in the late 1990s to investigate the role of TCF4 in B-lymphocytes (*185*). Several additional mouse models have since been generated, including two that incorporated pathogenic variants within the bHLH (*212–214*). One of these mice expressed a truncated Tcf4 protein, $Tcf4^{+/tr}$, to model dominant-negative function, while the other

bore CNS-specific *Tcf4* haploinsufficiency. In the former models, one mouse expresses the most prevalent pathogenic TCF4 mutation, R580W (R579W in mouse, $Tcf4^{R579W}$), and the other model has three arginine residues deleted, $Tcf4^{\Delta 574-579}$. With the exception of $Tcf4^{+/tr}$, these mice have been behaviorally characterized to phenocopy PTHS clinical symptoms including deficits in motor coordination and associative and spatial learning and memory, breathing abnormalities with increased hyperventilation frequency, and autistic-like behaviors of altered anxiety and sociability (*212*, *215*, *216*). Interestingly, these *Tcf4 mutant* mice also displayed enhanced LTP at the hippocampal SC-CA1 synapse. Subsequent work with *Tcf4* heterozygous and $Tcf4^{R579W}$ animals showed that the heightened LTP is due to NMDA receptor hyperfunction, which could be due to changes in NMDA receptor subunit composition as NMDA receptor-mediated currents in CA1 neurons of $Tcf4^{R579W}$ mice were sensitive to an antagonist selective for the NR2B subunit (*212*).

One main phenotypic difference is the altered acoustic startle response (ASR) and sensorimotor gating, in which Kennedy *et. al.* observed an enhanced response to the auditory stimulus but an attenuated pre-pulse inhibition (PPI) phenotype in $Tcf4^{+/-}$ mice, whereas Thaxton *et. al.* detected the opposite behavior. These conflicting results could be due to differences in age as younger *Tcf4* heterozygous and $Tcf4^{R579W}$ animals exhibited a similar pattern as $Tcf4^{+/-}$ mice with reduced sensorimotor gating. Nonetheless, the abnormal sensorimotor gating phenotype is consistent with the association of TCF4 variants in neuropsychiatric diseases such as schizophrenia, wherein patients have sensorimotor gating dysfunction (*217*–*219*).

Intriguingly, several phenotypes observed in the *Tcf4 mutant* mice modeling haploinsufficiency (e.g., $Tcf4^{+/-}$) or dominant-negative function ($Tcf4^{+/tr}$) are also seen in mice overexpressing Tcf4 in the CNS (*220*, *221*). These shared phenotypes include deficits in associative learning and memory and sensorimotor gating and NMDA receptor hyperfunction. Additionally, Tcf4 overexpression during brain development disrupted the organization of pyramidal cells in the

medial prefrontal cortex (mPFC), which is thought to be mediated by the activity of Tcf4 to transcriptionally activate genes involved in neuronal development (*221*). Overall, these studies highlight that, similar to the critical regulation of MeCP2 levels to maintain normal CNS function, control of TCF4 dosage is also important.

4.2.1.4 Therapeutic discovery for PTHS

The development of the aforementioned PTHS mouse models has provided tools to discover potential treatment strategies for PTHS. The numerous isoforms of TCF4 and detrimental effects of protein overexpression in mice present a challenge for TCF4-targeted gene therapy. However, a manuscript in preprint recently showed that embryonically and ubiquitously normalizing Tcf4 levels corrected behavioral deficits in *Tcf4* haploinsufficient mice, $Tcf4^{STOP/y}$, such as hyperactivity, deficits in spatial learning and memory, and heightened anxiety (*222*). Moreover, to mimic a potential viral-mediated gene therapy approach in the clinic, Cre-expressing AAV was delivered through intracerebroventricular (ICV) injection in neonatal mice. Such approach increased the *Tcf4* transcripts containing exon 10 (bHLH domain) and also reversed the behavioral abnormalities described above in addition to partial rescue of aberrant EEG characteristics. Interestingly, Tcf4 increase in specific neuronal populations only reversed some phenotypes, which could have implications in other treatment strategies that target other proteins or pathways. Nonetheless, this study demonstrates, for the first time that *in vivo Tcf4* normalization exerts beneficial effects in PTHS model mice.

To circumvent the potential challenges of TCF4-mediated gene therapy, modulation of proteins or pathways that contribute to the pathophysiology of PTHS could be an alternative route of intervention. One approach is to target transcriptional dysregulation caused by TCF4 functional loss as explored in a study that utilized the HDAC inhibitor, suberoylanilide hydroxamic acid (SAHA), which is currently approved for the treatment of T-cell lymphoma (*215*). SAHA corrected

behavioral cognitive deficits and normalized the enhanced LTP phenotype in *Tcf4*$^{+/-}$ animals. Similar behavioral reversal was observed with ICV administration of HDAC2-specific ASOs to reduce *Hdac2* levels. These results suggest that perhaps targeting HDAC activity could be beneficial for PTHS.

The previous study also reported that HDAC inhibition increased expression of the *Grin2a* gene, which expresses the NR2A subunit of the NMDA receptor, but not the *Grin2b* gene that encodes for the NR2B subunit (*215*). This finding is exciting in that a previous study demonstrated NMDA hyperfunction, possibly due to an increase in the NR2B subunit, as the basis for enhanced LTP phenotype in *Tcf4 mutant* animals (*212*). Moreover, the shift in NMDA receptor subunit towards NR2A has also been observed in RTT mice and genetic reduction and NMDA receptor antagonism with ketamine exerts beneficial effects in correcting RTT-like phenotypes (*139*, *223*–*225*). Given the overlapping clinical and preclinical phenotypes of RTT and PTHS, it is hypothesized that there is rationale to determine the effects of ketamine, which is currently under clinical investigation for RTT (ClinicalTrials.gov, number NCT03633058), in PTHS. Analogously, as described further below, another family of glutamate receptors, the metabotropic glutamate receptors (mGlu) are also implicated in synaptic transmission, which positions them as possible therapeutic targets for PTHS and other *MECP2*-related neurodevelopmental disorders.

1.2 Metabotropic Glutamate Receptors (mGlu)

The metabotropic glutamate (mGlu) and ionotropic glutamate (iGlu) receptors are both expressed throughout the CNS and bind to the neurotransmitter glutamate to regulate neurotransmission. Both receptor families work together in the CNS as comprehensively reviewed in (*226*). However, mGlu receptors are unique from iGlu receptors, which are ligand-gated ion channels, in that they are G-protein coupled receptors (GPCRs) that modulate excitatory transmission through their coupling with effector systems via guanosine-5'-triphosphate (GTP)-binding proteins. The eight

mGlu receptors ($mGlu_1$ – $mGlu_8$) are classified into three subgroups (Group I – III) depending on sequence homology, pharmacology and function (*227*). In short and generally, post-synaptically expressed Group I mGlu receptors ($mGlu_1$ and $mGlu_5$) mostly couple to G_q proteins to activate phospholipase C (PLC), resulting in calcium mobilization. $mGlu_2$ and $mGlu_3$ receptors are in the Group II subgroup, $G_{i/o}$-coupled, leading to inhibition of adenylyl cyclase (AC) activity, and enriched in both pre- and post-synapses of neurons. Group II mGlu receptors ($mGlu_4$, $mGlu_6$, $mGlu_7$ and $mGlu_8$) also modulate AC activity via $G_{i/o}$ proteins but are predominantly localized in pre-synaptic terminals.

All mGlu receptors resemble other family C GPCRs and are distinct from other GPCRs by the presence of a large, N-terminus extracellular domain (ECD) in addition to the conserved regions of the cysteine-rich domain (CRD), seven-helix transmembrane domain (TMD) and intracellular C-terminus tail (CTD) (Figure 4). The large ECD is also known as the Venus flytrap domain (VFD) or ligand-binding domain as it serves as the orthosteric binding site of ligands including the endogenous ligand glutamate. The region of binding for allosteric modulators is the TMD, which allows for subtype selectivity. Allosteric modulators have the capacity to alter the binding and/or activity of an orthosteric ligand. As illustrated in (*227*), positive allosteric modulators (PAM) enhance the function of the receptor, whereas negative allosteric modulators (NAM) inhibit the receptor. One of the first studies to characterize the activity and binding of a PAM for mGlu receptors utilized chimeric receptors and mutagenesis to identify TMD-specific binding regions of $mGlu_1$-selective compounds, and to illustrate the effect of the PAMs in increasing the affinity of an agonist for the $mGlu_1$ receptors and in enhancing the potency of these receptors (*228*). Since then, several reports have utilized similar approaches to map TMD-specific binding regions of PAMs and NAMs, including compounds that are selective for $mGlu_2$ (*229*, *230*).

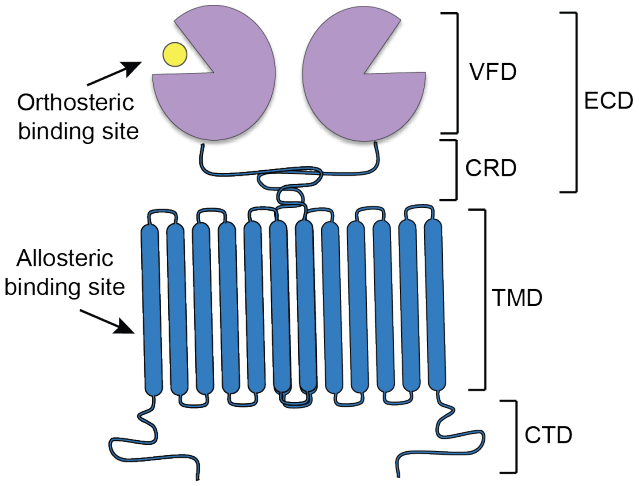

Figure 4: Schematic of the mGlu receptor. Domains of the mGlu receptor are illustrated along with the orthosteric and allosteric binding sites of ligands. mGlu receptors are constitutive dimers and only one promoter is shown. Extracellular domain (ECD), Venus flytrap domain (VFD), cysteine-rich domain (CRD), transmembrane domain (TMD), c-terminus domain (CTD), ligand e.g. glutamate (yellow circle).

mGlu receptors are obligate dimers, with dimerization occurring at several interfaces within the receptor (*231*). Structural and biochemical studies have shown that mGlu receptors form covalently linkages through cysteine residues within the extracellular CRD (*232*–*234*). Additional functional analyses later showed that ligand binding in a cleft between the two VFD lobes of the monomer induces conformational changes that determine the degree of activity (*233*–*235*). In particular, the VFD, normally at the resting form ("open-open"), achieves an active state upon ligand binding and closure of both lobes. The active state can either be "closed-open" or "closed-closed" depending on whether one or two ligands are bound and leading to partial or full receptor activity, respectively. Moreover, the conformational changes at the ligand interface cause rearrangement of more C-terminal regions such as the TMD via the CRD, and the TMD from each monomer directly associates, a phenomena that does not happen at the resting state (*234*, *236*). Interestingly, a recent report highlighted that, at least in the case of $mGlu_2$, glutamate binding only leads to partial activation and a PAM or $G_{i/o}$ protein is needed for full activation (*237*).

These reports have not only shown homodimerization but also heterodimerization within the mGlu receptor subtypes and other GPCRs (*231*, *238*). For example, the existence of $mGlu_{2/3}$ and $mGlu_{2/4}$ heterodimers have been found *in vitro* and *in vivo* (*238–241*). Studies on the functional consequences of mGlu receptor heterodimerization are still minimal but emerging, including a recent study describing that $mGlu_{2/4}$ receptors differentially regulate synaptic transmission in the mPFC (*242*). Thus, the discovery and functional characterization of these mGlu receptor heterodimer populations in native tissues are crucial as they could have potential implications for the development of treatments for CNS disorders.

1.2.1 Group II mGlu receptors: Expression, signaling, and regulation

The $mGlu_2$ and $mGlu_3$ receptor subtypes make up the Group II mGlu receptor group and are encoded by the *GRM2* and *GRM3* genes, respectively. Early characterization of these receptors illustrated high sequence homology (~70%) (*243–245*). This has presented a challenge in the development of pharmacological (e.g., subtype-selective orthosteric ligands and allosteric modulators) and biochemical (e.g., antibodies) tools. Nonetheless, several pharmacological tools are available (most common are listed in Table 3), which has allowed the interrogation on the role of $mGlu_2$ and $mGlu_3$ receptors in CNS disorders as further outlined below.

Group II mGlu receptors are highly expressed in the CNS, with $mGlu_3$ receptors more widely distributed compared to $mGlu_2$. Both have high levels in the cortex, hippocampus and striatum, although this is thought to be developmentally regulated as $mGlu_2$ levels increase after birth, and the opposite is true for $mGlu_3$ (*246*, *247*). Within the hippocampus, $mGlu_2$ is localized within the terminals of mossy fibers and the perforant path, whereas $mGlu_3$ is primarily expressed in the CA1 (*246*, *248*, *249*). Thus, $mGlu_2$ is characterized as a pre-synaptic receptor, whereas $mGlu_3$ is found primarily in post-synaptic neurons as well as in glia. Moreover, group II mGlu receptors are located in extra-synaptic sites of terminals with $mGlu_3$ receptors at peri-synaptic sites or locations

near the post-synaptic density (PSD) (*246*). At these extra-synaptic sites, $mGlu_{2/3}$ receptors are thought to be activated by excess glutamate release.

The differences in synaptic localization between the group II mGlu receptors have implications in their physiological functions. As highlighted shortly above, $mGlu_2$ and $mGlu_3$ predominantly couple to $G_{i/o}$ proteins. Through this coupling, $mGlu_{2/3}$ receptors mediate signaling pathways associated with AC, specifically inhibiting the enzyme and decrease cyclic-AMP (cAMP) production. Through the βγ subunit, these receptors can also indirectly modulate the activity of other proteins such as the G-protein-gated inwardly rectifying potassium channels (GIRK) and the extracellular signal-regulated kinase 1/2 (ERK1/2) proteins that are part of the mitogen-activated protein kinase (MAPK) family (*250*).

The activity of $mGlu_{2/3}$ receptors is regulated by their direct interactions with other proteins, which have been identified throughout the years (*250*–*256*). Many of these proteins are PSD-95/Discs-large/ZO1 (PDZ) scaffold proteins, including protein interacting with protein kinase C (PICK), glutamate receptor-interacting protein (GRIP), syntenin and the Na^+/H^+ exchanger regulatory factors 1 and 2 (NHERF) proteins, which bind to a motif in the CTD of these receptors (*253*, *256*). These scaffold proteins are thought to regulate the localization of $mGlu_{2/3}$ receptors, while other proteins modulate their signaling. In particular, protein kinase A (PKA) has been shown to phosphorylate $mGlu_2$ and $mGlu_3$ at a conserved serine residue in the CTD, which prevents G-protein coupling, thereby inhibiting the function of these receptors at pre-synaptic terminals (*251*, *252*). It was later shown that the PKA-mediated phosphorylation of $mGlu_3$, but not $mGlu_2$, can be dephosphorylated by protein phosphatase 2Cα (PP2Cα) (*254*). Another distinct regulation between the group II mGlu receptors is their sensitivity to GPCR kinases (GRKs) and β-arrestins. Again, $mGlu_3$ but not $mGlu_2$, was desensitized by GRK2 and GRK3 and internalized by β-arrestins upon agonist or glutamate binding due to a unique CTD sequence in $mGlu_3$ (*250*, *257*).

The functional consequences of these diverse regulation mechanisms are further complicated by the presence of splice variants. To date, additional isoforms have not been identified for $mGlu_2$. However, in addition to the full-length protein, $mGlu_3$ has four splice variants, stemming from intragenic deletions within the six exons. These variants, GRM3Δ2, GRM3Δ4, and GRM3Δ2Δ3, are due to deletions in exons 2, 4, and 2 and 3, respectively (*258*). Deletion of exon 2 removes the transcription start site, precluding the formation of a protein. GRM3Δ4, on the other hand, encodes a truncated protein that lacks the TMD and expresses a novel C-terminal tail. The retention of GRM3Δ4 in the membrane and expression in the human brain suggests it could have functional consequences, including heterodimerization with full-length $mGlu_3$ to exert a dominant-negative effect; this latter effect has recently been reported (*259*). Additionally, a report suggested that the expression of the GRM3Δ4 variant may be altered in neuropsychiatric patients with single nucleotide polymorphisms (SNPs) that confer risk for disease (*260*).

1.2.2 $mGlu_{2/3}$ receptors and synaptic plasticity

Elucidation of synaptic localization and cellular expression has allowed for the characterization of the distinct roles of group II mGlu receptors in modulating synaptic transmission. The predominant presence of $mGlu_2$ receptors at pre-synaptic terminals suggests that it is generally involved in inhibition of neurotransmitter release at excitatory synapses. $mGlu_2$ receptors have been primarily linked to the induction of LTD, especially at the mossy fiber-CA3 and perforant path synapses projecting to the dentate gyrus, CA1 and CA3 of the hippocampus (*261*, *262*). Recent studies have shown that $mGlu_2$'s role in dampening excitatory transmission is not limited to the hippocampus as it also induces LTD in excitatory synapses in the basal ganglia and PFC, thus implicating the receptor in disorders such as Parkinson's disease and depression, respectively (*263*, *264*). Specifically, use of the orthosteric agonist LY379268 caused LTD that was not observed in $mGlu_2$ knockout animals (*263*), and antagonism using the subtype selective NAM VU6001966 inhibited LTD at thalamic-PFC synapses (*264*). The latter study on LTD in the PFC

has been observed previously using the $mGlu_2$ PAM BINA, wherein $mGlu_2$ activation blocked increased post-synaptic currents (*265*).

On the other hand, $mGlu_3$ receptors at the post-synaptic terminals modulate neuronal excitability and have been mostly linked to LTP induction. A recent study showed that the orthosteric agonist LY354740 led to an enhancement of SC-CA1 LTP (*266*), and a subsequent report confirmed that the effects of LY379268 were blocked in the presence of the $mGlu_3$ NAM VU0650786 (*267*). However, $mGlu_3$ is not exclusively in post-synaptic neurons as reports of $mGlu_3$ activation, such as with the endogenous ligand NAAG, inhibit LTD at the perforant path-dentate gyrus synapse, whereas $mGlu_3$'s inhibition reverses the NAAG-mediated LTD inhibition (*268*, *269*). It is possible that the latter effects are mediated by $mGlu_3$ expressed in glia given previous reports that NAAG is released only at heightened neuronal activity and is sufficient to inhibit cAMP in cultured astrocytes (*270*, *271*). A recent report demonstrated that $mGlu_3$ activation by pairing LY379268 with the $mGlu_3$ selective NAM VU0650786 impaired SC-CA1 LTP through its interaction with β-adrenergic receptors within astrocytes (*272*). The effects of increased cAMP and impaired LTP were not observed in the presence of a glial toxin. Moreover, LY379268 in the presence of VU0650786 reversed LY379268's disruption of contextual fear memory, a phenotype that is observed with β-adrenergic receptor antagonism. Therefore, these findings suggest that activation of astrocytic-specific $mGlu_3$ causes cognitive dysfunction.

1.2.3 Role of Group II mGlu receptors in neuropsychiatric disorders

The utility of knockout rodent models and selective pharmacological tools have assisted in illuminating the significance of group II mGlu receptors in several neurological and neuropsychiatric disorders. Here, the following will focus primarily on the role of $mGlu_{2/3}$ receptors in depression and schizophrenia. However, these receptors have also shown to be neuroprotective, especially the activity of $mGlu_3$ receptors in glial cells, and to mediate motor

dysfunction in Parkinson's disease, pain and stress (*263*, *273–278*). Furthermore, anxiolytic effects of both $mGlu_{2/3}$ activation and antagonism have been demonstrated (*279–282*), which complicates the use of $mGlu_{2/3}$ compounds for anxiety.

$mGlu_{2/3}$ receptors have been implicated in depression due to recent preclinical studies using $mGlu_{2/3}$ antagonists and subtype selective NAMs. Chaki *et. al.* first demonstrated that $mGlu_{2/3}$ antagonism decreased the time of immobility of animals in the forced swim test (FST) and tail suspension test (TST), which are both a measure of antidepressant effects (*283*). The effects observed with $mGlu_{2/3}$ antagonism, including the orthosteric antagonist LY341495, is similar to ketamine, an NMDA receptor antagonist that exerts rapid antidepressant effects within the mPFC (*284*, *285*).

Many studies have begun to elucidate the mechanisms underlying the antidepressant effects of $mGlu_{2/3}$ antagonism as well as the role of each receptor subtype. One study reported that LY341495's effects in the FST were not observed in $mGlu_2$ knockout mice, thereby suggesting that $mGlu_2$ mediates antidepressant effects (*286*). However, several $mGlu_3$ NAMs, including VU0650786 have shown efficacy in TST (*287*). VU0650786 was also employed to assess the contribution of $mGlu_3$ in modulating LTD in the mPFC; in these studies, $mGlu_3$ inhibition blocked LTD from excitatory inputs within the mPFC and from the basolateral amygdala (*282*, *288*). These effects were consistent with knockdown of $mGlu_3$ from PFC pyramidal cells, suggesting that post-synaptic $mGlu_3$ receptors are important for facilitating LTD in the PFC. Similar effects were observed in thalamocortical LTD (*264*). Interestingly, the $mGlu_2$ NAM VU6001966 also inhibited LTD from thalamic inputs, but through a pre-synaptic mechanism. Moreover, both compounds independently exerted antidepressant effects in FST and TST, as well as corticosterone stress-induced anhedonia. This set of findings suggests that both $mGlu_2$ and $mGlu_3$ work in concert to

enhance synaptic transmission to the mPFC, and thus highlight the use of $mGlu_{2/3}$ antagonists for depression.

The potential of $mGlu_{2/3}$ antagonists as treatment for depression are further supported by reports of altered $mGlu_{2/3}$ expression in the PFC of patients with major depressive disorder (*289*, *290*). Interestingly, a recent paper reported on a clinical trial on the use of the group II mGlu receptor NAM decoglurant for depression (*291*). Unfortunately, decoglurant had no effect on depression or cognition, although it was noted that a high placebo effect was observed. Given the abundant efficacy of orthosteric antagonists in preclinical models, the lack of effects with the $mGlu_{2/3}$ receptor suggest that orthosteric antagonists may be more efficacious than NAMs.

In contrast to the efficacy of $mGlu_{2/3}$ antagonism for depression, schizophrenia is thought to benefit from activation of group II mGlu receptors. The relationship of $mGlu_{2/3}$ receptors and schizophrenia is strongly substantiated by clinical data. Both receptors have been found to be decreased in post-mortem samples of schizophrenia patients (*292*, *293*). Congruently, $mGlu_{2/3}$ knockout models exhibit phenotypes consistent with several of the symptom domains present in schizophrenia patients, which is a disorder characterized by negative, positive and cognitive symptoms. In a neurodevelopmental model of schizophrenia, in which prenatal stress induces schizophrenia-like phenotypes, $mGlu_2$ and $mGlu_3$ are decreased in the frontal cortex (*294*). Thus, targeting $mGlu_{2/3}$ receptors has the potential to intervene at each symptom domain.

Many current treatments for schizophrenia inhibit the D2 dopamine receptors to dampen the hyperdopaminergic condition that leads to the positive symptoms of the disease. However, these current regimens do not alleviate negative and cognitive symptoms. Many clinical and preclinical studies have demonstrated that NMDA receptor hypofunction is a hallmark of schizophrenia, suggesting that glutamatergic dysfunction could also contribute to the disease (*295*). The role of

$mGlu_{2/3}$ receptors in schizophrenia was first shown by Moghaddam *et. al.*, wherein treatment with LY345470 to activate these receptors reversed phenotypes induced by the NMDA receptor antagonist phencyclidine (PCP) (*296*). Many $mGlu_{2/3}$ agonists have since shown efficacy in reversing phenotypes of NMDA hypofunction in model animals, which include hyperactivity, sensorimotor gating deficits, and working memory impairments (*249*, *267*, *280*, *297*–*302*). The preclinical efficacy prompted clinical trials, specifically with the $mGlu_{2/3}$ agonist LY2140023. The initial study held promise in treating positive and negative symptoms (*301*). Unfortunately, subsequent and larger clinical trials showed that LY2140023 lacked efficacy (*303*–*305*).

The utility of $mGlu_{2/3}$ knockout mice has allowed the interrogation of the contribution of each receptor in mediating the effects of nonselective agonists. For example, the attenuation of PCP-induced hyperlocomotion by LY379268 was mediated by $mGlu_2$ (*298*). This suggested that $mGlu_2$ activation may play a role in the positive symptoms of schizophrenia, and the $mGlu_2$ PAM BINA showed promise in reversing hallucinogen-induced phenotypes, such as excitatory neurotransmission and stereotypic head-twitching induced (*265*). Another $mGlu_2$ PAM, LY487379 also reversed phenotypes of hyperlocomotion and attenuated PPI (*306*). A caveat to the use of $mGlu_2$ PAMs are their ability to induce impairments in cognitive function, as has been shown previously (*307*). However, one study demonstrated that the $mGlu_2$ PAM SAR218645 corrected episodic memory and working memory in pharmacological and genetic model mice of schizophrenia (*308*). These findings show that $mGlu_2$ PAMs could potentially exert efficacy in improving all symptom domains of schizophrenia. Two clinical trials have since been conducted, with one trial reporting that AstraZeneca's drug AZD8529 had no beneficial effect (*309*). The other trial using JNJ-40411813 demonstrated some cognitive efficacy (*310*); however, the clinical progression of this $mGlu_2$ PAM has appeared to have been halted.

$mGlu_3$ has garnered attention given genetic evidence from schizophrenia patients. Specifically, SNPs in the $mGlu_3$ gene, *GRM3*, have been detected and linked to poor performance in prefrontocortical- and hippocampal-based tests that measure working and spatial memory (*311*–*316*). These cognitive deficits in patients are also observed in $mGlu_3$ knockout mice which show impairments in hippocampal synaptic plasticity and deficits in reference, working and spatial memory (*317*–*320*). The importance of $mGlu_3$ function has also been shown in mice modeling schizophrenia, as $mGlu_{2/3}$ agonism can reverse working memory deficits (*266*, *267*, *296*, *300*), while the combination of $mGlu_2$ agonism and $mGlu_3$ antagonism does not (*321*). Lastly, a functional relationship between $mGlu_3$ and $mGlu_5$ has been demonstrated in the mPFC, specifically in how $mGlu_3$-induced LTD requires $mGlu_5$ activation (*278*, *322*). This has also been recently observed in the hippocampus, wherein $mGlu_3$ and $mGlu_5$ work in concert to modulate a temporal-dependent form of associative learning and memory (*267*). These findings suggest that $mGlu_3$ PAMs bear the potential to improve cognitive function. Additionally, given the neuroprotective role of $mGlu_3$, it is conceivable that activation of both $mGlu_3$ and $mGlu_5$ could exert beneficial effects across all symptom domains.

1.2.4 Relationship of $mGlu_{2/3}$ receptors and *MECP2*-related disorders

The reason for the detailed introduction on group II mGlu receptors is because of their association with neurodevelopmental disorders and ASD with previous preclinical studies showing that the antagonism of $mGlu_{2/3}$ can reverse ASD-associated and Fragile X syndrome (FXS) phenotypes (*323*, *324*). The potential role of $mGlu_2$ and $mGlu_3$ receptors in RTT is highlighted by transcriptomic analyses in mouse models and human samples. Several studies have shown that male *Mecp2 mutant* animals display decreased $mGlu_2$ and $mGlu_3$ mRNA and/or protein expression (*68*, *121*, *123*). The altered expression of these receptors is also conserved in cortical post-mortem samples from patients with RTT (*122*, *124*). *Mecp2 mutant* animals exhibit impaired LTP and LTD at the hippocampal SC-CA1 synapse (*69*–*71*) as well as impairments in learning and memory tasks,

such as contextual fear conditioning, novel object recognition and spatial memory (*70*, *74*, *78*, *82*, *83*, *97*, *325*). These cognitive deficits are also observed in $mGlu_3$ knockout mice, which show impairments in reference, working and spatial memory (*317–320*). $mGlu_2$ knockout mice also show attenuated hippocampal synaptic plasticity, such as LTD, albeit at different synapses (e.g. perforant path-CA1 or mossy fiber-CA3), which could be associated with abnormal spatial learning and memory observed in $mGlu_{2/3}$ knockout animals (*261*, *262*, *317*, *326*).

With the phenotypic overlap of cognitive dysfunction between *Mecp2 mutant* animals and $mGlu_{2/3}$ knockout mice, it is likely that $mGlu_{2/3}$ activation could reverse the deficits observed in RTT mice. Unfortunately, some reports have shown that $mGlu_{2/3}$ activation with LY379268 did not reverse working memory impairments in mice, which were induced by the NMDA receptor antagonist, MK-801 (*327*). Additionally, NAAG-mediated $mGlu_3$ activation inhibited LTP at the perforant path-dentate gyrus synapses (*269*). However, several studies have demonstrated that pharmacological activation of $mGlu_2$ and/or $mGlu_3$ modulates SC-CA1 LTP and behavioral learning and memory (*266*, *267*, *299*, *328*). In particular, $mGlu_{2/3}$ receptor activation enhanced LTP and reversed serotonergic-dependent deficits in novel objection recognition (*266*, *299*). On the other hand, $mGlu_3$ activation has been determined to be sufficient in correcting novel object recognition deficits in animal models of NAGG peptidase inhibitors, as well as attenuated PCP-induced LTP and trace fear acquisition (*267*, *328*). These findings suggest a complex role of group II mGlu receptors that could be dependent on the disease, brain region or circuity, and pharmacological tools. Nevertheless, group II mGlu receptor modulation could potentially reverse phenotypes in RTT.

In contrast to *Mecp2 mutant* animals, MeCP2-overexpressing mice exhibit abnormal enhancement of cognitive phenotypes, including LTP, LTD and contextual and cued fear learning and memory (*105*, *171*, *329*). In this regard, $mGlu_{2/3}$ antagonism would logically have beneficial

normalization effects. Several studies have shown that orthosteric $mGlu_{2/3}$ antagonists inhibit LTD at different hippocampal synapses, including a report in which an antagonist attenuated the heightened LTD phenotype in a FXS model mouse (*269*, *324*). However, as alluded to above, this approach is complicated by findings of nonspecific $mGlu_{2/3}$ or $mGlu_3$ activation, as well as $mGlu_2$ selective PAMs in impairing LTP and/or disrupting contextual fear memory (*269*, *272*, *307*). In these paradigms, the effects of $mGlu_{2/3}$ or $mGlu_3$ activation are likely due to the activity of $mGlu_3$ in glial cells (*269*, *272*, *274*). Interestingly, MeCP2 deficiency in glial cells exerts non-cell autonomous negative effects on nearby neurons; this is thought to be due to excessive glutamate release (*38*, *40*, *41*). Given the critical regulation of normal MeCP2 levels, MeCP2 overexpression in glia may also have negative influence. Thus, $mGlu_{2/3}$ activation could mediate this *Mecp2*-induced neurotoxicity, a previously illustrated role for $mGlu_{2/3}$ agonists in protecting mouse-derived primary striatal neurons from NMDA receptor-mediated toxicity *in vitro*, as well as in partially shielding hippocampal CA1 neurons from ischemic-induced apoptosis *in vivo* (*273*, *274*). Further studies are needed to elucidate the physiological and behavioral impact of $mGlu_{2/3}$ modulation in the context of MeCP2 overexpression.

The relationship between group II mGlu receptors and PTHS is even more complex in that contrasting synaptic plasticity and behavioral cognition phenotypes are observed in PTHS model mice. *Tcf4 mutant* mice exhibit enhanced LTP but deficits in associative learning and memory tasks (*212*, *215*). Thus, how $mGlu_{2/3}$ modulation could impact these cognitive phenotypes is unclear. However, TCF4 variants have been implicated in schizophrenia (*218*, *330*, *331*) and *Tcf4* haploinsufficiency causes aberrant morphological, synaptic and behavioral phenotypes related to the mPFC (*213*, *220*, *221*, *332*, *333*), a region associated with psychiatric symptoms and the action of $mGlu_{2/3}$ modulation in alleviating neuropsychiatric-like phenotypes (*264*, *265*, *282*, *284*, *293*, *322*, *334*). In particular, $mGlu_{2/3}$ agonists have shown efficacy in reversing phenotypes in mice modeling NMDA receptor hypofunction, such as sensorimotor gating and hyperactivity, and

increased post-synaptic currents in the mPFC (*249*, *265*, *280*, *296*, *297*, *299*, *300*, *302*, *335*); these are also abnormalities observed in *Tcf4 mutant* animals (*212*, *215*, *220*, *222*). Therefore, it is probable that similar modulation of $mGlu_{2/3}$ receptors that are employed for neuropsychiatric disorders, specifically schizophrenia could exert beneficial effects in PTHS.

Lastly, group II mGlu receptors have been associated with ASD-like phenotypes in addition to learning and memory such as anxiety, motor and social behaviors. For example, $mGlu_{2/3}$ activation normalizes motor and social deficits in mice with autism-like phenotypes; conversely, antagonism reverses hyperlocomotion in NMDA receptor hypofunction model mice (*279*–*281*, *323*). Interestingly, $mGlu_{2/3}$ activation and antagonism both have anxiolytic effects, of which activation of $mGlu_{2/3}$ receptors has been observed in patients (*279*–*281*, *336*). Both the clinical population and preclinical models of *MECP2*-related disorders exhibit abnormalities within these phenotypic domains, and preclinical investigations have shown that these phenotypes are receptive to small molecule intervention (*124*, *133*, *134*, *136*, *137*, *171*, *173*, *215*, *337*). Based on these overall results, we hypothesize that $mGlu_{2/3}$ modulation could potentially have efficacy in several or specific symptoms of *MECP2*-related disorders.

1.3 Harnessing Clinical Data for Therapeutic Discovery

Clinical data are powerful tools in translational research, particularly in defining disease etiology and pathophysiology, as well as therapeutic discovery and development. In regard to *MECP2*-related disorders, several observational clinical trials such as natural history studies (e.g. the RTT Natural History Study from 2006 to 2015 (ClinicalTrials.gov, number NCT00299312) and RTT-related disorders, including MDS (NCT02738281)), biobanking research (e.g., NCT02705677), and characterization of neurophysiological features (e.g., NCT03077308), have been or are currently being conducted. These studies all aim to understand disease manifestation and progression, as well as to identify potential biomarkers, and numerous reports have ranged from

genotype-phenotype correlations to severity and frequency of phenotypes (*52*, *166*, *338–350*). Although such observational studies are limited for PTHS, these published findings have also followed the progression of phenotypes such as epilepsy and breathing abnormalities, as well as presented genotype-phenotype correlations (*178*, *209*, *210*, *351*, *352*).

The availability of these clinical data is also useful in basic scientific research and preclinical therapeutic drug discovery efforts. For example, the correlations between mutations and clinical severity provide insights into more relevant or translational animal models. The characterization of neurophysiological phenotypes also affords potential translational biomarkers to identify treatment efficacy. Furthermore, the availability of patient samples facilitates the identification of novel treatment options. In regard to the goals of this dissertation, data obtained from autopsy samples from RTT patients have led to two critical areas of study: (1) Evaluation on the impact of *MECP2* mutations on treatment feasibility; and (2) Identification of novel treatment options for atypical RTT (*MECP2* mutation-negative) and *MECP2*-related disorders using small molecules modulating proteins related to the disease.

1.4 Dissertation Goals

MECP2-related neurodevelopmental disorders are rare, pediatric diseases with devastating outcomes. The complex pathophysiology of these disorders has raised challenges in developing effective treatments. However, *MECP2*-related disorders exhibit comparable phenotypes both in the clinic and in preclinical animal models, which proposes the possibility that these disorders could be responsive to similar therapeutic strategies. Clinical and transcriptomic could provide insights into these mutual and potential therapeutic targets. My dissertation project will explore two arms of the therapeutic drug discovery efforts, genetic and pharmacological interventions, and employ preclinical animal models of disease and several molecular biology and *in vivo* neuropharmacology techniques to evaluate the safety and efficacy of these treatment strategies.

In Chapters 2 and 3, I will address the safety and efficacy of MeCP2 genetic supplementation in a RTT mouse model harboring a clinically prevalent MeCP2 mutation, as well as in mice modeling PTHS. Chapter 4 will discuss the efficacy of pharmacologically targeting the group II mGlu receptors, two proteins for which we have observed significant decreases in expression in autopsy brain samples from RTT patients, in alleviating the cognitive symptoms of RTT and MDS model mice. I will conclude with the potential implications of these preclinical studies and future directions. Overall, this dissertation aims to provide information pertinent to the clinical trajectory of gene therapy and potential novel therapeutics targets for *MECP2*-related neurodevelopmental disorders.

CHAPTER 2

GENETIC INCREASE OF MeCP2 IN HYPOMORPHIC MUTANT RETT SYNDROME MOUSE MODEL

Work presented in this chapter was published in Genes, Brain and Behavior (*100*).

Summary of findings depicted in Figure 5 and detailed in Table 1.

2.1. Abstract

De novo loss-of-function mutations in methyl-CpG-binding protein 2 (MeCP2) lead to the neurodevelopmental disorder Rett syndrome (RTT). Despite promising results from strategies aimed at increasing MeCP2 levels, additional studies exploring how hypomorphic MeCP2 mutations impact the therapeutic window are needed. Here, we investigated the consequences of genetically introducing a wild-type *MECP2* transgene in the *Mecp2 R133C* mouse model of RTT. The *MECP2* transgene reversed the majority of RTT-like phenotypes exhibited by male and female *Mecp2 R133C* mice. However, three core symptom domains were adversely affected in female $Mecp2^{R133C/+}$ animals; these phenotypes resemble those observed in disease contexts of excess MeCP2. Parallel control experiments in $Mecp2^{Null/+}$ mice linked these adverse effects to the hypomorphic *R133C* mutation. Collectively, these data provide evidence regarding the safety and efficacy of genetically overexpressing functional MeCP2 in *Mecp2 R133C* mice and suggest that personalized approaches may warrant consideration for the clinical assessment of MeCP2-targeted therapies.

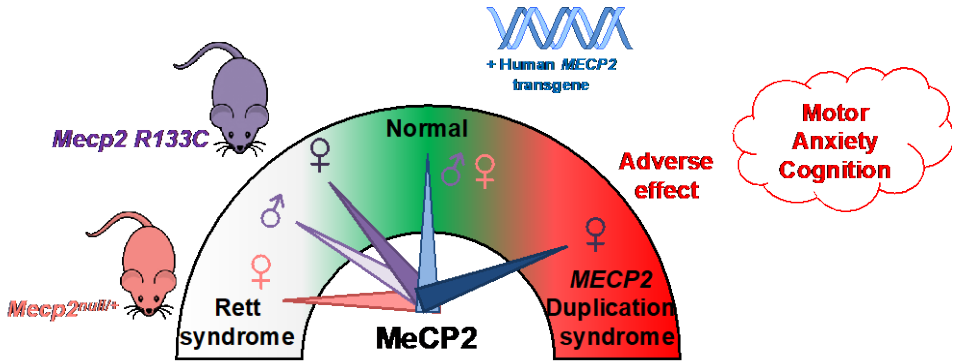

Figure 5: Summary of MeCP2 supplementation effects in *Mecp2 mutant* mice. Female *Mecp2 R133C* (purple ♀, dark purple arrow) animals exhibit less severe Rett syndrome phenotypes than male *Mecp2 R133C* (purple ♂, light purple arrow) and female *Mecp2*$^{Null/+}$ (pink ♀ / arrow) mice. Addition of human *MECP2* transgene normalizes phenotypes of male *Mecp2 R133C* and female *Mecp2*$^{Null/+}$ animals (light blue arrow), whereas adverse effects mimicking *MECP2* Duplication syndrome in motor, anxiety and cognition domains are observed in female *Mecp2 R133C* mice (dark blue arrow).

2.2. Introduction

Rett syndrome is a rare neurodevelopmental disorder that is predominantly seen in female individuals and is characterized by a period of developmental regression in early childhood. Although it has been 20 years since the discovery of the gene causing RTT (*47*), therapeutic treatments remain elusive. The majority of RTT cases (90-95%) are due to loss-of-function (LOF) mutations in *methyl-CpG-binding protein 2* (*MECP2*), a gene that is expressed from the X-chromosome and encodes for the methyl reader protein (MeCP2). Seminal findings in preclinical hemizygous *Mecp2 null* models have described that RTT symptoms are reversible if MeCP2 levels are restored to those of wild type mice, even after disease onset (*71*, *101*). Several studies have since shown that viral delivery of human *MECP2* in hemizygous and heterozygous *Mecp2 null* mice can achieve similar effects in reducing symptom severity and increasing survival (*93*, *112*, *113*, *115*, *116*, *119*). These data support the hypothesis that restoring MeCP2 function by supplying the wild-type protein using gene therapy could be a viable treatment option for RTT.

Three primary challenges arise with assessing the value of gene therapy as a therapeutic strategy for RTT. First, proper brain function has remarkably precise requirements for MeCP2 dosage, as even 2x MeCP2 overexpression is also detrimental, and is the molecular basis of another neurodevelopmental disorder known as *MECP2* Duplication syndrome (MDS). MDS has been modeled in mice and, interestingly, there are clusters of symptoms that appear to overlap with those in RTT models, while additional symptoms oppose those seen in RTT (*105*, *168*). For example, seizures are common clinically in both disorders as well as in mouse models of the two diseases. In contrast, anxiety, motor coordination and learning and memory phenotypes are antiparallel, with deficits observed in RTT models that oppose phenotypes seen in MDS model mice.

The second and third challenges arise from the fact that RTT patients are a heterogeneous clinical population, and their diversity has the potential to impact the therapeutic window. In contrast to the *Mecp2 null* mice that have traditionally been used to assess the efficacy of prospective therapeutics, the RTT patient population is variable in regard to symptom severity, which is impacted by X-chromosome inactivation (XCI) and the specific pathological *MECP2* mutation. XCI, a random process of silencing one X-chromosome in somatic cells (*353*), leaves female RTT patients and *Mecp2* heterozygous mice mosaic for the wild-type (WT) and mutant MeCP2. Although the majority of RTT patients display a random XCI pattern, XCI can be skewed, whereby the expression of the X chromosome with the mutant *MECP2* allele can be expressed at substantially higher or lower levels compared to the WT allele. Several studies have reported skewed XCI in RTT patients, including familial (e.g. (*53*, *354*)) and sporadic (e.g. (*51*)) cases, with the majority suggesting that a relationship exists between skewed XCI (i.e. favoring WT MeCP2) and milder disease severity. This has also been illustrated in *Mecp2* heterozygous mice, whereby more WT MeCP2 cells leads to milder phenotypic severity (*49*, *355*, *356*).

Similarly, correlations exist between each patient's specific *MECP2* mutation and symptom severity (*357*, *58*, *60*). Pathogenic *MECP2* mutations can render the protein completely nonfunctional via truncation or diminished stability, or partially functional through subtle disruption of key domains. The latter situation creates a hypomorphic mutation, in which some critical functions of MeCP2 are retained, and include the most prominent pathological mutations such as *R133C*, *R306C* and *R294X*, as well as other sporadic mutations, e.g. *P152A* (*83*, *95*, *98*, *358*). These retained features of MeCP2 include the ability to bind to DNA or recruit a complex of the co-repressors nuclear receptor co-repressor 2 (NCoR)/silencing mediator for retinoid or thyroid-hormone receptors (SMRT) to regulate gene transcription. Thus far, the majority of preclinical studies regarding gene therapy have addressed the efficacy and safety of this treatment in models of complete LOF mutations, including *T158M* and *R255X* (*74*, *82*, *116*). With the exception of a study that investigated the effects of increased MeCP2 dosage in the context of the hypomorphic mutation *R306C* (*95*), the feasibility of such treatment for patients bearing hypomorphic mutations has been understudied and would provide valuable information to the field.

We focused here on the hypomorphic mutation *R133C*, which is 1) one of the eight most common mutations found in patients, 2) accounts for 7% of the current patient population (*57*), and 3) leads to a mild form of RTT (*58*, *60*, *359*, *360*). This mild severity is thought to be attributed to the *R133C* mutant MeCP2 protein retaining some ability to bind to DNA (*91*, *98*). *Mecp2 R133C* mice have been previously shown to exhibit some RTT-like phenotypes, in particular increased phenotypic score and decreased survival, but these phenotypes are milder in comparison to *Mecp2 null* mice (*98*).

In this current report, we further validated the *Mecp2 R133C* model of RTT by conducting an extensive behavioral phenotypic characterization of male and female mice. We then crossed MDS mice (*MECP2*$^{Tg1/o}$) and *Mecp2 R133C* mice to introduce a human *MECP2* transgene (termed

MECP2$^{Tg1/o}$; *Mecp2*$^{R133C/y}$ or *MECP2*$^{Tg1/o}$; *Mecp2*$^{R133C/+}$) and demonstrate reversibility of several symptoms in male and female mice. Interestingly, however, we observed that female *MECP2*$^{Tg1/o}$; *Mecp2*$^{R133C/+}$ mice demonstrate some phenotypes that are similar to MDS mice, suggesting a potential safety risk for MeCP2 overexpression in the *R133C* context. In a parallel experiment, heterozygous *Mecp2 null* (*Mecp2*$^{Null/+}$) mice with the *MECP2* transgene were indistinguishable from WT littermates, further supporting that the MDS-like phenotypes observed in the female *Mecp2*$^{R133C/+}$ mice are attributable to the hypomorphic *R133C* mutation. In short, we present the first empirical evidence demonstrating that the consequences of introducing a functional MeCP2 in a female mouse model of RTT bearing a hypomorphic *MECP2* mutation are contingent on mutation and symptom.

2.4. Materials and Methods

Animals: All animals used in the present study were group housed with food and water given ad libitum and maintained on a 12 hr light/dark cycle. Animals were cared for in accordance with the National Institutes of Health *Guide for the Care and Use of Laboratory Animals*. All studies were approved by the Vanderbilt Institutional Animal Care and Use Committee and took place during the light phase. *Mecp2 R133C* (B6.129P2(C)-*Mecp2*$^{tm6.1Bird}$/J, stock no. 026848) mice were cryorecovered and *Mecp2*$^{Null/+}$ (B6.129P2(C)-*Mecp2*$^{tm1.1Bird}$/J, stock no. 003890) were obtained from The Jackson Laboratory (Bar Harbor, ME, USA). *MECP2*$^{Tg1/o}$ mice (C57Bl6 background) were generously shared by Dr. Jeffrey Neul (Vanderbilt University). Experimental mice were obtained by crossing female *Mecp2*$^{R133C/+}$ and male *MECP2*$^{Tg1/o}$ mice. Male and female mice were aged until the predicted symptomatic ages (6 weeks and 20 weeks old, respectively) for all experiments. Analogously, female *Mecp2*$^{Null/+}$ were crossed with male *MECP2*$^{Tg1/o}$ mice, and female mice were aged to 20 weeks old for experiments.

Behavioral Assays: All behavioral experiments were conducted during predicted symptomatic ages (6-13 weeks male mice; 20-28 weeks female mice) at the Vanderbilt Mouse Neurobehavioral Core. Each mouse was utilized in multiple assays and conducted in the following order: acoustic startle response, accelerated rotarod, open field, elevated zero maze, 3-chamber social preference, contextual fear conditioning, and whole-body plethysmograph; a minimum of 4 days elapsed between each assay. For each assay, mice were habituated to the testing room for at least 30 min prior to the experiment. Quantification was performed either by a researcher blinded to the genotype or by automated software.

Hindlimb Clasping: Mice were suspended by their tail for 1 min, which was video recorded and analyzed by a blinded reviewer. Recording occurred every 2 weeks within a 6-week span starting

from 6 weeks old (male) or 20 weeks old (females). Clasping was defined as the number of seconds spent either clasping one or more paws, or knuckling the digits of the paw.

Acoustic Startle Response and Pre-Pulse Inhibition (PPI): Mice were placed in individual acoustic startle chambers (Med Associates Inc, St. Albans, VT) and after a 5 min acclimation period, followed the testing paradigm of 61 trials previously described in (*361*). Mice were first presented with five 120 dB startle stimulus alone, which was averaged and presented as the acoustic startle response (in arbitrary units). Then, animals were exposed to nine rounds of pseudo-randomized presentations of the following trials (intertrial interval varied pseudo-randomly between 9 and 21 sec): no stimulus, startle pulse alone (120 dB), highest pre-pulse noise alone (80 dB), and three varying pre-pulses (70, 75, or 80 dB; 20 msec) followed by a startle pulse (120 dB, 50 msec interstimulus interval). Background noise of 65 dB was presented continuously. Percent PPI was calculated as 100 x (mean acoustic startle response [ASR] - mean ASR in pre-pulse plus pulse trials) / mean ASR in startle pulse trials.

Accelerated Rotarod: Mice were placed on a rotarod (Ugo Basile, Med Associates Inc, St. Albans, VT, USA) that accelerated from 4 to 40 rpm over 5 min with a 10 min maximum per test. Each animal was tested 3 times a day for 3 days with 1 hr between trials. The latency to fall was recorded as the time that the mice fall from the rod or time at which the mice turn with the rod twice. Data are presented as an average latency to fall of the 3 testing days.

Open Field: Mice were placed in the activity chamber for 30 min and locomotor activity was quantified as beam breaks in the X, Y and Z axis using Activity Monitor software (Med Associates Inc, St. Albans, VT, USA).

Elevated Zero Maze: Mice were placed on a continuous circular platform with two closed and two open regions for 5 min under full light conditions (~700 lux in the open regions, ~400 lux in the

closed regions). The time spent exploring the open regions, as well as distanced traveled in both open and closed regions, was quantified by ANY-maze software (Stoelting, Wood Dale, IL, USA).

3-chamber Social Preference Assay: Mice were placed in a standard three-chamber apparatus and allowed to habituate for 5 min. The mice were then exposed to a novel mouse (stranger 1) and an empty cup for 7 min. Immediately after, the animals were exposed to a novel stranger ("novel mouse") in addition to stranger 1 ("familiar mouse") for 7 min. Stranger mice were of the same sex and strain, as well as ≤5 weeks younger as experimental mice. In between experimental mice, chamber placement of stranger mice and cups were switched. Time spent in the chambers were quantified using ANY-maze software (Stoelting, Wood Dale, IL, USA).

Contextual Fear Conditioning: Mice were habituated to the room for 2 hrs on the day prior to fear conditioning and for 1 hr before conditioning and contextual testing. On conditioning day, mice were placed into an operant chamber with a shock grid (Med Associates Inc, St. Albans, VT, USA) in the presence of a 10% vanilla odor cue. Following a 3 min habituation period, mice were exposed to two mild (0.7 mA) 1 sec foot shocks spaced 30 sec apart that were preceded by a tone. Mice remained in the context for an additional 30 sec after the second foot shock. On test day, 24 hrs after conditioning, mice were placed back into the same operant chamber with a 10% vanilla odor cue for 5 min, and the percentage of time spent freezing was measured by Video Freeze software (Med Associates Inc, St. Albans, VT, USA). Due to high baseline freezing (pre-tone shock), the freezing percentage on the contextual test day was subtracted by the baseline freezing on conditioning day.

Whole Body Plethysmography (WBP): Unrestrained mice were placed in a WBP recording chamber (Buxco, two-site system, DSI, New Brighton, MN, USA) with a continuous inflow of air (1 liter/min). After a habituation period of 1 hr, respiratory measurements were made for 30 min.

Analysis was performed using FinePointe ResearchSuite (version 2.3.1.9). Apneas, defined as pauses spanning twice the average expiratory time of the previous 2 min, were quantified using the FinePointe apnea software patch. Only points of motion-free recording were analyzed. Periods of movement were removed (i) automatically by the FinePointe apnea software, (ii) manually by identifying points where the D-chamber volume exceeded the normal breath range, and (iii) at points where the researcher was present during the recording noted activity.

Total Protein Preparation: The cortex, cerebellum and hippocampus were microdissected from naïve 6-week male and 20-week female mice that were of separate cohorts from the mice that underwent behavior to avoid changes in gene expression that may occur after behavioral testing. Total protein was prepared as previously described in (*362*). Briefly, tissue samples were homogenized using a hand-held motorized mortar and pestle in radioimmunoprecipitation assay buffer (RIPA) containing 10 mM Tris-HCl, 150 mM NaCl, 1 mM ethylenediaminetetraacetic acid (EDTA), 0.1% sodium dodecyl sulfate (SDS), 1% Triton X-100, and 1% deoxycholate (Sigma, St. Louis, MO, USA). After homogenization, samples were centrifuged and the supernatant was collected. Protein concentration was determined using a bicinchoninic acid (BCA) protein assay (Pierce, ThermoFisher, Waltham, MA, USA).

SDS-Page and Western Blotting: As previously described in (*362*), 50 µg of total protein was electrophoretically separated using a 4-20% SDS polyacrylamide gel and transferred onto a nitrocellulose membrane (Bio-Rad, Hercules, CA, USA). Membranes were blocked in Odyssey blocking buffer (LI-COR, Lincoln, NE, USA) for 1 hr at room temperature. Membranes were probed with primary antibodies overnight at 4 °C: rabbit anti-MeCP2 (1:1000, Millipore cat no. 07-013, Burlington, MA, USA) and mouse anti-Gapdh (1:1000, ThermoFisher cat. no. MA5-15738, Waltham, MA, USA), followed by the fluorescent secondary antibodies: goat anti-rabbit (800 nm, 1:5000, LI-COR, Lincoln, NE, USA) and goat anti-mouse (680 nm, 1:10,000, LI-COR, Lincoln,

NE, USA). Fluorescence was detected using the Odyssey (LI-COR, Lincoln, NE, USA) imaging system at the Vanderbilt University Medical Center Molecular Cell Biology Resource (MCBR) Core and then quantified using the Image Studio Lite software (LI-COR, Lincoln, NE, USA). Values were normalized to Gapdh and compared relative to wild-type controls.

Statistical Analyses: Statistics were carried out using Prism 8 (GraphPad) and Excel (Microsoft). All data shown represent mean ± SEM. Statistical significance between genotypes was determined using mixed-effects analysis, or 1- or 2-way ANOVA with Sidak's, Tukey's or t-test post-hoc, or unpaired t-test. Sample size and statistical tests are specified in each figure legend with p-values represented as *$p < 0.05$, **$p < 0.01$, ***$p < 0.001$, and ****$p < 0.0001$ for within-genotype comparison.

2.6. Results

2.6.1. *Mecp2 R133C* mice exhibit RTT-like phenotypes

Male mice harboring the *R133C* mutation (*Mecp2*$^{R133C/y}$) have been previously characterized as exhibiting RTT-like phenotypes such as decreased survival, increased phenotypic score (an aggregate measurement of six parameters including general condition, breathing and hindlimb clasping (*363*)) and altered anxiety behavior compared to wild-type (WT) mice (*98*). To expand these observations to more quantitative phenotypes, we began by assessing weight deficits in both male and female (*Mecp2*$^{R133C/+}$) *Mecp2 R133C* mice. We found that, regardless of sex, decreased weight was observed as early as 5 weeks old and maintained at older ages (Figure 6A, mixed-effects analysis, male: $F(1,47) = 93.09$, $p < 0.0001$, female: $F(1,66) = 26.65$, $p < 0.0001$). Similarly, hindlimb clasping was pronounced in male and female *Mecp2 R133C* mice, as shown in the representative images (Figure 6B). Blinded scoring of video recordings illustrated the increased hindlimb clasping in *Mecp2 R133C* mice compared to WT littermates (Figure 6B, t-test, male: $t(44) = 6.630$, $p < 0.0001$, female: $t(61) = 5.362$, $p < 0.0001$). The clasping phenotype was also maintained from weeks 6-13 in male *Mecp2*$^{+/y}$ and 20-28 in female *Mecp2*$^{R133C/+}$ animals (ANOVA, male: $F(1,44) = 43.95$, $p < 0.0001$, female: $F(1,61) = 28.83$, $p < 0.0001$).

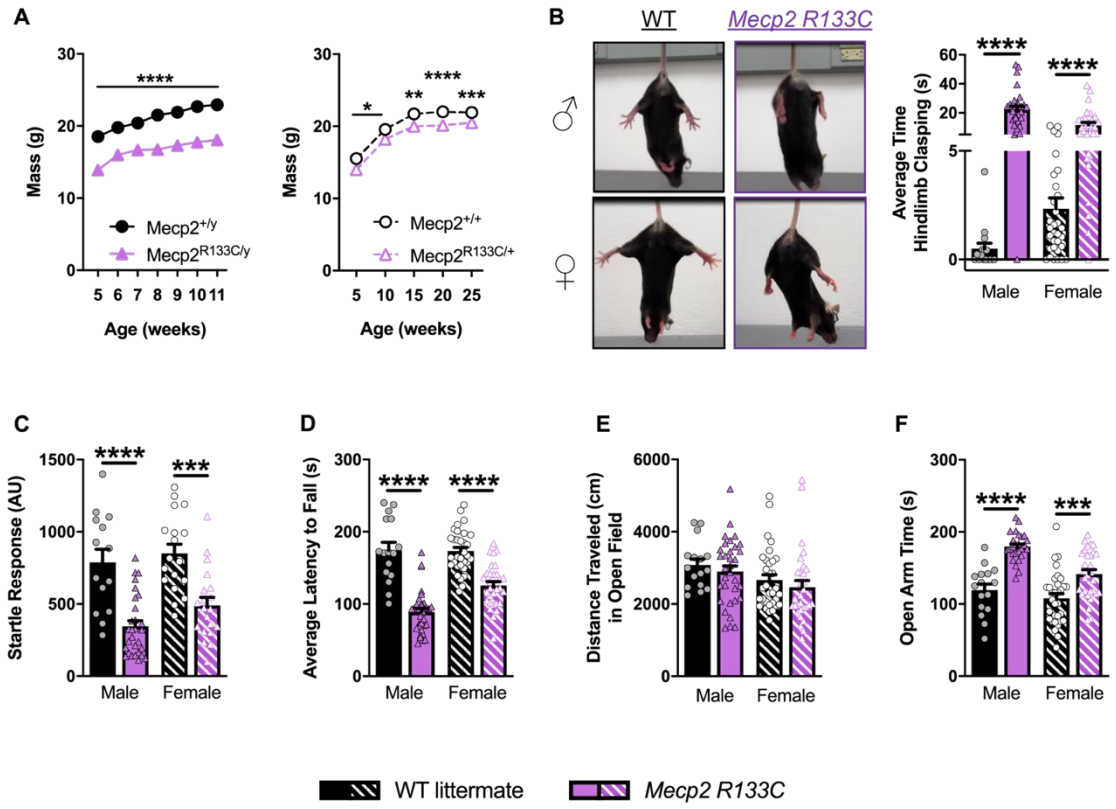

Figure 6: RTT-like neurological phenotypes are observed in male and female *Mecp2 R133C* mice. (A) Attenuated weight across all ages (5-11 week-old males (n = 11-28 per genotype), and 5-25 week-old females, n = 14-25 per genotype)). (B-F) *Mecp2 R133C* mice exhibited hindlimb clasping (representative images shown, B), attenuated acoustic startle response to a 120dB stimulus (C), decreased latency to fall on an accelerated rotarod (D), normal spontaneous locomotor activity in the open field task (E), and increased time spent in the open arms of an elevated zero maze (F). n = 15-33 per genotype in males, n = 18-32 per genotype in females. Mixed-effects analysis with Sidak's post-hoc test, or unpaired t-test. *within-genotype comparison. *p < 0.05, ** p < 0.01, *** p < 0.001, **** p < 0.0001. WT = filled or patterned black bars or closed or open black circles. *Mecp2 R133C* = filled or patterned purple bars or closed or open purple triangles. Male = filled, closed. Female = patterned, open.

We then conducted a behavioral battery that incorporates evaluation of a series of phenotypes that have been reported to be abnormal in various mouse models of RTT (*62*, *72*) and that we have used for previous studies (*136*, *137*, *362*) (Figure 7). Given the prior observation that *Mecp2 R133C* mice exhibited milder severity compared to *Mecp2 null* mice (*98*), these studies used 6-12 week-old male and 20-26 week-old female mice. This battery tested for the following

behaviors: acoustic startle response, motor coordination, spontaneous locomotor activity, anxiety, social behavior and social recognition/preference, contextual fear conditioning, and breathing abnormalities. As assessments of sensorimotor gating, we evaluated the acoustic startle response as well as pre-pulse inhibition (PPI). Both sexes of *Mecp2 R133C* mice exhibited an attenuated acoustic startle response to a 120 decibel (dB) stimulus (Figure 6C, t-test, male: t (41) = 5.287, p < 0.0001, female: t (36) = 4.326, p < 0.001). However, no difference in percentage of PPI was observed in male or female *Mecp2 R133C* mice compared to WT littermates (ANOVA, male: F (1,41) = 1.226, p > 0.05, female: F (1,35) =1.275, p > 0.05). These data suggest that, while basal startle reactivity is impaired, *Mecp2 R133C* mice display normal sensorimotor gating.

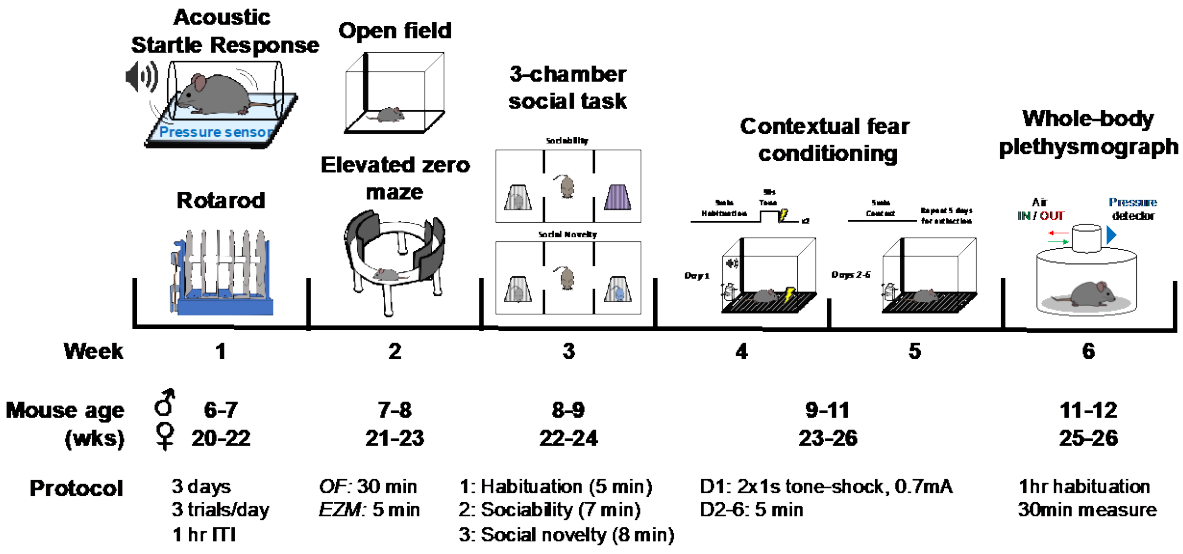

Figure 7: Behavioral battery to assess phenotypes in *Mecp2 R133C* mice. ♀ (female), ♂ (male).

We next measured performance in an accelerated rotarod to determine motor dysfunction. Both sexes of *Mecp2 R133C* mice displayed decreased average latency to fall, indicative of attenuated motor coordination (Figure 6D, t-test, male: t (47) = 8.055, p < 0.0001, female: t (60) = 6.345, p < 0.0001). Given this deficit, we assessed spontaneous locomotor activity in an open field, as gross motor deficits could impact more subtle phenotypic measures of anxiety, cognition, and sociability.

We observed no locomotor activity changes in *Mecp2 R133C* mice compared to WT littermates (Figure 6E, t-test, male: $t(40) = 0.7135$, $p > 0.05$, female: $t(60) = 0.8408$, $p > 0.05$), suggesting that the rotarod deficit is specific to motor coordination and not gross motor function. We then utilized an elevated zero maze to evaluate anxiety-related behavior. Although male *Mecp2*$^{R133C/y}$ mice exhibited decreased total distance traveled (t-test, male: $t(35) = 2.434$, $p < 0.05$, female: $t(60) = 1.692$, $p > 0.05$), both male and female *Mecp2 R133C* mice spent more time in the open arms compared to the WT littermates, indicative of decreased anxiety behavior (Figure 6F, t-test, male: $t(35) = 6.785$, $p < 0.0001$, female: $t(60) = 3.821$, $p < 0.001$).

To evaluate social behavior as well as learning and memory phenotypes, we utilized a 3-chamber discrimination task. In this assay, both *Mecp2*$^{R133C/+}$ and *Mecp2*$^{R133C/y}$ mice were comparable to sex-matched WT littermates, spending more time with the stranger mouse ("stranger 1") over an inanimate object (in this case, an empty cup) (ANOVA, male: $F(2,70) = 257.0$, $p < 0.0001$, female: $F(2,96) = 179.9$, $p < 0.0001$), which suggests normal sociability. However, when presented with a novel mouse ("novel") in addition to the familiar mouse ("familiar") from the sociability phase, both sexes of *Mecp2 R133C* mice failed to demonstrate the same preference for the novel stranger as littermates, spending equal time with both stranger mice (Figure 8A, ANOVA, male: $F(2,68) = 108.8$, $p < 0.0001$ (*Mecp2*$^{+/y}$), $p > 0.05$ (*Mecp2*$^{R133C/y}$), female: $F(2,96) = 135.3$, $p < 0.05$ (*Mecp2*$^{+/+}$), $p > 0.05$ (*Mecp2*$^{R133C/+}$)). This result is indicative of a deficit in social preference and/or impaired social memory.

We further assessed learning and memory using a contextual fear conditioning test, which measures freezing to a previously aversive stimulus as a proxy of memory. On day 1, the mice were trained to associate their environment with a mild foot shock. Irrespective of genotype, male and female mice responded to the aversive stimulus (ANOVA, male: $F(2,70) = 34.37$, $p < 0.0001$, female: $F(2,110) = 138.8$, $p < 0.0001$), suggesting normal sensory and short-term memory

acquisition. To evaluate the long-term memory component, mice were placed back in the same context 24 hours after shock administration (training day), and only male *Mecp2*$^{R133C/y}$ mice exhibited decreased freezing behavior (Figure 8B, t-test, male: t (35) = 2.465, $p < 0.05$, female: t (55) = 0.9306, $p > 0.05$). In contrast, female *Mecp2*$^{R133C/+}$ mice showed contextual freezing at levels comparable to littermate controls.

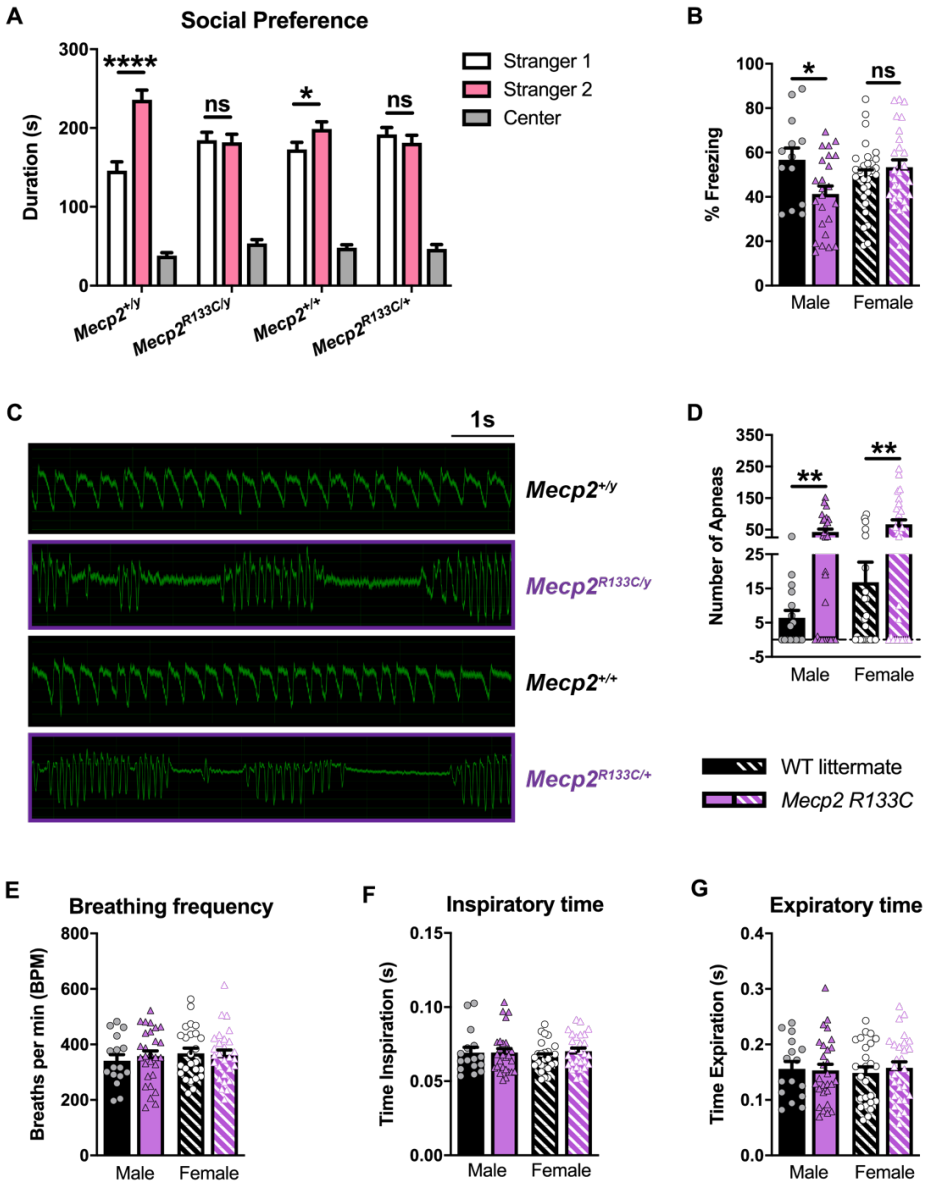

Figure 8: Male and female *Mecp2 R133C* mice exhibit differential phenotypes in social preference, contextual fear conditioning, and respiratory function. (A) Contrary to WT littermates that spend more time with novel (pink)

than familiar (white) mice in a 3-chamber social preference task, *Mecp2 R133C* mice did not show preference for the novel mouse. (B) Only male *Mecp2*$^{R133C/y}$ displayed decreased percent freezing in contextual fear conditioning 24 hours after training. (C-D) Increased apneas were observed in *Mecp2 R133C* mice, both quantitatively and qualitatively as shown in representative whole-body plethysmography traces. (E-G) *Mecp2 R133C* mice exhibited normal respiratory parameters for breathing frequency, inspiratory time and expiratory time. n = 13-29 per genotype in males, n = 21-30 per genotype in females. 2-way ANOVA with t-test post-hoc, or unpaired t-test. *within-genotype comparison. ns (not significant), *p < 0.05, **p < 0.01, ****p < 0.0001. WT = filled or patterned black bars. *Mecp2 R133C* = filled or patterned purple bars. Male = filled, closed. Female = patterned, open.

Lastly, we investigated the presence of breathing abnormalities, particularly apneas, which are observed in RTT mouse models and patients. Apneas, characterized as “breath-holding” or hypoventilation, are preceded by periods of hyperventilation (*364*) and can be quantified using whole-body plethysmography. We observed that both male and female *Mecp2 R133C* mice exhibited apneas (Figure 8C-D, t-test, male: $t(42) = 3.067$, $p < 0.01$, female: $t(51) = 3.108$, $p < 0.01$) without significant changes in other breathing parameters such as frequency and times of inspiration or expiration (Figure 8E-G, t-test, all $p > 0.05$, male: $t(42) = 0.5755$ (breathing frequency), $t(42) = 0.04122$ (inspiration time), $t(42) = 0.1622$ (expiration time), female: $t(51) = 0.1999$ (breathing frequency), $t(51) = 1.253$ (inspiration time), $t(51) = 0.5968$ (expiration time)).

2.6.2. MeCP2 protein expression in *Mecp2 R133C* mice with and without *MECP2* transgene is brain region- specific

The milder phenotypes in *Mecp2 R133C* mice and RTT patients have been linked to some preserved MeCP2 expression and function, as had been previously characterized both *in vitro* and *ex vivo* (*91*, *98*, *365*). Therefore, we hypothesized that the mutant MeCP2 protein is stably expressed in *Mecp2 R133C* mice. Using Western blotting, we detected both WT MeCP2 and GFP-tagged *R133C* MeCP2. Interestingly, in male *Mecp2*$^{R133C/y}$ mice, the total level of MeCP2 protein was dependent on the brain region, with unchanged expression in the cortex and

cerebellum, but decreased in the hippocampus compared to WT littermates (Figure 9A, t-test, t (8) = 0.4178, p > 0.05 (cortex), t (9) = 2.330, p > 0.05 (cerebellum), t (10) = 2.966, p < 0.05 (hippocampus)). In female *Mecp2*$^{R133C/+}$ mice, we quantified WT and mutant MeCP2, and observed that total MeCP2 expression was similar to WT littermates regardless of brain region (Figure 9B, t-test, all p > 0.05, t (10) = 1.456 (cortex), t (9) = 0.1474 (cerebellum), t (10) = 1.700 (hippocampus)). Moreover, by comparing the relative expression of these two forms of MeCP2 in female mice, we also observed variability in heterogeneity both between samples and across brain regions, with some mice expressing more of the *R133C* mutant than WT MeCP2, more of WT MeCP2 than the *R133C* mutant protein, or equal amounts of both proteins.

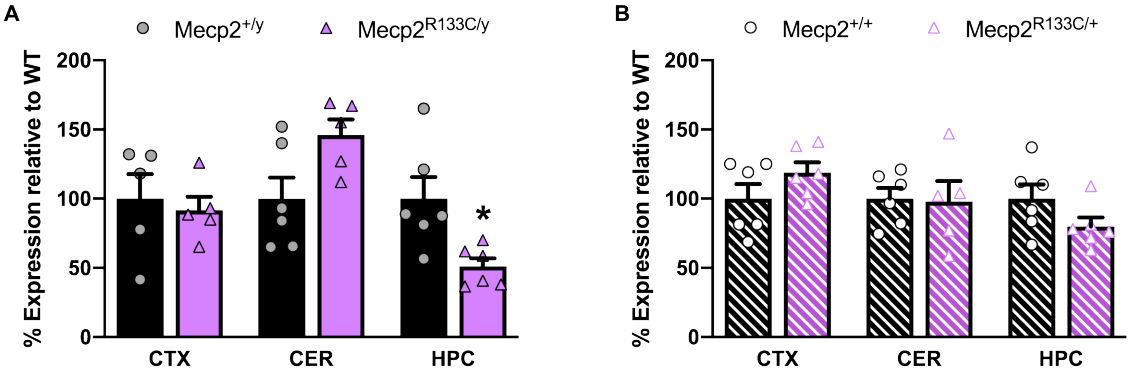

Figure 9: Basal MeCP2 protein expression in *Mecp2 R133C* mice varies by brain region in *Mecp2*$^{R133C/y}$ mice and is unchanged in *Mecp2*$^{R133C/+}$ mice. (A) Total MeCP2 protein is unchanged in the cortex and cerebellum of *Mecp2*$^{R133C/y}$ mice but is decreased in the hippocampus. (B) Compared to WT littermates, *Mecp2*$^{R133C/+}$ mice express normal total MeCP2 levels in the cortex (CTX), cerebellum (CER), and hippocampus (HPC). Total expression is a sum of WT and R133C mutant MeCP2 levels. n = 5-6 per genotype. Unpaired t-test. *p < 0.05. WT = filled or patterned black bars. *Mecp2 R133C* = filled or patterned purple bars. Male = filled, closed. Female = patterned, open.

We posited that introduction of a WT human *MECP2* transgene would further increase protein expression in *Mecp2 R133C* animals and might elicit unique effects in male versus female mice. To address our hypothesis, we took advantage of a well-characterized *MECP2* Duplication

syndrome (MDS) mouse model, *MECP2*$^{Tg1/o}$ (*105*), which expresses a WT human *MECP2* transgene, and have now been bred to the same C57Bl6 congenic background as the *R133C* mutation(*74*). Similar to the approach in (*74*), we then bred MDS mice with *Mecp2 R133C* mice to genetically introduce the human *MECP2* transgene (Figure 10). This breeding strategy led to our experimental mice, male *MECP2*$^{Tg1/o}$*; Mecp2*$^{R133C/y}$ and female *MECP2*$^{Tg1/o}$*; Mecp2*$^{R133C/+}$ animals, which we compared to the following controls: *Mecp2*$^{+/y}$ or *Mecp2*$^{+/+}$, *MECP2*$^{Tg1/o}$ and *Mecp2*$^{R133C/y}$ or *Mecp2*$^{R133C/+}$. Again, we assessed MeCP2 protein expression in the cortex, hippocampus and cerebellum from these mice. Compared to WT littermates, total MeCP2 protein was increased in MDS mice, *MECP2*$^{Tg1/o}$, regardless of sex and brain region (Figure 11, ANOVA, overall p-value indicated, male: $F(3,18) = 7.584$, $p < 0.01$ (cortex), $F(3,19) = 7.894$, $p < 0.01$ (cerebellum), $F(3,20) = 3.654$, $p < 0.05$ (hippocampus), female: $F(3,20) = 37.58$, $p < 0.0001$ (cortex), $F(3,19) = 8.113$, $p < 0.01$ (cerebellum), $F(3,20) = 21.24$, $p < 0.0001$ (hippocampus)). A similar observation was seen in the cortex and cerebellum of *MECP2*$^{Tg1/o}$*; Mecp2*$^{R133C/y}$ and *MECP2*$^{Tg1/o}$*; Mecp2*$^{R133C/+}$ mice, which was not surprising given the stable expression in the *Mecp2 R133C* mice alone. Interestingly, hippocampal MeCP2 expression in female *MECP2*$^{Tg1/o}$*; Mecp2*$^{R133C/+}$ mice (Figure 11F) was comparable to that of WT littermates despite *Mecp2*$^{R133C/+}$ mice expressing MeCP2 protein at WT levels. Nonetheless, regardless of brain region, addition of the *MECP2* transgene increased WT MeCP2 levels in *Mecp2*$^{R133C/+}$ mice as indicated by a rightward shift in the expression of the WT protein in *MECP2*$^{Tg1/o}$*; Mecp2*$^{R133C/+}$ mice compared to that in *Mecp2*$^{R133C/+}$ mice. Additionally, since MeCP2 protein expression was similar between *MECP2*$^{Tg1/o}$ and *MECP2*$^{Tg1/o}$*; Mecp2*$^{R133C/y}$ or *MECP2*$^{Tg1/o}$*; Mecp2*$^{R133C/+}$ mice in most brain areas, we posited that the introduction of an *MECP2* transgene in *Mecp2 R133C* mice could cause the development of MDS-like phenotypes.

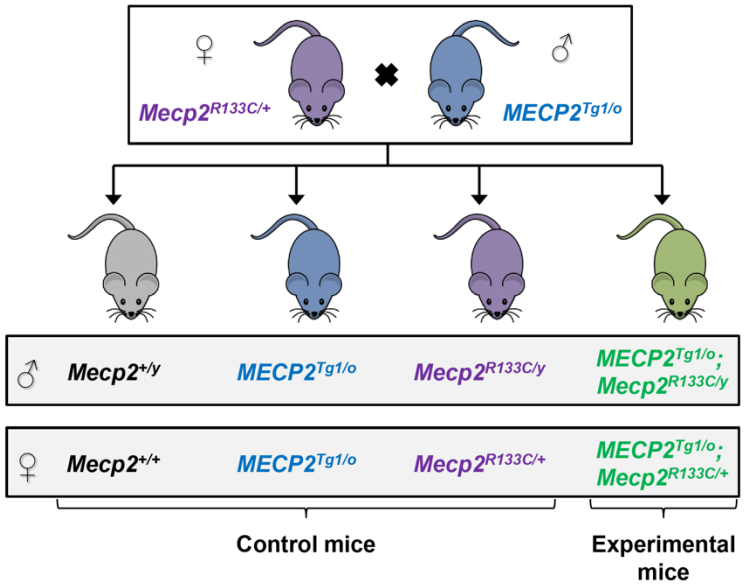

Figure 10: Breeding scheme to generate *Mecp2 R133C* mice expressing an *MECP2* transgene. Male *MECP2*$^{Tg1/o}$ mice (blue) were bred with female *Mecp2*$^{R133C/+}$ (purple) animals to introduce the human *MECP2* transgene and generate the experimental mice *MECP2*$^{Tg1/o}$*; Mecp2*$^{R133C/y}$ and *MECP2*$^{Tg1/o}$*; Mecp2*$^{R133C/+}$ (green). Wild-type (gray), *MECP2*$^{Tg1/o}$, and *Mecp2*$^{R133C/y}$ or *Mecp2*$^{R133C/+}$ littermates were used as controls.

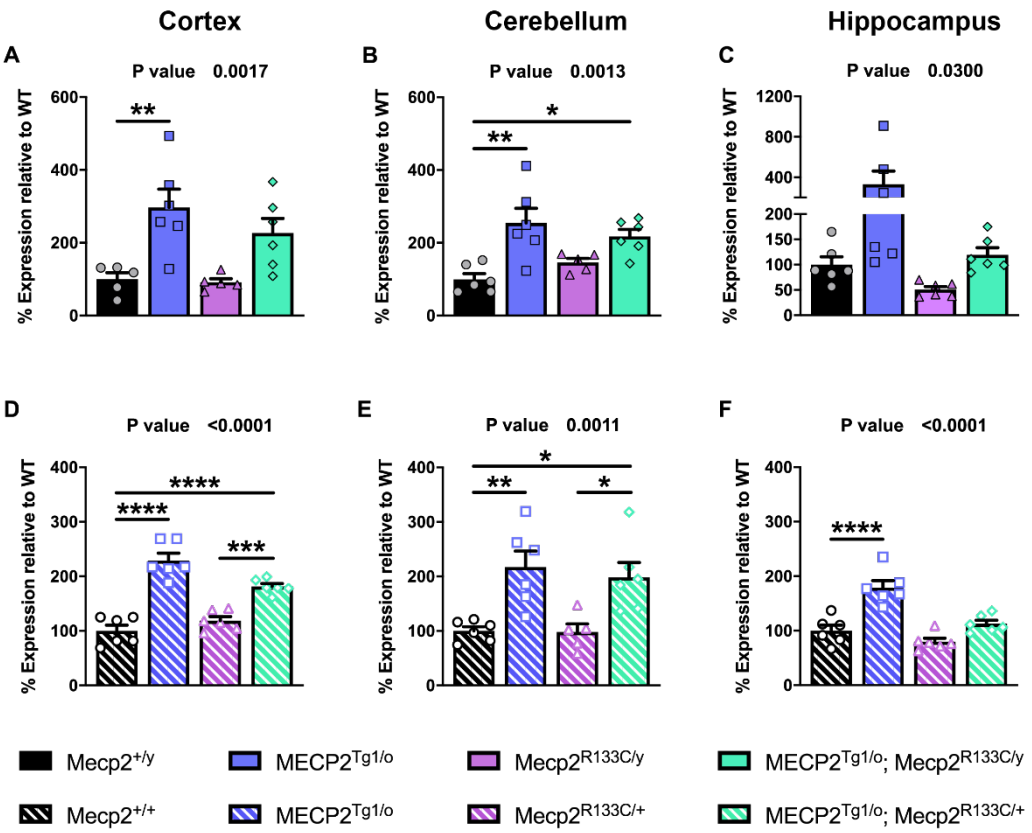

Figure 11: Impact of *MECP2* transgene on MeCP2 protein expression in *Mecp2 R133C* mice.

(A-F) Compared to WT littermates, male and female *MECP2*$^{Tg1/o}$ mice demonstrate increased MeCP2 expression in the cortex, cerebellum and hippocampus. Addition of the *MECP2* transgene in *Mecp2*$^{R133C/y}$ and *Mecp2*$^{R133C/+}$ mice increased total MeCP2 protein in the cortex and cerebellum, but not in the hippocampus. Total expression is a sum of WT and R133C mutant MeCP2 levels. n = 5-6 per genotype. 1-way ANOVA with Tukey's post-hoc test. Overall p-value indicated at the top of each graph. *p < 0.05, **p < 0.01, ***p < 0.001, ****p < 0.0001. WT = black bars or circles. *MECP2*$^{Tg1/o}$ = blue bars or squares. *Mecp2 R133C* = purple bars or triangles. *MECP2*$^{Tg1/o}$*; Mecp2 R133C* = green bars or diamonds. Male = filled or closed. Female = patterned or open.

2.6.3. Phenotypic reversal in male *Mecp2*$^{R133C/y}$ mice with a wild-type *MECP2* transgene

We first investigated the phenotypic consequences of expressing a WT *MECP2* allele in the male global mutant *R133C* context mice by conducting the aforementioned behavioral battery. We observed reversal of *Mecp2*$^{R133C/y}$-associated phenotypes, including the weight deficit and

hindlimb clasping phenotype, at all ages (Figure 12A-B, p-value indicated for *MECP2*$^{Tg1/o;}$ *Mecp2*$^{R133C/y}$ vs *Mecp2*$^{R133C/y}$ comparison, (weight) mixed-effects analysis, $F(3,99) = 53.56$, $p < 0.0001$, (hindlimb clasping) ANOVA, $F(3,95) = 58.71$, $p < 0.0001$ (overall), $F(3,95) = 58.71$, $p < 0.0001$ (at each age range). Moreover, the addition of WT *MECP2* in *Mecp2*$^{R133C/y}$ mice reversed acoustic startle response deficiency (Figure 12C, ANOVA, $F(3,89) = 14.05$, $p < 0.0001$ (*MECP2*$^{Tg1/o;}$ *Mecp2*$^{R133C/y}$ vs *Mecp2*$^{R133C/y}$)), abnormal social preference (Figure 12D, ANOVA, $F(2,160) = 200.9$, $p < 0.001$ (*MECP2*$^{Tg1/o;}$ *Mecp2*$^{R133C/y}$ familiar mouse vs novel mouse)), and increased apneas (Figure 12E, ANOVA, $F(3,93) = 10.56$, $p < 0.001$ (*MECP2*$^{Tg1/o;}$ *Mecp2*$^{R133C/y}$ vs *Mecp2*$^{R133C/y}$)). The effect on respiratory function was restricted to the apnea phenotype as no changes were observed in breathing frequency as well as inspiratory and expiratory times (ANOVA, all $p > 0.05$, $F(3,93) = 0.8194$ (breathing frequency), $F(3,93) = 0.3889$ (inspiratory time), $F(3,93) = 0.6070$ (expiratory time)).

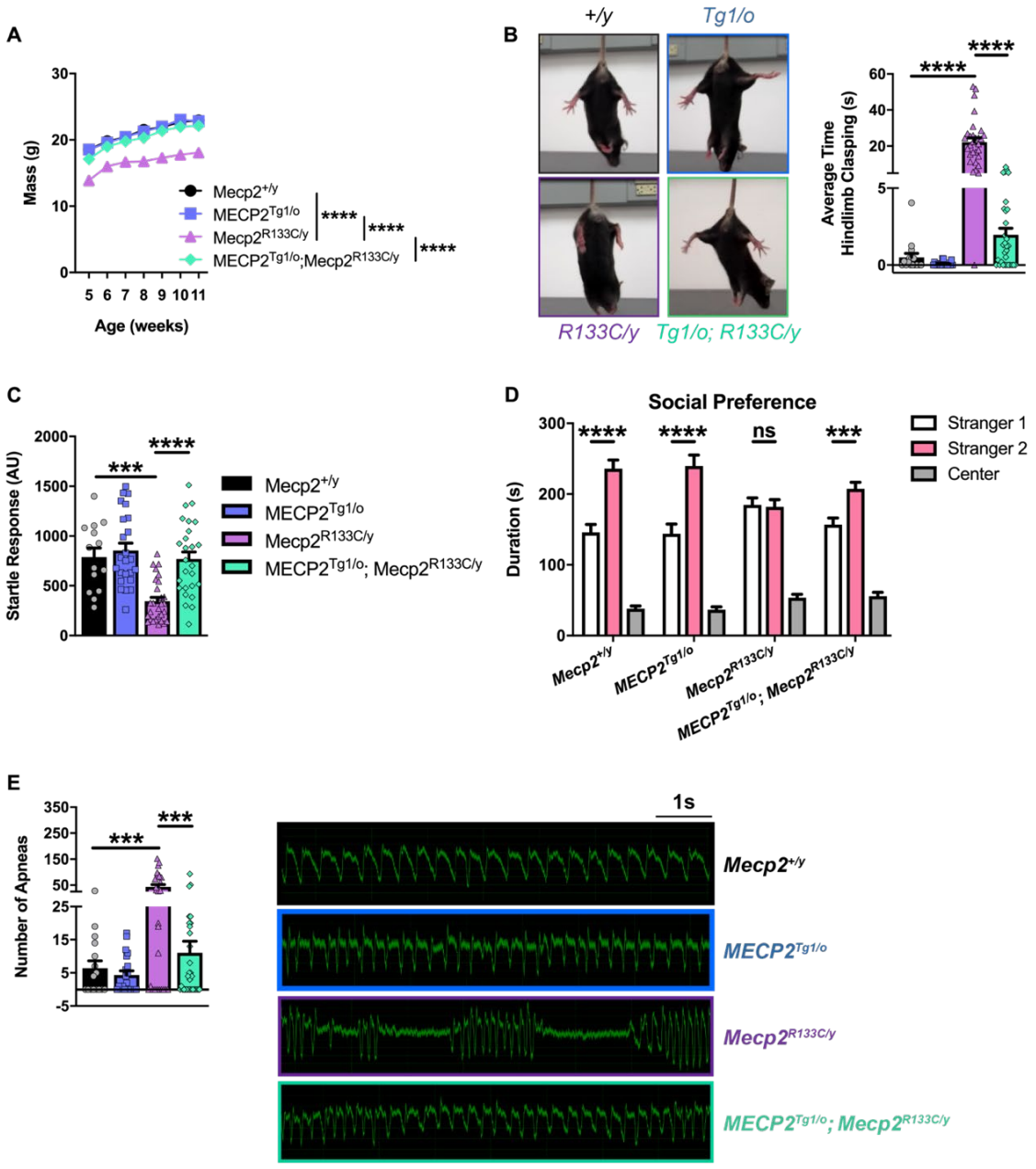

Figure 12: Wild-type *MECP2* corrects abnormal behaviors observed in *Mecp2*$^{R133C/y}$ mice. (A-E) Weight deficit (n = 11-32 per genotype) (A), hindlimb clasping (n = 16-31 per genotype) (B), attenuated acoustic startle response (n = 14-29 per genotype) (C), lack of social preference (n = 15-30 per genotype) (D), and increased apneas (n = 16-32 per genotype) (E) in *Mecp2*$^{R133C/y}$ mice were normalized in *MECP2*$^{Tg1/o}$*; Mecp2*$^{R133C/y}$ mice. Male *MECP2*$^{Tg1/o}$ mice also exhibited normal behavior in these assays when compared to WT littermates. Representative hindlimb clasping and apnea traces are shown. Mixed-effects analysis, or 1- or 2-way ANOVA with Tukey's or t-test post-hoc. ns (not significant), ** $p < 0.01$, *** $p < 0.001$, **** $p < 0.0001$. WT = filled black bars or circles. *MECP2*$^{Tg1/o}$ = filled blue bars or squares. *Mecp2*$^{R133C/y}$ = filled purple bars or triangles. *MECP2*$^{Tg1/o}$*; Mecp2*$^{R133C/y}$ = filled green bars or diamonds.

When comparing the phenotype of RTT and MDS mice, several phenotypes consistently present in a bi-directional manner. These phenotypes include anxiety, motor coordination and associative learning and memory in the form of contextual fear freezing (*79*, *105*, *366*, *367*). We observed the bi-directionality of these phenotypes, in which *Mecp2*$^{R133C/y}$ mice exhibited attenuated anxiety, motor coordination and contextual freezing, whereas *MECP2*$^{Tg1/o}$ mice displayed contrasting phenotypes of increased anxiety, and abnormally enhanced performance in the accelerated rotarod and contextual fear conditioning tasks (Figure 13A-C, ANOVA, $F(3,83) = 43.22$, $p < 0.01$ (*Mecp2*$^{+/y}$ vs *MECP2*$^{Tg1/o}$), $p < 0.0001$ (*Mecp2*$^{+/y}$ vs *Mecp2*$^{R133C/y}$) (anxiety), $F(3,99) = 49.10$, $p < 0.0001$ (*Mecp2*$^{+/y}$ vs *MECP2*$^{Tg1/o}$ and *Mecp2*$^{+/y}$ vs *Mecp2*$^{R133C/y}$) (motor coordination), $F(3,80) = 13.69$, $p < 0.05$ (*Mecp2*$^{+/y}$ vs *MECP2*$^{Tg1/o}$ and *Mecp2*$^{+/y}$ vs *Mecp2*$^{R133C/y}$) (contextual fear conditioning)). Introduction of an *MECP2* transgene in the *Mecp2*$^{R133C/y}$ mice reversed these deficits to WT levels, which further established phenotypic reversal in male *Mecp2*$^{R133C/y}$ mice (Figure 13A-C, ANOVA, p-valued indicated for *MECP2*$^{Tg1/o}$; *Mecp2*$^{R133C/y}$ vs *Mecp2*$^{R133C/y}$ comparison, $p < 0.0001$ (anxiety), $p < 0.0001$ (motor coordination), $p < 0.01$ (contextual fear conditioning).

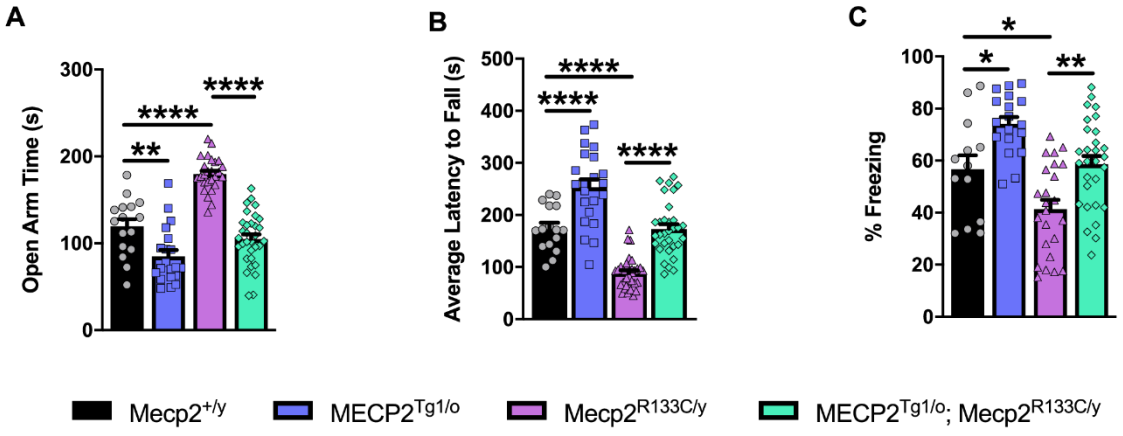

Figure 13: Bi-directionally affected phenotypes are reversed in *Mecp2*$^{R133C/y}$ mice after expression of an *MECP2* transgene. (A-C) Opposing phenotypes were observed in *MECP2*$^{Tg1/o}$ and *Mecp2*$^{R133C/y}$ mice in anxiety-related behavior (n = 16-32 per genotype) (A), motor coordination (n = 16-33 per genotype) (B), contextual fear learning and

memory (n = 13-29 per genotype) (C). Introducing the *MECP2* transgene in *Mecp2*$^{R133C/y}$ mice normalized these phenotypes to WT levels. 1-way ANOVA with Tukey's post-hoc test. *p < 0.05, **p < 0.01, ****p < 0.0001. WT = filled black bars or circles. *MECP2*$^{Tg1/o}$ = filled blue bars or squares. *Mecp2*$^{R133C/y}$ = filled purple bars or triangles. *MECP2*$^{Tg1/o}$; *Mecp2*$^{R133C/y}$ = filled green bars or diamonds.

2.6.4. Phenotype-specific effect in female *Mecp2*$^{R133C/+}$ mice with wild-type *MECP2* transgene

The beneficial effects observed with the introduction of an *MECP2* transgene in male *Mecp2*$^{R133C/y}$ mice were anticipated, as global MeCP2 disruption would be predicted to result in increased severity, and consequently, a larger window before MDS-like phenotypes are observed. We next investigated if this reversal would also hold true in female *Mecp2*$^{R133C/+}$ mice as they 1) are mosaic for mutant and wild-type MeCP2, 2) exhibit milder phenotypes than male mice, and 3) show normal baseline MeCP2 protein levels in the cortex, hippocampus and cerebellum (Figure 9B). Furthermore, the MeCP2 protein expression in *MECP2*$^{Tg1/o}$; *Mecp2*$^{R133C/+}$ mice was increased and comparable to that in *MECP2*$^{Tg1/o}$ mice in most brain regions (Figure 11D-F).

General physical characteristics, specifically weight and hindlimb clasping, were similar in *MECP2*$^{Tg1/o}$; *Mecp2*$^{R133C/+}$ mice and WT littermates across age (Figure 14A-B, p-value indicated for *MECP2*$^{Tg1/o}$; *Mecp2*$^{R133C/+}$ vs *Mecp2*$^{R133C/+}$ comparison, (weight) mixed-effects analysis, $F(3,135) = 11.36$, $p < 0.01$ (5, 10 and 25 weeks old), $p < 0.0001$ (15 and 20 weeks old), (hindlimb clasping) ANOVA, $F(3,125) = 21.23$, $p < 0.0001$ (overall), $F(3,125) = 21.54$, $p < 0.001$ (22-25 weeks old), $p < 0.0001$ (20-23 and 24-28 weeks old)), suggesting that increasing *MECP2* dosage corrected weight deficits and the clasping phenotype. This reversal effect with the *MECP2* transgene was also observed in the attenuated acoustic startle response and lack of social preference in *Mecp2*$^{R133C/+}$ mice (Figure 14C-D, ANOVA, $F(3,74) = 9.971$, $p < 0.0001$ (*MECP2*$^{Tg1/o}$; *Mecp2*$^{R133C/+}$ vs *Mecp2*$^{R133C/+}$) (acoustic startle response), $F(2,204) = 239.6$, $p <$

0.01, (*MECP2*$^{Tg1/o}$; *Mecp2*$^{R133C/+}$ familiar mouse vs novel mouse) (social preference)). As illustrated in the representative traces and number of apneas, *MECP2*$^{Tg1/o}$; *Mecp2*$^{R133C/+}$ mice showed comparable apneas to WT littermates, again without changes in other breathing parameters (Figure 14E, ANOVA, p-value indicated for *MECP2*$^{Tg1/o}$; *Mecp2*$^{R133C/+}$ vs *Mecp2*$^{R133C/+}$ comparison, $F(3,107) = 12.67$, $p < 0.0001$ (apnea), $F(3,107) = 1.007$, $p > 0.05$ (breathing frequency), $F(3,107) = 1.353$, $p > 0.05$ (inspiratory time), $F(3,107) = 0.3095$, $p > 0.05$ (expiration time)).

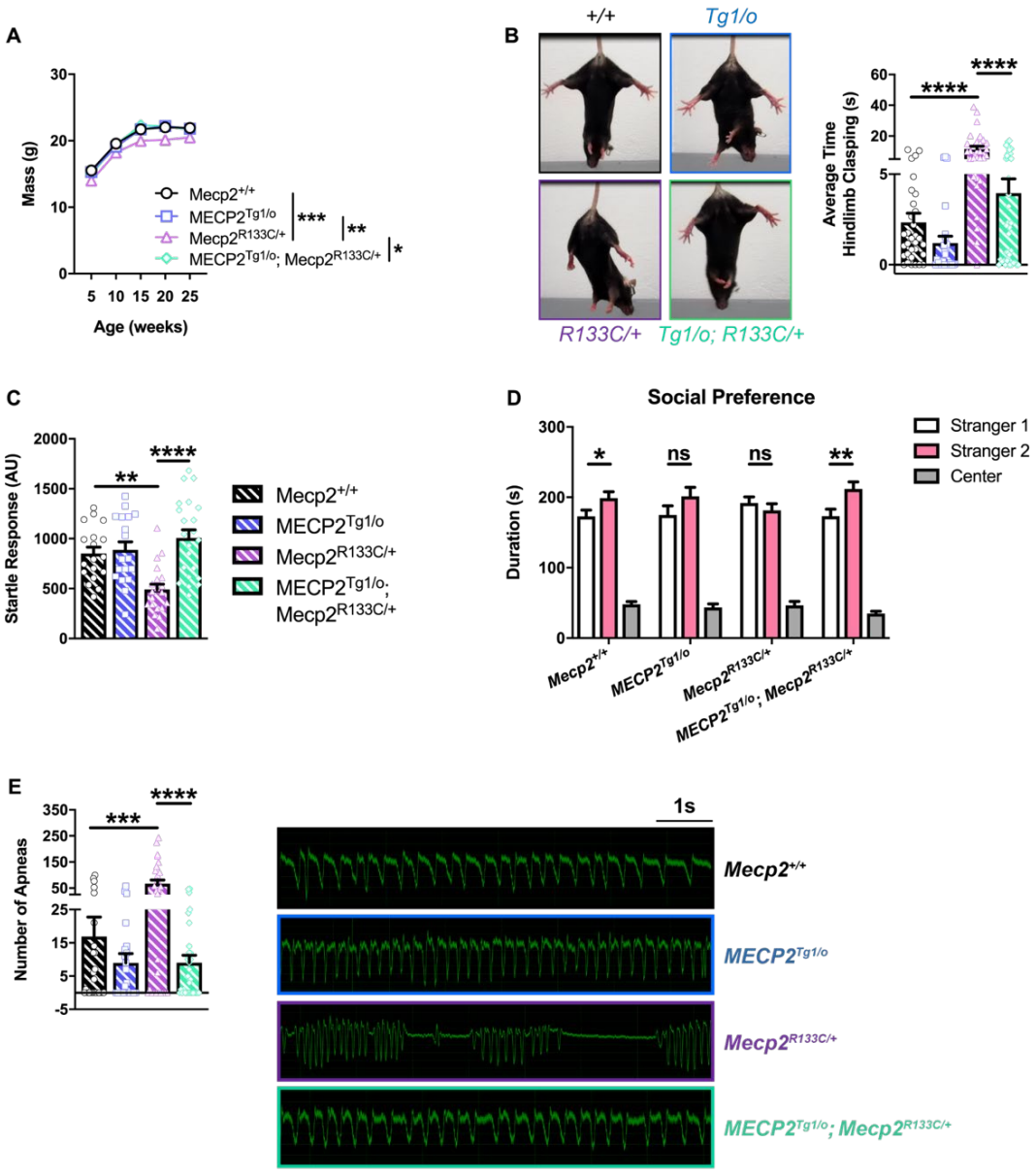

Figure 14: Additional wild-type *MECP2* normalizes a subset of phenotypes in *Mecp2*$^{R133C/+}$ mice. (A-E) *MECP2*$^{Tg1/o}$*; Mecp2*$^{R133C/+}$ mice exhibited similar weight (n = 14-26 per genotype) (A), hindlimb clasping behavior (n = 26-40 per genotype) (B), acoustic startle response (n = 18-22 per genotype) (C), social preference (n = 25-31 per genotype) (D), and number of apneas (n = 25-33 per genotype) (E) as WT littermates, illustrating a reversal of abnormal phenotypes observed in *Mecp2*$^{R133C/+}$ mice. Representative hindlimb clasping and apnea traces are shown. Mixed-effects analysis, or 1- or 2-way ANOVA with Tukey's or t-test post-hoc. ns (not significant), *p < 0.05, **p < 0.01, ***p < 0.001, ****p < 0.0001. WT = patterned black bars or open circles. *MECP2*$^{Tg1/o}$ = patterned blue bars or open squares. *Mecp2*$^{R133C/+}$ = patterned purple bars or open triangles. *MECP2*$^{Tg1/o}$*; Mecp2*$^{R133C/+}$ = patterned green bars or open diamonds.

We next evaluated the performance of *MECP2*$^{Tg1/o}$*; Mecp2*$^{R133C/+}$ mice in the bi-directionally affected symptom domains of anxiety, motor coordination and associative learning and memory. Similar to their male counterparts, female *MECP2*$^{Tg1/o}$ mice displayed increased anxiety, enhanced performance in the accelerated rotarod, and an excessive contextual fear conditioning response (Figure 15A-C, ANOVA, p-value indicated for *Mecp2*$^{+/+}$ vs *MECP2*$^{Tg1/o}$ comparison, $F(3,123) = 21.46$, $p < 0.05$ (anxiety), $F(3,125) = 38.86$, $p < 0.0001$ (motor coordination), $F(3,111) = 12.63$, $p < 0.0001$ (contextual fear conditioning)). Notably, these phenotypes were also observed in *MECP2*$^{Tg1/o}$*; Mecp2*$^{R133C/+}$ mice, which although not as robust as *MECP2*$^{Tg1/o}$ mice alone, were significantly different from WT littermates (ANOVA, p-value indicated for *Mecp2*$^{+/+}$ vs *MECP2*$^{Tg1/o}$*; Mecp2*$^{R133C/+}$ comparison, $F(3,123) = 21.46$, $p < 0.05$ (anxiety), $F(3,125) = 38.86$, $p < 0.001$ (motor coordination), $F(3,111) = 12.63$, $p < 0.01$ (contextual fear conditioning)). To confirm that these MDS-like phenotypes were linked to preserved function of the *R133C* allele, we applied a similar approach in introducing the *MECP2* transgene in *Mecp2*$^{Null/+}$ mice. In contrast to the *Mecp2*$^{R133C/+}$ mice, *MECP2*$^{Tg1/o}$*; Mecp2*$^{Null/+}$ animals were not significantly different from their WT counterparts in all three assays (Figure 15D-F, all $p > 0.05$ for *Mecp2*$^{+/+}$ vs *MECP2*$^{Tg1/o}$*; Mecp2*$^{Null/+}$ comparison, $F(3,60) = 7.374$ (anxiety), $F(3,67) = 30.82$ (motor coordination), $F(3,58) = 21.01$ (contextual fear conditioning)). Aside from the anxiety-related behavior, wherein *MECP2*$^{Tg1/o}$ mice did not spend less time in the open arms, *MECP2*$^{Tg1/o}$*; Mecp2*$^{Null/+}$ were significantly different from *MECP2*$^{Tg1/o}$ mice in motor coordination and contextual freezing (ANOVA, p-value indicated for *MECP2*$^{Tg1/o}$ vs *MECP2*$^{Tg1/o}$*; Mecp2*$^{R133C/+}$ comparison, $F(3,60) = 7.374$, $p > 0.05$ (anxiety), $F(3,67) = 30.82$, $p < 0.05$ (motor coordination), $F(3,58) = 21.01$, $p < 0.05$ (contextual fear conditioning)). Altogether, these results suggest that expression of the *MECP2* transgene in the clinically relevant *Mecp2*$^{R133C/+}$ genetic background may result in “MDS-like” phenotypes, and potentially points to a narrower therapeutic window for MeCP2-targeted therapeutics when used with mild hypomorphic mutations.

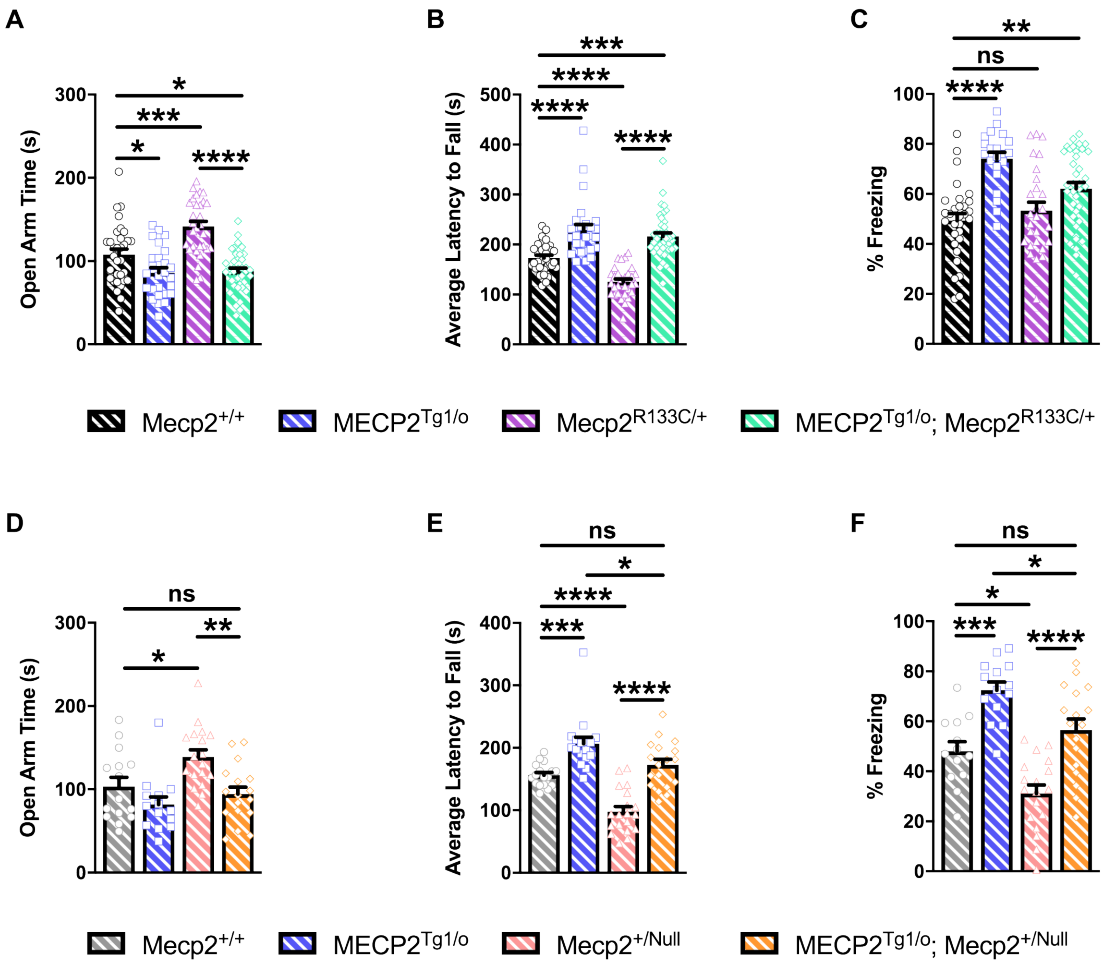

Figure 15: *Mecp2*$^{R133C/+}$ mice with additional wild-type *MECP2* develop MDS-like phenotypes in anxiety, motor and cognitive assays. *MECP2*$^{Tg1/o}$ and *Mecp2*$^{R133C/+}$ or *Mecp2*$^{Null/+}$ mice exhibited contrasting phenotypes in anxiety-related behavior (A, D), motor coordination (B, E), and contextual fear learning and memory (D, F). (A-C) *MECP2*$^{Tg1/o}$; *Mecp2*$^{R133C/+}$ mice phenocopied *MECP2*$^{Tg1/o}$ mice and significantly differed from WT littermates, with enhanced anxiety (A), motor coordination (B) and contextual freezing (C). n = 21-40 per genotype. (D-F) In contrast, *MECP2*$^{Tg1/o}$; *Mecp2*$^{Null/+}$ mice were indistinguishable from WT littermates and/or significantly different from *MECP2*$^{Tg1/o}$. n = 13-19 per genotype. 1-way ANOVA with Tukey's post-hoc test. Ns (not significant), *p < 0.05, **p < 0.01, ***p < 0.001, ****p < 0.0001. WT = patterned black or grey bars or open circles. *MECP2*$^{Tg1/o}$ = patterned blue bars or open squares. *Mecp2*$^{R133C/+}$ = patterned purple bars or open triangles. *MECP2*$^{Tg1/o}$; *Mecp2*$^{R133C/+}$ = patterned green bars or open diamonds. *Mecp2*$^{Null/+}$ = patterned pink bars or open triangles. *MECP2*$^{Tg1/o}$; *Mecp2*$^{Null/+}$ = patterned orange bars or open diamonds.

2.7. Discussion

In the past decade, gene therapy research for RTT has significantly increased, emerging as a feasible and exciting treatment option (*93*, *112*, *113*, *115*, *116*, *119*). Most recently, a report described the efficacy and safety of a self-complementary AAV9 (scAAV9) encoding for the human *MECP2* in male *Mecp2 null* mice and non-human primate models (*119*). While encouraging, the majority of preclinical studies regarding gene therapy for RTT have not examined safety in the context of mosaic females (with the notable exception of (*113*) and (*118*)). Furthermore, these preclinical studies do not address the impact of hypomorphic MeCP2 mutations on therapeutic index, except for the study by (*95*), which illustrated the effects of increasing MeCP2 expression in male mice that were hemizygous for the missense mutation *R306C*. It is widely accepted that many missense *MECP2* mutations are correlative with milder clinical severity as a result of preserved protein function and stability. In this study, we sought to complement existing efforts to generate MeCP2-based therapeutics by addressing aspects of this diverse clinical landscape. Specifically, we asked whether a 1x increase in MeCP2 dosage from conception would rescue phenotypes in *Mecp2*$^{R133C/y}$ and *Mecp2*$^{R133C/+}$ mice without evoking MDS-like adverse effects.

The *R133C* mutation is one of most common mutations in patients but it also leads to a mild presentation of the disease, similar to *R306C* (*60*, *357*, *359*). Here, we behaviorally validated the *Mecp2 R133C* mice as a hypomorphic mutant mouse model of RTT. Both male and female *Mecp2 R133C* mice exhibited RTT-like phenotypes, with the exception of a normal contextual fear response in female *Mecp2*$^{R133C/+}$ mice, which differs from what is commonly observed in *Mecp2*$^{Null/+}$ animals (*70*, *79*, *124*, *137*, *368*). This further supports the clinical observation that the *R133C* mutation is not a functional *null* allele, but rather is hypomorphic and conveys a milder phenotype. Additionally, our data are in agreement with previous reports of *Mecp2 R133C* and *Mecp2 R306C* mice, as well as constitutive hypomorphic *Mecp2*$^{flox/y}$ mice, which have a 50% reduction in MeCP2 expression (*72*, *95*, *98*, *325*, *369*). The lack of abnormal PPI contrasted from previous findings

wherein enhanced PPI was observed in *Mecp2*$^{tm1.1Jae}$ heterozygous females, *Mecp2*$^{flox/y}$ mice, and glutamatergic- or GABAergic-specific *Mecp2* knockout mice (*139*, *72*, *325*, *370*). However, compared to these studies, which utilized older mice of different background strains, we evaluated PPI at 6-7 weeks of age for both male and female *Mecp2 R133C* mice to account for the hearing loss that mice of the C57Bl6 background strain begin to experience at 8 weeks of age. Therefore, it is possible that older *Mecp2 R133C* mice could exhibit altered PPI.

As has been previously posited (*98*), the milder phenotypes seen in the *Mecp2 R133C* animals are likely attributed to partial functional loss of MeCP2. This hypothesis was supported by our protein expression data demonstrating that expression of the *R133C allele* was comparable to WT MeCP2 in two brain regions, cortex and cerebellum, in these mice. Interestingly, we observed a decrease in hippocampal MeCP2 protein expression in male *Mecp2*$^{R133C/y}$ mice that was not observed in female *Mecp2*$^{R133C/+}$ mice. While mosaicism would be predicted to dilute the mutant allele's aggregate impact on hippocampal MeCP2 expression, this sex-specific disconnect could explain the associative learning and memory phenotype that was distinct between the male and female *Mecp2 R133C* animals, where only male mice exhibited a contextual fear conditioning deficit.

To model an optimal 1x rescue of MeCP2 protein, we genetically introduced a human *MECP2* transgene into *Mecp2 R133C* mice. We demonstrated that all of the abnormal phenotypes observed in male *Mecp2*$^{R133C/y}$ mice were reversed to that of wild-type behavior when the *MECP2* transgene was expressed, which is highly encouraging. These reversal effects support the conclusion that global MeCP2 mutation or loss broadens the range in which MeCP2 can be increased before MDS-like phenotypes emerge. Our results are similar to previous studies illustrating that genetically increasing MeCP2 expression in male *Mecp2 R306C* mice corrected several RTT-like phenotypes such as deficits in motor function and contextual fear learning and

memory (*95*). In addition, other MeCP2-targeting genetic strategies, such as postnatal reactivation of *Mecp2*, neuronal-specific germline introduction of *Tau-Mecp2*, and viral delivery of human *MECP2* in *Mecp2 null* mice improved phenotypes (*71*, *101*, *102*, *112*, *113*, *115*, *116*, *119*). Collectively, these findings support the potential use of MeCP2-targeted approaches for male RTT patients with the *R133C* mutation.

To address the impact of a hypomorphic mutation in a mosaic context, which would occur in female patients, we evaluated the consequences of this genetic strategy in female *Mecp2*$^{R133C/+}$ mice. Encouragingly, the majority of the RTT-like phenotypes in *Mecp2*$^{R133C/+}$ mice were normalized with the additional *MECP2* transgene. These findings are in agreement with previous reports of phenotypic reversal with systemic delivery of full-length MeCP2 in female *Mecp2*$^{Null/+}$ mice, increased MeCP2 expression in *Mecp2 T158M* mice or germline introduction of human *MECP2* in mice harboring the *R255X* mutation (*74*, *82*, *113*, *118*). While increased expression of *MECP2* was able to correct a number of deficits in female *Mecp2 R133C* mice, three phenotypes, anxiety, motor coordination and contextual fear conditioning, were mildly yet significantly “over-corrected”, and the resulting phenotypes mirrored those of MDS model animals. These data are different from a previous report where genetically increasing MeCP2 protein expression in female *Mecp2 T158M* or *R255X* mice reversed motor coordination and contextual freezing to WT behavior levels (*74*, *82*). Interestingly, despite lacking an anxiolytic phenotype, the female *Mecp2 R255X* mice were unaffected with addition of the *MECP2* transgene. However, the *R255X* mutation is different from the *R133C* mutation in that no protein is produced in *Mecp2 R255X* mice (*74*). Similarly, the *T158M* mutation decreases protein expression and renders the protein nonfunctional, causing a more severe form of the disorder, similar to *Mecp2 null* animals (*98*). Furthermore, the motor coordination phenotype observed in the *Mecp2*$^{R133C/+}$ mice with the *MECP2* transgene was different from a previous study showing that virally-delivered MeCP2 post-symptom onset improved attenuated motor behavior in *Mecp2*$^{Null/+}$ mice (*113*), as well as a recent report that pre-

symptom onset delivery of viral MeCP2 did not affect motor coordination in *Mecp2*$^{Null/+}$ mice (*118*). Nonetheless, these previous studies are all in agreement with our results showing that, in *Mecp2*$^{Null/+}$ mice, addition of the *MECP2* transgene reversed attenuated anxiety and performance in motor coordination and contextual freezing tasks to levels seen in WT littermates. Altogether, our data suggest that the development of MDS-like phenotypes is due to the impact that the *R133C* MeCP2 mutation has on therapeutic index.

We believe that this study provides important information regarding the feasibility of increasing MeCP2 expression in mosaic female RTT model mice engineered to have a common hypomorphic mutation in MeCP2. Our findings illustrate the promise of MeCP2-targeted therapies for male and female RTT patients with an *R133C MECP2* mutation. However, our data suggest that careful consideration may be required to avoid adverse effects when considering dosage of prospective MeCP2-based therapeutics in female *R133C* RTT patients, as preserved function may result in a narrowing of the therapeutic window. One caveat to our studies is that our genetic approach increases MeCP2 levels from conception, which is different from current MeCP2-targeted treatment strategies that deliver viral MeCP2 after disease onset. It has been hypothesized that post-mitotic neurons may be more forgiving with regard to the amount of MeCP2 that can be delivered before adverse effects present. It is unknown whether this same caveat can also be applied to efficacy, where post-mitotic neurons could be less responsive to a 1x increase in MeCP2 protein. Future experiments will be required to determine if either scenario is true, and, if so, what impact this has on therapeutic development. In summary, this study contributes valuable safety data to ongoing efforts to develop MeCP2-targeted therapeutics that are both safe and effective. Furthermore, these studies highlight the need for similar investigations in other pathological hypomorphic mutations of RTT, and their inclusion in preclinical development efforts.

CHAPTER 3

GENETIC INCREASE OF MeCP2 IN PITT-HOPKINS SYNDROME MOUSE MODEL

Summary of findings depicted in Figure 16 and detailed in Table 2.

Supplementary tables pertaining to RNA-sequencing data are provided as external files.

3.1 Abstract

Pitt-Hopkins syndrome (PTHS) is a rare neurodevelopmental disorder caused by loss-of-function (LOF) mutations in the *Transcription Factor 4* (*TCF4*) gene. Interestingly, PTHS closely resembles Rett syndrome (RTT), another neurodevelopmental disorder caused by LOF mutations in a related gene, *Methyl-CpG-Binding Protein 2* (*MECP2*). These two disorders share molecular and behavioral phenotypes, including cognitive and motor dysfunction, in both the preclinical and clinical settings. Based upon this phenotypic/symptom overlap, and the potential clinical application of normalizing *MECP2* gene dosage for RTT, we investigated the hypothesis that genetic supplementation of MeCP2 would reverse the abnormal phenotypes in PTHS model mice that are Tcf4 haploinsufficient, *Tcf4*$^{+/-}$. Genetic introduction of a wild-type *MECP2* transgene from MeCP2-overexpressing mice to *Tcf4*$^{+/-}$ mice reversed the phenotypes of *Tcf4*$^{+/-}$ animals, specifically hyperlocomotion, attenuated anxiety and contextual fear learning and memory deficit. Molecular experiments suggest that MeCP2 does not impact Tcf4 expression, suggesting a more complex relationship between these two proteins. Subsequent total RNA-sequencing studies identified creatine- and myelination-associated genes and pathways as likely explanations of the behavioral effects. However, creatine metabolites were unchanged in *Tcf4*$^{+/-}$ animals and reduced expression of myelination markers in *Tcf4*$^{+/-}$ mice were not changed with the *MECP2* transgene. Studies are ongoing to determine the mechanism(s) underlying the behavioral reversal. Overall, our preclinical data suggest that the treatment strategy of increasing MeCP2 dosage could potentially be leveraged for PTHS.

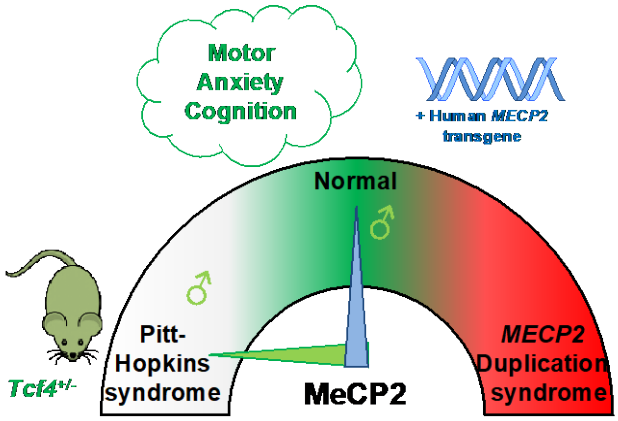

Figure 16: Summary of MeCP2 supplementation effects in *Tcf4 mutant* mice. Addition of human *MECP2* transgene (blue arrow) normalizes phenotypes of male *Tcf4*$^{+/-}$ animals (green arrow) in motor, anxiety and cognition domains.

3.2 Introduction

Pitt-Hopkins syndrome (PTHS) is a rare neurodevelopmental disorder that is characterized by autism-associated symptoms including microcephaly, intellectual disability, speech and motor dysfunction, breathing abnormalities, and seizures (*175*, *177*, *178*). Nearly 30 years after the original patient observations (*183*), two independent reports linked PTHS with *de novo* loss-of-function (LOF) or dominant-negative mutations in *Transcription Factor 4* (*TCF4*), a gene located on chromosome 18 (*205*, *206*). The encoded class I basic helix-loop-helix (bHLH) protein or E-protein, TCF4, imparts its transcriptional activity through homo- or hetero-dimerization with TCF4 variants or other bHLH transcription factors (*371*). There are at least 18 characterized isoforms, which differ primarily due to the structure of the N-terminus (*196*). As such, TCF4 variants can lack all or some of the N-terminal transactivation domain (AD1) and/or the nuclear localization signal, which impacts the degree of transcriptional activity or subcellular localization of TCF4, respectively. All variants, however, contain the C-terminal bHLH domain that is functionally essential for the DNA-binding ability of TCF4, as well as the AD2 region that is sufficient for TCF4's activity and acts in a synergistic fashion with AD1 if present.

Variability in TCF4 expression and function is further compounded in PTHS by the presence of *TCF4* mutations. Although the majority of pathogenic mutations in TCF4 are located within the bHLH domain (*201*, *208*), numerous mutations, such as gene deletions, have been identified throughout the *TCF4* gene (*181*). Each mutation imparts varying modifications, including protein instability, subcellular localization alterations and functional impairments that modify homo- or hetero-dimerization formation and DNA-binding capability, which all ultimately affect the transcriptional activity of TCF4 (*208*, *371*). The array of pathogenic mutations and consequent functional changes in TCF4 could, in part, influence the phenotypic diversity observed in patients as well as pose a challenge in treatment strategies aimed to replace the TCF4 gene or protein and/or enhance the function of TCF4. Regardless of this potential challenge, research efforts focused on genetic normalization of TCF4 expression and/or function are ongoing. These are supported by a study showing that a slight increase in Tcf4 levels in *Tcf4*$^{+/-}$ mice rescued hippocampal-dependent cognitive deficits and a recent report illustrating that post-natal increase of Tcf4 levels in *Tcf4 mutant* animals reversed similar phenotypes in addition to hyperactivity, heightened anxiety and EEG abnormalities (*215*, *222*). Conversely, overexpressing Tcf4 in mice resulted in altered cortical development and deficits in sensorimotor gating and associative learning and memory in fear conditioning tasks (*220*, *221*). While these studies suggest that TCF4-based replacement may be therapeutically advantageous, they also highlight a potentially narrow therapeutic window, and thus warrant exploration of other treatment options.

In this study, we investigated the feasibility of leveraging *Methyl-CpG-binding Protein 2* (*MECP2*)-targeted gene therapy, which is currently being strongly explored for Rett syndrome (RTT), another rare neurodevelopmental disorder. Recent studies using preclinical rodent models of RTT, which is predominantly caused by LOF mutations in *MECP2*, have shown that genetic normalization of MeCP2 gene dosage before or after symptom onset rescues phenotypes (*93*, *112*, *113*, *115*, *116*, *119*). Interestingly, prior to the connection of PTHS to *TCF4* variants, patients

were historically diagnosed with other disorders, including RTT, due to the similarity in symptoms (*372*). The clinical similarity between PTHS and RTT is also conserved in preclinical models of these disorders, suggesting that treatment for one could be efficacious for the other. PTHS model mice that are haploinsufficient for *Tcf4* (*Tcf4*$^{+/-}$) display abnormal dendritic complexity that is seen in *Mecp2 null* animals or other RTT mouse models with compromised MeCP2 protein function or expression (*332*, *373*). Such structural abnormalities translate to physiological aberrations as *Tcf4* and *Mecp2 mutant* mice exhibit synaptic plasticity deficiencies, including impaired long-term hippocampal synaptic plasticity (*70*, *212*, *215*). At the behavioral level, seizures, attenuated anxiety, and cognitive deficits, such as in the form of impaired fear learning and memory, are also observed in these disease model mice (*70*, *137*, *212*, *215*, *374*, *375*). Notably, these shared characteristics of motor, anxiety and cognitive dysfunction between PTHS and RTT are antiparallel to those of a related disorder that has increased MeCP2 expression, *MECP2* Duplication syndrome (MDS) (*105*, *168*).

Given the overlap in symptomology between RTT and PTHS, as well as the contrasting phenotypes of both diseases with MDS, we explored here the hypothesis that increasing MeCP2 expression would reverse phenotypes in *Tcf4*$^{+/-}$ animals. For genetic supplementation of MeCP2, we crossed *Tcf4*$^{+/-}$ and MDS model mice, *MECP2*$^{Tg1/o}$, to congenitally introduce a wild-type functional MeCP2 allele into *Tcf4*$^{+/-}$ animals. The increased MeCP2 dosage reversed abnormal phenotypes of *Tcf4*$^{+/-}$ animals, specifically hyperlocomotion, attenuated anxiety and deficits in associative learning and memory. Although increasing MeCP2 levels did not influence the expression of *Tcf4*, transcriptomic studies revealed a relatively small set of differentially expressed genes (DEGs) and molecular pathways that were significantly altered in *Tcf4*$^{+/-}$ and *MECP2*$^{Tg1/o}$; *Tcf4*$^{+/-}$ animals, in particular those that are involved in creatine production and myelination. Globally, however, the RNA sequencing results suggest minimal overlap between genes changed in the context of MeCP2 overexpression or Tcf4 loss. Given that creatine

deficiency has been implicated in other neurodevelopmental disorders such as RTT (*376*, *377*) and that myelination defects have been previously shown as characteristics of *Tcf4*$^{+/-}$ animals (*378*), we interrogated the hypothesis that MeCP2 supplementation rescues creatine deficiency and hypomyelination. Here, we show that *Tcf4*$^{+/-}$ mutant animals do not have altered plasma creatine and creatinine metabolite composition. We did confirm reduced myelination in *Tcf4*$^{+/-}$ mice, but observed no effect of the *MECP2* transgene. Further analysis of the RNA-sequencing data is ongoing to uncover potential molecular mechanisms.

Overall, our data here provide proof-of-concept results that, preclinically, PTHS may be amenable to treatment aimed at increasing MeCP2 dosage. Additionally, the behavioral efficacy observed could be explained by the normalization of disrupted genes and pathways. In short, this study proposes that *MECP2*-based therapeutic strategies could be leveraged for PTHS.

3.4 Materials and Methods

Animals: All animals used in the present study were group housed with food and water given ad libitum and maintained on a 12 hr light/dark cycle. Animals were cared for in accordance with the National Institutes of Health *Guide for the Care and Use of Laboratory Animals*. All studies were approved by the Vanderbilt Institutional Animal Care and Use Committee and took place during the light phase. *Tcf4*$^{+/-}$ mice were cryorecovered from The Jackson Laboratory (B6;129-Tcf4^{tm1Zhu}/J, stock no. 013598), and maintained by breeding male *Tcf4*$^{+/-}$ with female WT C57BL/6Jx129S F1 hybrid mice (The Jackson Laboratory, B6129SF1/J, stock no. 101043). *MECP2*$^{Tg1/o}$ mice (C57BL/6J background) were generously shared by Dr. Jeffrey Neul (Vanderbilt University). Experimental mice were obtained by crossing *Tcf4*$^{+/-}$ and *MECP2*$^{Tg1/o}$ mice. Male mice were aged until the predicted symptomatic age of 20 weeks old for all experiments. Mice used for behavioral experiments were different from those utilized for molecular assays, with the exception of the creatine/creatinine detection.

Total Protein Extraction: The cortex, hippocampus, striatum and cerebellum were microdissected from naïve 20-25 week-old mice. Total protein was prepared as previously described in (*362*). Briefly, tissue samples were homogenized using a hand-held motorized mortar and pestle in radioimmunoprecipitation assay buffer (RIPA) containing 10 mM Tris-HCl, 150 mM NaCl, 1 mM ethylenediaminetetraacetic acid (EDTA), 0.1% sodium dodecyl sulfate (SDS), 1% Triton X-100, and 1% deoxycholate (Sigma, St. Louis, MO, USA). After homogenization, samples were centrifuged and the supernatant was collected. Protein concentration was determined using a bicinchoninic acid (BCA) protein assay (Pierce, ThermoFisher, Waltham, MA, USA).

SDS-PAGE and Western Blotting: 50 µg of total protein from the cortex, hippocampus, striatum and cerebellum was electrophoretically separated using a 4-20% (for MeCP2) or 12% (for Tcf4) SDS polyacrylamide gel and transferred onto a nitrocellulose membrane (Criterion™ Blotter, Bio-

Rad, Hercules, CA, USA (for MeCP2)) or a PVDF membrane (iBlot2, ThermoFisher, Waltham, MA, USA (for Tcf4)). Membranes were blocked in TBS Odyssey blocking buffer (LI-COR) for 1 hr at room temperature. Membranes were blocked in TBS Odyssey blocking buffer (LI-COR, Lincoln, NE, USA) for 1 hr at room temperature. Membranes were probed with primary antibodies overnight at 4 °C: rabbit anti-MeCP2 (1:1000, Millipore cat no. 07-013, Burlington, MA, USA), rabbit anti-Tcf4 (1:1000, ProteinTech cat no. 22337-1-AP, Rosemont, IL, USA) and mouse anti-Gapdh (1:1000, ThermoFisher cat. no. MA5-15738, Waltham, MA, USA), followed by the fluorescent secondary antibodies: goat anti-rabbit (800 nm, 1:5000, LI-COR, Lincoln, NE, USA) and goat anti-mouse (680 nm, 1:10,000, LI-COR, Lincoln, NE, USA). Fluorescence was detected using the Odyssey Infrared Imager (LI-COR, Lincoln, NE, USA) at the Vanderbilt University Medical Center Molecular Cell Biology Resource (MCBR) Core then quantified using the Image Studio Lite software (LI-COR, Lincoln, NE, USA). Values were normalized to Gapdh and compared relative to wild-type controls.

Total RNA Extraction: The cortex, hippocampus, striatum and cerebellum were microdissected from naïve 20-25 week-old mice. Total RNA was prepared from tissue samples using TRIzol Reagent (ThermoFisher, Waltham, MA, USA) and isolated using a RNeasy Mini Kit (Qiagen, Hilden, Germany) in accordance with the manufacturer's instructions. Total RNA was DNase-treated with RNase-Free DNase Set (Qiagen, Hilden, Germany). Using one set of RNA samples from all the brain regions mentioned above, cDNA from 2 µg of total RNA was synthesized using SuperScript™ VILO™ cDNA Synthesis Kit (ThermoFisher cat no. 11754050, Waltham, MA, USA) for qRT-PCR analysis. A different set of RNA samples from the hippocampus and striatum were used for RNA-sequencing analysis.

Quantitative Real-Time PCR (qRT-PCR): qRT-PCR (CFX96, Bio-Rad Hercules, CA, USA, equipment located at the Vanderbilt University Medical Center MCBR core) on 50 ng /9 µL cDNA

from the cortex, hippocampus, striatum and cerebellum was run in duplicate using PowerUp™ SYBR™ Green Master Mix (ThermoFisher cat no. A25742, Waltham, MA, USA) with the following primers (5' to 3'): *Mecp2* (exon 4, forward: ATGAGACTGTGCTCCCCATC, reverse: TTTTCTCACCAAGGGTGGAC, 80 bp), *Tcf4* (exon 18, forward: CCCAGACCAAGCTCCTGATT, reverse: CATGTGATTCGCTGCGTCTC, 194 bp), *Gamt* (exons 1-2, forward: CCCTATATGCATGCGCTAG, reverse: TAATCCAGTGTTCCTCTATGGG, 124 bp) and *Gapdh* (exon 6, forward: CGACTTCAACAGCAACTCCC, reverse: GCCGTATTCATTGTCATACCAGG, 106 bp). All primer sequences were designed using Primer3 and constructed by Sigma through the Vanderbilt University Medical Center MCBR core. Ct values for each sample were normalized to *Gapdh* expression and analyzed using the delta−delta Ct method as described in (*137*). Values exceeding two times the standard deviation were classified as outliers. Each value was compared to the average delta-Ct value acquired for wild-type controls and calculated as percent-relative to the average control delta-Ct.

RNA-sequencing (RNA-seq) Analysis: Extracted RNA samples were sent to Genewiz (South Plainfield, NJ), wherein samples were quantified using Qubit 2.0 Fluorometer (Life Technologies, Carlsbad, CA, USA) and RNA integrity was checked using Agilent TapeStation 4200 (Agilent Technologies, Palo Alto, CA, USA). Further analysis, including RNA library preparation, sequencing, and initial bioinformatics analysis, were also conducted by Genewiz.

Library Preparation with Poly A Selection: RNA sequencing libraries were prepared using the NEBNext Ultra RNA Library Prep Kit for Illumina following manufacturer's instructions (NEB, Ipswich, MA, USA). Briefly, mRNAs were first enriched with Oligo(dT) beads. Enriched mRNAs were fragmented for 15 min at 94 °C. First strand and second strand cDNAs were subsequently synthesized. cDNA fragments were end repaired and adenylated at 3'ends, and universal adapters were ligated to cDNA fragments, followed by index addition and library enrichment by

limited-cycle PCR. The sequencing libraries were validated on the Agilent TapeStation (Agilent Technologies, Palo Alto, CA, USA), and quantified by using Qubit 2.0 Fluorometer (Invitrogen, Carlsbad, CA) as well as by quantitative PCR (KAPA Biosystems, Wilmington, MA, USA).

HiSeq Sequencing: The sequencing libraries were pooled and clustered on 4 lanes of a Flowcell. After clustering, the Flowcell was loaded on the Illumina HiSeq instrument (4000 or equivalent) according to manufacturer's instructions. The samples were sequenced using a 2x150 bp Paired End (PE) configuration. Image analysis and base calling were conducted by the HiSeq Control Software (HCS). Raw sequence data (.bcl files) generated from Illumina HiSeq was converted into FASTQ files and de-multiplexed using Illumina's bcl2fastq 2.17 software. One mismatch was allowed for index sequence identification.

Data Analysis: After investigating the quality of the raw data, sequence reads were trimmed to remove possible adapter sequences and nucleotides with poor quality using Trimmomatic v.0.36. The trimmed reads were mapped to the *Mus musculus* reference genome available on ENSEMBL using the STAR aligner v.2.5.2b. The STAR aligner is a splice aligner that detects splice junctions and incorporates them to help align the entire read sequences. BAM files were generated as a result of this step. Unique gene hit counts were calculated by using feature Counts from the Subread package v.1.5.2. Only unique reads that fell within exon regions were counted. After extraction of gene hit counts, the gene hit counts table was used for downstream differential expression analysis. Using DESeq2, a comparison of gene expression between the groups of samples was performed. The Wald test was used to generate p-values and Log2 fold-changes. Genes with adjusted p-values < 0.05 were called as differentially expressed genes for each comparison. Gene ontology (GO) and pathway analysis was performed on the statistically significant set of genes by utilizing the freely available online bioinformatics resource tools DAVID Functional Annotation Bioinformatics Microarray Analysis (https://david.ncifcrf.gov) and

Reactome Pathway Database (https://reactome.org). The GO list, which includes biological processes (BP), cellular component (CC) and molecular function (MF), was generated along with a list of statistically significant pathways from the Kyoto Encyclopedia of Genes and Genomes (KEGG) Pathway Database. All raw RNA-seq data will be stored at the National Institutes of Health Sequence Read Archive (SRA) upon publication.

Behavioral Assays: All behavioral experiments were conducted from the predicted symptomatic age (20-26 weeks) at the Vanderbilt Mouse Neurobehavioral (MNL) Core. Each mouse was utilized in multiple assays and conducted in the following order: open field, elevated zero maze, and contextual fear conditioning; a minimum of 3 days elapsed between each assay. For each assay, mice were habituated to the testing room for 1 hr prior to the experiment. Quantification was performed either by a researcher blinded to the genotype or by automated software.

Open Field: Mice were placed in an activity chamber for 1 hr and locomotor and vertical activities were quantified as beam breaks in the X, Y and Z axis using Activity Monitor software (Med Associates Inc, St. Albans, VT, USA).

Elevated Zero Maze: Mice were placed on a continuous circular platform with two closed and two open regions for 5 min under full light conditions (~700 lux in the open regions, ~400 lux in the closed regions). The time spent exploring the open regions were quantified by ANY-maze software (Stoelting, Wood Dale, IL, USA).

Contextual Fear Conditioning: Mice were habituated to the room for 1 hr before conditioning and each contextual testing day. On conditioning day, mice were placed into an operant chamber with a shock grid (Med Associates Inc, St. Albans, VT, USA) in the presence of a 10% vanilla odor cue. Following a 3-min habituation period, mice were exposed to one mild (0.7mA) 1 sec foot

shock that was preceded by a 30 sec tone. Mice remained in the context for an additional 30 sec after the foot shock. On test day, 24 hours after conditioning, mice were placed back into the same operant chamber with a 10% vanilla odor cue for 5 min, and the percentage of time spent freezing was measured by Video Freeze software (Med Associates Inc, St. Albans, VT, USA). A nociception assay was also performed by applying a series of mild foot-shocks of increasing intensity 20 sec apart and progressing as follows: 0.05, 0.1, 0.2, 0.3, 0.4, 0.5, 0.6, and 0.7 mA. Startle response was binarily scored (0 = no response, 1 = response) and visually quantified as a movement that is different from their normal exploratory motion (e.g. jump or running away).

Metabolite analysis: Blood samples from isofluorane-anesthesized mice were collected by cardiac puncture and kept on ice until plasma samples were separated by 700xg centrifugation for 10 min at 4 °C. A commercial enzyme-linked immunosorbent assay (ELISA) assay kit (Abcam, cat no. ab65340, Cambridge, MA) was used to measure creatine and creatinine concentrations in accordance with manufacturer's instructions. Fluorescence (Ex/Em = 538/587 nm) was measured using a Flexstation III (Molecular Devices, San Jose, CA).

Statistical Analyses: Statistics were carried out using Prism 8.0 (GraphPad) and Excel (Microsoft). All data shown represent Mean ± SEM. Statistical significance between genotypes was determined using 1-way or 2-way ANOVA with Sidak's or Tukey's post-hoc test. Sample size and statistical test are specified in each figure legend or on the graph above the error bars.

3.6 Results

3.6.1 Abnormal phenotypes in *Tcf4*$^{+/-}$ mice are reversed with increased MeCP2 dosage

Genetic supplementation of MeCP2 from conception has been previously conducted in several mouse models of Rett syndrome (RTT), including mice that have decreased MeCP2 protein expression and function, as well as mice that stably express MeCP2 yet have compromised protein function (*74*, *82*, *94*, *95*, *99*, *100*). The latter context is mimicked in PTHS model mice that are haploinsufficient for *Tcf4*, *Tcf4*$^{+/-}$, wherein MeCP2 mRNA and protein expression are unchanged relative to wild-type (WT) littermates across several brain regions, including the cortex, hippocampus, striatum and cerebellum (Figure 17). In these previous RTT studies, one method to increase MeCP2 levels consists of introducing a functional human *MECP2* allele, which is expressed by the *MECP2* Duplication syndrome (MDS) model mice, *MECP2*$^{Tg1/o}$, to the mutant mice of interest. We utilized this method and bred *MECP2*$^{Tg1/o}$ with *Tcf4*$^{+/-}$ mice to generate *MECP2*$^{Tg1/o}$*; Tcf4*$^{+/-}$ animals that express one copy each of the *Tcf4* and human *MECP2* alleles in addition to the endogenous mouse *Mecp2* allele (Figure 18). Given that MeCP2 is stably expressed in *Tcf4*$^{+/-}$ mice, it is not surprising that, regardless of brain region, we observed an increase in MeCP2 mRNA and protein in *MECP2*$^{Tg1/o}$*; Tcf4*$^{+/-}$, animals that have the *MECP2* transgene; these mice resemble *MECP2*$^{Tg1/o}$ mice in terms of elevated MECP2 expression (Figure 17).

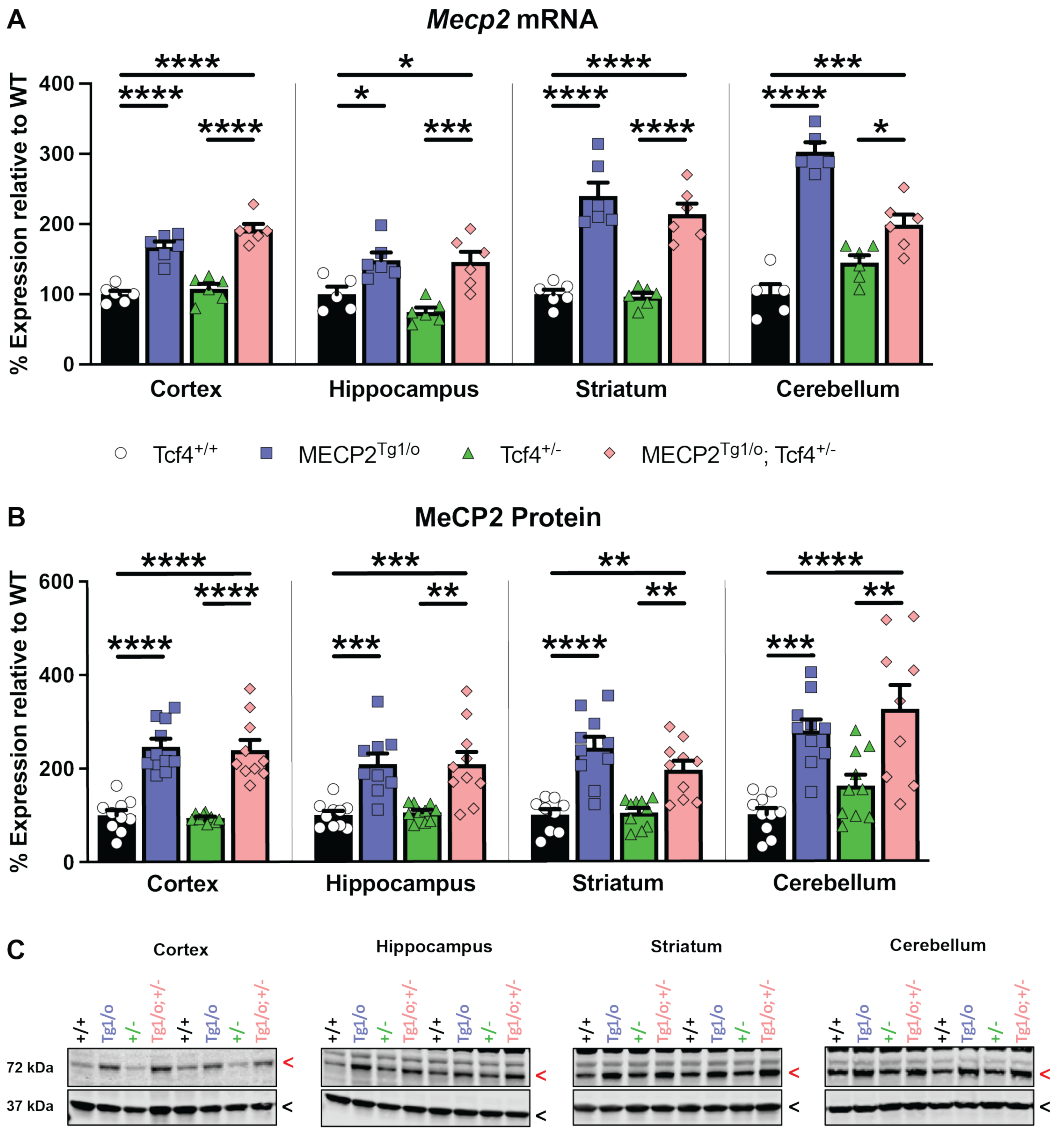

Figure 17: Introduction of an *MECP2* transgene increases MeCP2 expression in *Tcf4*$^{+/-}$ mice. (A-B) Compared to WT littermates (*Tcf4*$^{+/+}$), *MECP2*$^{Tg1/o}$ and *MECP2*$^{Tg1/o}$*; Tcf4*$^{+/-}$ mice exhibit a similar increase in MeCP2 transcript and protein levels in the cortex, hippocampus, striatum and cerebellum. MeCP2 expression in *Tcf4*$^{+/-}$ animals is unchanged relative to that of WT littermates. (C) Representative images of immunoblots for MeCP2/Mecp2 (72 kDa, red arrow) and Gapdh (35 kDa, black arrow). mRNA: n = 5-6 mice per genotype. Protein: n = 9-10 mice per genotype. 1-way ANOVA with Tukey's post-hoc test. *p < 0.05, **p < 0.01, ***p < 0.001, ****p < 0.0001. Open circle / black bars = *Tcf4*$^{+/+}$, blue squares/bars = *MECP2*$^{Tg1/o}$, green triangles/bars = *Tcf4*$^{+/-}$, pink diamonds/bars = *MECP2*$^{Tg1/o}$*; Tcf4*$^{+/-}$.

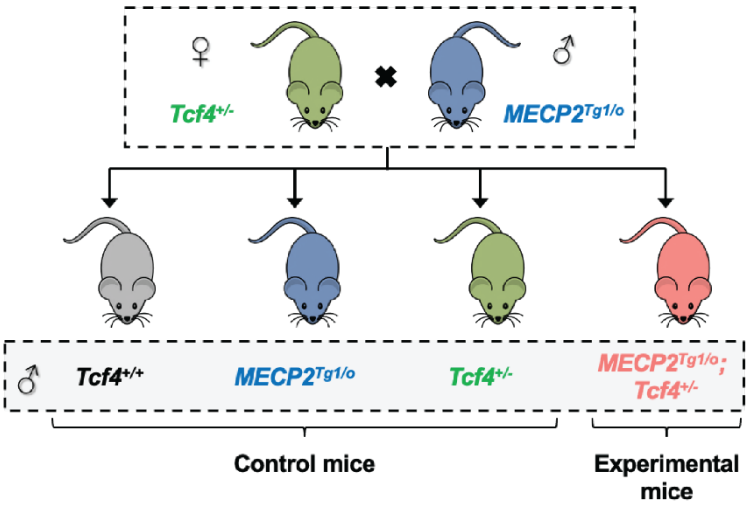

Figure 18: Breeding strategy to introduce the *MECP2* transgene into *Tcf4*$^{+/-}$ mice. Breeding scheme to genetically introduce the *MECP2* transgene from *MECP2*$^{Tg1/o}$ mice into *Tcf4*$^{+/-}$ animals. Male mice (20-25 weeks old) were used for all experiments.

The increased levels of MeCP2 raised the possibility that *MECP2*$^{Tg1/o}$*; Tcf4*$^{+/-}$ mice might develop MDS-like phenotypes as previously observed in RTT mice with partial loss-of-function mutations in MeCP2 (*99*, *100*). Therefore, we conducted a behavioral battery (Figure 19) to assess the phenotypes of *MECP2*$^{Tg1/o}$*; Tcf4*$^{+/-}$ animals, focusing on previously identified abnormal behavioral characteristics of various PTHS model mice. As illustrated in Figure 20A-B, *Tcf4*$^{+/-}$ mice behaved significantly different from WT littermates by exhibiting enhanced distance traveled in an open field chamber throughout the one-hour test. This hyperlocomotor activity was not observed in *MECP2*$^{Tg1/o}$*; Tcf4*$^{+/-}$ animals, indicating a reversal effect of the *MECP2* transgene. In this open field arena, vertical or rearing activity, characterized as a mouse standing on both hind paws in an upright posture, is also evaluated; *Tcf4*$^{+/-}$ mice displayed a significant increase in this behavior compared to WT littermates (Figure 20C). Rearing has been linked to anxiety-related behavior (*379*); therefore, we performed another assay of anxiety using an elevated zero maze apparatus. In this test, *Tcf4*$^{+/-}$ animals spent more time in the open, fully lighted regions of the maze, signifying attenuated anxiety (Figure 20D). In both measures of anxiety, *MECP2*$^{Tg1/o}$*; Tcf4*$^{+/-}$ animals display

anxiogenic behavior compared to *Tcf4*$^{+/-}$ mice and spent a similar amount in the open arms as their WT counterparts, again refuting our initial hypothesis of the potential development of MDS-like phenotypes.

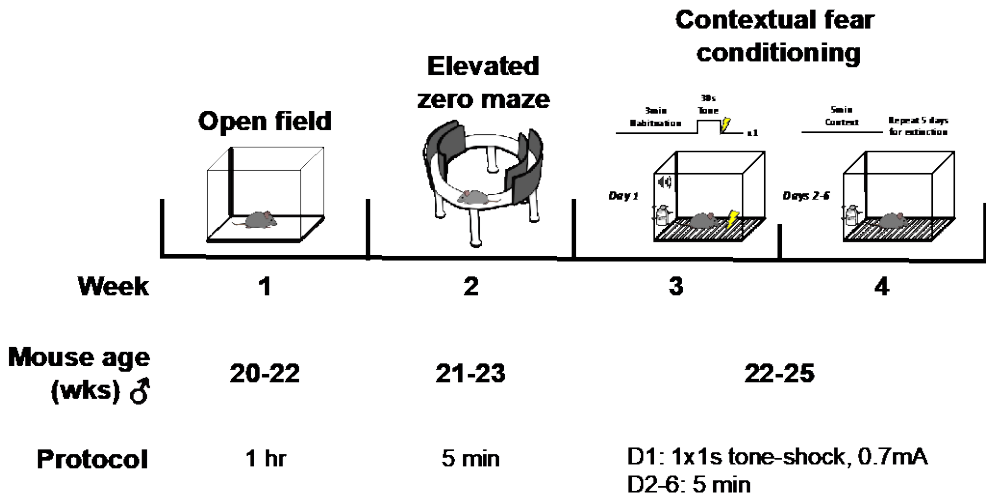

Figure 19: Behavioral battery to assess effects of the *MECP2* transgene in *Tcf4*$^{+/-}$ mice. ♂ (male).

Lastly, we assessed associative learning and memory using a classical Pavlovian contextual fear conditioning task. On training day, mice were placed in a chamber with vanilla odor (unconditioned stimulus) and presented with a conditioned stimulus (foot shock). Regardless of genotype, all mice responded to the foot shock; however, *MECP2*$^{Tg1/o}$ animals demonstrated increased freezing prior to and after the foot shock compared to all other genotypes. Twenty-four hours after training, mice were placed back in the same context (chamber with vanilla odor), and *Tcf4*$^{+/-}$ animals exhibited attenuated percent freezing compared to WT littermates, indicative of a deficit in associative learning and memory (Figure 20E). This phenotype is in contrast to *MECP2*$^{Tg1/o}$ mice, which displayed enhanced percent freezing. Moreover, the contextual fear conditioning deficit was reversed to the level of WT littermates when the *MECP2* transgene was added to *Tcf4*$^{+/-}$ mice. These observations were not due to differences in response to the conditioned stimulus as

no genotypic discrepancies were seen in a nociception assay, wherein mice were presented with several foot shocks of increasing intensity.

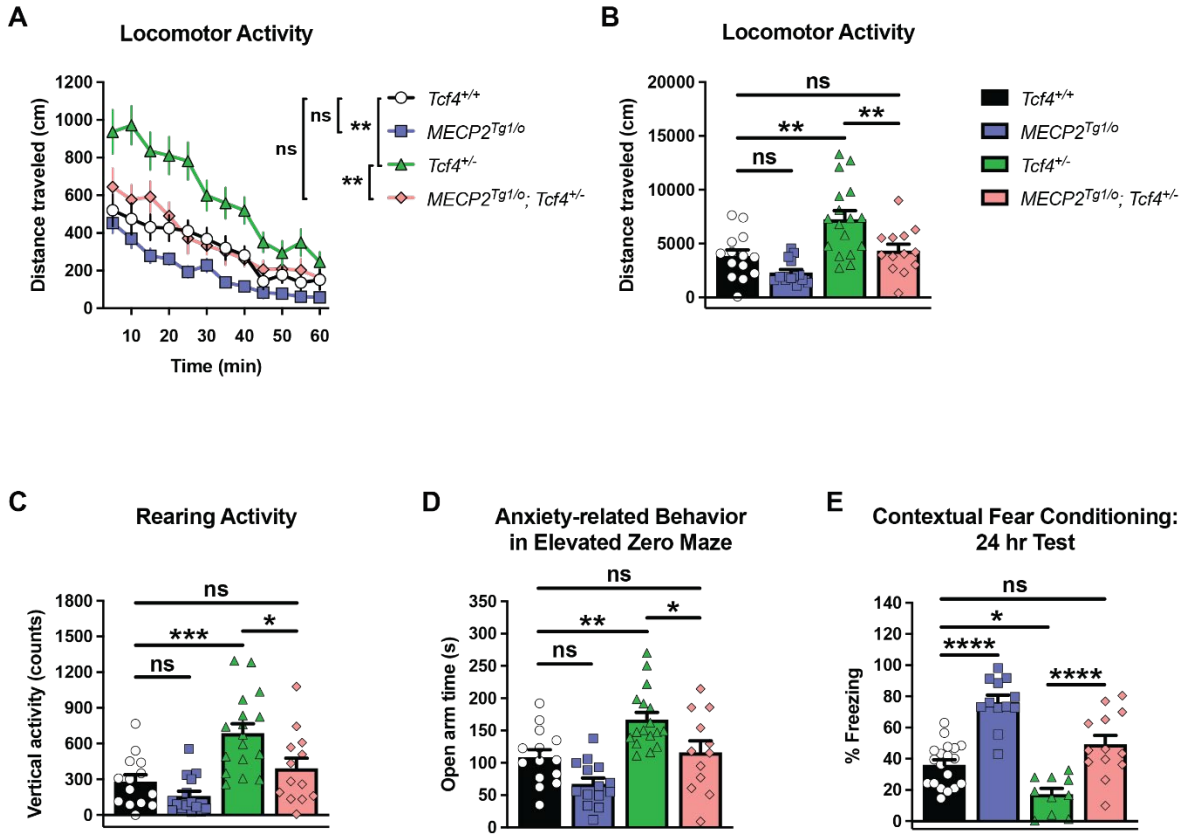

Figure 20: Increasing MeCP2 levels reverses abnormal phenotypes in *Tcf4*$^{+/-}$ mice. (A-B) *Tcf4*$^{+/-}$ mice exhibit hyperlocomotive activity in an open field chamber, which is maintained throughout the majority of the duration of the test. (C-D) Indicated by enhanced vertical activity in an open field chamber and increased time spent in the open arms of an elevated zero maze, *Tcf4*$^{+/-}$ mice display decreased anxiety-related behavior. (E) Compared to WT littermates, *Tcf4*$^{+/-}$ mice have a deficit in contextual fear learning and memory, as signified by decreased percent freezing in the contextual fear conditioning task. In all behavioral assays, *MECP2*$^{Tg1/o}$*; Tcf4*$^{+/-}$ animals do not behave statistically different from WT littermates. n = 10-19 mice per genotype. 1- or 2-way ANOVA with Tukey's post-hoc test. *p < 0.05, **p < 0.01, ***p < 0.001, ****p < 0.0001, ns (not significant). Open circle / black bars = *Tcf4*$^{+/+}$, blue squares/bars = *MECP2*$^{Tg1/o}$, green triangles/bars = *Tcf4*$^{+/-}$, pink diamonds/bars = *MECP2*$^{Tg1/o}$*; Tcf4*$^{+/-}$.

3.6.2 Increasing MeCP2 expression does not affect *Tcf4* levels yet imparts global transcriptomic changes

The reversal effect of increased MeCP2 dosage in a context of normal MeCP2 protein and function is surprising given previous studies of adverse effects in the form of MDS-like phenotypes when MeCP2 is overexpressed (*99*, *100*). However, this is encouraging from the view of PTHS therapeutic discovery, and we posited at least two possible underlying molecular scenarios. First, we hypothesized that Tcf4 is a downstream target of MeCP2, which, like Tcf4, acts a transcriptional regulator. We assessed mRNA expression of Tcf4 in several brain regions, including the cortex, hippocampus, striatum and cerebellum. As illustrated in Figure 21A, *Tcf4* transcript is decreased in *Tcf4*$^{+/-}$ animals without and with the *MECP2* transgene when compared to WT littermates across brain regions. Additionally, *Tcf4* mRNA is unchanged in *MECP2*$^{Tg1/o}$ mice. The numerous isoforms of Tcf4 presents a challenge in detecting protein expression. However, we did detect several isoforms of Tcf4 in the cerebellum, which is where Tcf4 is highly expressed (*204*), and observed similar results in that Tcf4 levels are decreased in both *Tcf4*$^{+/-}$ and *MECP2*$^{Tg1/o;}$ *Tcf4*$^{+/-}$ animals. These data indicate that the additional copy of MeCP2 does not impact Tcf4 levels and suggest that the behavioral effects observed in the *MECP2*$^{Tg1/o;}$ *Tcf4*$^{+/-}$ mice could perhaps be due to functional compensation rather than normalization of Tcf4 expression.

To test this possibility, we performed total RNA-sequencing (RNA-seq) analysis using hippocampal and striatal samples from the four genotypes of interest (n = 6 per genotype per brain region) as these two brain regions are thought to be critically involved in the behavioral phenotypes observed in *Tcf4*$^{+/-}$ mice (*204*). In each brain region, we individually compared all mutant animals, *MECP2*$^{Tg1/o}$, *Tcf4*$^{+/-}$ and *MECP2*$^{Tg1/o;}$ *Tcf4*$^{-/-}$, against the WT (*Tcf4*$^{+/+}$) mice. RNA-seq quality control is summarized in Supplementary Table 1. RNA-seq experiments and bioinformatics analysis were conducted by Genewiz. RNA extraction, mRNA enrichment and cDNA library preparation were performed on individual samples, and sequencing of each sample

was conducted with paired-end 150 base pair high-throughput sequencing using Illumina HiSEq 4000. Following trimming of sequence reads, an average quality score of 35 was obtained in all samples. Over 15 million high-quality reads were obtained per sample, of which 93.3% +/- 0.5% were unique reads and 98.7% +/- 0.08% were mapped to the Mus musculus GRCm38 reference genome available on ENSEMBL (Supplementary Table 1).

Using differential sequencing analysis with DESeq2, we identified 787 and 126 differentially expressed genes (DEGs) with false discovery rate (FDR) < 0.05 from the hippocampus and striatum, respectively, in *Tcf4*$^{+/-}$ animals (Figure 21B, Supplementary Table 2). In *MECP2*$^{Tg1/o}$ mice, the number of DEGs were slightly lower, as only 221 hippocampal and 77 striatal genes were altered. Regardless of genotype, the majority of these DEGs were not impacted by the addition of the *MECP2* transgene or reduction of *Tcf4* levels, as these "unchanged" genes were commonly disrupted in both *Tcf4*$^{+/-}$ or *MECP2*$^{Tg1/o}$ and *MECP2*$^{Tg1/o}$*; Tcf4*$^{+/-}$ mice (Figure 22A-B). One exception is in the striatal DEG set for *MECP2*$^{Tg1/o}$ animals, in which half of the genes were unchanged or "normalized" with the *Tcf4 haploinsufficiency* (Figure 22B).

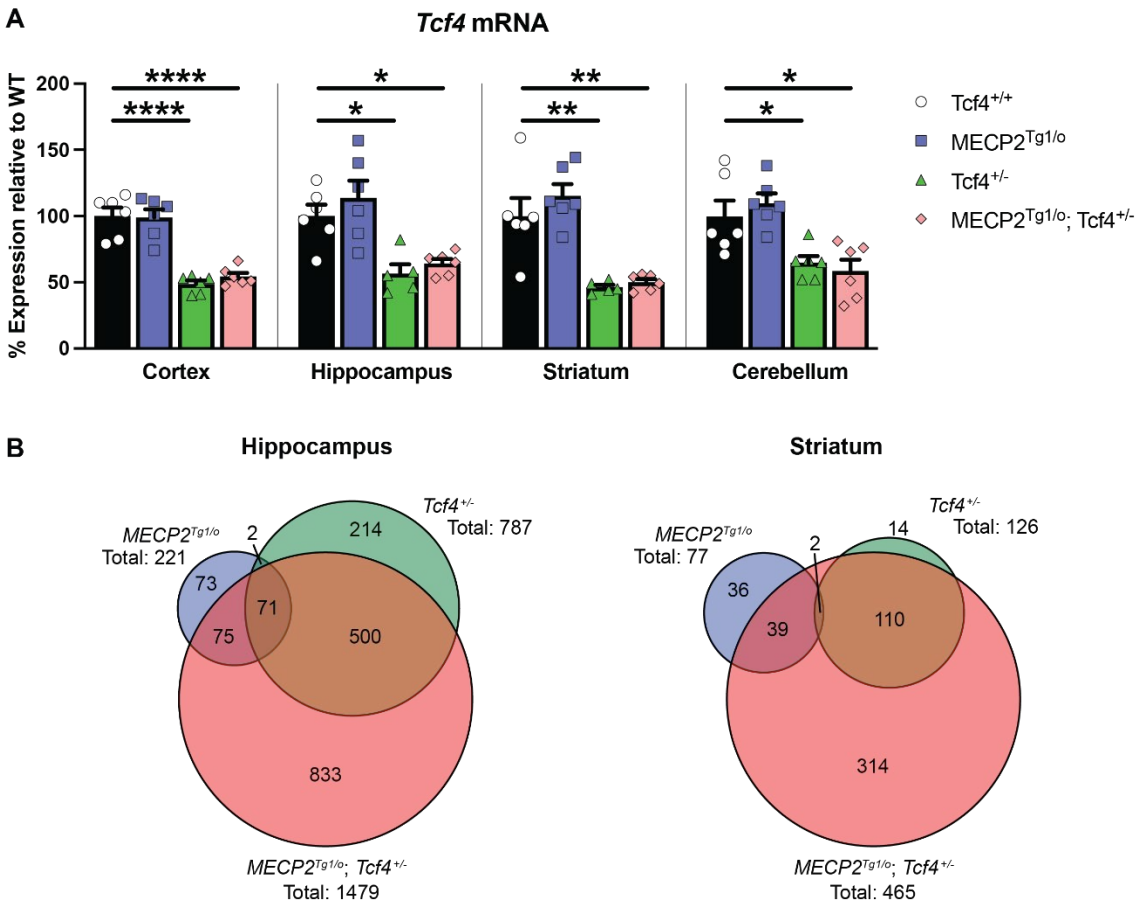

Figure 21: Increased MeCP2 dosage does not affect *Tcf4* expression but elicits global transcriptomic changes. (A) *Tcf4* mRNA expression is decreased in the cortex, hippocampus, striatum and cerebellum of *Tcf4*$^{+/-}$ and *MECP2*$^{Tg1/o}$; *Tcf4*$^{+/-}$ mice. (B) Total RNA-sequencing analysis reveals unique and similar DEGs from the hippocampal and striatal samples of the three mutant mice assessed compared to WT animals. n = 5-6 mice per genotype. 1-way ANOVA with Tukey's post-hoc test. *p < 0.05, **p < 0.01, ****p < 0.0001. Open circle / black bars = *Tcf4*$^{+/+}$, blue squares/bars = *MECP2*$^{Tg1/o}$, green triangles/bars = *Tcf4*$^{+/-}$, pink diamonds/bars = *MECP2*$^{Tg1/o}$; *Tcf4*$^{+/-}$.

In the *Tcf4*$^{+/-}$ mice, approximately 27% (215) and 11% (14) of the hippocampal and striatal DEGs, were normalized with the *MECP2* transgene (Figure 22A, Supplementary Table 3). In the hippocampus, the normalized DEGs were evenly distributed between decreased (14.0%, 110 genes) and increased (13.3%, 105 genes) DEGs. Interestingly, decreased DEGs (11 genes vs 3 increased genes) disproportionately consisted of the normalized DEGs in the striatum, although this is certainly skewed due to the low number of increased genes (4) that were disrupted in *Tcf4*$^{+/-}$

striatal samples. When compared to the hippocampus of *Tcf4*$^{+/-}$ animals, a similar distribution of normalized genes was observed in the hippocampus of *MECP2*$^{Tg1/o}$ mice (31%, 77 DEGs) (Figure 22B); however, more of the normalized genes were initially decreased (55 genes vs 20 increased genes), which mirrored the striatal gene set in *Tcf4*$^{+/-}$. Moreover, approximately half of striatal DEGs in *MECP2*$^{Tg1/o}$ were normalized (47%, 36 genes) and equally distributed amongst decreased (24.7%, 19 genes) and increased (22.1%, 17 genes) DEGs. More genes in *MECP2*$^{Tg1/o}$ appear to be impacted; however, in either brain region, the number of DEGs is much lower than in *Tcf4*$^{+/-}$. Furthermore, the equal distribution of normalized vs unchanged genes in the hippocampus for each transgenic animal suggest that the *MECP2* transgene and *Tcf4 haploinsufficiency* favorably elicit its effects in the hippocampus. However, regardless of genotype and brain region, these normalized genes were not as robustly changed ($-2 < \log_2$ Fold Change (FC) > 2) (Figure 22C-F).

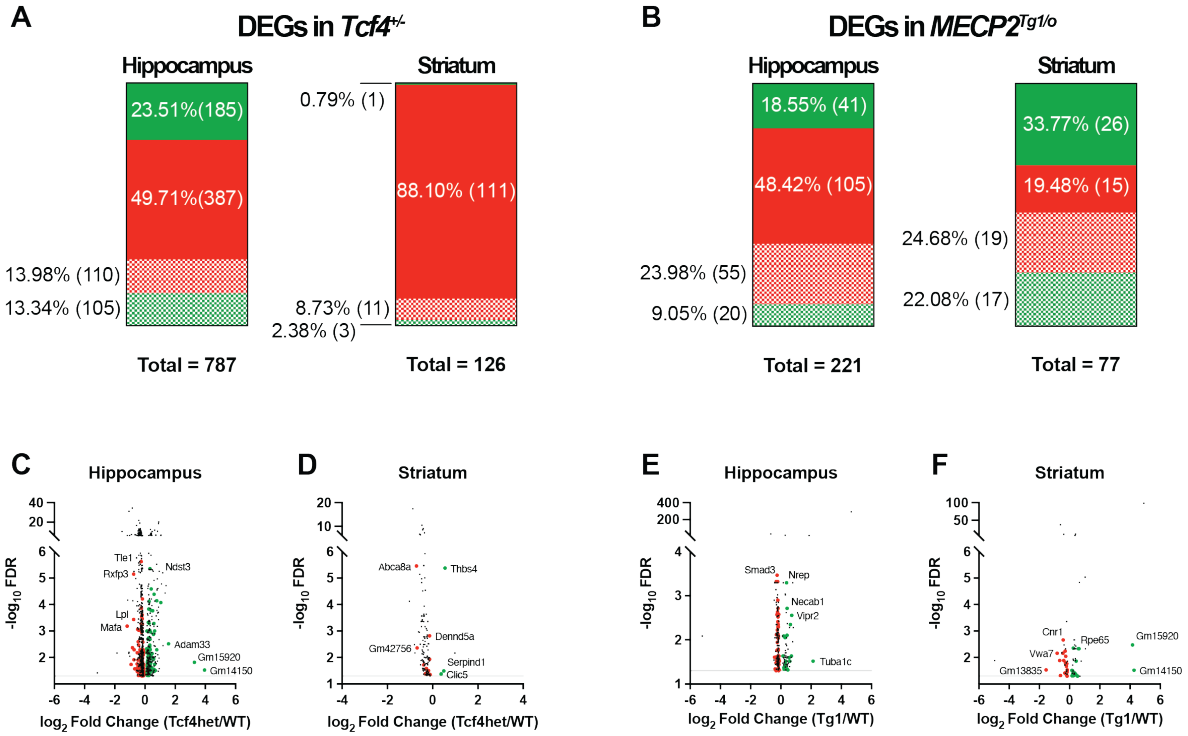

Figure 22: Normalization of altered genes in *Tcf4*$^{+/-}$ and *MECP2*$^{Tg1/o}$ animals. (A-B) Comparative analysis between DEGs (increased in green, decreased in red) within each brain region reveal a subset that is disrupted (unchanged) in *Tcf4*$^{+/-}$ or *MECP2*$^{Tg1/o}$ mice and normalized (checkered) with the *MECP2* transgene or reduction of *Tcf4* expression, respectively (i.e. normalized in the *MECP2*$^{Tg1/o}$; *Tcf4*$^{+/-}$ animals. The number of DEGs and percent of the total DEGs are indicated. (C-F) Volcano plots illustrating the $\log_2$ Fold Change of normalized (green or red for increased or decreased, respectively) and unchanged (black) DEGs. DEGs are genes with FDR < 0.05 or $-\log_{10}$ FDR > 1.30. Some normalized genes are labeled. n = 6 mice per genotype.

We then conducted gene ontology (GO) functional enrichment analysis using the DAVID Functional Annotation Tool on the normalized DEGs, regardless of magnitude or direction and genotype, and discovered that the majority of the identified hippocampal genes were involved in neuronal development and/or function (Supplementary Table 4A-B). This is consistent with previous studies illustrating the role of Tcf4 and MeCP2 in brain development and function especially in regard to cortical and hippocampal neurons (*20*, *36*, *68*, *102*, *202*, *203*, *332*, *333*, *380–382*). A similar GO enrichment was observed in the normalized striatal genes of *MECP2*$^{Tg1/o}$

animals (Supplementary Table 4B), suggesting that the impact of *Tcf4 haploinsufficiency* is widespread in the brain. In contrast, GO analysis with the normalized striatal DEGs in *Tcf4*$^{+/-}$ mice revealed a variety of roles that were not necessarily neuronal-specific (Supplementary Table 4A); again, this could be influenced by the low number of normalized genes compared to the hippocampal dataset.

3.6.3 Analysis of MeCP2- and TCF4-regulated genes highlights potential dysregulation of creatine pathway in *Tcf4*$^{+/-}$ mice.

Focusing on the impact of increased MeCP2 expression in *Tcf4*$^{+/-}$ animals, we further determined the importance of genes that had been "normalized" in *Tcf4*$^{+/-}$ mice by conducting a comparative analysis of genes regulated by MeCP2 and/or Tcf4. The genes that are transcriptionally activated or repressed by MeCP2 or Tcf4 were previously identified using brain tissue from mice lacking or overexpressing MeCP2, or cells expressing TCF4 (*15*, *378*). As illustrated in Figure 23A, several of the normalized DEGs have been shown to be regulated by MeCP2 or Tcf4. However, only 9 genes were predicted to be both MeCP2- and Tcf4-regulated, 8 from the hippocampus and 1 from the striatum. The gene from the striatum, guanidinoacetate methyltransferase (*Gamt*), was of particular interest due to its role in a group of disorders known as cerebral creatine deficiencies (CDDs), which are metabolic disorders characterized by neurological symptoms of intellectual disability and epilepsy, in addition to creatine deficiency (*383*). CDDs are caused by mutations in one of three genes encoding for proteins involved in creatine production or transport, arginine: glycine amidinotransferase (AGAT), GAMT, or creatine transporter (SLC6A8) (*383*). Of these three genes, *GAMT* has been implicated in RTT (*384*); additionally, alterations in creatine and creatinine are also linked to the pathophysiology of RTT (*376*, *377*, *385*). Moreover, we performed pathway analysis of these normalized genes using the Reactome Pathway Database and discovered that creatine metabolism was predicted to be significantly altered. Therefore, we

proceeded to establish the expression of Gamt and whether creatine and creatinine levels are also disrupted in *Tcf4*$^{+/-}$ animals.

Evaluation of Gamt mRNA and protein expression using a cohort of samples independent from the RNA-seq samples showed that it was unchanged in the hippocampus or striatum of *Tcf4*$^{+/-}$ mice (Figure 23B-E). This discrepancy between the RNA-seq and qRT-PCR or Western blot could be due to the small change in Gamt expression in *Tcf4*$^{+/-}$ mice in the RNA-seq study ($\log_2$ fold change of -0.28). Nonetheless, we analyzed plasma creatine and creatinine levels using an ELISA-based fluorescence assay. Regardless of genotype, we detected normal creatinine and creatine levels in the plasma of these animals (Figure 23F-H). This is consistent with the normal expression of Gamt, and suggests that creatine deficiency is not characteristic of *Tcf4*$^{+/-}$ animals.

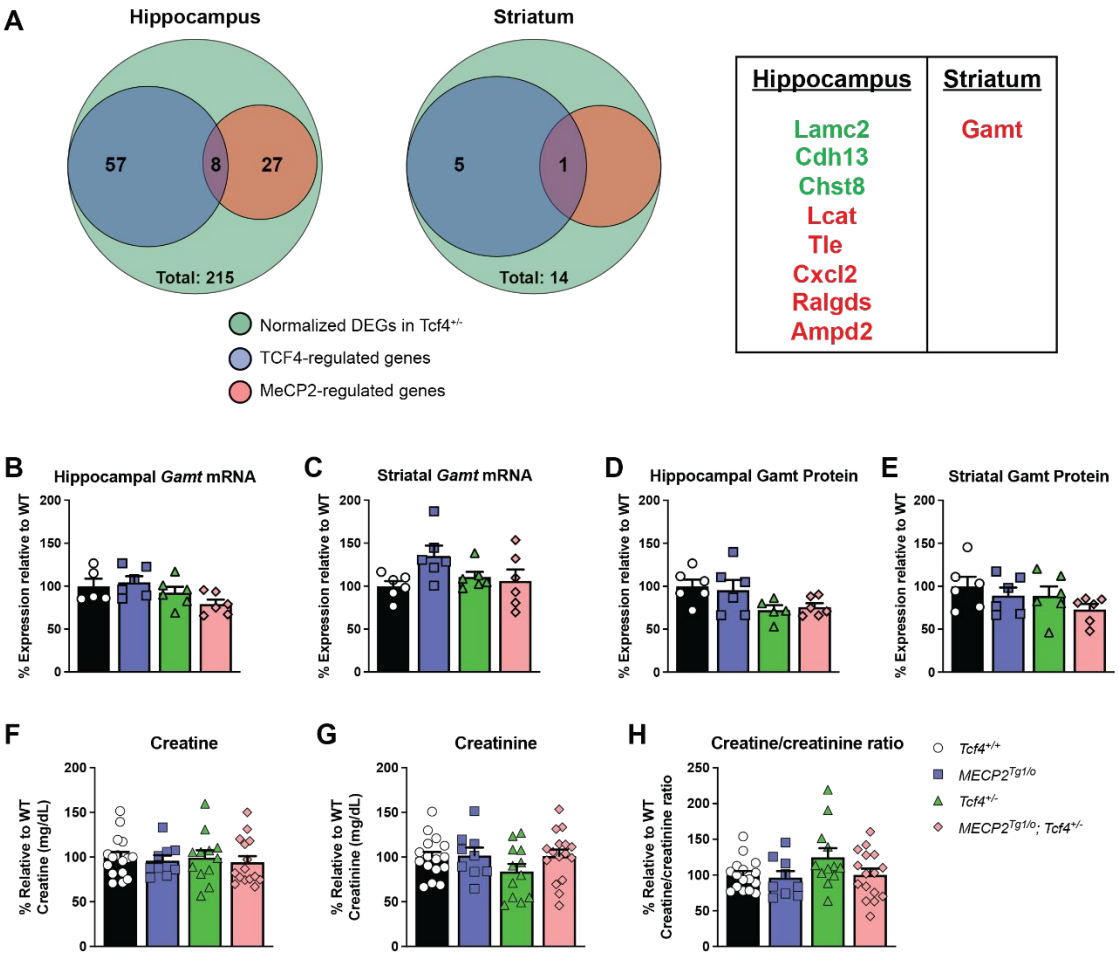

Figure 23: Transcriptomic analysis illustrate genes regulated by both MeCP2 and Tcf4. (A) Several hippocampal and striatal DEGs that are disrupted in *Tcf4*$^{+/-}$ animals and normalized with the *MECP2* transgene are also regulated by both Tcf4 and MeCP2. Originally upregulated genes in green and downregulated genes in red. (B-E) *Gamt* mRNA and protein expression in the hippocampus and striatum is unchanged across the genotypes assessed (n = 5-6 mice per genotype). (F-G) Creatine and creatinine concentration, and plasma creatine/creatinine ratio are not changed in plasma samples of all genotypes assessed (n = 12-16 mice per genotype). 1-way ANOVA with Tukey's post-hoc test.

3.6.4 Transcriptomic studies illustrate myelination-associated genes and pathways that could underlie behavioral reversal in *Tcf4*$^{+/-}$ mice

We next focused on the DEGs from only the *MECP2*$^{Tg1/o}$*; Tcf4*$^{+/-}$ animals with the idea that the addition of the *MECP2* transgene elicited changes specifically in the context of Tcf4 haploinsufficiency (Supplementary Table 2). We performed separate GO analyses for the

individual gene sets of each brain region in only the *MECP2*$^{Tg1/o}$; *Tcf4*$^{+/-}$ group and discovered enrichment of myelination-associated biological processes (BP), molecular function (MF) and cellular component (CC) (Figure 24A-B, Supplementary Table 5). To further delineate whether these pathways are conserved in both brain regions, we first conducted comparative analysis of DEGs in only the *MECP2*$^{Tg1/o}$; *Tcf4*$^{+/-}$ group, and identified 64 genes that were common in both the hippocampus and striatum (Figure 24C). GO analysis using these shared genes also identified myelination-associated pathways as significantly altered (Figure 24D, Supplementary Table 5), which further supports the importance of myelination in PTHS mice and/or in the mechanisms of MeCP2 supplementation's beneficial effects in PTHS mice. Moreover, it has been previously observed that myelination and expression of myelination-associated genes and proteins are also altered in other mouse models of syndromic autism spectrum disorders including RTT (*Mecp2*$^{Null/y}$), phosphatase and tensin homolog deleted on chromosome 10 (PTEN)-associated autism (homozygous *Pten* mutation), and Tuberous sclerosis (TSC, *Tsc1* neuronal-specific deletion) in addition to PTHS (*378*, *386*, *387*). Therefore, we determined whether the increase in MeCP2 expression reversed the myelination defects that have been previously characterized in *Tcf4*$^{+/-}$ animals.

A

Category	GO Term	Description	# of Genes	Fold Enrichment	-log10 p-value
BP	GO:0032291	Axon ensheathment in central nervous system	6	10.191	3.705
BP	GO:0022010	Central nervous system myelination	6	10.191	3.705
BP	GO:0014003	Oligodendrocyte development	7	4.693	2.474
BP	GO:0042552	Myelination	15	3.295	3.749
BP	GO:0008366	Axon ensheathment	15	3.239	3.670
BP	GO:0007272	Ensheathment of neurons	15	3.239	3.670
BP	GO:0048709	Oligodendrocyte differentiation	12	3.185	2.878
MF	GO:0019911	Structural constituent of myelin sheath	3	15.379	1.854
CC	GO:0043209	Myelin sheath	23	2.471	3.795

B

Category	GO Term	Description	# of Genes	Fold Enrichment	-log10 p-value
BP	GO:0048713	Regulation of oligodendrocyte differentiation	5	7.657	2.400
BP	GO:0014003	Oligodendrocyte development	4	6.932	1.708
BP	GO:0048709	Oligodendrocyte differentiation	9	6.173	3.983
BP	GO:0042552	Myelination	9	5.109	3.415
BP	GO:0008366	Axon ensheathment	9	5.022	3.365
BP	GO:0007272	Ensheathment of neurons	9	5.022	3.365
CC	GO:0043218	Compact myelin	3	9.365	1.400
CC	GO:0043209	Myelin sheath	18	4.989	6.911

C

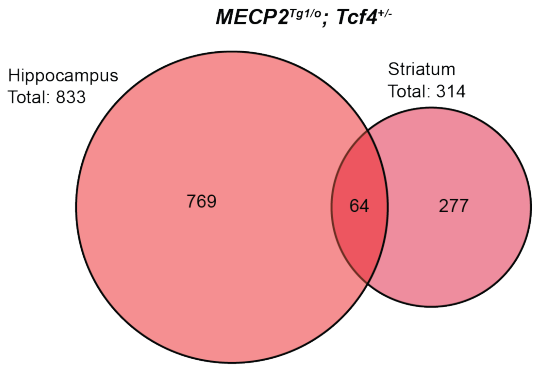

D

Category	GO Term	Description	# of Genes	Fold Enrichment	-log10 (p-value)
BP	GO:0022010	Central nervous system myelination	2	39.802	1.316
BP	GO:0032291	Axon ensheathment in central nervous system	2	39.802	1.316
BP	GO:0042552	Myelination	4	10.294	2.180
BP	GO:0008366	Axon ensheathment	4	10.119	2.159
BP	GO:0007272	Ensheathment of neurons	4	10.119	2.159
BP	GO:0048709	Oligodendrocyte differentiation	3	9.329	1.399
CC	GO:0043209	Myelin sheath	8	10.776	5.137
MF	GO:0019911	Structural constituent of myelin sheath	2	124.933	1.806

Figure 24: Transcriptomic studies illustrate myelination-associated genes and pathways as enriched in *MECP2$^{Tg1/o}$; Tcf4$^{+/-}$* mice. (A-B) GO analysis of hippocampal and striatal DEGs only in *MECP2$^{Tg1/o}$; Tcf4$^{+/-}$* animals reveals enrichment of myelination-associated pathways. (C-D) Comparative analysis of DEGs found only in *MECP2$^{Tg1/o}$; Tcf4$^{+/-}$* mice detects a subset of genes that are common between the hippocampus and striatum. Subsequent GO analysis of these 64 DEGs identifies significant enrichment of pathways related to myelination.

We evaluated the expression of markers for mature myelinating-oligodendrocytes (OLs), myelin oligodendrocyte glycoprotein (MOG) and 2',3'-Cyclic nucleotide 3'-phosphodiesterase (CNP) in total protein lysates from the cortex of WT, *MECP2*$^{Tg1/o}$, *Tcf4*$^{+/-}$, and *MECP2*$^{Tg1/o}$; *Tcf4*$^{+/-}$ animals. Similar to previous findings in the medial prefrontal cortex (*378*), *Tcf4*$^{+/-}$ mice exhibit hypomyelination with decreased expression of MOG, but not CNP, without changes in the immature OL marker, NG2 chondroitin sulphate proteoglycan (NG2) (Figure 25). However, compared to WT, *MECP2*$^{Tg1/o;}$ *Tcf4*$^{+/-}$ animals also have decreased levels of these myelination markers. These data suggest that although myelination defects are observed in *Tcf4*$^{+/-}$ mice, increasing MeCP2 expression does not correct this abnormal phenotype and therefore, myelination does not underlie the behavioral reversal effects. We anticipate that the identification of myelination pathways that appeared to be affected only in the *MECP2*$^{Tg1/o;}$ *Tcf4*$^{+/-}$ mice was due to the relatively small changes that were identified in these genes in the RNA sequencing study.

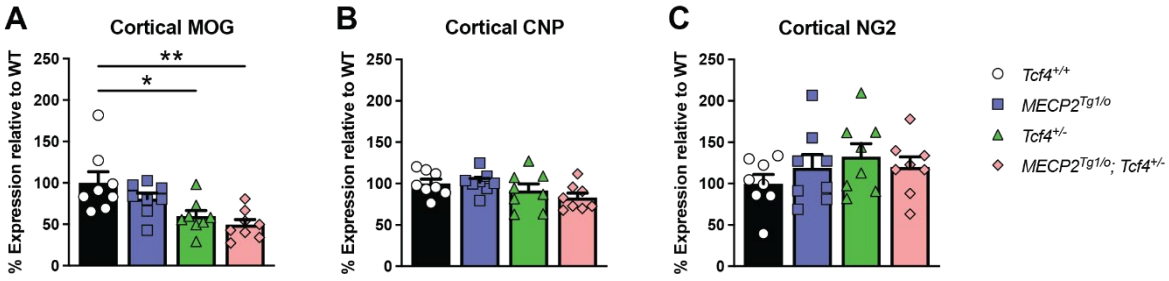

Figure 25: Myelination defects in *Tcf4*$^{+/-}$ animals are not changed with an *MECP2*$^{Tg1/o}$ transgene. (A) Decreased expression of the mature OL myelination marker MOG is decreased in the cortex of *Tcf4*$^{+/-}$ without and with the *MECP2* transgene. (B-C) Mature OL marker CNP and immature OL marker NG2 are unchanged in the cortex. n = 8 mice per genotype. 1-way ANOVA with Tukey's post-hoc. *p < 0.05, **p < 0.01.

3.7 Discussion

The need for an effective therapeutic intervention for PTHS has paralleled the increase in identification of patients with PTHS. The monogenicity of PTHS makes gene therapy an intriguing possibility given this approach's previous success in neurological disorders such as spinal muscular atrophy (*388*–*391*). A recent study demonstrated that a viral-mediated strategy to increase Tcf4 levels postnatally in the brain of *Tcf4* haploinsufficient mice exerts beneficial effects in several behavioral domains (*222*). However, the challenge of TCF4-targeted gene therapy is a potentially narrow therapeutic window as overexpression of Tcf4 in mice disrupted brain development and led to deficits in sensorimotor gating and associative learning and memory (*220*, *221*). An alternative approach is to leverage RTT therapeutics for PTHS given the overlapping symptomology of these two disorders. In particular, here we studied the safety and efficacy of genetic MeCP2 supplementation in PTHS model mice, *Tcf4*$^{+/-}$.

We utilized a breeding strategy previously conducted by us and other labs in mouse models of RTT to introduce a wild-type human *MECP2* transgene in *Tcf4*$^{+/-}$ animals (*74*, *99*, *100*). The *MECP2* transgene increased MeCP2 expression in several brain regions of the *Tcf4*$^{+/-}$ animals at similar levels as the MDS mice, thereby validating our genetic approach. Remarkably, increasing MeCP2 levels had favorable effects, reversing behavioral phenotypes characteristic of *Tcf4 mutant* animals including hyperactivity, anxiety-like behavior and attenuated learning and memory. These beneficial effects are in agreement with previous studies of RTT mice using the same approach (*74*, *82*, *99*, *100*). However, this result is also perplexing, as *Tcf4*$^{+/-}$ animals had normal MeCP2 levels and previous studies have demonstrated the manifestation of abnormal MDS-like phenotypes in the context of MeCP2 overexpression, which are likely due to the retention of normal MeCP2 expression and partial function (*99*, *100*). Nonetheless, we show for the first time proof-of-concept data on the feasibility of genetic MeCP2 supplementation for PTHS.

The lack of adverse effects associated with increased MeCP2 suggested that TCF4 levels could be impacted and/or MeCP2 and TCF4 share common pathways which are disrupted with Tcf4 haploinsufficiency and normalized with the addition of the *MECP2* transgene. The former hypothesis was negated, as *MECP2*$^{Tg1/o;}$ *Tcf4*$^{+/-}$ animals displayed decreased *Tcf4* mRNA and protein across several brain regions, similar to the *Tcf4*$^{+/-}$ mice. To interrogate the second possibility, we conducted total RNA-sequencing analysis of hippocampal and striatal samples from all four genotypes and compared dysregulated genes and pathways in the mutant animals to that of their WT counterparts. A set of genes were disrupted in *Tcf4*$^{+/-}$ mice, and also normalized with the *MECP2* transgene. One of these genes from the striatum, *Gamt*, is regulated by both MeCP2 and TCF4 as previously identified through other transcriptomic studies (*15*, *331*). Gamt is also involved in creatine production, which was of interest given a group of intellectual disability disorders characterized by cerebral creatine deficiencies, and the reports of altered levels of creatine and its metabolite, creatinine in RTT patients (*376*, *377*, *383*). Therefore, it was conceivable that creatine deficiency is a characteristic of PTHS and that increasing MeCP2 would normalize this metabolic dysfunction thereby alleviating the behavioral phenotypes. However, plasma creatine and creatinine levels were normal in *Tcf4*$^{+/-}$ animals, suggesting that creatine is not involved in the effects of the *MECP2* transgene. Still, it is plausible that creatine deficiency is a hallmark of PTHS in the clinical population as has been observed in RTT patients. One potential mechanism for decreased creatine is the increase activity of creatine kinase (CK), which breaks down creatine to its metabolites phosphocreatine and creatinine (*392*). The *CK* gene has four E-box regions in its enhancer, positing the possibility that TCF4 regulates the expression of this gene as has been previously shown *in vitro* (*205*). Thus, further studies should assess whether creatine or creatinine levels are altered in PTHS patients as these findings would have implications for treatment as well as serve as biomarkers to evaluate treatment efficacy and/or disease progression.

The other set of genes of interest from the hippocampus and striatum of *MECP2*$^{Tg1/o;}$ *Tcf4*$^{+/-}$ animals are involved in myelination, as characterized using GO analysis. Defects in myelination have been observed through brain imaging of PTHS patients (*393*). Congruently, hypomyelination using the markers for myelinating mature oligodendrocytes was reported in the cortex of *Tcf4 mutant* animals (*378*). Given this precedent, the enrichment of myelination-associated processes appeared to be significant. Using cortical samples, we confirmed the previous report of attenuated expression of myelination markers in *Tcf4*$^{+/-}$ mice. However, we also detected the same reduction in the *MECP2*$^{Tg1/o;}$ *Tcf4*$^{+/-}$ animals, suggesting that myelination defects were not reversed with the *MECP2* transgene. These results are consistent with the previously observed function of MeCP2 as a negative regulator of myelin genes (*394*). In such case, MeCP2 overexpression would also cause myelination dysfunction, as has been documented been documented in patients with MDS (*395*, *396*). Other studies, however, have shown the opposite in that MeCP2 acts as positive regulator of myelin and that restoration of MeCP2 levels in glia partially reversed myelin gene expression in *Mecp2 null* mice (*397*, *398*). With the latter role of MeCP2 as a transcriptional activator of myelin-associated genes, it would be logical that increasing MeCP2 in a hypomyelination context such as in *Tcf4 mutant* animals would impart beneficial effects. However, it is also possible that too much MeCP2 would cause aberrant myelination.

The mechanisms underlying the behavioral reversal with increased MeCP2 expression are still unclear. The transcriptomic data demonstrate that many of the normalized genes are involved in neuronal development and function. Therefore, it is likely that increasing MeCP2 expression from conception impacts the functional loss of TCF4 in regulating brain development. To mitigate the developmental effects of increased MeCP2, as well as mimic the ideal gene therapy strategy potentially used in the clinic, an alternative approach would be to increase MeCP2 expression postnatally and after symptom onset. In such case, the viral vectors expressing MeCP2 that have been used in preclinical RTT investigations could be employed.

Overall, these data demonstrate the promise for leveraging the MeCP2-targeted gene therapy for PTHS. Further analysis of the abundant transcriptomic data is needed to elucidate which genes and/or pathways are playing a role in MeCP2's beneficial effects, which could have implications in the utility of MeCP2-targeted gene therapy for other atypical RTT disorders.

CHAPTER 4

PHARMACOLOGICAL MODULATION OF GROUP II METABOTROPIC GLUTAMATE RECEPTORS IN MOUSE MODELS OF RETT SYNDROME AND *MECP2* DUPLICATION SYNDROME

Summary of findings depicted in Figure 26.

4.1 Abstract

Rett syndrome (RTT) and *MECP2* Duplication syndrome (MDS) have opposing molecular origins in relation to expression and function of the transcriptional regulator Methyl-CpG-binding protein 2 (MeCP2). Several clinical and preclinical phenotypes, however, are shared between these disorders. Modulation of MeCP2 levels has recently emerged as a potential treatment option for both of these diseases. However, toxicity concerns remain with these approaches. Here, we focus on pharmacologically modulating the group II metabotropic glutamate receptors (mGlu), $mGlu_2$ and $mGlu_3$, which are two downstream targets of MeCP2 that are bidirectionally affected in expression in RTT patients and mice ($Mecp2^{Null/+}$) versus an MDS mouse model ($MECP2^{Tg1/o}$). $Mecp2^{Null/+}$ and $MECP2^{Tg1/o}$ animals also exhibit contrasting phenotypes in trace fear acquisition, a form of temporal associative learning and memory, with trace fear deficiency observed in $Mecp2^{Null/+}$ mice and abnormally enhanced trace fear acquisition in $MECP2^{Tg1/o}$ animals. In $Mecp2^{Null/+}$ mice, treatment with the $mGlu_{2/3}$ agonist LY379268 reverses the deficit in trace fear acquisition, and $mGlu_{2/3}$ antagonism with LY341495 normalizes the abnormal trace fear learning and memory phenotype in $MECP2^{Tg1/o}$ mice. Altogether, these data highlight the role of group II mGlu receptors in RTT and MDS and demonstrate that both $mGlu_2$ and $mGlu_3$ may be potential therapeutic targets for these disorders.

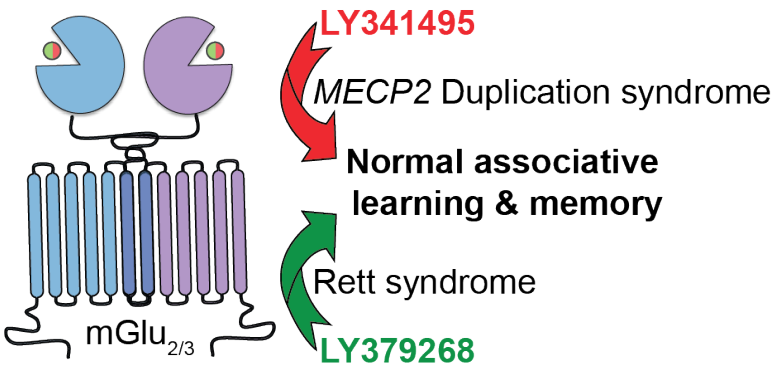

Figure 26: $mGlu_{2/3}$ receptor modulation in RTT and MDS model mice. Activation (green, LY379268) or inhibition (red, LY341495) of $mGlu_{2/3}$ receptors in mouse models of Rett syndrome (RTT) and *MECP2* Duplication syndrome (MDS), respectively, normalizes abnormal phenotypes of associative learning and memory, specifically trace fear acquisition.

4.2 Introduction

MECP2-associated disorders are X-linked monogenic neurodevelopmental diseases that are caused by abnormal expression and/or function of the protein Methyl-CpG-binding protein 2 (MeCP2), which is encoded on the X chromosome. Rett syndrome (RTT) is caused by loss-of-function (LOF) mutations in *MECP2*, and is observed most often in females (*21*, *47*). The multi-domain clinical symptoms of RTT, including motor dysfunction, impaired social skills, cognitive decline, and breathing abnormalities, overlap with another *MECP2*-associated disorder, *MECP2* Duplication syndrome (MDS), which is caused by multiple copies of the *MECP2* gene. Due to random X chromosome inactivation in females, patients diagnosed with MDS are predominantly male (*161*, *162*). The symptoms observed in RTT patients are recapitulated in mice that ubiquitously or cell type-specifically lack *Mecp2* or express functionally mutated *Mecp2* (*65*, *70*, *74–79*, *82*, *85*, *86*, *95–101*, *325*, *368*, *369*, *399–402*). Similarly, clinical characteristics of MDS are observed in mouse models that either have global or neuronal-specific *MECP2* overexpression (*105*, *168*). Interestingly, many phenotypes in RTT mice are antiparallel to those observed in MDS model animals, including anxiety, motor abnormalities, and cognitive function. For example, RTT

mice display deficits in associative learning and memory in a fear conditioning task; in contrast, MDS mice exhibit abnormally enhanced learning in this task in addition to impairments in extinction of fear-learned behavior (*70*, *105*, *168*, *329*, *366*).

Previous studies in RTT models have shown that genetic normalization of *MECP2,* even after disease onset, can rescue many phenotypes in *Mecp2* mutant mice, supporting the feasibility of treating the disorder (*71*, *93*, *112–120*). Promisingly, recent studies have also demonstrated that abnormal phenotypes in MDS mice can be improved post-symptom onset with genetic manipulations, including normalization of MeCP2 dosage with antisense oligonucleotides (*94*, *171*). Pharmacological approaches targeting genes/pathways downstream of MeCP2 could also have potential in treating symptom domains of RTT and MDS. For example, in mice with MeCP2 over-expression in neurons (*Tau-Mecp2*), pharmacological antagonism of $GABA_A$ receptors can alleviate symptoms (*173*). Comparably, studies have determined that modulation of receptors involved in neurotransmission and that are sensitive to MeCP2 dosage can improve phenotypes in RTT mice (*124*, *128*, *129*, *136*, *137*, *143–145*). These include the Trkb, glutamatergic AMPA, metabotropic glutamate (mGlu), and muscarinic acetylcholine receptors, which were initially identified in expression studies in RTT patient and mouse samples (*15*, *68*, *121–124*, *136*, *137*). The association of these receptors with neurological and neurodevelopmental disorders, as well as the advent of selective modulators, make these receptors potential therapeutic targets for new drug candidates.

The expression of the group II mGlu receptors, $mGlu_2$ and $mGlu_3$, has been consistently demonstrated to be affected by MeCP2 dosage in patient and preclinical samples (*15*, *68*, *122–124*). Additionally, these dimeric receptors have been implicated in neuropsychiatric disorders such as schizophrenia and depression (*311*, *313*, *314*, *403*, *404*). Studies using subtype-selective modulators, preclinical knockout mouse models, and clinical genetic associations have shown

that $mGlu_3$ has a vital role in cognition, specifically in hippocampal and prefrontal cortical function (*264*, *266*, *267*, *269*, *272*, *288*, *311*, *316*, *319*, *320*, *405*). $mGlu_2$ has also been shown to be involved in cognition, as $mGlu_2$-selective positive allosteric modulators (PAMs) improve learning and memory in rodent models of schizophrenia (*308*, *406*). Given the molecular studies demonstrating the relationship of MeCP2 and the group II mGlu receptors, as well as the association of these receptors with cognition, we posited that $mGlu_2$ and $mGlu_3$ may play critical roles in the etiology or treatment of the cognitive phenotypes observed in RTT and MDS.

In this study, we show that $mGlu_2$ and $mGlu_3$ receptor levels are decreased in temporal cortex samples from RTT patient autopsies. Expression of these receptors is also reciprocally decreased and increased in the hippocampus of *Mecp2*$^{Null/+}$ and *MECP2*$^{Tg1/o}$ mice, respectively. Based on these findings, we tested the hypothesis that an $mGlu_{2/3}$ agonist or antagonist would positively affect behavior in *Mecp2*$^{Null/+}$ and *MECP2*$^{Tg1/o}$ mice in a hippocampal-dependent behavioral cognitive assay. We show here that activation of $mGlu_{2/3}$ receptors reverses deficient trace fear acquisition in *Mecp2*$^{Null/+}$ animals, whereas $mGlu_{2/3}$ antagonism normalizes the abnormal enhanced trace fear acquisition phenotype in *MECP2*$^{Tg1/o}$ mice. Collectively, these data demonstrate that both $mGlu_2$ and $mGlu_3$ receptors are implicated in the cognitive function of RTT and MDS model mice, and that modulation of $mGlu_{2/3}$ activity may be beneficial in alleviating cognitive symptoms of these two disorders.

4.4 Materials and Methods

Animals: All animals used in the present study were group housed with food and water given ad libitum and maintained on a 12 hr light/dark cycle. Animals were cared for in accordance with the National Institutes of Health Guide for the Care and Use of Laboratory Animals. All studies were approved by the Vanderbilt Institutional Animal Care and Use Committee and took place during the light phase. *MECP2*$^{Tg1/o}$ mice (FVB-Tg(MECP2)1Hzo/J, stock no. 008679) were cryorecovered and *Mecp2*$^{Null/+}$ (B6.129P2(C)-*Mecp2*$^{tm1.1Bird}$/J, stock no. 003890) were obtained from The Jackson Laboratory. Given that *MECP2*$^{Tg1/o}$ mice on the FVB/N background are prone to retinal degeneration, we utilized the F1 generation or hybrid mice (FVB/N x C57BL/6) for our studies as described previously (*172*, *407*). These F1 hybrid mice were generated by crossing *MECP2*$^{Tg1/o}$ mice (FVB/N background) with WT C57BL/6J mice (The Jackson Laboratory, stock no. 000664). To reflect the predominantly male clinical population in MDS (*161*), male *MECP2*$^{Tg1/o}$ mice (8-12 weeks old) were used for all experiments. Similarly, as a reflection of the predominantly female RTT patient population, female *Mecp2*$^{Null/+}$ mice were utilized and aged to at least 20 weeks of age prior to experiments. *Mecp2*$^{Null/+}$ animals were maintained on a C57BL/6J background by breeding *Mecp2*$^{Null/+}$ with WT C57BL/6J mice (The Jackson Laboratory, stock no. 000664).

Total Protein Preparation: The cortex and hippocampus were microdissected from 8-9 week-old male WT littermates and *MECP2*$^{Tg1/o}$ mice, and 20-25 week-old female *Mecp2*$^{+/+}$ and *Mecp2*$^{Null/+}$ animals. Total protein was prepared as previously described in (*362*). Briefly, tissue samples were homogenized using a hand-held motorized mortar and pestle in radioimmunoprecipitation assay buffer (RIPA) containing 10 mM Tris-HCl, 150 mM NaCl, 1 mM ethylenediaminetetraacetic acid (EDTA), 0.1% sodium dodecyl sulfate (SDS), 1% Triton X-100, and 1% deoxycholate. After homogenization, samples were centrifuged and the supernatant was

collected. Protein concentration was determined using a bicinchoninic acid (BCA) protein assay (Pierce).

SDS-Page and Western Blotting: As previously described in (*362*), 50 µg of total protein was electrophoretically separated using a 4-20% SDS polyacrylamide gel and transferred onto a nitrocellulose membrane (iBlot2, ThermoFisher (for $mGlu_2$ and $mGlu_3$); Criterion™ Blotter, Bio-Rad (for MeCP2)). Membranes were blocked in TBS Odyssey blocking buffer (LI-COR) for 1hr at room temperature. Membranes were probed with primary antibodies overnight at 4 °C: mouse anti-$mGlu_2$ (1:1000 Abcam, cat. no. ab15672), rabbit anti-$mGlu_3$ (1:1000, Alomone, cat. no. AGC_012), rabbit anti-MeCP2 (1:1000, Millipore, cat. no. 07-013), rabbit anti-vGlut2 (1:1000, Cell Signaling Technology, cat. no. 71555) and mouse anti-Gapdh (1:1000, ThermoFisher, cat. no. MA5-15738), followed by the fluorescent secondary antibodies: goat anti-rabbit (800 nm, 1:5000, LI-COR, cat. no. 926-32211) and goat anti-mouse (680 nm, 1:10,000, LI-COR, cat. no. 926-68020). Fluorescence was detected using the Odyssey (LI-COR) imaging system at the Vanderbilt University Medical Center Molecular Cell Biology Resource (MCBR) Core and then quantified using the Image Studio Lite software (LI-COR). Values were normalized to Gapdh and compared relative to controls (WT littermates or *Mecp2*$^{+/+}$).

Total RNA Extraction and cDNA Synthesis: For total RNA extraction of human temporal cortex samples, frozen samples were obtained from the University of Maryland Brain and Tissue Bank and the Harvard Brain Tissue Resource Center, which are Brain and Tissue Repositories of the National Institutes of Health NeuroBioBank (neurobiobank.nih.gov). For mouse total RNA extraction, the cortex and hippocampus were microdissected from 8-9 week-old male WT littermates and *MECP2*$^{Tg1/o}$ mice, and 20-25 week-old female *Mecp2*$^{+/+}$ and *Mecp2*$^{Null/+}$ animals. Total RNA was prepared from tissue samples using TRIzol Reagent (ThermoFisher) and isolated using a RNeasy Mini Kit (Qiagen) in accordance with manufacturer's instructions. Total RNA was

DNase-treated with RNase-Free DNase Set (Qiagen), and cDNA from 2 µg of total RNA was synthesized using a SuperScript™ VILO™ cDNA Synthesis Kit (ThermoFisher, cat. no. 11754050).

Quantitative Real-Time PCR (qRT-PCR): qRT-PCR (CFX96, Bio-Rad, Vanderbilt University Medical Center MCBR Core) on 50 ng / 9 µL cDNA was run in duplicate using TaqMan™ Fast Universal PCR Master Mix (2X), no AmpErase™ UNG (Life Technologies, cat. no. 4352042) and Life Technologies gene expression assays for human *GRM2* (Hs00968358_m1), *GRM3* (Hs00932301_m1) and *G6PD* (Hs00166169_m1), and mouse *Grm2* (Mm01235831_m1), *Grm3* (Mm00725298_m1) and *Gapdh* (Mm99999915_g1). Similar qRT-PCR was performed using PowerUp™ SYBR™ Green Master Mix (ThermoFisher, cat. no. A25742) with the following primers (5' to 3'): *Mecp2* (exon 4, forward: ATGAGACTGTGCTCCCCATC, reverse: TTTTCTCACCAAGGGTGGAC) and *Gapdh* (exon 6, forward: CGACTTCAACAGCAACTCCC, reverse: GCCGTATTCATTGTCATACCAGG). All primers used for SYBR qRT-PCR were designed using Primer3 and constructed by Sigma through the Vanderbilt University Medical Center MCBR Core. Ct values for each sample were normalized to G6PD/Gapdh expression and analyzed using the delta−delta Ct method as described in (*137*). Values exceeding two times the standard deviation were classified as outliers. Each value was compared to the average delta-Ct value acquired for control human samples or wild-type mice (WT littermate or $Mecp2^{+/+}$) and calculated as percent-relative to the average control delta-Ct.

Drugs: LY379268 ($mGlu_{2/3}$ agonist) and LY341495 ($mGlu_{2/3}$ antagonist) were purchased from Tocris. All drugs used for behavioral experiments were diluted in 10% Tween-80.

Behavioral Assays: All behavioral experiments were conducted at predicted symptomatic ages (8-12 week-old $MECP2^{Tg1/o}$ and 20-25 week-old $Mecp2^{Null/+}$ mice) at the Vanderbilt Mouse

Neurobehavioral Lab (MNL) Core. All experiments were preceded by intraperitoneal (i.p.) injections of the following drugs (T_{max} in parentheses): vehicle (10% Tween-80), LY379268 (1mg/kg, 30 min) or LY341495 (3mg/kg, 20 min pre-LY379268 administration or 30 min). Quantification was performed either by a researcher blinded to the genotype and/or by automated software.

Open Field: Mice were placed in the activity chamber for 30 min and locomotor activity was quantified as beam breaks in the X, Y and Z axis using Activity Monitor software (Med Associates Inc).

Trace Fear Conditioning: Mice were habituated to the room for 1 hour before all tests. On acquisition or conditioning day, mice were treated with compounds or vehicle prior to being placed into an operant chamber with a shock grid (Med Associates Inc.) in the presence of a 10% vanilla odor cue. Modified from previous studies (*267*, *408*), mice were acclimated for 1 min and exposed to a mild 1 sec foot shock (0.5 mA for WT littermate and *MECP2*$^{Tg1/o}$ mice, and 0.7mA for *Mecp2*$^{+/+}$ and *Mecp2*$^{Null/+}$ animals) that was preceded by a 15 sec tone. A precise 30 sec interval or "trace" separated the tone and shock. Three or four tone-trace-shock pairings were applied, 240 sec apart, for the *MECP2*$^{Tg1/o}$ or *Mecp2*$^{Null/+}$ mouse lines, respectively. Percentage of time spent freezing during each trace was measured by Video Freeze software (Med Associates Inc.).

Statistical Analyses: Statistics were carried out using Prism 9 (GraphPad) and Excel (Microsoft). All data shown represent mean ± SEM. Statistical significance between genotypes was determined using Student's t-test, or 2-way ANOVA with Sidak's or Tukey's post-hoc. Sample size (denoted as "n"), statistical test and results of statistical analyses are specified in each figure legend.

4.6 Results

4.6.1 Group II mGlu receptor expression is decreased in clinical and preclinical RTT samples

We first investigated the expression of $mGlu_2$ and $mGlu_3$ in post-mortem brain tissue from female patients clinically diagnosed with RTT. Complementing our previous studies in the motor cortex and cerebellum (*124*, *136*, *137*), we obtained fourteen temporal cortex samples (Brodmann area 20 or 38, BA 20 or BA 38) from female RTT patients characterized as having truncation mutations in *MECP2* (*R168X*, *R255X*, and *R270X*) and fourteen age-, sex- and post-mortem interval (PMI)-matched controls (Table 4). qRT-PCR analyses revealed decreased levels of *GRM2* and *GRM3* mRNA in the temporal cortex of RTT patients (Figure 27A), which is in agreement with previous transcriptomic analyses of other brain regions, including the cerebellum and frontal, motor and temporal cortices (*121*, *122*, *124*).

Decreased expression of $mGlu_2$ and $mGlu_3$ mRNA has also been observed in preclinical RTT mouse models, particularly in the cortex of male *Mecp2 null* mice (*15*, *68*, *123*). Consistent with these transcriptomic studies, we found significantly reduced *Grm2* mRNA expression in the cortex of naïve 20-25 week old female $Mecp2^{Null/+}$ animals compared to the wild-type (WT) controls, $Mecp2^{+/+}$ (Figure 27B). Interestingly, cortical *Grm3* mRNA was not statistically different between the mutant and control mice. Given that $mGlu_2$ and $mGlu_3$ have both been linked to cognitive function, specifically hippocampal-dependent cognition (*317*, *318*), we assessed *Grm2* and *Grm3* transcript levels in the hippocampus, and found that hippocampal *Grm2* and *Grm3* mRNA levels were also attenuated in $Mecp2^{Null/+}$ animals (Figure 27C).

Next, we determined whether altered expression of $mGlu_2$ and $mGlu_3$ in $Mecp2^{Null/+}$ mice was maintained at the protein level. As illustrated in the representative immunoblots, both $mGlu_2$ and $mGlu_3$ proteins were decreased in the cortex of $Mecp2^{Null/+}$ animals (Figure 27D-E, antibody

validated using $mGlu_3$ global knockout animals that have been previously characterized in (*267*)). Compared to their WT counterparts, *Mecp2*$^{Null/+}$ mice exhibited significant reductions of monomer, dimer and total (sum of monomer and dimer) $mGlu_2$ protein, whereas $mGlu_3$ levels were significantly reduced at the levels of the monomeric and total protein (Figure 27E). Additionally, the decreased expression of $mGlu_2$ and $mGlu_3$ protein was also observed in the hippocampus of *Mecp2*$^{Null/+}$ mice, which is in agreement with the transcript expression data (Figure 27F-G). Notably, for both receptors, the dimer and total protein levels were significantly decreased in *Mecp2*$^{Null/+}$ animals without differences in the control synaptic protein vGlut2 (Figure 27G). These clinical and preclinical data provided rationale for investigating the role and therapeutic potential of group II mGlu receptors in RTT and related disorders.

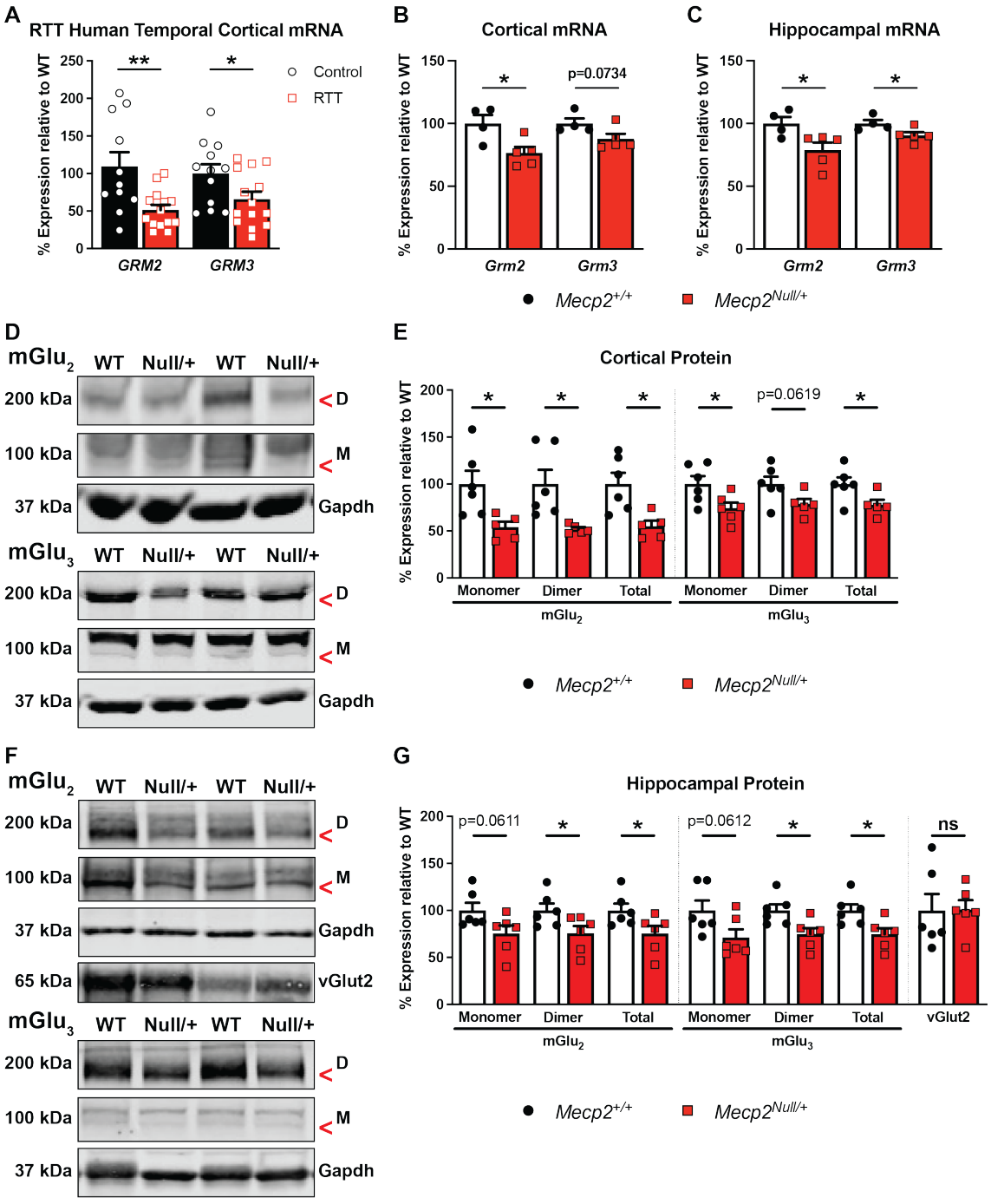

Figure 27: mGlu$_2$ and mGlu$_3$ expression is decreased in RTT patients and mice. (A) Compared to controls (black bars / white circles, n = 11-12), *GRM2* and *GRM3* mRNA are both decreased in RTT patients in temporal cortex autopsy samples (red bars / white squares, n = 14). RTT patient samples used in this study have truncated MeCP2 mutations, specifically R168X, R255X and R270X (see Table 4). (B-C) Compared to *Mecp2*$^{+/+}$ animals (red bars / squares, n = 4-5), *Grm2* and/or *Grm3* mRNA levels are decreased in 20-25 week-old *Mecp2*$^{Null/+}$ mice (white bars / black circles, n = 4-5). (D) Representative immunoblots illustrating cortical dimeric ("D", 200 kDa) and monomeric ("M", 100 kDa) forms

of $mGlu_2$ or $mGlu_3$ and Gapdh (37 kDa) loading control in *Mecp2*$^{+/+}$ ("WT") and *Mecp2*$^{Null/+}$ ("Null/+") animals. (E) Cortical $mGlu_2$ and $mGlu_3$ protein expression (total = monomer + dimer) is decreased in *Mecp2*$^{Null/+}$ mice (n = 5-6) relative to *Mecp2*$^{+/+}$ animals (n = 5-6). (F) Representative immunoblots for hippocampal proteins as in (D) with the addition of $vGlut_2$ (65 kDa). (G) Compared to *Mecp2*$^{+/+}$ animals (n = 5-6), $mGlu_2$ and $mGlu_3$ proteins are reduced in the hippocampus of *Mecp2*$^{Null/+}$ mice (n = 5-6). $vGlut_2$ is unchanged between genotypes. Student's t-test. ns (not significant), *p<0.05, **p<0.01.

4.6.2 Group II mGlu receptor expression is increased in *MECP2*$^{Tg1/o}$ mice

We further explored the molecular relationship of $mGlu_2$ and $mGlu_3$ with MeCP2 using a rodent MDS model, *MECP2*$^{Tg1/o}$, and tested the hypothesis that increased MeCP2 expression in the *MECP2*$^{Tg1/o}$ context also enhances $mGlu_2$ and $mGlu_3$ expression. Similar to the use of symptomatic female *Mecp2*$^{Null/+}$ animals to reflect the clinical population, we utilized 8-9 week old male *MECP2*$^{Tg1/o}$ mice and WT littermates to assess protein and mRNA expression in the hippocampus. In agreement with previous reports (*105*, *168*, *171*, *362*), MeCP2 mRNA and protein expression were increased in *MECP2*$^{Tg1/o}$ mice compared to WT littermates (Figure 28A-C). Comparably, *Grm2* and *Grm3* mRNA levels were also significantly increased in *MECP2*$^{Tg1/o}$ animals (Figure 28A). To determine if this effect was also observed at the protein level, we evaluated $mGlu_2$ and $mGlu_3$ protein expression. As illustrated in the representative immunoblots, expression of both receptors was increased in *MECP2*$^{Tg1/o}$ animals (Figure 28B). In Figure 28C, quantification of expression showed that statistical significance was observed for the expression of the monomer, dimer and total (sum of monomer and dimer) protein for $mGlu_2$, and the level of the dimer and total $mGlu_3$ protein was significantly different between *MECP2*$^{Tg1/o}$ mice and WT littermates. These overexpression data of group II mGlu receptors suggested that these proteins could potentially contribute to the abnormal phenotypes in MDS mice, which could be amenable to receptor modulation.

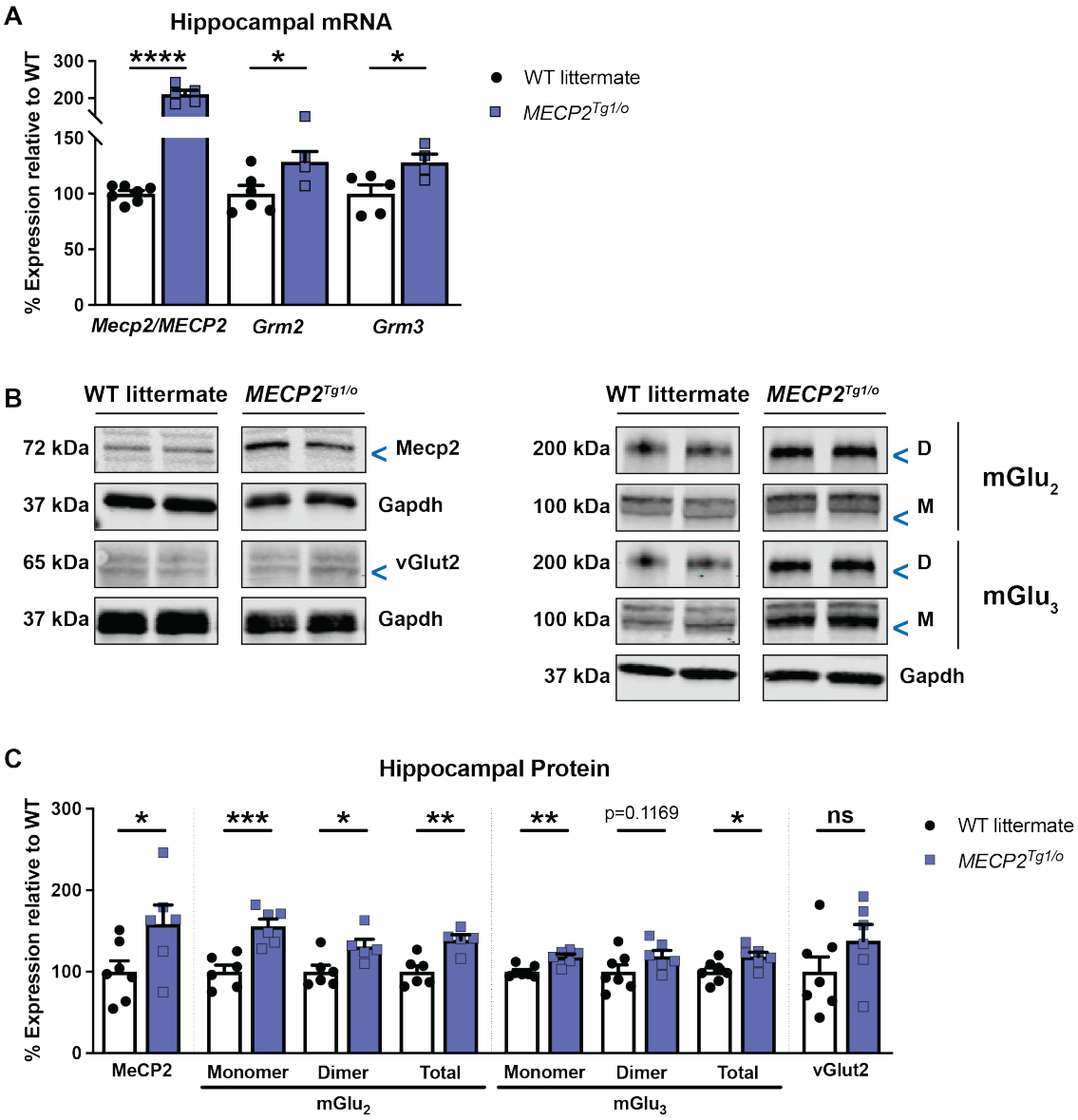

Figure 28: Hippocampal $mGlu_2$ and $mGlu_3$ expression is increased in MDS mice. (A) Compared to WT littermates (white bars / black circles, n = 5-7), *Mecp2/MECP2, Grm2* and *Grm3* transcripts are increased in the hippocampus of 8-9 week-old *MECP2*$^{Tg1/o}$ mice (blue bars / squares, n = 4-5). (B) Representative immunoblots illustrating MeCP2 (72 kDa), $mGlu_2$ or $mGlu_3$ dimer ("D", 200 kDa) and monomer ("M", 100 kDa), vGlut2 (65 kDa), and Gapdh (37 kDa) loading control in hippocampal samples of WT littermates and *MECP2*$^{Tg1/o}$ mice. (C) Protein expression of MeCP2, $mGlu_2$, and $mGlu_3$ (total = monomer + dimer) is increased in *MECP2*$^{Tg1/o}$ mice (n = 5-6) relative to WT littermates (n = 6-7). $vGlut_2$ is unchanged between genotypes. Student's t-test. ns (not significant), *p<0.05, **p<0.01, ***p<0.001, ****p<0.0001.

4.6.3 RTT and MDS mice exhibit abnormal and bidirectional phenotypes in trace fear acquisition

Numerous studies have characterized RTT model mice as exhibiting abnormal phenotypes in cognition, specifically in associative learning and memory, which is often assessed using a cued or contextual fear conditioning assay (*70*, *74*, *79*, *82*, *83*, *97*, *99*, *100*, *136*, *137*, *366*, *368*). Interestingly, a recent study highlighted the role of $mGlu_3$ in mediating a temporal- and hippocampal-dependent associative learning and memory phenotype known as trace fear acquisition or conditioning (*267*). Prior to investigating the relationship of $mGlu_{2/3}$ receptors and trace fear conditioning in a RTT mouse model, we first characterized the trace fear behavior of *Mecp2*$^{Null/+}$ animals. In this task, the mice were trained to associate their environment and presented tone with an aversive stimulus in the form of a mild foot shock (0.7 mA); the "trace" period that separates the tone and shock presentations is thought to enhance learning (Figure 29A). As shown in Figure 29B, increases in percent freezing in *Mecp2*$^{+/+}$ animals paralleled the increase in tone-trace-shock pairings (black symbols), reflecting learning behavior. However, we demonstrate here that *Mecp2*$^{Null/+}$ mice exhibit abnormal trace fear acquisition, as illustrated by the attenuated percent freezing compared to their *Mecp2*$^{+/+}$ counterparts. In particular, freezing behavior was significantly different between *Mecp2*$^{+/+}$ and *Mecp2*$^{Null/+}$ animals at the last trace period (T4), suggesting a deficit in trace fear acquisition.

Similar to RTT model mice, MDS mice have been shown to exhibit abnormal phenotypes in cued or contextual fear associative learning and memory (*105*, *168*, *171–173*, *329*, *362*). However, as in RTT model animals, phenotypes in trace fear conditioning have not been assessed in mice modeling MDS. WT littermate and *MECP2*$^{Tg1/o}$ animals were subjected to a similar trace fear acquisition paradigm as RTT mice, with the notable differences of a milder foot shock intensity (0.5 mA) and reduced number of tone-trace-shock pairings (Figure 29C). These changes were performed to account for the high percent freezing phenotype that MDS mice exhibit in fear

conditioning assays (*105*, *168*, *171–173*, *329*, *362*). Compared to WT littermates, *MECP2*$^{Tg1/o}$ mice displayed enhanced trace fear acquisition during the last trace period measured (T3, Figure 29D). This abnormal enhancement in trace fear acquisition was in contrast to the deficient phenotype in *Mecp2*$^{Null/+}$ animals; coupled with the increases in expression of $mGlu_2$ and $mGlu_3$ in the hippocampus of *MECP2*$^{Tg1/o}$ mice, we hypothesized that these changes in trace fear behavior might be sensitive to $mGlu_{2/3}$ receptor modulation.

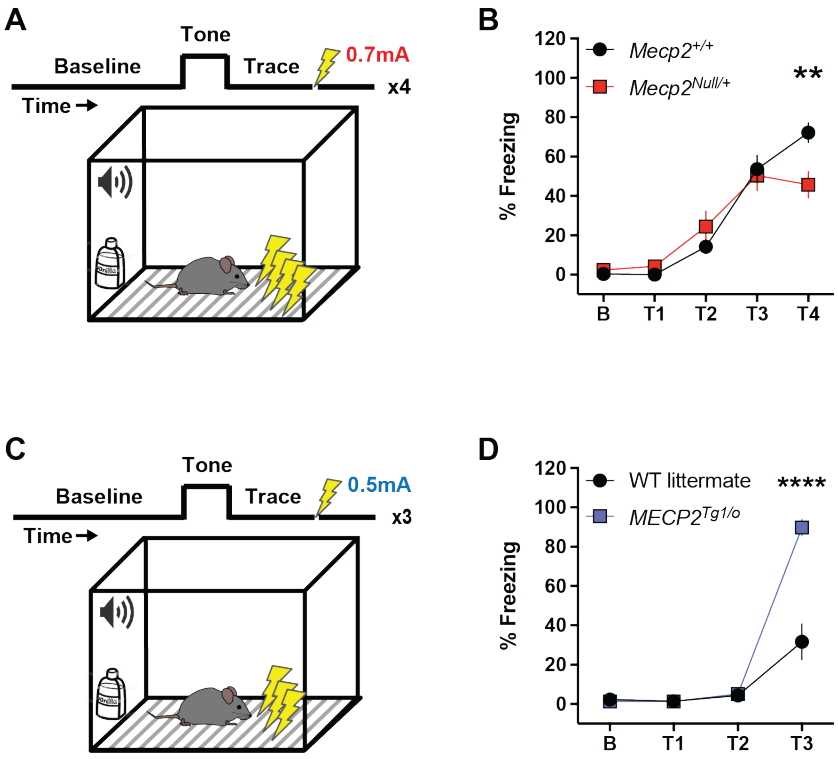

Figure 29: Contrasting phenotypes in trace fear conditioning between *Mecp2*$^{Null/+}$ and *MECP2*$^{Tg1/o}$ animals. (A) Diagram illustrating the trace fear conditioning paradigm. Mice are trained to associate their environment (context and tone) with an aversive stimulus in the form of a mild foot shock (0.7 mA), with a temporal component (trace) separating the tone and shock. Four tone-trace-shock pairings are presented and percent freezing during the trace period is measured as a proxy for fear learning behavior. (B) Compared to *Mecp2*$^{+/+}$ mice (black circles, n = 17), 20-25 week-old *Mecp2*$^{Null/+}$ animals (red squares, n = 12) display attenuated percent freezing during the fourth trace period (T4). (C) Diagram illustrating the trace fear conditioning paradigm in WT littermates and *MECP2*$^{Tg1/o}$ animals. The protocol mentioned above in RTT mice is followed with notable differences in the foot shock intensity (0.5 mA) and the number

of tone-trace-shock pairings (three). (D) Compared to WT littermates (black circles, n = 11), 8-12 week-old *MECP2*$^{Tg1/o}$ animals (blue squares, n = 10) exhibit increased percent freezing during the third trace period (T3). 2-way ANOVA with Sidak's post-hoc test. **p<0.01, ****p<0.0001.

4.6.4 $mGlu_{2/3}$ activation reverses deficits in trace fear acquisition in *Mecp2*$^{Null/+}$ mice

Detection and quantitation of a trace fear acquisition deficit in RTT mice allowed us to then test the hypothesis that administration of a nonselective $mGlu_{2/3}$ agonist, LY379268, to increase receptor activity would improve this abnormal cognitive phenotype in *Mecp2*$^{Null/+}$ animals. Animals were intraperitoneally administered either vehicle (10% Tween-80) or 1mg/kg LY379268 30 minutes prior to trace fear conditioning (Figure 30A). LY379268 treatment reversed the trace fear acquisition deficit in vehicle-treated *Mecp2*$^{Null/+}$ mice with statistical significance observed between vehicle- and LY379268-treated *Mecp2*$^{Null/+}$ mice at trace periods 2 (T2) and 4 (T4) (Figure 30B-D). The increased freezing behavior at period T2 was only observed in *Mecp2*$^{Null/+}$ animals (Figure 30C), suggesting an increased sensitivity to LY379268 in the mutant mice compared to their WT counterparts. In contrast, *Mecp2*$^{+/+}$ animals did not exhibit a significant change in response to LY379268 at any of the trace periods measured. To eliminate the possibility that the increased percent freezing in *Mecp2*$^{Null/+}$ animals was due to hypolocomotive effects of LY379268, as has previously been shown in WT animals (*280*, *298*, *409*), we placed the mice in an open field chamber and monitored spontaneous locomotor activity. 1mg/kg LY379268 did not change the distance traveled of *Mecp2*$^{+/+}$ or *Mecp2*$^{Null/+}$ animals, which already have reduced locomotion at baseline.

To further validate that the reversal effects in trace fear conditioning were due to $mGlu_{2/3}$ modulation by LY379268 and not an off-target result, we administered the $mGlu_{2/3}$ orthosteric antagonist LY341495 (3mg/kg) prior to LY379268 treatment (Figure 30E). LY341495 blocked the

effect of LY379268 in *Mecp2*$^{Null/+}$ mice, specifically at trace periods T2-T4 (Figure 30F-I). In these trace periods, the freezing behavior of vehicle-treated *Mecp2*$^{Null/+}$ animals was indistinguishable from *Mecp2*$^{Null/+}$ mice that received both LY341495 and LY379268. Importantly, the ability of LY341495 to block LY379268's increased freezing effect at period T2 in *Mecp2*$^{Null/+}$ animals suggests that the left-shifted response of the mutant animals to LY379268 is a consequence of $mGlu_{2/3}$ modulation (Figure 30G). Interestingly, co-administration of LY379268 and LY341495 to *Mecp2*$^{+/+}$ animals decreased percent freezing at trace periods T3-T4 (Figure 30H-I). Again, this could potentially be due to alterations in locomotor activity; however, assessment of distance traveled in an open field assay revealed no locomotor effects of LY341495 and LY379268 co-administration in either the *Mecp2*$^{+/+}$ and *Mecp2*$^{+/-}$ mice. Overall, these data support the ability of $mGlu_{2/3}$ activation to enhance the trace fear acquisition response in *Mecp2*$^{Null/+}$ animals.

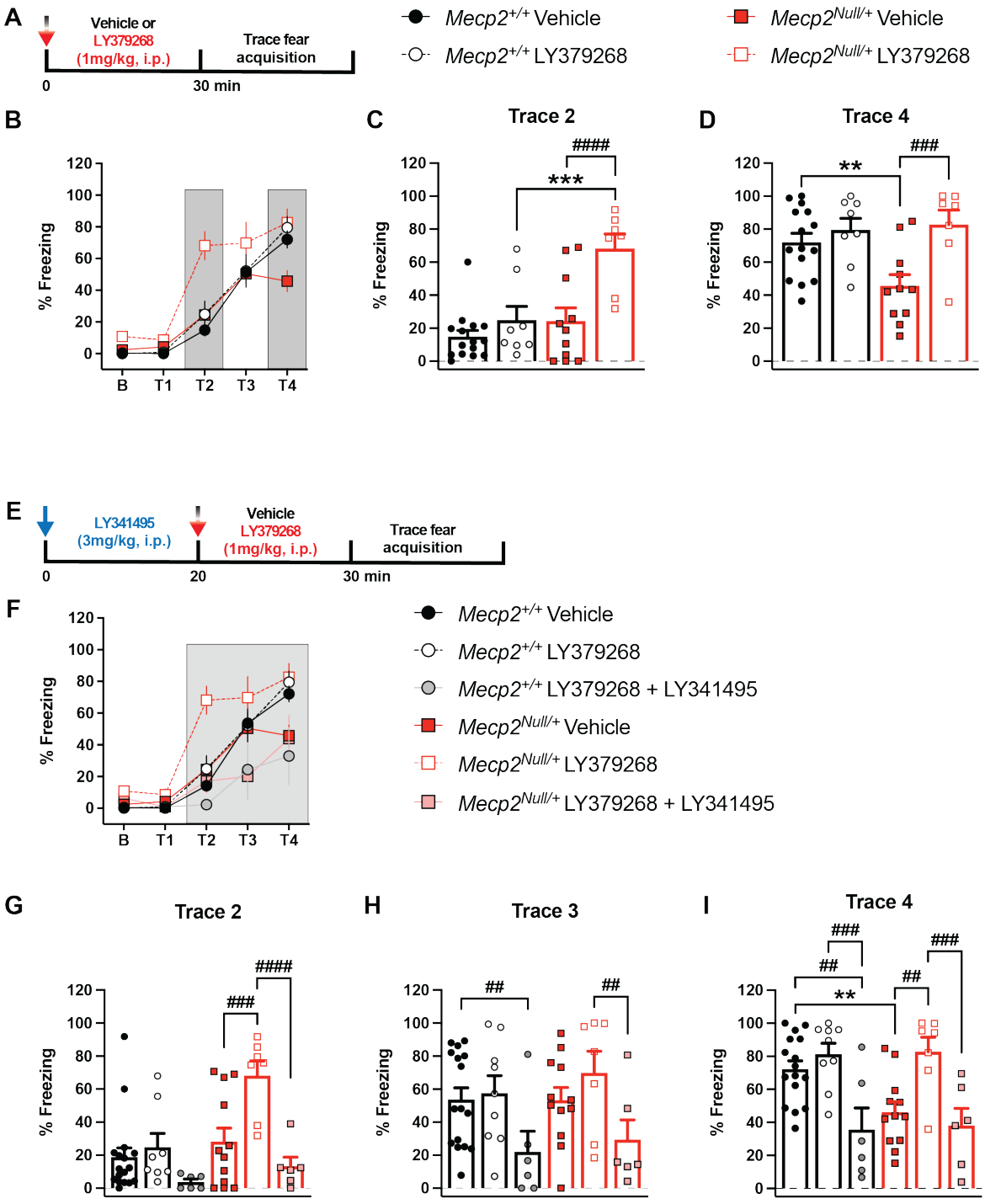

Figure 30: Attenuated trace fear acquisition in *Mecp2*$^{Null/+}$ mice is improved with group II mGlu receptor activation. (A) Diagram illustrating timeline of drug administration prior to trace fear conditioning. Mice are treated intraperitoneally (i.p.) with vehicle (10% Tween-80) or 1 mg/kg LY379268 ($mGlu_{2/3}$ agonist) 30 minutes prior to placement in the fear conditioning box. (B-D) Treatment with LY379268 increases trace fear acquisition in *Mecp2*$^{Null/+}$ mice (red bars, vehicle: closed red squares, n = 15; LY379268: open red squares, n = 7). Freezing behavior in *Mecp2*$^{+/+}$

mice (black bars) is not different between the treatment groups, vehicle (closed black circles, n = 15) and LY379268 (open black circles, n = 8). Analysis of trace periods T2 and T4 (dark grey) are shown in (C) and (D), respectively. (E) Diagram illustrating timeline of co-drug administration of LY341495 ($mGlu_{2/3}$ antagonist) and LY379268 prior to trace fear conditioning. LY341495 (3 mg/kg, i.p.) is administered 20 minutes prior to LY379268 (1 mg/kg, i.p.). (F-I) Co-administration of LY341495 and LY379268 blocked the reversal effect of LY379268 in *Mecp2*$^{Null/+}$ animals (red bars, vehicle: closed red squares, n = 12; LY341495 + LY379268: pink squares, n = 6) at trace periods T2-T4. Percent freezing in *Mecp2*$^{+/+}$ mice (black bars) is decreased with co-administration of LY341495 and LY379268, particularly at trace periods T3-T4 (vehicle: closed black circles, n = 17; LY341495 + LY379268: grey circles, n = 6). Analysis of trace periods T2-T4 (dark grey) is shown in (G-I). 20-25 week-old mice. 2-way ANOVA with Tukey's post-hoc test. *between-genotypes. $^{\#}$within-genotypes. **p<0.01, ***p<0.001, $^{\#\#}$p<0.01, $^{\#\#\#}$p<0.001, $^{\#\#\#\#}$p<0.0001.

4.6.5 $mGlu_{2/3}$ antagonism normalizes abnormal trace fear acquisition phenotype in *MECP2*$^{Tg1/o}$ mice

Given the beneficial effects of activating $mGlu_{2/3}$ in RTT mice, which display opposite trace fear conditioning phenotypes from MDS mice, we then posited the converse hypothesis: that inhibiting $mGlu_{2/3}$ could alleviate the abnormal increase in trace fear behavior in *MECP2*$^{Tg/o}$ animals. Prior to trace fear conditioning, animals were intraperitoneally administered either vehicle (10% Tween-80) or the nonselective orthosteric $mGlu_{2/3}$ antagonist LY341495 (3mg/kg) (Figure 31A). LY341495 treatment did not affect trace fear behavior in WT littermates (Figure 31B-C). However, *MECP2*$^{Tg1/o}$ animals administered LY341495 exhibited significantly reduced percent freezing at the last tone-trace-shock pairing (T3) compared to vehicle-treated *MECP2*$^{Tg1/o}$ mice (Figure 31C). Notably, LY341495-treated *MECP2*$^{Tg1/o}$ mice displayed comparable freezing behavior to vehicle-treated WT counterparts. To rule out potential locomotor effects of $mGlu_{2/3}$ inhibition with the nonselective antagonist, we placed vehicle- and LY341495-treated animals in an open field chamber. At baseline, *MECP2*$^{Tg1/o}$ mice presented with hypolocomotor activity compared to WT littermates. Importantly, regardless of genotype, LY341495 administration did not affect distance traveled in the open field task, which is in agreement with previous studies using systemic

administration of LY341495 (*284*, *286*). Overall, these data suggest that $mGlu_{2/3}$ antagonism has positive effects in normalizing enhanced trace fear behavior in *MECP2*$^{Tg1/o}$ animals.

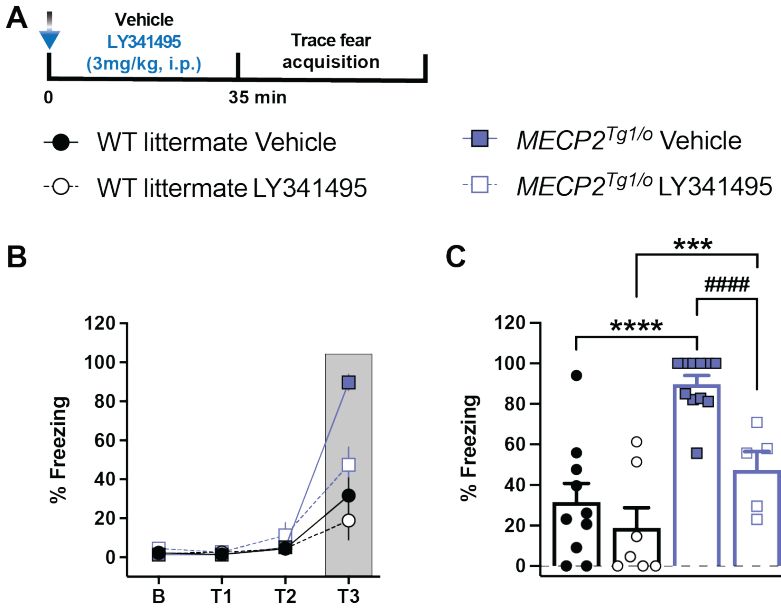

Figure 31: Group II mGlu receptor antagonism normalizes enhanced trace fear acquisition in *MECP2*$^{Tg1/o}$ mice. (A) Diagram illustrating the timeline of LY341495 administration prior to trace fear conditioning. Mice are treated intraperitoneally (i.p.) with vehicle (10% Tween-80) or 3 mg/kg LY341495 ($mGlu_{2/3}$ antagonist) 35 minutes prior to placement in the fear conditioning box. (B-C) LY341495 treatment significantly decreases the enhanced trace fear acquisition phenotype in *MECP2*$^{Tg1/o}$ mice (blue bars, vehicle: closed blue squares, n = 11; LY341495: open blue squares, n = 5) but not in WT littermates (white bars, vehicle: closed black circles, n = 10; LY341495: open black circles, n = 7). Analysis of trace period T3 (dark grey) is shown in (C). 8-12 week-old mice. 2-way ANOVA with Tukey's post-hoc test. *between-genotypes. $^{\#}$within-genotypes. ***p<0.001, ****p<0.0001, $^{\#\#\#\#}$p<0.0001.

4.8 Discussion

Our understanding of *MECP2*-associated disorders has developed tremendously in the past 20 years. However, despite the monogenicity of these disorders and the link of MeCP2 protein expression and/or function to each disease, no effective treatment is currently available for RTT or MDS. Promisingly, recent studies have demonstrated that genetic manipulations of *MECP2* and pharmacological modulations of downstream targets of the protein improve phenotypes in preclinical rodent models of RTT (*93*, *112*–*119*, *124*, *128*, *129*, *136*, *137*, *143*–*145*) and MDS (*94*, *171*, *173*). In this study, we aimed to capitalize on previous reports by investigating two potential therapeutic targets, $mGlu_2$ and $mGlu_3$, and employing pharmacological modulators of these receptors to evaluate effects in RTT ($Mecp2^{Null/+}$) and MDS ($MECP2^{Tg1/o}$) mouse models.

$mGlu_2$ and $mGlu_3$ are group II mGlu receptors that have been robustly implicated in neuropsychiatric disorders (*334*, *403*, *404*, *410*, *411*). Their role in neurodevelopmental disorders is limited; however, $mGlu_3$ has been shown to be involved in the cognitive phenotypes of Fragile X syndrome (FXS) (*324*) and $mGlu_{2/3}$ receptors have been implicated in autism-like phenotypes in a rat model of autism (*323*). Moreover, expression studies demonstrate that both $mGlu_2$ and $mGlu_3$ are decreased in male $Mecp2^{Null/y}$ mice and patients diagnosed with RTT (*15*, *68*, *121*–*124*). Here, we further support these data by showing attenuated $mGlu_2$ and $mGlu_3$ expression in the temporal cortex of RTT autopsy samples from patients with truncating mutations in MeCP2. Altered levels of these receptors are conserved in a female RTT mouse model, $Mecp2^{Null/+}$, specifically in the cortex and hippocampus. Since RTT and MDS are due to loss-of-function mutations and multiple copies of *MECP2*, respectively, and given the role of MeCP2 as a transcriptional activator (*15*), we posited that $mGlu_2$ and $mGlu_3$ expression would be increased in MDS. In the hippocampus of $MECP2^{Tg1/o}$ mice, we confirmed previous studies showing increased MeCP2 expression (*105*, *168*, *362*) and also observed increased $mGlu_2$ and $mGlu_3$ mRNA and

protein expression. These findings suggest that group II mGlu receptors may be targets of MeCP2 transcriptional regulation, whether through direct or indirect mechanisms.

These molecular data provided our rationale to further explore $mGlu_2$ and $mGlu_3$ in the behavioral phenotypes of RTT and MDS, focusing on the learning and memory phenotypes given the role of group II mGlu receptors in cognition. Numerous studies have established that RTT and MDS mice have contrasting characteristics in contextual fear conditioning, a hippocampal-dependent learning and memory paradigm (*70*, *105*, *137*, *168*, *172*, *173*, *329*, *362*, *366*). In particular, RTT mice exhibit deficits in contextual fear conditioning, whereas MDS mice display an abnormal enhancement of this behavior. Several studies have described a similar hippocampal-dependent cognitive task that relies on both the spatial and temporal factors of learning and memory called trace fear conditioning (*408*, *412–414*). Excitingly, our group has demonstrated a specific role for $mGlu_3$ in trace fear acquisition (*267*). Before exploring the relationship of $mGlu_{2/3}$ receptors and trace fear conditioning in mouse models of *MECP2*-associated disorders, we first characterized the behavior of both $Mecp2^{Null/+}$ and $MECP2^{Tg1/o}$ animals in this cognitive task, which has not yet been investigated. Here, we extend previous studies in cognitive domains to show that $Mecp2^{Null/+}$ mice exhibit a deficit in trace fear acquisition. Conversely, $MECP2^{Tg1/o}$ animals have an abnormal enhanced trace fear acquisition phenotype, which supports the bidirectional behavioral phenotypes of cognition in mouse models of these two disorders.

These data prompted us to test our hypothesis that $mGlu_{2/3}$ modulation could improve abnormal cognitive phenotypes in $Mecp2^{Null/+}$ and $MECP2^{Tg1/o}$ mice using the trace fear paradigm. Previous preclinical studies have shown that $mGlu_3$ activation and $mGlu_2$ positive allosteric modulators improve deficits in cognitive tasks (*272*, *308*, *406*). Given that both receptors are decreased in $Mecp2^{Null/+}$ mice, it is likely that the function of both $mGlu_2$ and $mGlu_3$ is also disrupted. Therefore, we activated both receptors using a nonselective $mGlu_{2/3}$ agonist, LY379268. Excitingly, in

Mecp2$^{Null/+}$ animals, LY379268 rescued deficiencies in trace fear acquisition. Interestingly, we observed a left-shifted response to LY379268 that was specific to *Mecp2*$^{Null/+}$ mice. This could be attributed to a ceiling effect of the trace fear paradigm, for example the strong shock intensity, on the baseline trace fear behavior of *Mecp2*$^{+/+}$ animals, which has also been previously observed in WT animals (*267*), or to a potential sensitivity of the receptors to agonist in the *Mecp2*$^{Null/+}$ context. Importantly, LY379268's effect in augmenting freezing behavior in *Mecp2*$^{Null/+}$ was completely blocked by the $mGlu_{2/3}$ antagonist, LY341495, suggesting that LY379268 mediates its effects via $mGlu_2$ and $mGlu_3$ in the trace fear acquisition paradigm in RTT mice.

In contrast to the effects seen in *Mecp2*$^{Null/+}$ animals, inhibition of $mGlu_{2/3}$ receptors with LY341495 reversed the abnormally enhanced trace fear acquisition of *MECP2*$^{Tg1/o}$ mice. The lack of LY341495's effect in WT animals suggests that the heightened trace fear phenotype in *MECP2*$^{Tg1/o}$ mice is driven, in part, by the increased expression of the $mGlu_2$ and/or $mGlu_3$ receptors. The bidirectionality in $mGlu_{2/3}$ modulation to alleviate the abnormal behavioral cognition in *Mecp2*$^{Null/+}$ and *MECP2*$^{Tg1/o}$ animals parallels the contrasting trace fear phenotypes. These together may indicate that, in both the RTT and MDS contexts where both receptors are affected, one or both of the group II mGlu receptors are needed to mediate this form of associative learning and memory.

In *MECP2*$^{Tg1/o}$ and *Mecp2*$^{Null/+}$ mice, the functional consequences of altered $mGlu_2$ and $mGlu_3$ receptor expression, such as in impacting long-term synaptic plasticity in the hippocampal Schaffer collateral-CA1 (SC-CA1) synapse, remains to be elucidated. Previous reports have demonstrated that SC-CA1 long-term potentiation (LTP) is bidirectionally altered in *Mecp2 mutant* and *MECP2*$^{Tg1/o}$ animals (*69*–*71*, *105*, *171*). Additionally, in *Mecp2 mutant* mice, NMDA antagonism has been shown to reverse LTP deficits (*138*). Although no studies have yet shown whether NMDA function is implicated in MDS, NMDA dysregulation has been associated with the

enhanced LTP phenotype of mice modeling a related disorder, Pitt-Hopkins syndrome (*212*, *215*). Coupling these data with previous evidence illustrating that $mGlu_{2/3}$ receptors play a role in NMDA-mediated LTP at the SC-CA1 synapses (*266*), it is therefore possible that $mGlu_{2/3}$ modulation may correct abnormal SC-CA1 LTP in RTT and MDS animals. However, empirical studies are needed to demonstrate this theory.

In conclusion, we have demonstrated that the expression of $mGlu_2$ and $mGlu_3$ is altered in RTT clinical samples and bidirectionally affected in *Mecp2*$^{Null/+}$ and *MECP2*$^{Tg1/o}$ animals, indicating a potential role of group II mGlu receptors in RTT and MDS phenotypes. Correspondingly, we establish that *Mecp2*$^{Null/+}$ and *MECP2*$^{Tg1/o}$ mice present abnormal and contrasting phenotypes in trace fear conditioning, a temporal-dependent form of associative learning and memory. Pharmacological $mGlu_{2/3}$ activation or antagonism exerted efficacy in modulating trace fear behavior of *Mecp2*$^{Null/+}$ and *MECP2*$^{Tg1/o}$ mice, respectively. Altogether, our data provide novel evidence that $mGlu_2$ and $mGlu_3$ are implicated in neurodevelopmental disorders, particularly in RTT and MDS.

4.9 Acknowledgements

We acknowledge the donation of samples from RTT patient families, and we thank the University of Maryland Brain and Tissue Bank, the Harvard Brain Tissue Resource Center, the National Institutes of Health NeuroBioBank and Rettsyndrome.org, for their assistance in obtaining the valuable resource of autopsy samples.

CHAPTER 5

CONCLUSION

The goals of this dissertation stemmed from the assessment and utility of clinical data from RTT patients and consisted of interrogating two arms of the therapeutic drug discovery efforts, genetic and pharmacological interventions, for *MECP2*-related neurodevelopmental disorders. With focus on these two interventions, this research aimed to address two areas of study: (1) Evaluation on the impact of *MECP2* mutations on treatment feasibility; and (2) Identification of novel treatment options for atypical RTT (*MECP2* mutation-negative) and *MECP2*-related disorders using small molecules modulating proteins related to the disease.

5.1 Influence of *MECP2* mutations on treatment safety and efficacy

Extensive behavioral characterization demonstrated the efficacy of genetic supplementation of *MECP2* in mouse models of typical and atypical RTT, specifically PTHS. However, the manifestation of MDS-like adverse effects in the typical RTT mice harboring the hypomorphic and clinically prevalent MeCP2 mutation R133C highlights potential toxicity issues with MeCP2-targeted gene therapy especially in the context of stable expression and functional retention of the MeCP2 protein. More studies are needed to determine if such safety concerns are specific to the R133C mutation studied here or are conserved in all hypomorphic *MECP2* mutations. Several studies have shown that the safety issues of MeCP2 supplementation appear to be restricted in hypomorphic contexts (*74*, *82*, *99*). Still, many *MECP2* mutations that lead to stable protein expression and function have yet to be assessed.

The observed effectiveness of MeCP2 supplementation in PTHS model mice is promising for the treatment of PTHS as well as other related *MECP2* mutation-negative disorders such as *FOXG1* syndrome and *CDKL5* deficiency disorder. Leveraging current treatment strategies of other neurodevelopmental disorders for PTHS is not a new concept; a current Phase II clinical trial is

evaluating RTT-related therapeutics (targeting IGF-1 pathway using NNZ-2591) for PTHS (ClinicalTrials.gov, number NCT05025332). The premise is that targeting the IGF receptor and signaling will improve symptoms in PTHS, a similar mechanism through which trofinetide exerts its effects in RTT. This is due to studies showing that several proteins in the IGF signaling pathway are decreased in *in vitro* TCF4 knockdown studies (*331*, *415*). One of these proteins is IGF-2, which has been implicated in synaptogenesis and learning and memory (*416*, *417*), and activates the same receptor as IGF-1.

The mechanisms underlying the beneficial effects of MeCP2 supplementation in PTHS are still unclear; however, transcriptomics analyses have provided investigative tools. Comparison of these data with transcriptomic information from other related disorders regardless of species, as had been previously done (*121*, *122*, *124*, *378*), would also be insightful in delineating pathways or proteins that are commonly dysregulated between these disorders, which could have clinical implications in treatment selection. To illustrate the utility of transcriptomic data for several disorders, one group of genes of interest from the RNA-sequencing studies was myelination-associated genes. Myelination dysfunction and aberrant white matter are characteristics in patients and preclinical models of several ASDs, including RTT, MDS, PTEN-associated ASD, PTHS and TSC (*378*, *386*, *396*, *418–420*). The studies conducted here recapitulate findings of hypomyelination in PTHS model mice. Although increasing MeCP2 expression did not reverse the attenuated expression of myelination markers, these data supported evidence that targeting myelination regulation could be a potential therapeutic avenue. Recent studies with TSC model mice have shown that perhaps mTOR dysregulation could underlie myelination defects, specifically through the increase of the neuronal connective tissue growth factor (CTGF), which disrupts OL maturation (*386*, *387*). Interestingly, our RNA-seq data indicated that *Ctgf* was increased in *Tcf4*$^{+/-}$ animals with the *MECP2* transgene, which is consistent with the lack of rescue in hypomyelination. Moreover, most of the ASDs mentioned above are associated with mTOR

dysregulation, and is one of the downstream effectors within the IGF signaling pathway (*418*, *421*). Thus, targeting the mTOR pathway to reverse myelination dysfunction and secondary effects, such as synaptic transmission and behavioral abnormalities, could be exploited for several disorders.

Although the positive effects of MeCP2 supplementation in two disorders are encouraging and provide proof-of-concept data, it is imperative to establish whether the effect is also observed with more translatable gene therapy methods using viral vectors expressing MeCP2 as well as the evaluation of translatable neurophysiological features with the use of EEG and auditory and/or visual ERPs. Moreover, the temporal effects of MeCP2 increase should also be assessed. The genetic studies conducted here provided for increased MeCP2 expression throughout development and during pre-symptomatic phases, which is a different context from the ideal clinical approach employing virally-mediated gene therapy after birth and post-symptom onset. To mimic the clinical strategy, one potential approach is to deliver AAV-expressing MeCP2 in adult symptomatic animals. Another method is to use an inducible Cre that targets an additional WT *Mecp2* allele with a STOP cassette in *Mecp2 or Tcf4* mutant animals. In this way, the Cre recombinase enzyme can be activated after symptom onset to allow transcription of the additional WT *Mecp2* allele. Regardless of the method, such studies will contribute to field of MeCP2-targeted gene therapy and our understanding of *MECP2*-related disorders.

The studies here were performed in the context of evaluating MeCP2-targeted therapeutics for RTT and PTHS; however, the bidirectionality of the phenotypes observed in regard to RTT or PTHS model mice compared to the MDS mice suggest that perhaps altering MeCP2 and TCF4 expression and function could be beneficial for MDS. For example, female *Mecp2 null* animals exhibited attenuated motor coordination, anxiety, and learning and memory; MeCP2-overexpressing mice display abnormal enhancements in these tasks. Similar contrasting

phenotypes, with the addition of hyperactivity, were observed when compared with the *Tcf4 haploinsufficient* animals. In the "rescue" or double transgenic animals with both the *Mecp2* or *Tcf4* deficiency and *MECP2* transgene, all these phenotypes in RTT, PTHS and MDS mice were normalized to that of WT animals. Excitingly, a recent study has shown that specific MeCP2 mutations, such as those that disrupt the recruitment of co-repressors via the NID domain, are able to ameliorate abnormal phenotypes caused by MeCP2 overexpression (*94*). On the other hand, mutations in MBD exacerbate MDS-like phenotypes. Our findings here with the *Mecp2 R133C* animals demonstrating MDS-like phenotypes upon *MECP2* transgene expression support the latter observation. Moreover, decreasing Tcf4 expression appears to reverse phenotypes of MDS mice, not only behaviorally but also at transcriptome level, as genes involved in neurodevelopment and neuronal function and disrupted in MDS mice are normalized in the rescue animals. Disrupting Tcf4 expression and function in MDS could possibly be deleterious in practice given Tcf4's role in normal brain development; however, modulating pathways or genes that are shared between these two proteins and/or disorders could be favorable. Therefore, as alluded to above, targeting MeCP2 through the same viral method or convergent pathways among these disorders has implications for a broad clinical population, including MDS patients.

5.2 Identification of novel treatment options for *MECP2*-related disorders

Correction of behavioral cognitive phenotypes, specifically in trace fear conditioning in RTT and MDS mice using a small molecule approach, illustrates that two mGlu receptors may be potential therapeutic targets for these disorders. The reversal effects are consistent with the cognitive improvement exerted by $mGlu_2$ and/or $mGlu_3$ modulation in models of neuropsychiatric disorders such as schizophrenia and depression. Thus, the studies here contribute to the rationale for developing small molecules that target group II mGlu receptors simultaneously or selectively to mediate pathological symptoms, including impaired cognitive function. These data also raise

several possibilities or directions regarding synaptic function and the interplay of these two mGlu receptors alone or with other proteins.

Hippocampal short-term and long-term synaptic plasticity, especially paired-pulse ratio (PPR) and LTP has been used as a correlate to associative learning and memory. An unanswered question in these studies is the effect of $mGlu_{2/3}$ modulation on the synaptic physiology profiles of RTT and MDS mice. RTT mice, similar to NMDA receptor hypofunction models of schizophrenia, exhibit SC-CA1 LTP deficits (*267*, *300*, *422–426*). Conversely, MDS mice exhibit heightened LTP, although there are conflicting reports regarding this phenotype (*105*, *168*, *171*). Another bidirectional phenotype between RTT and MDS mice is PPR, which is attenuated and increased, respectively. It would be prudent to evaluate how $mGlu_{2/3}$ activation mediates synaptic transmission in RTT and MDS. As previously shown, it is likely that only $mGlu_3$ plays a role in SC-CA1 LTP (*267*, *272*). Utility of subtype-selective positive or negative allosteric modulators would help delineate the contribution of these two mGlu receptors in facilitating the cognitive effects. Along the same lines, PAMs and NAMs could be employed *in vivo* to determine whether both receptors are required for improvement of trace fear conditioning in these model mice.

Additionally, while the studies here show that $mGlu_{2/3}$ receptor modulation can affect the changes in trace fear behavior in RTT and MDS model mice, other proteins could also be involved, especially the $mGlu_5$ receptor. Deletion of $mGlu_5$ from CA1 pyramidal cells induces deficits in trace fear conditioning (*267*, *408*). Additionally, the effects of LY379268 in augmenting trace fear acquisition are dependent on the concerted effort of both $mGlu_3$ and $mGlu_5$ (*267*), a relationship that has been previously characterized in the prefrontal cortex (*322*). In regard to MDS, $mGlu_5$ has been linked to abnormal hippocampal synaptic plasticity and behavioral dysfunction observed in MDS animals (*329*). There are also previous reports demonstrating the relationship of $mGlu_5$ and RTT, specifically decreased $mGlu_5$ expression in RTT patients and mouse models, the role

of $mGlu_5$ in mediating hippocampal synaptic plasticity, and the beneficial effects of pharmacologically activating $mGlu_5$ in RTT mice (*136*, *427*). These several lines of evidence suggest that the group II mGlu receptors and $mGlu_5$ are key players in modulating trace fear behavior in RTT and MDS animals. Thus, it is probable that the interplay of these three receptors is needed to regulate trace fear conditioning in RTT and MDS mice. Further studies are needed to elucidate this possibility, but this collective effort could have potential implications in treatment strategies for RTT and MDS.

Although the studies here focused on the role of $mGlu_{2/3}$ receptors on cognitive function, other symptom domains in RTT and MDS could be responsive to $mGlu_{2/3}$ modulation. Several studies have shown that activation of group II mGlu receptors can mediate anxiety-related behavior, both in having anxiolytic and anxiogenic effects, and hyperlocomotor activity especially in models of NMDA receptor hypofunction (*279*–*281*, *323*). $mGlu_{2/3}$ receptor antagonism also normalizes abnormal anxiety and motor phenotypes (*279*–*281*). Therefore, targeting the group II mGlu receptors, either simultaneously or selectively, could be advantageous across many symptoms of the RTT and MDS, and future studies should assess these potential effects in rodent models of these disorders.

In regard to RTT, the reversal effects of $mGlu_{2/3}$ activation in *Mecp2 null* animals are consistent with the human-derived data of attenuated $mGlu_2$ and $mGlu_3$ levels. However, expression data from post-mortem human samples also postulate that perhaps the effects of group II mGlu receptor modulation is dependent on the type and domain localization of the *MECP2* mutation (Figure 32). For example, mutations in the MBD lead to decrease levels of $mGlu_2$ and $mGlu_3$, and specifically, the T158M mutation affect both receptors. Interestingly, $mGlu_2$ expression appears to be sensitive to mutations in all MeCP2 functional domains compared to $mGlu_3$, which may suggest that $mGlu_2$ receptor modulation could have exert efficacy in a broader population of RTT patients.

Moreover, both receptors are also attenuated in *MECP2* mutation-negative samples, which represents samples from patients diagnosed with RTT but do not have mutations in *MECP2*. Thus, it is possible that atypical RTT disorders could benefit from $mGlu_{2/3}$-targeted therapy. Future studies should assess $mGlu_{2/3}$ activation in MeCP2 point mutant mouse models, as well as mice modeling atypical RTT disorders, to determine the effect of MeCP2 mutation on symptomatic treatment strategies.

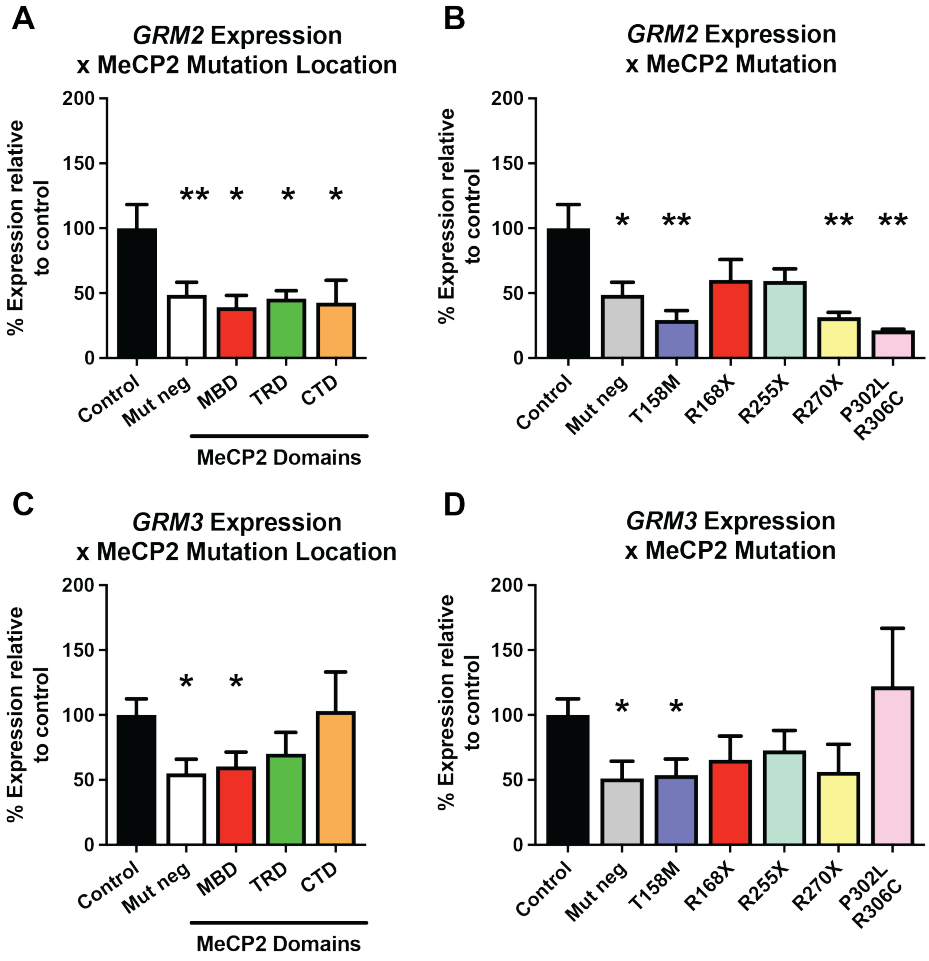

Figure 32: mGu_2 and $mGlu_3$ mRNA expression is dependent on MeCP2 mutation. *GRM2* (A-B) and *GRM3* (C-D) levels in RTT (n = 42) are dependent on the location of the mutation within the protein domain (A, C) and the type of mutation (B, D; common mutations are shown). Control samples (n = 11-12) are from sex-, age- and post-mortem interval-matched samples of typical patients. All samples are from the temporal cortex, Brodmann areas 20 and 38. The *MECP2* mutation-negative (Mut Neg) designation represents samples from patients clinically diagnosed with RTT

but lacking a mutation in *MECP2*. Student's unpaired t-test, *p < 0.05, **p < 0.05. MeCP2 domains: methyl-CpG-binding domain (MBD), transcriptional repressor domain (TRD), C-terminus (CTD).

In conclusion, this dissertation aimed to provide information pertinent to the clinical trajectory of MeCP2-targeted gene therapy and potential novel therapeutic targets for *MECP2*-related neurodevelopmental disorders. The collected preclinical data has implications for precision or personalized medicine of *MECP2*-related neurodevelopmental disorders.

TABLES

Phenotype	- *MECP2* transgene			+ *MECP2* transgene		
	R133C/y	***R133C/+***	***Null/+***	***R133C/y***	***R133C/+***	***Null/+***
Decreased weight	✓	✓	Inconclusive	+	+	Inconclusive
Decreased survival			✓			+
Seizures			✓			+
Hindlimb clasping[#]	✓	✓	✓	+	+	+
Decreased acoustic startle response	✓	✓	n/a	+	+	n/a
Apneas	✓	✓	✓	+	+	+
Decreased social preference	✓	✓	✓	+	+	+
Decreased anxiety	✓	✓	✓	+	-	+
Decreased motor coordination[#]	✓	✓	✓	+	-	+
Decreased contextual freezing[#]	✓		✓	+	-	+

[#] *Statistically different between Mecp2$^{R133C/+}$ and Mecp2$^{null/+}$*

+ (beneficial effect in improving phenotype); - (MDS-like phenotype/adverse effect)

Table 1: Behavioral phenotyping comparison in *Mecp2 mutant* mice with and without an *MECP2* transgene.

Phenotype	*Tcf4*$^{+/-}$	
	- *MECP2* transgene	**+ *MECP2* transgene**
Tcf4 transcript	✓	No effect
Mecp2 transcript + protein	No change	-
Hyperactivity	✓	+
Decreased anxiety	✓	+
Decreased contextual freezing	✓	+
+ (beneficial effect in improving phenotype); *- (MDS-like phenotype/adverse effect)*		

Table 2: Molecular and behavioral comparison in *Tcf4 mutant* mice with and without an *MECP2* transgene.

Activity	Compound	Selectivity	Effects in preclinical investigations
Agonist	LY354740	Group II	Anti-psychotic (*296*, *297*) Neuroprotection (*273*) Anxiolytic (*279*)
	LY379268	Group II	Neuroprotection (*273*) Anti-psychotic (*280*, *297–300*) Anti-depressant (*276*, *335*) Pro-cognitive (*267*, *299*) Anxiolytic / anxiogenic (*280*)
Antagonist	LY341495	Group II > Group III > Group I	Anxiolytic (*281*) Antidepressant (*284*) Stress resilience (*277*)
PAM	LY487379	$mGlu_2$	Anti-psychotic (*306*)
	BINA	$mGlu_2$	Anti-psychotic (*265*)
NAM	VU6001966	$mGlu_2$	Antidepressant (*264*)
	VU0650786	$mGlu_3$	Antidepressant (*264*, *287*, *405*)

Table 3: List of common compounds targeting the Group II mGlu receptors.

Code	AN Number	Age	Sex	PMI (hr)	Mutation	%XCI	Region	Sub-reg	Cause of Death
Rett-1	AN19242	10	F	N/A	R255X	63.9	Cortex	BA20	
Rett-3	AN15579	11	F	9.6	R255X	38.9	Cortex	BA38	
Rett-4	AN04573	12	F	5	R270X	49.1	Cortex	BA20	
Rett-5	AN08016	8	F	2.9	R255X		Cortex	BA38	
Rett-6	AN02091	24	F	15.78	R255X		Cortex	BA20	
Rett-7	AN04121	10	F	23.5	R270X		Cortex	BA38	
Rett-13	AN13266	33	F	23.67	R270X		Cortex	BA38	
Rett-16	AN15264	35	F	25.37	R168X		Cortex	BA38	
Rett-23	AN07309	12	F	16.83	R255X		Cortex	BA38	
Rett-26	AN17849	12	F	3.08	R168X		Cortex	BA38	
Rett-27	AN14876	26	F	17.05	R270X		Cortex	BA38	
Rett-32	AN05266	21	F	19.68	R168X		Cortex	BA38	
Rett-33	AN09497	27	F	32.08	R255X		Cortex	BA38	
Rett-37	AN05357	12	F	8.13	R168X		Cortex	BA38	

Rett	Age	PMI
AVG	**18.1**	**15.6**
SEM	**2.5**	**2.6**

Code	UMBN	Age	Sex	PMI (hr)	Mutation	%XCI	Region	Sub-reg	Cause of Death
CTL-3	#5161	10	F	22	None		Cortex	BA38	Accidental Hanging, S15
CTL-4	#5554	13	F	15	None		Cortex	BA38	Suicidal Hanging, S9
CTL-6	#5844	42	F	12	None		Cortex	BA38	Cardiac Arrythmia, S11
CTL-7	#5566	15	F	23	None		Cortex	BA38	Hypertrophic Cardiomyopathy, S11
CTL-8	#5309	14	F	8	None		Cortex	BA38	Streptococcal Toxic Shock, S13
CTL-9	#4330	19	F	19	None		Cortex	BA38	Unaffected Control, 4430S9
CTL-10	#5446	18	F	18	None		Cortex	BA38	Unaffected Control, 5446S11
CTL-11	#5538	19	F	24	None		Cortex	BA38	Unaffected Control, 5538S11
CTL-12	#5644	30	F	23	None		Cortex	BA38	Unaffected Control, 5644S9
CTL-13	#5646	21	F	23	None		Cortex	BA38	Unaffected Control, 5646S11
CTL-14	#5669	25	F	29	None		Cortex	BA38	Unaffected Control, 5669S11
CTL-15	#5670	17	F	22	None		Cortex	BA38	Unaffected Control, 5670S11
CTL-16	#5751	25	F	24	None		Cortex	BA38	Unaffected Control, 5751S11

CTL	Age	PMI
AVG	**20.6**	**20.2**
SEM	**2.3**	**1.6**

Table 4: Human temporal cortex sample data. PMI = post mortem interval, XCI = X chromosome inactivation. *cause of death in RTT samples is not specified.

REFERENCES

1. S. Vidal *et al.*, Genetic landscape of rett syndrome spectrum: improvements and challenges. *Int. J. Mol. Sci.* **20** (2019).
2. M. D'Esposito *et al.*, Isolation, physical mapping, and northern analysis of the X-linked human gene encoding methyl CpG-binding protein, MECP2. *Mamm. Genome*. **7**, 533–535 (1996).
3. N. A. Quaderi *et al.*, Genetic and physical mapping of a gene encoding a methyl CpG binding protein, Mecp2, to the mouse X chromosome. *Genomics*. **22**, 648–651 (1994).
4. J. F. Coy, Z. Sedlacek, D. Bächner, H. Delius, A. Poustka, A complex pattern of evolutionary conservation and alternative polyadenylation within the long 3"-untranslated region of the methyl-CpG-binding protein 2 gene (MeCP2) suggests a regulatory role in gene expression. *Hum. Mol. Genet.* **8**, 1253–1262 (1999).
5. G. N. Mnatzakanian *et al.*, A previously unidentified MECP2 open reading frame defines a new protein isoform relevant to Rett syndrome. *Nat. Genet.* **36**, 339–341 (2004).
6. S. Kriaucionis, A. Bird, The major form of MeCP2 has a novel N-terminus generated by alternative splicing. *Nucleic Acids Res.* **32**, 1818–1823 (2004).
7. X. Nan, P. Tate, E. Li, A. Bird, DNA methylation specifies chromosomal localization of MeCP2. *Mol. Cell. Biol.* **16**, 414–421 (1996).
8. R. J. Klose *et al.*, DNA binding selectivity of MeCP2 due to a requirement for A/T sequences adjacent to methyl-CpG. *Mol. Cell*. **19**, 667–678 (2005).
9. J. C. Hansen, R. P. Ghosh, C. L. Woodcock, Binding of the Rett syndrome protein, MeCP2, to methylated and unmethylated DNA and chromatin. *IUBMB Life*. **62**, 732–738 (2010).
10. P. J. Skene *et al.*, Neuronal MeCP2 is expressed at near histone-octamer levels and globally alters the chromatin state. *Mol. Cell*. **37**, 457–468 (2010).
11. M. Mellén, P. Ayata, S. Dewell, S. Kriaucionis, N. Heintz, MeCP2 binds to 5hmC enriched within active genes and accessible chromatin in the nervous system. *Cell*. **151**, 1417–1430 (2012).
12. J. U. Guo *et al.*, Distribution, recognition and regulation of non-CpG methylation in the adult mammalian brain. *Nat. Neurosci.* **17**, 215–222 (2014).
13. H. W. Gabel *et al.*, Disruption of DNA-methylation-dependent long gene repression in Rett syndrome. *Nature*. **522**, 89–93 (2015).
14. S. Lagger *et al.*, MeCP2 recognizes cytosine methylated tri-nucleotide and di-nucleotide sequences to tune transcription in the mammalian brain. *PLoS Genet.* **13**, e1006793 (2017).
15. M. Chahrour *et al.*, MeCP2, a key contributor to neurological disease, activates and represses transcription. *Science*. **320**, 1224–1229 (2008).
16. X. Nan *et al.*, Transcriptional repression by the methyl-CpG-binding protein MeCP2 involves a histone deacetylase complex. *Nature*. **393**, 386–389 (1998).
17. M. J. Lyst *et al.*, Rett syndrome mutations abolish the interaction of MeCP2 with the NCoR/SMRT co-repressor. *Nat. Neurosci.* **16**, 898–902 (2013).
18. R. C. Samaco, J. L. Neul, Complexities of Rett syndrome and MeCP2. *J. Neurosci.* **31**, 7951–7959 (2011).
19. M. J. Lyst, A. Bird, Rett syndrome: a complex disorder with simple roots. *Nat. Rev. Genet.* **16**, 261–275 (2015).
20. J. Guy, H. Cheval, J. Selfridge, A. Bird, The role of MeCP2 in the brain. *Annu. Rev. Cell Dev. Biol.* **27**, 631–652 (2011).
21. L. M. Lombardi, S. A. Baker, H. Y. Zoghbi, MECP2 disorders: from the clinic to mice and back. *J. Clin. Invest.* **125**, 2914–2923 (2015).
22. J. I. Young *et al.*, Regulation of RNA splicing by the methylation-dependent transcriptional repressor methyl-CpG binding protein 2. *Proc. Natl. Acad. Sci. USA*. **102**, 17551–17558

(2005).
23. J. P. Buschdorf, W. H. Strätling, A WW domain binding region in methyl-CpG-binding protein MeCP2: impact on Rett syndrome. *J. Mol. Med.* **82**, 135–143 (2004).
24. S. W. Long, J. Y. Y. Ooi, P. M. Yau, P. L. Jones, A brain-derived MeCP2 complex supports a role for MeCP2 in RNA processing. *Biosci. Rep.* **31**, 333–343 (2011).
25. S. S. Maxwell, G. J. Pelka, P. P. Tam, A. El-Osta, Chromatin context and ncRNA highlight targets of MeCP2 in brain. *RNA Biol.* **10**, 1741–1757 (2013).
26. D. V. C. Brito, K. Gulmez Karaca, J. Kupke, L. Frank, A. M. M. Oliveira, MeCP2 gates spatial learning-induced alternative splicing events in the mouse hippocampus. *Mol. Brain*. **13**, 156 (2020).
27. J. O'Brien, H. Hayder, Y. Zayed, C. Peng, Overview of microrna biogenesis, mechanisms of actions, and circulation. *Front. Endocrinol. (Lausanne)*. **9**, 402 (2018).
28. T.-L. Cheng *et al.*, MeCP2 suppresses nuclear microRNA processing and dendritic growth by regulating the DGCR8/Drosha complex. *Dev. Cell*. **28**, 547–560 (2014).
29. K. E. Szulwach *et al.*, Cross talk between microRNA and epigenetic regulation in adult neurogenesis. *J. Cell Biol.* **189**, 127–141 (2010).
30. T.-L. Cheng *et al.*, Regulation of mRNA splicing by MeCP2 via epigenetic modifications in the brain. *Sci. Rep.* **7**, 42790 (2017).
31. O. Glaich *et al.*, DNA methylation directs microRNA biogenesis in mammalian cells. *Nat. Commun.* **10**, 5657 (2019).
32. K. Tsujimura *et al.*, miR-199a Links MeCP2 with mTOR Signaling and Its Dysregulation Leads to Rett Syndrome Phenotypes. *Cell Rep.* **12**, 1887–1901 (2015).
33. Y. Li *et al.*, Global transcriptional and translational repression in human-embryonic-stem-cell-derived Rett syndrome neurons. *Cell Stem Cell*. **13**, 446–458 (2013).
34. S. Ricciardi *et al.*, Reduced AKT/mTOR signaling and protein synthesis dysregulation in a Rett syndrome animal model. *Hum. Mol. Genet.* **20**, 1182–1196 (2011).
35. N. Mellios *et al.*, MeCP2-regulated miRNAs control early human neurogenesis through differential effects on ERK and AKT signaling. *Mol. Psychiatry*. **23**, 1051–1065 (2018).
36. M. D. Shahbazian, B. Antalffy, D. L. Armstrong, H. Y. Zoghbi, Insight into Rett syndrome: MeCP2 levels display tissue- and cell-specific differences and correlate with neuronal maturation. *Hum. Mol. Genet.* **11**, 115–124 (2002).
37. N. Kishi, J. D. Macklis, MECP2 is progressively expressed in post-migratory neurons and is involved in neuronal maturation rather than cell fate decisions. *Mol. Cell. Neurosci.* **27**, 306–321 (2004).
38. N. Ballas, D. T. Lioy, C. Grunseich, G. Mandel, Non-cell autonomous influence of MeCP2-deficient glia on neuronal dendritic morphology. *Nat. Neurosci.* **12**, 311–317 (2009).
39. I. Maezawa, S. Swanberg, D. Harvey, J. M. LaSalle, L.-W. Jin, Rett syndrome astrocytes are abnormal and spread MeCP2 deficiency through gap junctions. *J. Neurosci.* **29**, 5051–5061 (2009).
40. I. Maezawa, L.-W. Jin, Rett syndrome microglia damage dendrites and synapses by the elevated release of glutamate. *J. Neurosci.* **30**, 5346–5356 (2010).
41. D. T. Lioy *et al.*, A role for glia in the progression of Rett's syndrome. *Nature*. **475**, 497–500 (2011).
42. B. Hagberg, J. Aicardi, K. Dias, O. Ramos, A progressive syndrome of autism, dementia, ataxia, and loss of purposeful hand use in girls: Rett's syndrome: report of 35 cases. *Ann. Neurol.* **14**, 471–479 (1983).
43. A. Rett, [On a unusual brain atrophy syndrome in hyperammonemia in childhood]. *Wien. Med. Wochenschr.* **116**, 723–726 (1966).
44. D. D. Armstrong, The neuropathology of Rett syndrome--overview 1994. *Neuropediatrics*. **26**, 100–104 (1995).
45. J. L. Neul *et al.*, Rett syndrome: revised diagnostic criteria and nomenclature. *Ann. Neurol.*

68, 944–950 (2010).
46. H. Leonard, S. Cobb, J. Downs, Clinical and biological progress over 50 years in Rett syndrome. *Nat. Rev. Neurol.* **13**, 37–51 (2017).
47. R. E. Amir *et al.*, Rett syndrome is caused by mutations in X-linked MECP2, encoding methyl-CpG-binding protein 2. *Nat. Genet.* **23**, 185–188 (1999).
48. D. A. Adler *et al.*, The X-linked methylated DNA binding protein, Mecp2, is subject to X inactivation in the mouse. *Mamm. Genome*. **6**, 491–492 (1995).
49. D. Braunschweig, T. Simcox, R. C. Samaco, J. M. LaSalle, X-Chromosome inactivation ratios affect wild-type MeCP2 expression within mosaic Rett syndrome and Mecp2-/+ mouse brain. *Hum. Mol. Genet.* **13**, 1275–1286 (2004).
50. H. Y. Zoghbi, A. K. Percy, R. J. Schultz, C. Fill, Patterns of X chromosome inactivation in the Rett syndrome. *Brain Dev.* **12**, 131–135 (1990).
51. G. P. S. Knudsen *et al.*, Increased skewing of X chromosome inactivation in Rett syndrome patients and their mothers. *Eur. J. Hum. Genet.* **14**, 1189–1194 (2006).
52. J. L. Neul *et al.*, The array of clinical phenotypes of males with mutations in Methyl-CpG binding protein 2. *Am. J. Med. Genet. B, Neuropsychiatr. Genet.* **180**, 55–67 (2019).
53. Q. Zhang *et al.*, Familial cases and male cases with MECP2 mutations. *Am. J. Med. Genet. B, Neuropsychiatr. Genet.* **174**, 451–457 (2017).
54. M. Topçu *et al.*, Somatic mosaicism for a MECP2 mutation associated with classic Rett syndrome in a boy. *Eur. J. Hum. Genet.* **10**, 77–81 (2002).
55. L. Villard, MECP2 mutations in males. *J. Med. Genet.* **44**, 417–423 (2007).
56. J. Christodoulou, A. Grimm, T. Maher, B. Bennetts, RettBASE: The IRSA MECP2 variation database-a new mutation database in evolution. *Hum. Mutat.* **21**, 466–472 (2003).
57. S. Fyfe, A. Cream, N. de Klerk, J. Christodoulou, H. Leonard, InterRett and RettBASE: International Rett Syndrome Association databases for Rett syndrome. *J. Child Neurol.* **18**, 709–713 (2003).
58. D. Young *et al.*, The relationship between MECP2 mutation type and health status and service use trajectories over time in a Rett syndrome population. *Res. Autism Spectr. Disord.* **5**, 442–449 (2011).
59. S. M. Kyle, N. Vashi, M. J. Justice, Rett syndrome: a neurological disorder with metabolic components. *Open Biol*. **8** (2018).
60. V. A. Cuddapah *et al.*, Methyl-CpG-binding protein 2 (MECP2) mutation type is associated with disease severity in Rett syndrome. *J. Med. Genet.* **51**, 152–158 (2014).
61. R. R. Shah, A. P. Bird, MeCP2 mutations: progress towards understanding and treating Rett syndrome. *Genome Med.* **9**, 17 (2017).
62. W. Li, L. Pozzo-Miller, Beyond Widespread Mecp2 Deletions to Model Rett Syndrome: Conditional Spatio-Temporal Knockout, Single-Point Mutations and Transgenic Rescue Mice. *Autism Open Access*. **2012**, 5 (2012).
63. D. M. Katz *et al.*, Preclinical research in Rett syndrome: setting the foundation for translational success. *Dis. Model. Mech.* **5**, 733–745 (2012).
64. L. Ricceri, B. De Filippis, G. Laviola, Mouse models of Rett syndrome: from behavioural phenotyping to preclinical evaluation of new therapeutic approaches. *Behav. Pharmacol.* **19**, 501–517 (2008).
65. G. M. Jentarra *et al.*, Abnormalities of cell packing density and dendritic complexity in the MeCP2 A140V mouse model of Rett syndrome/X-linked mental retardation. *BMC Neurosci.* **11**, 19 (2010).
66. J. V. Deng *et al.*, MeCP2 in the nucleus accumbens contributes to neural and behavioral responses to psychostimulants. *Nat. Neurosci.* **13**, 1128–1136 (2010).
67. M. V. C. Nguyen *et al.*, MeCP2 is critical for maintaining mature neuronal networks and global brain anatomy during late stages of postnatal brain development and in the mature adult brain. *J. Neurosci.* **32**, 10021–10034 (2012).

68. F. Bedogni *et al.*, Defects during mecp2 null embryonic cortex development precede the onset of overt neurological symptoms. *Cereb. Cortex*. **26**, 2517–2529 (2016).
69. Y. Asaka, D. G. M. Jugloff, L. Zhang, J. H. Eubanks, R. M. Fitzsimonds, Hippocampal synaptic plasticity is impaired in the Mecp2-null mouse model of Rett syndrome. *Neurobiol. Dis.* **21**, 217–227 (2006).
70. P. Moretti *et al.*, Learning and memory and synaptic plasticity are impaired in a mouse model of Rett syndrome. *J. Neurosci.* **26**, 319–327 (2006).
71. J. Guy, J. Gan, J. Selfridge, S. Cobb, A. Bird, Reversal of neurological defects in a mouse model of Rett syndrome. *Science*. **315**, 1143–1147 (2007).
72. H.-T. Chao *et al.*, Dysfunction in GABA signalling mediates autism-like stereotypies and Rett syndrome phenotypes. *Nature*. **468**, 263–269 (2010).
73. S. Cohen *et al.*, Genome-wide activity-dependent MeCP2 phosphorylation regulates nervous system development and function. *Neuron*. **72**, 72–85 (2011).
74. M. R. Pitcher *et al.*, Rett syndrome like phenotypes in the R255X Mecp2 mutant mouse are rescued by MECP2 transgene. *Hum. Mol. Genet.* **24**, 2662–2672 (2015).
75. E. C. Ballinger *et al.*, Mecp2 Deletion from Cholinergic Neurons Selectively Impairs Recognition Memory and Disrupts Cholinergic Modulation of the Perirhinal Cortex. *eNeuro*. **6** (2019).
76. M. Shahbazian *et al.*, Mice with truncated MeCP2 recapitulate many Rett syndrome features and display hyperacetylation of histone H3. *Neuron*. **35**, 243–254 (2002).
77. R. C. Samaco *et al.*, Loss of MeCP2 in aminergic neurons causes cell-autonomous defects in neurotransmitter synthesis and specific behavioral abnormalities. *Proc. Natl. Acad. Sci. USA*. **106**, 21966–21971 (2009).
78. D. Goffin *et al.*, Rett syndrome mutation MeCP2 T158A disrupts DNA binding, protein stability and ERP responses. *Nat. Neurosci.* **15**, 274–283 (2011).
79. R. C. Samaco *et al.*, Female Mecp2(+/-) mice display robust behavioral deficits on two different genetic backgrounds providing a framework for pre-clinical studies. *Hum. Mol. Genet.* **22**, 96–109 (2013).
80. J. M. Bissonnette, L. R. Schaevitz, S. J. Knopp, Z. Zhou, Respiratory phenotypes are distinctly affected in mice with common Rett syndrome mutations MeCP2 T158A and R168X. *Neuroscience*. **267**, 166–176 (2014).
81. E. Wegener *et al.*, Characterization of the MeCP2R168X knockin mouse model for Rett syndrome. *PLoS One*. **9**, e115444 (2014).
82. J. M. Lamonica *et al.*, Elevating expression of MeCP2 T158M rescues DNA binding and Rett syndrome-like phenotypes. *J. Clin. Invest.* **127**, 1889–1904 (2017).
83. J. K. Merritt, B. E. Collins, K. R. Erickson, H. Dong, J. L. Neul, Pharmacological readthrough of R294X Mecp2 in a novel mouse model of Rett Syndrome. *Hum. Mol. Genet.* (2020).
84. H.-W. Dong *et al.*, Detection of neurophysiological features in female R255X MeCP2 mutation mice. *Neurobiol. Dis.*, 105083 (2020).
85. J. Guy, B. Hendrich, M. Holmes, J. E. Martin, A. Bird, A mouse Mecp2-null mutation causes neurological symptoms that mimic Rett syndrome. *Nat. Genet.* **27**, 322–326 (2001).
86. R. Z. Chen, S. Akbarian, M. Tudor, R. Jaenisch, Deficiency of methyl-CpG binding protein-2 in CNS neurons results in a Rett-like phenotype in mice. *Nat. Genet.* **27**, 327–331 (2001).
87. T. M. Yusufzai, A. P. Wolffe, Functional consequences of Rett syndrome mutations on human MeCP2. *Nucleic Acids Res.* **28**, 4172–4179 (2000).
88. S. Kudo *et al.*, Functional analyses of MeCP2 mutations associated with Rett syndrome using transient expression systems. *Brain Dev.* **23 Suppl 1**, S165-73 (2001).
89. S. Kudo *et al.*, Heterogeneity in residual function of MeCP2 carrying missense mutations in the methyl CpG binding domain. *J. Med. Genet.* **40**, 487–493 (2003).
90. A. Kumar *et al.*, Analysis of protein domains and Rett syndrome mutations indicate that

multiple regions influence chromatin-binding dynamics of the chromatin-associated protein MECP2 in vivo. *J. Cell Sci.* **121**, 1128–1137 (2008).
91. R. P. Ghosh, R. A. Horowitz-Scherer, T. Nikitina, L. M. Gierasch, C. L. Woodcock, Rett syndrome-causing mutations in human MeCP2 result in diverse structural changes that impact folding and DNA interactions. *J. Biol. Chem.* **283**, 20523–20534 (2008).
92. V. Kruusvee *et al.*, Structure of the MeCP2-TBLR1 complex reveals a molecular basis for Rett syndrome and related disorders. *Proc. Natl. Acad. Sci. USA*. **114**, E3243–E3250 (2017).
93. R. Tillotson *et al.*, Radically truncated MeCP2 rescues Rett syndrome-like neurological defects. *Nature*. **550**, 398–401 (2017).
94. M. V. Koerner *et al.*, Toxicity of overexpressed MeCP2 is independent of HDAC3 activity. *Genes Dev.* **32**, 1514–1524 (2018).
95. L. D. Heckman, M. H. Chahrour, H. Y. Zoghbi, Rett-causing mutations reveal two domains critical for MeCP2 function and for toxicity in MECP2 duplication syndrome mice. *Elife*. **3** (2014).
96. A. Lawson-Yuen *et al.*, Ube3a mRNA and protein expression are not decreased in Mecp2R168X mutant mice. *Brain Res.* **1180**, 1–6 (2007).
97. L. R. Schaevitz, N. B. Gómez, D. P. Zhen, J. E. Berger-Sweeney, MeCP2 R168X male and female mutant mice exhibit Rett-like behavioral deficits. *Genes Brain Behav.* **12**, 732–740 (2013).
98. K. Brown *et al.*, The molecular basis of variable phenotypic severity among common missense mutations causing Rett syndrome. *Hum. Mol. Genet.* **25**, 558–570 (2016).
99. B. E. Collins, J. K. Merritt, K. R. Erickson, J. L. Neul, Safety and efficacy of genetic MECP2 supplementation in the R294X mouse model of Rett syndrome. *Genes Brain Behav.*, e12739 (2021).
100. S. A. D. Vermudez *et al.*, Profiling beneficial and potential adverse effects of MeCP2 overexpression in a hypomorphic Rett syndrome mouse model. *Genes Brain Behav.*, e12752 (2021).
101. S. Luikenhuis, E. Giacometti, C. F. Beard, R. Jaenisch, Expression of MeCP2 in postmitotic neurons rescues Rett syndrome in mice. *Proc. Natl. Acad. Sci. USA*. **101**, 6033–6038 (2004).
102. L. Robinson *et al.*, Morphological and functional reversal of phenotypes in a mouse model of Rett syndrome. *Brain*. **135**, 2699–2710 (2012).
103. N. C. Derecki *et al.*, Wild-type microglia arrest pathology in a mouse model of Rett syndrome. *Nature*. **484**, 105–109 (2012).
104. J. Wang *et al.*, Wild-type microglia do not reverse pathology in mouse models of Rett syndrome. *Nature*. **521**, E1-4 (2015).
105. A. L. Collins *et al.*, Mild overexpression of MeCP2 causes a progressive neurological disorder in mice. *Hum. Mol. Genet.* **13**, 2679–2689 (2004).
106. E. Giacometti, S. Luikenhuis, C. Beard, R. Jaenisch, Partial rescue of MeCP2 deficiency by postnatal activation of MeCP2. *Proc. Natl. Acad. Sci. USA*. **104**, 1931–1936 (2007).
107. D. G. M. Jugloff *et al.*, Targeted delivery of an Mecp2 transgene to forebrain neurons improves the behavior of female Mecp2-deficient mice. *Hum. Mol. Genet.* **17**, 1386–1396 (2008).
108. C. Bodda *et al.*, Mild overexpression of Mecp2 in mice causes a higher susceptibility toward seizures. *Am. J. Pathol.* **183**, 195–210 (2013).
109. M. Alvarez-Saavedra, M. A. Sáez, D. Kang, H. Y. Zoghbi, J. I. Young, Cell-specific expression of wild-type MeCP2 in mouse models of Rett syndrome yields insight about pathogenesis. *Hum. Mol. Genet.* **16**, 2315–2325 (2007).
110. K. K. Gadalla *et al.*, Gene therapy for Rett syndrome: prospects and challenges. *Future Neurol.* **10**, 467–484 (2015).

111. S. E. Sinnett, S. J. Gray, Recent endeavors in MECP2 gene transfer for gene therapy of Rett syndrome. *Discov Med*. **24**, 153–159 (2017).
112. K. K. E. Gadalla *et al.*, Improved survival and reduced phenotypic severity following AAV9/MECP2 gene transfer to neonatal and juvenile male Mecp2 knockout mice. *Mol. Ther.* **21**, 18–30 (2013).
113. S. K. Garg *et al.*, Systemic delivery of MeCP2 rescues behavioral and cellular deficits in female mouse models of Rett syndrome. *J. Neurosci.* **33**, 13612–13620 (2013).
114. V. Matagne *et al.*, A codon-optimized Mecp2 transgene corrects breathing deficits and improves survival in a mouse model of Rett syndrome. *Neurobiol. Dis.* **99**, 1–11 (2017).
115. S. E. Sinnett *et al.*, Improved MECP2 Gene Therapy Extends the Survival of MeCP2-Null Mice without Apparent Toxicity after Intracisternal Delivery. *Mol. Ther. Methods Clin. Dev.* **5**, 106–115 (2017).
116. K. K. E. Gadalla *et al.*, Development of a Novel AAV Gene Therapy Cassette with Improved Safety Features and Efficacy in a Mouse Model of Rett Syndrome. *Mol. Ther. Methods Clin. Dev.* **5**, 180–190 (2017).
117. M. Luoni *et al.*, Whole brain delivery of an instability-prone Mecp2 transgene improves behavioral and molecular pathological defects in mouse models of Rett syndrome. *Elife*. **9** (2020).
118. V. Matagne *et al.*, Severe offtarget effects following intravenous delivery of AAV9-MECP2 in a female mouse model of Rett syndrome. *Neurobiol. Dis.* **149**, 105235 (2021).
119. S. Powers *et al.*, Rett syndrome gene therapy improves survival and ameliorates behavioral phenotypes in MeCP2 null (S51.002). *Neurology* (2019).
120. S. E. Sinnett, E. Boyle, C. Lyons, S. J. Gray, Engineered microRNA-based regulatory element permits safe high-dose miniMECP2 gene therapy in Rett mice. *Brain* (2021).
121. S. Ben-Shachar, M. Chahrour, C. Thaller, C. A. Shaw, H. Y. Zoghbi, Mouse models of MeCP2 disorders share gene expression changes in the cerebellum and hypothalamus. *Hum. Mol. Genet.* **18**, 2431–2442 (2009).
122. P. Lin *et al.*, Transcriptome analysis of human brain tissue identifies reduced expression of complement complex C1Q Genes in Rett syndrome. *BMC Genomics*. **17**, 427 (2016).
123. N. L. Pacheco *et al.*, RNA sequencing and proteomics approaches reveal novel deficits in the cortex of Mecp2-deficient mice, a model for Rett syndrome. *Mol. Autism*. **8**, 56 (2017).
124. R. G. Gogliotti *et al.*, Total RNA sequencing of rett syndrome autopsy samples identifies the M4 muscarinic receptor as a novel therapeutic target. *J. Pharmacol. Exp. Ther.* **365**, 291–300 (2018).
125. K. A. Aldinger *et al.*, Transcriptome data of temporal and cingulate cortex in the Rett syndrome brain. *Sci. Data*. **7**, 192 (2020).
126. Z. Zhou *et al.*, Brain-specific phosphorylation of MeCP2 regulates activity-dependent Bdnf transcription, dendritic growth, and spine maturation. *Neuron*. **52**, 255–269 (2006).
127. Q. Chang, G. Khare, V. Dani, S. Nelson, R. Jaenisch, The disease progression of Mecp2 mutant mice is affected by the level of BDNF expression. *Neuron*. **49**, 341–348 (2006).
128. M. Ogier *et al.*, Brain-derived neurotrophic factor expression and respiratory function improve after ampakine treatment in a mouse model of Rett syndrome. *J. Neurosci.* **27**, 10912–10917 (2007).
129. W. Li *et al.*, A small-molecule TrkB ligand restores hippocampal synaptic plasticity and object location memory in Rett syndrome mice. *Dis. Model. Mech.* **10**, 837–845 (2017).
130. E. S. Na *et al.*, D-cycloserine improves synaptic transmission in an animal model of Rett syndrome. *PLoS One*. **12**, e0183026 (2017).
131. A. M. Baker *et al.*, Central penetration and stability of N-terminal tripeptide of insulin-like growth factor-I, glycine-proline-glutamate in adult rat. *Neuropeptides*. **39**, 81–87 (2005).
132. M. M. Ramsey, M. M. Adams, O. J. Ariwodola, W. E. Sonntag, J. L. Weiner, Functional characterization of des-IGF-1 action at excitatory synapses in the CA1 region of rat

hippocampus. *J. Neurophysiol.* **94**, 247–254 (2005).
133. D. Tropea *et al.*, Partial reversal of Rett Syndrome-like symptoms in MeCP2 mutant mice. *Proc. Natl. Acad. Sci. USA*. **106**, 2029–2034 (2009).
134. J. Castro *et al.*, Functional recovery with recombinant human IGF1 treatment in a mouse model of Rett Syndrome. *Proc. Natl. Acad. Sci. USA*. **111**, 9941–9946 (2014).
135. M. R. Pitcher *et al.*, Insulinotropic treatments exacerbate metabolic syndrome in mice lacking MeCP2 function. *Hum. Mol. Genet.* **22**, 2626–2633 (2013).
136. R. G. Gogliotti *et al.*, mGlu5 positive allosteric modulation normalizes synaptic plasticity defects and motor phenotypes in a mouse model of Rett syndrome. *Hum. Mol. Genet.* **25**, 1990–2004 (2016).
137. R. G. Gogliotti *et al.*, mGlu7 potentiation rescues cognitive, social, and respiratory phenotypes in a mouse model of Rett syndrome. *Sci. Transl. Med.* **9** (2017).
138. S. M. Weng, F. McLeod, M. E. S. Bailey, S. R. Cobb, Synaptic plasticity deficits in an experimental model of rett syndrome: long-term potentiation saturation and its pharmacological reversal. *Neuroscience*. **180**, 314–321 (2011).
139. M. Kron *et al.*, Brain activity mapping in Mecp2 mutant mice reveals functional deficits in forebrain circuits, including key nodes in the default mode network, that are reversed with ketamine treatment. *J. Neurosci.* **32**, 13860–13872 (2012).
140. D. M. Katz, F. S. Menniti, R. J. Mather, N-Methyl-D-Aspartate Receptors, Ketamine, and Rett Syndrome: Something Special on the Road to Treatments? *Biol. Psychiatry*. **79**, 710–712 (2016).
141. A. Lekman *et al.*, Rett syndrome: biogenic amines and metabolites in postmortem brain. *Pediatr. Neurol.* **5**, 357–362 (1989).
142. J.-C. Viemari *et al.*, Mecp2 deficiency disrupts norepinephrine and respiratory systems in mice. *J. Neurosci.* **25**, 11521–11530 (2005).
143. J.-C. Roux, E. Dura, A. Moncla, J. Mancini, L. Villard, Treatment with desipramine improves breathing and survival in a mouse model for Rett syndrome. *Eur. J. Neurosci.* **25**, 1915–1922 (2007).
144. S. Zanella *et al.*, Oral treatment with desipramine improves breathing and life span in Rett syndrome mouse model. *Respir. Physiol. Neurobiol.* **160**, 116–121 (2008).
145. T. Bittolo *et al.*, Pharmacological treatment with mirtazapine rescues cortical atrophy and respiratory deficits in MeCP2 null mice. *Sci. Rep.* **6**, 19796 (2016).
146. A. P. Abdala *et al.*, Effect of Sarizotan, a 5-HT1a and D2-like receptor agonist, on respiration in three mouse models of Rett syndrome. *Am. J. Respir. Cell Mol. Biol.* **50**, 1031–1039 (2014).
147. L. Pozzo-Miller, S. Pati, A. K. Percy, Rett syndrome: reaching for clinical trials. *Neurotherapeutics*. **12**, 631–640 (2015).
148. D. M. Katz *et al.*, Rett syndrome: crossing the threshold to clinical translation. *Trends Neurosci.* **39**, 100–113 (2016).
149. A. Nissenkorn, M. Kidon, B. Ben-Zeev, A Potential Life-Threatening Reaction to Glatiramer Acetate in Rett Syndrome. *Pediatr. Neurol.* **68**, 40–43 (2017).
150. Y. Naegelin *et al.*, Fingolimod in children with Rett syndrome: the FINGORETT study. *Orphanet J Rare Dis*. **16**, 19 (2021).
151. O. S. Khwaja *et al.*, Safety, pharmacokinetics, and preliminary assessment of efficacy of mecasermin (recombinant human IGF-1) for the treatment of Rett syndrome. *Proc. Natl. Acad. Sci. USA*. **111**, 4596–4601 (2014).
152. D. G. Glaze *et al.*, A Double-Blind, Randomized, Placebo-Controlled Clinical Study of Trofinetide in the Treatment of Rett Syndrome. *Pediatr. Neurol.* **76**, 37–46 (2017).
153. D. G. Glaze *et al.*, Double-blind, randomized, placebo-controlled study of trofinetide in pediatric Rett syndrome. *Neurology*. **92**, e1912–e1925 (2019).
154. H. M. O'Leary *et al.*, Placebo-controlled crossover assessment of mecasermin for the

treatment of Rett syndrome. *Ann Clin Transl Neurol*. **5**, 323–332 (2018).
155. J. Youakim, Trofinetide: A Novel Approach to Rett Syndrome (767). *Neurology*. **94** (2020).
156. J. Mancini *et al.*, Effect of desipramine on patients with breathing disorders in RETT syndrome. *Ann Clin Transl Neurol*. **5**, 118–127 (2018).
157. C. L. Smith-Hicks *et al.*, Randomized open-label trial of dextromethorphan in Rett syndrome. *Neurology*. **89**, 1684–1690 (2017).
158. D. Lugtenberg *et al.*, Structural variation in Xq28: MECP2 duplications in 1% of patients with unexplained XLMR and in 2% of male patients with severe encephalopathy. *Eur. J. Hum. Genet.* **17**, 444–453 (2009).
159. P. Giudice-Nairn *et al.*, The incidence, prevalence and clinical features of MECP2 duplication syndrome in Australian children. *J. Paediatr. Child Health*. **55**, 1315–1322 (2019).
160. M. B. Ramocki, Y. J. Tavyev, S. U. Peters, The MECP2 duplication syndrome. *Am. J. Med. Genet. A*. **152A**, 1079–1088 (2010).
161. M. B. Ramocki *et al.*, Autism and other neuropsychiatric symptoms are prevalent in individuals with MeCP2 duplication syndrome. *Ann. Neurol.* **66**, 771–782 (2009).
162. H. Van Esch *et al.*, Duplication of the MECP2 region is a frequent cause of severe mental retardation and progressive neurological symptoms in males. *Am. J. Hum. Genet.* **77**, 442–453 (2005).
163. W. Reardon *et al.*, Progressive cerebellar degenerative changes in the severe mental retardation syndrome caused by duplication of MECP2 and adjacent loci on Xq28. *Eur. J. Pediatr.* **169**, 941–949 (2010).
164. S. U. Peters *et al.*, Brief report: regression timing and associated features in MECP2 duplication syndrome. *J. Autism Dev. Disord.* **43**, 2484–2490 (2013).
165. D. Marafi *et al.*, Spectrum and time course of epilepsy and the associated cognitive decline in MECP2 duplication syndrome. *Neurology*. **92**, e108–e114 (2019).
166. S. U. Peters *et al.*, Phenotypic features in MECP2 duplication syndrome: Effects of age. *Am. J. Med. Genet. A*. **185**, 362–369 (2021).
167. S. U. Peters *et al.*, Characterizing the phenotypic effect of Xq28 duplication size in MECP2 duplication syndrome. *Clin. Genet.* **95**, 575–581 (2019).
168. E. S. Na *et al.*, A mouse model for MeCP2 duplication syndrome: MeCP2 overexpression impairs learning and memory and synaptic transmission. *J. Neurosci.* **32**, 3109–3117 (2012).
169. M. Tantra *et al.*, Mild expression differences of MECP2 influencing aggressive social behavior. *EMBO Mol. Med.* **6**, 662–684 (2014).
170. M. Jiang *et al.*, Dendritic arborization and spine dynamics are abnormal in the mouse model of MECP2 duplication syndrome. *J. Neurosci.* **33**, 19518–19533 (2013).
171. Y. Sztainberg *et al.*, Reversal of phenotypes in MECP2 duplication mice using genetic rescue or antisense oligonucleotides. *Nature*. **528**, 123–126 (2015).
172. R. C. Samaco *et al.*, Crh and Oprm1 mediate anxiety-related behavior and social approach in a mouse model of MECP2 duplication syndrome. *Nat. Genet.* **44**, 206–211 (2012).
173. E. S. Na, M. J. Morris, E. D. Nelson, L. M. Monteggia, GABAA receptor antagonism ameliorates behavioral and synaptic impairments associated with MeCP2 overexpression. *Neuropsychopharmacology*. **39**, 1946–1954 (2014).
174. D.-C. Cai *et al.*, MECP2 duplication causes aberrant GABA pathways, circuits and behaviors in transgenic monkeys: neural mappings to patients with autismMapping from transgenic monkeys to autism patients. *J. Neurosci.* (2020).
175. M. Zollino *et al.*, Diagnosis and management in Pitt-Hopkins syndrome: First international consensus statement. *Clin. Genet.* **95**, 462–478 (2019).
176. D. A. Sweetser *et al.*, in *GeneReviews*®, M. P. Adam et al., Eds. (University of Washington, Seattle, Seattle (WA), 1993).

177. G. Marangi *et al.*, The Pitt-Hopkins syndrome: report of 16 new patients and clinical diagnostic criteria. *Am. J. Med. Genet. A*. **155A**, 1536–1545 (2011).
178. S. Whalen *et al.*, Novel comprehensive diagnostic strategy in Pitt-Hopkins syndrome: clinical score and further delineation of the TCF4 mutational spectrum. *Hum. Mutat.* **33**, 64–72 (2012).
179. G. Marangi *et al.*, Proposal of a clinical score for the molecular test for Pitt-Hopkins syndrome. *Am. J. Med. Genet. A*. **158A**, 1604–1611 (2012).
180. J. D. Sweatt, Pitt-Hopkins Syndrome: intellectual disability due to loss of TCF4-regulated gene transcription. *Exp Mol Med*. **45**, e21 (2013).
181. G. Marangi, M. Zollino, Pitt-Hopkins Syndrome and Differential Diagnosis: A Molecular and Clinical Challenge. *J. Pediatr. Genet.* **4**, 168–176 (2015).
182. S. V. Mullegama, J. T. Alaimo, L. Chen, S. H. Elsea, Phenotypic and molecular convergence of 2q23.1 deletion syndrome with other neurodevelopmental syndromes associated with autism spectrum disorder. *Int. J. Mol. Sci.* **16**, 7627–7643 (2015).
183. D. Pitt, I. Hopkins, A syndrome of mental retardation, wide mouth and intermittent overbreathing. *Aust Paediatr J*. **14**, 182–184 (1978).
184. M. P. Forrest, M. J. Hill, A. J. Quantock, E. Martin-Rendon, D. J. Blake, The emerging roles of TCF4 in disease and development. *Trends Mol. Med.* **20**, 322–331 (2014).
185. Y. Zhuang, P. Cheng, H. Weintraub, B-lymphocyte development is regulated by the combined dosage of three basic helix-loop-helix genes, E2A, E2-2, and HEB. *Mol. Cell. Biol.* **16**, 2898–2905 (1996).
186. R. Benezra, R. L. Davis, D. Lockshon, D. L. Turner, H. Weintraub, The protein Id: a negative regulator of helix-loop-helix DNA binding proteins. *Cell*. **61**, 49–59 (1990).
187. X. H. Sun, N. G. Copeland, N. A. Jenkins, D. Baltimore, Id proteins Id1 and Id2 selectively inhibit DNA binding by one class of helix-loop-helix proteins. *Mol. Cell. Biol.* **11**, 5603–5611 (1991).
188. S. P. Rockman *et al.*, Id2 is a target of the beta-catenin/T cell factor pathway in colon carcinoma. *J. Biol. Chem.* **276**, 45113–45119 (2001).
189. J. Saarikettu, N. Sveshnikova, T. Grundström, Calcium/calmodulin inhibition of transcriptional activity of E-proteins by prevention of their binding to DNA. *J. Biol. Chem.* **279**, 41004–41011 (2004).
190. C. Murre *et al.*, Interactions between heterologous helix-loop-helix proteins generate complexes that bind specifically to a common DNA sequence. *Cell*. **58**, 537–544 (1989).
191. F. Guillemot *et al.*, Mammalian achaete-scute homolog 1 is required for the early development of olfactory and autonomic neurons. *Cell*. **75**, 463–476 (1993).
192. P. Persson, A. Jögi, A. Grynfeld, S. Påhlman, H. Axelson, HASH-1 and E2-2 are expressed in human neuroblastoma cells and form a functional complex. *Biochem. Biophys. Res. Commun.* **274**, 22–31 (2000).
193. A. Flora, J. J. Garcia, C. Thaller, H. Y. Zoghbi, The E-protein Tcf4 interacts with Math1 to regulate differentiation of a specific subset of neuronal progenitors. *Proc. Natl. Acad. Sci. USA*. **104**, 15382–15387 (2007).
194. J. Mulvaney, A. Dabdoub, Atoh1, an essential transcription factor in neurogenesis and intestinal and inner ear development: function, regulation, and context dependency. *J Assoc Res Otolaryngol*. **13**, 281–293 (2012).
195. M. Wedel *et al.*, Transcription factor Tcf4 is the preferred heterodimerization partner for Olig2 in oligodendrocytes and required for differentiation. *Nucleic Acids Res.* **48**, 4839–4857 (2020).
196. M. Sepp, K. Kannike, A. Eesmaa, M. Urb, T. Timmusk, Functional diversity of human basic helix-loop-helix transcription factor TCF4 isoforms generated by alternative 5’ exon usage and splicing. *PLoS One*. **6**, e22138 (2011).
197. M. E. Massari *et al.*, A conserved motif present in a class of helix-loop-helix proteins

activates transcription by direct recruitment of the SAGA complex. *Mol. Cell*. **4**, 63–73 (1999).
198. R. Bayly *et al.*, E2A-PBX1 interacts directly with the KIX domain of CBP/p300 in the induction of proliferation in primary hematopoietic cells. *J. Biol. Chem.* **279**, 55362–55371 (2004).
199. J. Zhang, M. Kalkum, S. Yamamura, B. T. Chait, R. G. Roeder, E protein silencing by the leukemogenic AML1-ETO fusion protein. *Science*. **305**, 1286–1289 (2004).
200. I. S. Skerjanc, J. Truong, P. Filion, M. W. McBurney, A splice variant of the ITF-2 transcript encodes a transcription factor that inhibits MyoD activity. *J. Biol. Chem.* **271**, 3555–3561 (1996).
201. L. de Pontual *et al.*, Mutational, functional, and expression studies of the TCF4 gene in Pitt-Hopkins syndrome. *Hum. Mutat.* **30**, 669–676 (2009).
202. T. Chen *et al.*, Tcf4 Controls Neuronal Migration of the Cerebral Cortex through Regulation of Bmp7. *Front. Mol. Neurosci.* **9**, 94 (2016).
203. M. Jung *et al.*, Analysis of the expression pattern of the schizophrenia-risk and intellectual disability gene TCF4 in the developing and adult brain suggests a role in development and plasticity of cortical and hippocampal neurons. *Mol. Autism*. **9**, 20 (2018).
204. H. Kim, N. C. Berens, N. E. Ochandarena, B. D. Philpot, Region and cell type distribution of TCF4 in the postnatal mouse brain. *Front. Neuroanat.* **14**, 42 (2020).
205. C. Zweier *et al.*, Haploinsufficiency of TCF4 causes syndromal mental retardation with intermittent hyperventilation (Pitt-Hopkins syndrome). *Am. J. Hum. Genet.* **80**, 994–1001 (2007).
206. J. Amiel *et al.*, Mutations in TCF4, encoding a class I basic helix-loop-helix transcription factor, are responsible for Pitt-Hopkins syndrome, a severe epileptic encephalopathy associated with autonomic dysfunction. *Am. J. Hum. Genet.* **80**, 988–993 (2007).
207. A. Brockschmidt *et al.*, Severe mental retardation with breathing abnormalities (Pitt-Hopkins syndrome) is caused by haploinsufficiency of the neuronal bHLH transcription factor TCF4. *Hum. Mol. Genet.* **16**, 1488–1494 (2007).
208. M. Sepp, P. Pruunsild, T. Timmusk, Pitt-Hopkins syndrome-associated mutations in TCF4 lead to variable impairment of the transcription factor function ranging from hypomorphic to dominant-negative effects. *Hum. Mol. Genet.* **21**, 2873–2888 (2012).
209. M. F. Bedeschi *et al.*, Impairment of different protein domains causes variable clinical presentation within Pitt-Hopkins syndrome and suggests intragenic molecular syndromology of TCF4. *Eur J Med Genet*. **60**, 565–571 (2017).
210. J. A. Rosenfeld *et al.*, Genotype-phenotype analysis of TCF4 mutations causing Pitt-Hopkins syndrome shows increased seizure activity with missense mutations. *Genet. Med.* **11**, 797–805 (2009).
211. V. Maduro *et al.*, Complex translocation disrupting TCF4 and altering TCF4 isoform expression segregates as mild autosomal dominant intellectual disability. *Orphanet J Rare Dis*. **11**, 62 (2016).
212. C. Thaxton *et al.*, Common Pathophysiology in Multiple Mouse Models of Pitt-Hopkins Syndrome. *J. Neurosci.* **38**, 918–936 (2018).
213. M. D. Rannals *et al.*, Psychiatric risk gene transcription factor 4 regulates intrinsic excitability of prefrontal neurons via repression of scn10a and KCNQ1. *Neuron*. **90**, 43–55 (2016).
214. M. D. Rannals *et al.*, Neurodevelopmental models of transcription factor 4 deficiency converge on a common ion channel as a potential therapeutic target for Pitt Hopkins syndrome. *Rare Dis.* **4**, e1220468 (2016).
215. A. J. Kennedy *et al.*, Tcf4 regulates synaptic plasticity, DNA methylation, and memory function. *Cell Rep.* **16**, 2666–2685 (2016).
216. C. M. Cleary, S. James, B. J. Maher, D. K. Mulkey, Disordered breathing in a Pitt-Hopkins

syndrome model involves Phox2b-expressing parafacial neurons and aberrant Nav1.8 expression. *Nat. Commun.* **12**, 5962 (2021).
217. J. Shi *et al.*, Common variants on chromosome 6p22.1 are associated with schizophrenia. *Nature*. **460**, 753–757 (2009).
218. H. Stefansson *et al.*, Common variants conferring risk of schizophrenia. *Nature*. **460**, 744–747 (2009).
219. N. R. Swerdlow, G. A. Light, Sensorimotor gating deficits in schizophrenia: Advancing our understanding of the phenotype, its neural circuitry and genetic substrates. *Schizophr. Res.* **198**, 1–5 (2018).
220. M. M. Brzózka, K. Radyushkin, S. P. Wichert, H. Ehrenreich, M. J. Rossner, Cognitive and sensorimotor gating impairments in transgenic mice overexpressing the schizophrenia susceptibility gene Tcf4 in the brain. *Biol. Psychiatry*. **68**, 33–40 (2010).
221. S. C. Page *et al.*, The schizophrenia- and autism-associated gene, transcription factor 4 regulates the columnar distribution of layer 2/3 prefrontal pyramidal neurons in an activity-dependent manner. *Mol. Psychiatry*. **23**, 304–315 (2018).
222. H. Kim *et al.*, Rescue of behavioral and electrophysiological phenotypes in a Pitt-Hopkins syndrome mouse model by genetic restoration of Tcf4 expression. *BioRxiv* (2021).
223. S. Durand *et al.*, NMDA receptor regulation prevents regression of visual cortical function in the absence of Mecp2. *Neuron*. **76**, 1078–1090 (2012).
224. S. B. Mierau, A. Patrizi, T. K. Hensch, M. Fagiolini, Cell-Specific Regulation of N-Methyl-D-Aspartate Receptor Maturation by Mecp2 in Cortical Circuits. *Biol. Psychiatry*. **79**, 746–754 (2016).
225. A. Patrizi *et al.*, Chronic Administration of the N-Methyl-D-Aspartate Receptor Antagonist Ketamine Improves Rett Syndrome Phenotype. *Biol. Psychiatry*. **79**, 755–764 (2016).
226. A. Reiner, J. Levitz, Glutamatergic signaling in the central nervous system: ionotropic and metabotropic receptors in concert. *Neuron*. **98**, 1080–1098 (2018).
227. C. M. Niswender, P. J. Conn, Metabotropic glutamate receptors: physiology, pharmacology, and disease. *Annu. Rev. Pharmacol. Toxicol.* **50**, 295–322 (2010).
228. F. Knoflach *et al.*, Positive allosteric modulators of metabotropic glutamate 1 receptor: characterization, mechanism of action, and binding site. *Proc. Natl. Acad. Sci. USA*. **98**, 13402–13407 (2001).
229. H. Schaffhauser *et al.*, Pharmacological characterization and identification of amino acids involved in the positive modulation of metabotropic glutamate receptor subtype 2. *Mol. Pharmacol.* **64**, 798–810 (2003).
230. A. Farinha *et al.*, Molecular determinants of positive allosteric modulation of the human metabotropic glutamate receptor 2. *Br. J. Pharmacol.* **172**, 2383–2396 (2015).
231. E. Doumazane *et al.*, A new approach to analyze cell surface protein complexes reveals specific heterodimeric metabotropic glutamate receptors. *FASEB J.* **25**, 66–77 (2011).
232. C. Romano, W. L. Yang, K. L. O'Malley, Metabotropic glutamate receptor 5 is a disulfide-linked dimer. *J. Biol. Chem.* **271**, 28612–28616 (1996).
233. N. Kunishima *et al.*, Structural basis of glutamate recognition by a dimeric metabotropic glutamate receptor. *Nature*. **407**, 971–977 (2000).
234. T. Muto, D. Tsuchiya, K. Morikawa, H. Jingami, Structures of the extracellular regions of the group II/III metabotropic glutamate receptors. *Proc. Natl. Acad. Sci. USA*. **104**, 3759–3764 (2007).
235. J. Kniazeff *et al.*, Closed state of both binding domains of homodimeric mGlu receptors is required for full activity. *Nat. Struct. Mol. Biol.* **11**, 706–713 (2004).
236. M. Tateyama, H. Abe, H. Nakata, O. Saito, Y. Kubo, Ligand-induced rearrangement of the dimeric metabotropic glutamate receptor 1alpha. *Nat. Struct. Mol. Biol.* **11**, 637–642 (2004).
237. A. M. Cao *et al.*, Allosteric modulators enhance agonist efficacy by increasing the

residence time of a GPCR in the active state. *Nat. Commun.* **12**, 5426 (2021).
238. J. Lee *et al.*, Defining the Homo- and Heterodimerization Propensities of Metabotropic Glutamate Receptors. *Cell Rep.* **31**, 107605 (2020).
239. S. Yin *et al.*, Selective actions of novel allosteric modulators reveal functional heteromers of metabotropic glutamate receptors in the CNS. *J. Neurosci.* **34**, 79–94 (2014).
240. J. Levitz *et al.*, Mechanism of assembly and cooperativity of homomeric and heteromeric metabotropic glutamate receptors. *Neuron*. **92**, 143–159 (2016).
241. D. Moreno Delgado *et al.*, Pharmacological evidence for a metabotropic glutamate receptor heterodimer in neuronal cells. *Elife*. **6** (2017).
242. Z. Xiang *et al.*, Input-specific regulation of glutamatergic synaptic transmission in the medial prefrontal cortex by mGlu2/mGlu4 receptor heterodimers. *Sci. Signal.* **14** (2021).
243. P. J. Flor *et al.*, Molecular cloning, functional expression and pharmacological characterization of the human metabotropic glutamate receptor type 2. *Eur. J. Neurosci.* **7**, 622–629 (1995).
244. L. Emile *et al.*, Molecular cloning, functional expression, pharmacological characterization and chromosomal localization of the human metabotropic glutamate receptor type 3. *Neuropharmacology*. **35**, 523–530 (1996).
245. P. J. Conn, J. P. Pin, Pharmacology and functions of metabotropic glutamate receptors. *Annu. Rev. Pharmacol. Toxicol.* **37**, 205–237 (1997).
246. F. Ferraguti, R. Shigemoto, Metabotropic glutamate receptors. *Cell Tissue Res.* **326**, 483–504 (2006).
247. C. E. McOmish, E. Y. Demireva, J. A. Gingrich, Developmental expression of mGlu2 and mGlu3 in the mouse brain. *Gene Expr Patterns*. **22**, 46–53 (2016).
248. G. Gu *et al.*, Distribution of metabotropic glutamate 2 and 3 receptors in the rat forebrain: Implication in emotional responses and central disinhibition. *Brain Res.* **1197**, 47–62 (2008).
249. R. A. Wright *et al.*, CNS distribution of metabotropic glutamate 2 and 3 receptors: transgenic mice and [^{3}H]LY459477 autoradiography. *Neuropharmacology*. **66**, 89–98 (2013).
250. L. Iacovelli *et al.*, Regulation of group II metabotropic glutamate receptors by G protein-coupled receptor kinases: mGlu2 receptors are resistant to homologous desensitization. *Mol. Pharmacol.* **75**, 991–1003 (2009).
251. H. Schaffhauser *et al.*, cAMP-dependent protein kinase inhibits mGluR2 coupling to G-proteins by direct receptor phosphorylation. *J. Neurosci.* **20**, 5663–5670 (2000).
252. Z. Cai *et al.*, Cyclic AMP-dependent protein kinase phosphorylates group III metabotropic glutamate receptors and inhibits their function as presynaptic receptors. *J. Neurochem.* **78**, 756–766 (2001).
253. H. Hirbec *et al.*, The PDZ proteins PICK1, GRIP, and syntenin bind multiple glutamate receptor subtypes. Analysis of PDZ binding motifs. *J. Biol. Chem.* **277**, 15221–15224 (2002).
254. M. Flajolet *et al.*, Protein phosphatase 2C binds selectively to and dephosphorylates metabotropic glutamate receptor 3. *Proc. Natl. Acad. Sci. USA*. **100**, 16006–16011 (2003).
255. A. Seebahn, M. Rose, R. Enz, RanBPM is expressed in synaptic layers of the mammalian retina and binds to metabotropic glutamate receptors. *FEBS Lett.* **582**, 2453–2457 (2008).
256. S. L. Ritter-Makinson *et al.*, Group II metabotropic glutamate receptor interactions with NHERF scaffold proteins: Implications for receptor localization in brain. *Neuroscience*. **353**, 58–75 (2017).
257. N. Abreu, A. Acosta-Ruiz, G. Xiang, J. Levitz, Mechanisms of differential desensitization of metabotropic glutamate receptors. *Cell Rep.* **35**, 109050 (2021).
258. L. J. Sartorius *et al.*, Alternative splicing of human metabotropic glutamate receptor 3. *J. Neurochem.* **96**, 1139–1148 (2006).

259. A. García-Bea, I. Bermudez, P. J. Harrison, T. A. Lane, A group II metabotropic glutamate receptor 3 (mGlu3, GRM3) isoform implicated in schizophrenia interacts with canonical mGlu3 and reduces ligand binding. *J. Psychopharmacol. (Oxford)*. **31**, 1519–1526 (2017).
260. L. J. Sartorius *et al.*, Expression of a GRM3 splice variant is increased in the dorsolateral prefrontal cortex of individuals carrying a schizophrenia risk SNP. *Neuropsychopharmacology*. **33**, 2626–2634 (2008).
261. M. Yokoi *et al.*, Impairment of hippocampal mossy fiber LTD in mice lacking mGluR2. *Science*. **273**, 645–647 (1996).
262. G. A. Higgins *et al.*, Pharmacological manipulation of mGlu2 receptors influences cognitive performance in the rodent. *Neuropharmacology*. **46**, 907–917 (2004).
263. K. A. Johnson, C. M. Niswender, P. J. Conn, Z. Xiang, Activation of group II metabotropic glutamate receptors induces long-term depression of excitatory synaptic transmission in the substantia nigra pars reticulata. *Neurosci. Lett.* **504**, 102–106 (2011).
264. M. E. Joffe *et al.*, mGlu2 and mGlu3 Negative Allosteric Modulators Divergently Enhance Thalamocortical Transmission and Exert Rapid Antidepressant-like Effects. *Neuron*. **105**, 46–59.e3 (2020).
265. M. A. Benneyworth *et al.*, A selective positive allosteric modulator of metabotropic glutamate receptor subtype 2 blocks a hallucinogenic drug model of psychosis. *Mol. Pharmacol.* **72**, 477–484 (2007).
266. N. Rosenberg, U. Gerber, J. Ster, Activation of Group II Metabotropic Glutamate Receptors Promotes LTP Induction at Schaffer Collateral-CA1 Pyramidal Cell Synapses by Priming NMDA Receptors. *J. Neurosci.* **36**, 11521–11531 (2016).
267. S. Dogra *et al.*, Activating mGlu3 Metabotropic Glutamate Receptors Rescues Schizophrenia-like Cognitive Deficits Through Metaplastic Adaptations Within the Hippocampus. *Biol. Psychiatry*. **90**, 385–398 (2021).
268. P. M. Lea, B. Wroblewska, J. M. Sarvey, J. H. Neale, beta-NAAG rescues LTP from blockade by NAAG in rat dentate gyrus via the type 3 metabotropic glutamate receptor. *J. Neurophysiol.* **85**, 1097–1106 (2001).
269. B. Pöschel, B. Wroblewska, U. Heinemann, D. Manahan-Vaughan, The metabotropic glutamate receptor mGluR3 is critically required for hippocampal long-term depression and modulates long-term potentiation in the dentate gyrus of freely moving rats. *Cereb. Cortex*. **15**, 1414–1423 (2005).
270. B. Wroblewska, M. R. Santi, J. H. Neale, N-acetylaspartylglutamate activates cyclic AMP-coupled metabotropic glutamate receptors in cerebellar astrocytes. *Glia*. **24**, 172–179 (1998).
271. J. H. Neale, R. Olszewski, A Role for N-Acetylaspartylglutamate (NAAG) and mGluR3 in Cognition. *Neurobiol. Learn. Mem.* **158**, 9–13 (2019).
272. A. G. Walker *et al.*, Co-Activation of Metabotropic Glutamate Receptor 3 and Beta-Adrenergic Receptors Modulates Cyclic-AMP and Long-Term Potentiation, and Disrupts Memory Reconsolidation. *Neuropsychopharmacology*. **42**, 2553–2566 (2017).
273. A. E. Kingston *et al.*, Neuroprotection by metabotropic glutamate receptor glutamate receptor agonists: LY354740, LY379268 and LY389795. *Eur. J. Pharmacol.* **377**, 155–165 (1999).
274. C. Corti *et al.*, The use of knock-out mice unravels distinct roles for mGlu2 and mGlu3 metabotropic glutamate receptors in mechanisms of neurodegeneration/neuroprotection. *J. Neurosci.* **27**, 8297–8308 (2007).
275. A. Poli *et al.*, Group II metabotropic glutamate receptors regulate the vulnerability to hypoxic brain damage. *J. Neurosci.* **23**, 6023–6029 (2003).
276. E. F. Sharpe, A. E. Kingston, D. Lodge, J. A. Monn, P. M. Headley, Systemic pre-treatment with a group II mGlu agonist, LY379268, reduces hyperalgesia in vivo. *Br. J. Pharmacol.* **135**, 1255–1262 (2002).

277. J. N. Highland, P. Zanos, P. Georgiou, T. D. Gould, Group II metabotropic glutamate receptor blockade promotes stress resilience in mice. *Neuropsychopharmacology*. **44**, 1788–1796 (2019).
278. M. E. Joffe *et al.*, Mechanisms underlying prelimbic prefrontal cortex mGlu3/mGlu5-dependent plasticity and reversal learning deficits following acute stress. *Neuropharmacology*. **144**, 19–28 (2019).
279. A. M. Linden *et al.*, Anxiolytic-like activity of the mGLU2/3 receptor agonist LY354740 in the elevated plus maze test is disrupted in metabotropic glutamate receptor 2 and 3 knock-out mice. *Psychopharmacology*. **179**, 284–291 (2005).
280. G. Imre *et al.*, Effects of the mGluR2/3 agonist LY379268 on ketamine-evoked behaviours and neurochemical changes in the dentate gyrus of the rat. *Pharmacol. Biochem. Behav.* **84**, 392–399 (2006).
281. M. F. O'Neill, C. Heron-Maxwell, M. W. Conway, J. A. Monn, P. Ornstein, Group II metabotropic glutamate receptor antagonists LY341495 and LY366457 increase locomotor activity in mice. *Neuropharmacology*. **45**, 565–574 (2003).
282. M. E. Joffe *et al.*, Frontal cortex genetic ablation of metabotropic glutamate receptor subtype 3 (mGlu3) impairs postsynaptic plasticity and modulates affective behaviors. *Neuropsychopharmacology* (2021).
283. S. Chaki *et al.*, MGS0039: a potent and selective group II metabotropic glutamate receptor antagonist with antidepressant-like activity. *Neuropharmacology*. **46**, 457–467 (2004).
284. K. Fukumoto, M. Iijima, S. Chaki, The Antidepressant Effects of an mGlu2/3 Receptor Antagonist and Ketamine Require AMPA Receptor Stimulation in the mPFC and Subsequent Activation of the 5-HT Neurons in the DRN. *Neuropsychopharmacology*. **41**, 1046–1056 (2016).
285. H. Koike, M. Iijima, S. Chaki, Effects of ketamine and LY341495 on the depressive-like behavior of repeated corticosterone-injected rats. *Pharmacol. Biochem. Behav.* **107**, 20–23 (2013).
286. S. D. Gleason *et al.*, mGlu2/3 agonist-induced hyperthermia: an in vivo assay for detection of mGlu2/3 receptor antagonism and its relation to antidepressant-like efficacy in mice. *CNS Neurol Disord Drug Targets*. **12**, 554–566 (2013).
287. J. L. Engers *et al.*, Discovery of a Selective and CNS Penetrant Negative Allosteric Modulator of Metabotropic Glutamate Receptor Subtype 3 with Antidepressant and Anxiolytic Activity in Rodents. *J. Med. Chem.* **58**, 7485–7500 (2015).
288. A. G. Walker *et al.*, Metabotropic glutamate receptor 3 activation is required for long-term depression in medial prefrontal cortex and fear extinction. *Proc. Natl. Acad. Sci. USA*. **112**, 1196–1201 (2015).
289. A. M. Feyissa *et al.*, Elevated level of metabotropic glutamate receptor 2/3 in the prefrontal cortex in major depression. *Prog. Neuropsychopharmacol. Biol. Psychiatry*. **34**, 279–283 (2010).
290. C. E. McOmish *et al.*, Lower [3H]LY341495 binding to mGlu2/3 receptors in the anterior cingulate of subjects with major depressive disorder but not bipolar disorder or schizophrenia. *J. Affect. Disord.* **190**, 241–248 (2016).
291. D. Umbricht *et al.*, Randomized, Double-Blind, Placebo-Controlled Trial of the mGlu2/3 Negative Allosteric Modulator Decoglurant in Partially Refractory Major Depressive Disorder. *J. Clin. Psychiatry*. **81** (2020).
292. J. González-Maeso *et al.*, Identification of a serotonin/glutamate receptor complex implicated in psychosis. *Nature*. **452**, 93–97 (2008).
293. S. Ghose, K. A. Gleason, B. W. Potts, K. Lewis-Amezcua, C. A. Tamminga, Differential expression of metabotropic glutamate receptors 2 and 3 in schizophrenia: a mechanism for antipsychotic drug action? *Am. J. Psychiatry*. **166**, 812–820 (2009).
294. F. Matrisciano, P. Tueting, S. Maccari, F. Nicoletti, A. Guidotti, Pharmacological activation

of group-II metabotropic glutamate receptors corrects a schizophrenia-like phenotype induced by prenatal stress in mice. *Neuropsychopharmacology*. **37**, 929–938 (2012).
295. B. Moghaddam, D. Javitt, From revolution to evolution: the glutamate hypothesis of schizophrenia and its implication for treatment. *Neuropsychopharmacology*. **37**, 4–15 (2012).
296. B. Moghaddam, B. W. Adams, Reversal of phencyclidine effects by a group II metabotropic glutamate receptor agonist in rats. *Science*. **281**, 1349–1352 (1998).
297. J. Cartmell, J. A. Monn, D. D. Schoepp, The metabotropic glutamate 2/3 receptor agonists LY354740 and LY379268 selectively attenuate phencyclidine versus d-amphetamine motor behaviors in rats. *J. Pharmacol. Exp. Ther.* **291**, 161–170 (1999).
298. M. L. Woolley, D. J. Pemberton, S. Bate, C. Corti, D. N. C. Jones, The mGlu2 but not the mGlu3 receptor mediates the actions of the mGluR2/3 agonist, LY379268, in mouse models predictive of antipsychotic activity. *Psychopharmacology*. **196**, 431–440 (2008).
299. J. M. Wierońska *et al.*, The reversal of cognitive, but not negative or positive symptoms of schizophrenia, by the $mGlu_2/_3$ receptor agonist, LY379268, is 5-HT_1A dependent. *Behav. Brain Res.* **256**, 298–304 (2013).
300. K. Blot *et al.*, Modulation of hippocampus-prefrontal cortex synaptic transmission and disruption of executive cognitive functions by MK-801. *Cereb. Cortex*. **25**, 1348–1361 (2015).
301. S. T. Patil *et al.*, Activation of mGlu2/3 receptors as a new approach to treat schizophrenia: a randomized Phase 2 clinical trial. *Nat. Med.* **13**, 1102–1107 (2007).
302. J. A. Monn *et al.*, Synthesis and pharmacological characterization of 4-substituted-2-aminobicyclo[3.1.0]hexane-2,6-dicarboxylates: identification of new potent and selective metabotropic glutamate 2/3 receptor agonists. *J. Med. Chem.* **56**, 4442–4455 (2013).
303. B. J. Kinon *et al.*, A multicenter, inpatient, phase 2, double-blind, placebo-controlled dose-ranging study of LY2140023 monohydrate in patients with DSM-IV schizophrenia. *J Clin Psychopharmacol*. **31**, 349–355 (2011).
304. D. H. Adams *et al.*, A long-term, phase 2, multicenter, randomized, open-label, comparative safety study of pomaglumetad methionil (LY2140023 monohydrate) versus atypical antipsychotic standard of care in patients with schizophrenia. *BMC Psychiatry*. **13**, 143 (2013).
305. A. M. Downing *et al.*, A Double-Blind, Placebo-Controlled Comparator Study of LY2140023 monohydrate in patients with schizophrenia. *BMC Psychiatry*. **14**, 351 (2014).
306. R. Galici, N. G. Echemendia, A. L. Rodriguez, P. J. Conn, A selective allosteric potentiator of metabotropic glutamate (mGlu) 2 receptors has effects similar to an orthosteric mGlu2/3 receptor agonist in mouse models predictive of antipsychotic activity. *J. Pharmacol. Exp. Ther.* **315**, 1181–1187 (2005).
307. P. Scholler *et al.*, Allosteric nanobodies uncover a role of hippocampal mGlu2 receptor homodimers in contextual fear consolidation. *Nat. Commun.* **8**, 1967 (2017).
308. G. Griebel *et al.*, The mGluR2 positive allosteric modulator, SAR218645, improves memory and attention deficits in translational models of cognitive symptoms associated with schizophrenia. *Sci. Rep.* **6**, 35320 (2016).
309. R. E. Litman *et al.*, AZD8529, a positive allosteric modulator at the mGluR2 receptor, does not improve symptoms in schizophrenia: A proof of principle study. *Schizophr. Res.* **172**, 152–157 (2016).
310. H. Salih *et al.*, Pharmacokinetic and pharmacodynamic characterisation of JNJ-40411813, a positive allosteric modulator of mGluR2, in two randomised, double-blind phase-I studies. *J. Psychopharmacol. (Oxford)*. **29**, 414–425 (2015).
311. M. F. Egan *et al.*, Variation in GRM3 affects cognition, prefrontal glutamate, and risk for schizophrenia. *Proc. Natl. Acad. Sci. USA*. **101**, 12604–12609 (2004).
312. B. T. Baune *et al.*, Association between genetic variants of the metabotropic glutamate

receptor 3 (GRM3) and cognitive set shifting in healthy individuals. *Genes Brain Behav.* **9**, 459–466 (2010).
313. S. M. Saini *et al.*, Meta-analysis supports GWAS-implicated link between GRM3 and schizophrenia risk. *Transl. Psychiatry*. **7**, e1196 (2017).
314. P. J. Harrison, L. Lyon, L. J. Sartorius, P. W. J. Burnet, T. A. Lane, The group II metabotropic glutamate receptor 3 (mGluR3, mGlu3, GRM3): expression, function and involvement in schizophrenia. *J. Psychopharmacol. (Oxford)*. **22**, 308–322 (2008).
315. R. Mössner *et al.*, Further evidence for a functional role of the glutamate receptor gene GRM3 in schizophrenia. *Eur. Neuropsychopharmacol.* **18**, 768–772 (2008).
316. Schizophrenia Working Group of the Psychiatric Genomics Consortium, Biological insights from 108 schizophrenia-associated genetic loci. *Nature*. **511**, 421–427 (2014).
317. L. Lyon *et al.*, Fractionation of spatial memory in GRM2/3 (mGlu2/mGlu3) double knockout mice reveals a role for group II metabotropic glutamate receptors at the interface between arousal and cognition. *Neuropsychopharmacology*. **36**, 2616–2628 (2011).
318. B. De Filippis *et al.*, The role of group II metabotropic glutamate receptors in cognition and anxiety: comparative studies in GRM2(-/-), GRM3(-/-) and GRM2/3(-/-) knockout mice. *Neuropharmacology*. **89**, 19–32 (2015).
319. R. Fujioka *et al.*, Comprehensive behavioral study of mGluR3 knockout mice: implication in schizophrenia related endophenotypes. *Mol. Brain*. **7**, 31 (2014).
320. M. Lainiola, C. Procaccini, A.-M. Linden, mGluR3 knockout mice show a working memory defect and an enhanced response to MK-801 in the T- and Y-maze cognitive tests. *Behav. Brain Res.* **266**, 94–103 (2014).
321. M.-L. Li *et al.*, LY395756, an mGluR2 agonist and mGluR3 antagonist, enhances NMDA receptor expression and function in the normal adult rat prefrontal cortex, but fails to improve working memory and reverse MK801-induced working memory impairment. *Exp. Neurol.* **273**, 190–201 (2015).
322. L. Di Menna *et al.*, Functional partnership between mGlu3 and mGlu5 metabotropic glutamate receptors in the central nervous system. *Neuropharmacology*. **128**, 301–313 (2018).
323. Y.-W. Chen *et al.*, Activation of mGluR2/3 underlies the effects of N-acetylcystein on amygdala-associated autism-like phenotypes in a valproate-induced rat model of autism. *Front. Behav. Neurosci.* **8**, 219 (2014).
324. C. H. Choi *et al.*, Pharmacological reversal of synaptic plasticity deficits in the mouse model of fragile X syndrome by group II mGluR antagonist or lithium treatment. *Brain Res.* **1380**, 106–119 (2011).
325. R. C. Samaco *et al.*, A partial loss of function allele of methyl-CpG-binding protein 2 predicts a human neurodevelopmental syndrome. *Hum. Mol. Genet.* **17**, 1718–1727 (2008).
326. B. De Filippis *et al.*, Modulation of Rho GTPases rescues brain mitochondrial dysfunction, cognitive deficits and aberrant synaptic plasticity in female mice modeling Rett syndrome. *Eur. Neuropsychopharmacol.* **25**, 889–901 (2015).
327. E. Sokolenko, M. R. Hudson, J. Nithianantharajah, N. C. Jones, The mGluR2/3 agonist LY379268 reverses NMDA receptor antagonist effects on cortical gamma oscillations and phase coherence, but not working memory impairments, in mice. *J. Psychopharmacol. (Oxford)*, 269881119875976 (2019).
328. R. T. Olszewski *et al.*, NAAG Peptidase Inhibitors Act via mGluR3: Animal Models of Memory, Alzheimer's, and Ethanol Intoxication. *Neurochem. Res.* **42**, 2646–2657 (2017).
329. B. J. Stansley *et al.*, Contextual fear extinction induces hippocampal metaplasticity mediated by metabotropic glutamate receptor 5. *Cereb. Cortex*. **28**, 4291–4304 (2018).
330. M. E. Talkowski *et al.*, Sequencing chromosomal abnormalities reveals neurodevelopmental loci that confer risk across diagnostic boundaries. *Cell*. **149**, 525–537

(2012).
331. H. Xia *et al.*, Building a schizophrenia genetic network: transcription factor 4 regulates genes involved in neuronal development and schizophrenia risk. *Hum. Mol. Genet.* **27**, 3246–3256 (2018).
332. H. Li *et al.*, Disruption of TCF4 regulatory networks leads to abnormal cortical development and mental disabilities. *Mol. Psychiatry*. **24**, 1235–1246 (2019).
333. Y. Zhang *et al.*, Transcription factor 4 controls positioning of cortical projection neurons through regulation of cell adhesion. *Mol. Psychiatry* (2021).
334. M. E. Joffe, P. J. Conn, Antidepressant potential of metabotropic glutamate receptor mGlu2 and mGlu3 negative allosteric modulators. *Neuropsychopharmacology*. **44**, 214–236 (2019).
335. C. A. Jones, A. M. Brown, D. P. Auer, K. C. F. Fone, The mGluR2/3 agonist LY379268 reverses post-weaning social isolation-induced recognition memory deficits in the rat. *Psychopharmacology*. **214**, 269–283 (2011).
336. E. Dunayevich *et al.*, Efficacy and tolerability of an mGlu2/3 agonist in the treatment of generalized anxiety disorder. *Neuropsychopharmacology*. **33**, 1603–1610 (2008).
337. X. Tang *et al.*, Pharmacological enhancement of KCC2 gene expression exerts therapeutic effects on human Rett syndrome neurons and Mecp2 mutant mice. *Sci. Transl. Med.* **11** (2019).
338. A. K. Percy *et al.*, Rett syndrome diagnostic criteria: lessons from the Natural History Study. *Ann. Neurol.* **68**, 951–955 (2010).
339. J. B. Lane *et al.*, Clinical severity and quality of life in children and adolescents with Rett syndrome. *Neurology*. **77**, 1812–1818 (2011).
340. C. A. Chapleau *et al.*, Detection of rarely identified multiple mutations in MECP2 gene do not contribute to enhanced severity in Rett syndrome. *Am. J. Med. Genet. A*. **161A**, 1638–1646 (2013).
341. J. L. Neul *et al.*, Developmental delay in Rett syndrome: data from the natural history study. *J. Neurodev. Disord.* **6**, 20 (2014).
342. J. T. Killian *et al.*, Pubertal development in Rett syndrome deviates from typical females. *Pediatr. Neurol.* **51**, 769–775 (2014).
343. D. C. Tarquinio *et al.*, Age of diagnosis in Rett syndrome: patterns of recognition among diagnosticians and risk factors for late diagnosis. *Pediatr. Neurol.* **52**, 585–91.e2 (2015).
344. D. C. Tarquinio *et al.*, The Changing Face of Survival in Rett Syndrome and MECP2-Related Disorders. *Pediatr. Neurol.* **53**, 402–411 (2015).
345. J. T. Killian *et al.*, Caretaker quality of life in rett syndrome: disorder features and psychological predictors. *Pediatr. Neurol.* **58**, 67–74 (2016).
346. D. C. Tarquinio *et al.*, Longitudinal course of epilepsy in Rett syndrome and related disorders. *Brain*. **140**, 306–318 (2017).
347. J. T. Killian *et al.*, Scoliosis in rett syndrome: progression, comorbidities, and predictors. *Pediatr. Neurol.* **70**, 20–25 (2017).
348. D. C. Tarquinio *et al.*, The course of awake breathing disturbances across the lifespan in Rett syndrome. *Brain Dev.* **40**, 515–529 (2018).
349. C. B. Buchanan *et al.*, Behavioral profiles in Rett syndrome: Data from the natural history study. *Brain Dev.* **41**, 123–134 (2019).
350. C. Cutri-French *et al.*, Comparison of core features in four Developmental Encephalopathies in the Rett Natural History Study. *Ann. Neurol.* (2020).
351. C. F. de Winter *et al.*, Phenotype and natural history in 101 individuals with Pitt-Hopkins syndrome through an internet questionnaire system. *Orphanet J Rare Dis*. **11**, 37 (2016).
352. S. Matricardi *et al.*, Epilepsy, electroclinical features, and long-term outcomes in Pitt-Hopkins syndrome due to pathogenic variants in the TCF4 gene. *Eur. J. Neurol.* (2021).
353. S. Augui, E. P. Nora, E. Heard, Regulation of X-chromosome inactivation by the X-

inactivation centre. *Nat. Rev. Genet.* **12**, 429–442 (2011).
354. N. Sirianni, S. Naidu, J. Pereira, R. F. Pillotto, E. P. Hoffman, Rett syndrome: confirmation of X-linked dominant inheritance, and localization of the gene to Xq28. *Am. J. Hum. Genet.* **63**, 1552–1558 (1998).
355. M. C. Ribeiro, J. L. MacDonald, Sex differences in Mecp2-mutant Rett syndrome model mice and the impact of cellular mosaicism in phenotype development. *Brain Res.* **1729**, 146644 (2020).
356. J. I. Young, H. Y. Zoghbi, X-chromosome inactivation patterns are unbalanced and affect the phenotypic outcome in a mouse model of rett syndrome. *Am. J. Hum. Genet.* **74**, 511–520 (2004).
357. J. L. Neul *et al.*, Specific mutations in methyl-CpG-binding protein 2 confer different severity in Rett syndrome. *Neurology*. **70**, 1313–1321 (2008).
358. A. A. Adegbola, M. L. Gonzales, A. Chess, J. M. LaSalle, G. F. Cox, A novel hypomorphic MECP2 point mutation is associated with a neuropsychiatric phenotype. *Hum. Genet.* **124**, 615–623 (2009).
359. H. Leonard *et al.*, Patients with the R133C mutation: is their phenotype different from patients with Rett syndrome with other mutations? *J. Med. Genet.* **40**, e52 (2003).
360. A. Bebbington *et al.*, Investigating genotype-phenotype relationships in Rett syndrome using an international data set. *Neurology*. **70**, 868–875 (2008).
361. D. J. Foster *et al.*, Antipsychotic-like Effects of M4 Positive Allosteric Modulators Are Mediated by CB2 Receptor-Dependent Inhibition of Dopamine Release. *Neuron*. **91**, 1244–1252 (2016).
362. N. M. Fisher *et al.*, Genetic Reduction or Negative Modulation of mGlu7 Does Not Impact Anxiety and Fear Learning Phenotypes in a Mouse Model of MECP2 Duplication Syndrome. *ACS Chem. Neurosci.* **9**, 2210–2217 (2018).
363. H. Cheval *et al.*, Postnatal inactivation reveals enhanced requirement for MeCP2 at distinct age windows. *Hum. Mol. Genet.* **21**, 3806–3814 (2012).
364. J.-M. Ramirez, C. S. Ward, J. L. Neul, Breathing challenges in Rett syndrome: lessons learned from humans and animal models. *Respir. Physiol. Neurobiol.* **189**, 280–287 (2013).
365. T. G. Kucukkal, E. Alexov, Structural, dynamical, and energetical consequences of rett syndrome mutation R133C in mecp2. *Comput. Math. Methods Med.* **2015**, 746157 (2015).
366. N. A. Stearns *et al.*, Behavioral and anatomical abnormalities in Mecp2 mutant mice: a model for Rett syndrome. *Neuroscience*. **146**, 907–921 (2007).
367. M. Santos, A. Silva-Fernandes, P. Oliveira, N. Sousa, P. Maciel, Evidence for abnormal early development in a mouse model of Rett syndrome. *Genes Brain Behav.* **6**, 277–286 (2007).
368. G. J. Pelka *et al.*, Mecp2 deficiency is associated with learning and cognitive deficits and altered gene activity in the hippocampal region of mice. *Brain*. **129**, 887–898 (2006).
369. B. Kerr, M. Alvarez-Saavedra, M. A. Sáez, A. Saona, J. I. Young, Defective body-weight regulation, motor control and abnormal social interactions in Mecp2 hypomorphic mice. *Hum. Mol. Genet.* **17**, 1707–1717 (2008).
370. X. Meng *et al.*, Manipulations of MeCP2 in glutamatergic neurons highlight their contributions to Rett and other neurological disorders. *Elife*. **5** (2016).
371. M. Forrest *et al.*, Functional analysis of TCF4 missense mutations that cause Pitt-Hopkins syndrome. *Hum. Mutat.* **33**, 1676–1686 (2012).
372. B. Schönewolf-Greulich *et al.*, Clinician's guide to genes associated with Rett-like phenotypes-Investigation of a Danish cohort and review of the literature. *Clin. Genet.* **95**, 221–230 (2019).
373. C. A. Chapleau *et al.*, Dendritic spine pathologies in hippocampal pyramidal neurons from Rett syndrome brain and after expression of Rett-associated MECP2 mutations. *Neurobiol.*

Dis. **35**, 219–233 (2009).
374. R. G. Wither *et al.*, Electrographic and pharmacological characterization of a progressive epilepsy phenotype in female MeCP2-deficient mice. *Epilepsy Res.* **140**, 177–183 (2018).
375. M. S. Fallah, J. H. Eubanks, Seizures in mouse models of rare neurodevelopmental disorders. *Neuroscience*. **445**, 50–68 (2020).
376. N. S. J. Halbach *et al.*, Altered carbon dioxide metabolism and creatine abnormalities in rett syndrome. *JIMD Rep.* **3**, 117–124 (2012).
377. J. L. Neul *et al.*, Metabolic signatures differentiate rett syndrome from unaffected siblings. *Front Integr Neurosci*. **14**, 7 (2020).
378. B. N. Phan *et al.*, A myelin-related transcriptomic profile is shared by Pitt-Hopkins syndrome models and human autism spectrum disorder. *Nat. Neurosci.* **23**, 375–385 (2020).
379. M. L. Seibenhener, M. C. Wooten, Use of the Open Field Maze to measure locomotor and anxiety-like behavior in mice. *J. Vis. Exp.*, e52434 (2015).
380. S. Mesman, R. Bakker, M. P. Smidt, Tcf4 is required for correct brain development during embryogenesis. *Mol. Cell. Neurosci.* **106**, 103502 (2020).
381. K. Braun, B. M. Häberle, M.-T. Wittmann, D. C. Lie, Enriched environment ameliorates adult hippocampal neurogenesis deficits in Tcf4 haploinsufficient mice. *BMC Neurosci.* **21**, 50 (2020).
382. L. M. Monteggia, E. T. Kavalali, Rett syndrome and the impact of MeCP2 associated transcriptional mechanisms on neurotransmission. *Biol. Psychiatry*. **65**, 204–210 (2009).
383. S. Stockler-Ipsiroglu, C. D. M. van Karnebeek, Cerebral creatine deficiencies: a group of treatable intellectual developmental disorders. *Semin Neurol*. **34**, 350–356 (2014).
384. F. Ehrhart *et al.*, Integrated analysis of human transcriptome data for Rett syndrome finds a network of involved genes. *World J Biol Psychiatry*. **21**, 712–725 (2020).
385. M. Freilinger *et al.*, Effects of creatine supplementation in Rett syndrome: a randomized, placebo-controlled trial. *J Dev Behav Pediatr*. **32**, 454–460 (2011).
386. L. Meikle *et al.*, A mouse model of tuberous sclerosis: neuronal loss of Tsc1 causes dysplastic and ectopic neurons, reduced myelination, seizure activity, and limited survival. *J. Neurosci.* **27**, 5546–5558 (2007).
387. E. Ercan *et al.*, Neuronal CTGF/CCN2 negatively regulates myelination in a mouse model of tuberous sclerosis complex. *J. Exp. Med.* **214**, 681–697 (2017).
388. R. S. Finkel *et al.*, Nusinersen versus Sham Control in Infantile-Onset Spinal Muscular Atrophy. *N. Engl. J. Med.* **377**, 1723–1732 (2017).
389. E. Mercuri *et al.*, Nusinersen versus Sham Control in Later-Onset Spinal Muscular Atrophy. *N. Engl. J. Med.* **378**, 625–635 (2018).
390. G. Acsadi *et al.*, Safety and efficacy of nusinersen in spinal muscular atrophy: The EMBRACE study. *Muscle Nerve*. **63**, 668–677 (2021).
391. R. S. Finkel *et al.*, Treatment of infantile-onset spinal muscular atrophy with nusinersen: final report of a phase 2, open-label, multicentre, dose-escalation study. *Lancet Child Adolesc. Health*. **5**, 491–500 (2021).
392. R. H. Andres, A. D. Ducray, U. Schlattner, T. Wallimann, H. R. Widmer, Functions and effects of creatine in the central nervous system. *Brain Res. Bull.* **76**, 329–343 (2008).
393. K. Goodspeed *et al.*, Pitt-Hopkins Syndrome: A Review of Current Literature, Clinical Approach, and 23-Patient Case Series. *J. Child Neurol.* **33**, 233–244 (2018).
394. K. Sharma, J. Singh, P. P. Pillai, E. E. Frost, Involvement of MeCP2 in Regulation of Myelin-Related Gene Expression in Cultured Rat Oligodendrocytes. *J. Mol. Neurosci.* **57**, 176–184 (2015).
395. H. Van Esch, in *GeneReviews(®)*, R. A. Pagon et al., Eds. (University of Washington, Seattle, Seattle (WA), 1993).
396. O. Philippe *et al.*, NF-κB signalling requirement for brain myelin formation is shown by

genotype/MRI phenotype correlations in patients with Xq28 duplications. *Eur. J. Hum. Genet.* **21**, 195–199 (2013).
397. M. V. C. Nguyen *et al.*, Oligodendrocyte lineage cells contribute unique features to Rett syndrome neuropathology. *J. Neurosci.* **33**, 18764–18774 (2013).
398. L. Buch *et al.*, Role of astrocytic MeCP2 in regulation of CNS myelination by affecting oligodendrocyte and neuronal physiology and axo-glial interactions. *Exp. Brain Res.* **236**, 3015–3027 (2018).
399. P. Moretti, J. A. Bouwknecht, R. Teague, R. Paylor, H. Y. Zoghbi, Abnormalities of social interactions and home-cage behavior in a mouse model of Rett syndrome. *Hum. Mol. Genet.* **14**, 205–220 (2005).
400. T. Gemelli *et al.*, Postnatal loss of methyl-CpG binding protein 2 in the forebrain is sufficient to mediate behavioral aspects of Rett syndrome in mice. *Biol. Psychiatry*. **59**, 468–476 (2006).
401. S. L. Fyffe *et al.*, Deletion of Mecp2 in Sim1-expressing neurons reveals a critical role for MeCP2 in feeding behavior, aggression, and the response to stress. *Neuron*. **59**, 947–958 (2008).
402. M. Adachi, A. E. Autry, H. E. Covington, L. M. Monteggia, MeCP2-mediated transcription repression in the basolateral amygdala may underlie heightened anxiety in a mouse model of Rett syndrome. *J. Neurosci.* **29**, 4218–4227 (2009).
403. J. Maksymetz, S. P. Moran, P. J. Conn, Targeting metabotropic glutamate receptors for novel treatments of schizophrenia. *Mol. Brain*. **10**, 15 (2017).
404. S. Chaki, mGlu2/3 Receptor Antagonists as Novel Antidepressants. *Trends Pharmacol. Sci.* **38**, 569–580 (2017).
405. M. E. Joffe, C. I. Santiago, J. L. Engers, C. W. Lindsley, P. J. Conn, Metabotropic glutamate receptor subtype 3 gates acute stress-induced dysregulation of amygdalo-cortical function. *Mol. Psychiatry*. **24**, 916–927 (2019).
406. A. Nikiforuk *et al.*, Effects of a positive allosteric modulator of group II metabotropic glutamate receptors, LY487379, on cognitive flexibility and impulsive-like responding in rats. *J. Pharmacol. Exp. Ther.* **335**, 665–673 (2010).
407. D. Zhang *et al.*, Altered visual cortical processing in a mouse model of MECP2 duplication syndrome. *Sci. Rep.* **7**, 6468 (2017).
408. J. Xu *et al.*, Hippocampal metaplasticity is required for the formation of temporal associative memories. *J. Neurosci.* **34**, 16762–16773 (2014).
409. G. Imre, The preclinical properties of a novel group II metabotropic glutamate receptor agonist LY379268. *CNS Drug Rev.* **13**, 444–464 (2007).
410. C. J. Swanson *et al.*, Metabotropic glutamate receptors as novel targets for anxiety and stress disorders. *Nat. Rev. Drug Discov.* **4**, 131–144 (2005).
411. A. G. Walker, P. J. Conn, Group I and group II metabotropic glutamate receptor allosteric modulators as novel potential antipsychotics. *Curr. Opin. Pharmacol.* **20**, 40–45 (2015).
412. M. D. McEchron, H. Bouwmeester, W. Tseng, C. Weiss, J. F. Disterhoft, Hippocampectomy disrupts auditory trace fear conditioning and contextual fear conditioning in the rat. *Hippocampus*. **8**, 638–646 (1998).
413. P. T. Huerta, L. D. Sun, M. A. Wilson, S. Tonegawa, Formation of temporal memory requires NMDA receptors within CA1 pyramidal neurons. *Neuron*. **25**, 473–480 (2000).
414. M.-G. Zhao *et al.*, Deficits in trace fear memory and long-term potentiation in a mouse model for fragile X syndrome. *J. Neurosci.* **25**, 7385–7392 (2005).
415. M. P. Forrest, A. J. Waite, E. Martin-Rendon, D. J. Blake, Knockdown of human TCF4 affects multiple signaling pathways involved in cell survival, epithelial to mesenchymal transition and neuronal differentiation. *PLoS One*. **8**, e73169 (2013).
416. D. Y. Chen *et al.*, A critical role for IGF-II in memory consolidation and enhancement. *Nature*. **469**, 491–497 (2011).

417. M. J. Schmeisser *et al.*, IκB kinase/nuclear factor κB-dependent insulin-like growth factor 2 (Igf2) expression regulates synapse formation and spine maturation via Igf2 receptor signaling. *J. Neurosci.* **32**, 5688–5703 (2012).
418. A. Y. Galvez-Contreras, D. Zarate-Lopez, A. L. Torres-Chavez, O. Gonzalez-Perez, Role of oligodendrocytes and myelin in the pathophysiology of autism spectrum disorder. *Brain Sci.* **10** (2020).
419. X.-R. Jin, X.-S. Chen, L. Xiao, Mecp2 deficiency in neuroglia: new progress in the pathogenesis of rett syndrome. *Front. Mol. Neurosci.* **10**, 316 (2017).
420. E. P. Harrington *et al.*, Oligodendrocyte PTEN is required for myelin and axonal integrity, not remyelination. *Ann. Neurol.* **68**, 703–716 (2010).
421. K. M. Huber, E. Klann, M. Costa-Mattioli, R. S. Zukin, Dysregulation of mammalian target of rapamycin signaling in mouse models of autism. *J. Neurosci.* **35**, 13836–13842 (2015).
422. J. L. Stringer, P. G. Guyenet, Elimination of long-term potentiation in the hippocampus by phencyclidine and ketamine. *Brain Res.* **258**, 159–164 (1983).
423. J. L. Stringer, L. J. Greenfield, J. T. Hackett, P. G. Guyenet, Blockade of long-term potentiation by phencyclidine and sigma opiates in the hippocampus in vivo and in vitro. *Brain Res.* **280**, 127–138 (1983).
424. E. J. Coan, W. Saywood, G. L. Collingridge, MK-801 blocks NMDA receptor-mediated synaptic transmission and long term potentiation in rat hippocampal slices. *Neurosci. Lett.* **80**, 111–114 (1987).
425. M. Pollard *et al.*, Synaptic transmission changes in fear memory circuits underlie key features of an animal model of schizophrenia. *Behav. Brain Res.* **227**, 184–193 (2012).
426. S. Percelay *et al.*, Functional Dysregulations in CA1 Hippocampal Networks of a 3-Hit Mouse Model of Schizophrenia. *Int. J. Mol. Sci.* **22** (2021).
427. X. Zhong, H. Li, Q. Chang, MeCP2 phosphorylation is required for modulating synaptic scaling through mGluR5. *J. Neurosci.* **32**, 12841–12847 (2012).